LEABHARLANN CHOLÁISTE NA TRÍONÓIDE, BAILE ÁTHA CLIATH | TRINITY COLLEGE LIBRARY DUBLIN
Ollscoil Átha Cliath | The University of Dublin

Terms and Conditions of Use of Digitised Theses from Trinity College Library Dublin

Copyright statement

All material supplied by Trinity College Library is protected by copyright (under the Copyright and Related Rights Act, 2000 as amended) and other relevant Intellectual Property Rights. By accessing and using a Digitised Thesis from Trinity College Library you acknowledge that all Intellectual Property Rights in any Works supplied are the sole and exclusive property of the copyright and/or other IPR holder. Specific copyright holders may not be explicitly identified. Use of materials from other sources within a thesis should not be construed as a claim over them.

A non-exclusive, non-transferable licence is hereby granted to those using or reproducing, in whole or in part, the material for valid purposes, providing the copyright owners are acknowledged using the normal conventions. Where specific permission to use material is required, this is identified and such permission must be sought from the copyright holder or agency cited.

Liability statement

By using a Digitised Thesis, I accept that Trinity College Dublin bears no legal responsibility for the accuracy, legality or comprehensiveness of materials contained within the thesis, and that Trinity College Dublin accepts no liability for indirect, consequential, or incidental, damages or losses arising from use of the thesis for whatever reason. Information located in a thesis may be subject to specific use constraints, details of which may not be explicitly described. It is the responsibility of potential and actual users to be aware of such constraints and to abide by them. By making use of material from a digitised thesis, you accept these copyright and disclaimer provisions. Where it is brought to the attention of Trinity College Library that there may be a breach of copyright or other restraint, it is the policy to withdraw or take down access to a thesis while the issue is being resolved.

Access Agreement

By using a Digitised Thesis from Trinity College Library you are bound by the following Terms & Conditions. Please read them carefully.

I have read and I understand the following statement: All material supplied via a Digitised Thesis from Trinity College Library is protected by copyright and other intellectual property rights, and duplication or sale of all or part of any of a thesis is not permitted, except that material may be duplicated by you for your research use or for educational purposes in electronic or print form providing the copyright owners are acknowledged using the normal conventions. You must obtain permission for any other use. Electronic or print copies may not be offered, whether for sale or otherwise to anyone. This copy has been supplied on the understanding that it is copyright material and that no quotation from the thesis may be published without proper acknowledgement.

An Electrochemical Study of Electroactive, Ferrocene-Terminated, Self-Assembled Monolayers

Michael Kinsella
03174387

A Thesis submitted to
The University of Dublin
for the degree of
Doctor of Philosophy

Department of Chemistry
University of Dublin
Trinity College

September 2006

TRINITY COLLEGE
2 7 MAY 2008
LIBRARY DUBLIN
THESIS
8431

DECLARATION

This thesis has not been submitted as an exercise for a degree at any other university. Except where stated, the work described therein was carried out by me alone.

I give permission for the Library to lend or copy this thesis upon request.

Signed: Michael Kinsella.

ACKNOLEDGEMENTS

Firstly my thanks go to my supervisor, Dr. Mike Lyons for all his guidance and support. Thanks to the Irish Research Council for Science, Engineering and Technology for funding my project. Thanks to Prof. Corish who as head of chemistry allowed me to use the departmental facilities. Thanks to Dr. Morton-Blake for discussions regarding the effect of the magnetic field and his molecular dynamics simulations. Thanks to Prof. Kelly who as head of postgraduate studies was always available to provide support if needed.

Thanks to Ray O'Brien and Conchiur MacGloinn for synthesising the compounds I've used in my project. Thanks to Dr. John O'Brien for his NMR work on these compounds.

I would also like to thank all the lads who've come through the lab for their company over the past three years. You've all made my time here very enjoyable. Special thanks to Johnny for the wind ups and teaching me to hit a sliotar, Brandon for the funny one-liners, Gar for some great nights spent over a few pints and finally thanks to Ray for just being Ray.

Very special thanks to my girlfriend Deirdre for always cheering me up effortlessly when things got difficult and always helping me out in any way she could.

Finally thanks to my Mam & Dad for their fantastic and unwavering support at all times. Time to enjoy your retirement folks…..

Abstract

Nanoscience includes the study of objects and systems in which at least one dimension is 1-100 nm. At these sizes, nanosystems can exhibit interesting and useful physical behaviours based on quantum phenomena. An area of Nanoscience that has received particular attention over the past 10 years is the area of molecular electronics. The concept of molecular electronics is an enticing alternative to extend Moore's Law beyond the foreseen limits of small-scale conventional silicon integrated circuits. This area was first proposed by Mulliken and Szent-Gyorgi in 1940 however it was not until 1974 when Ratner and Aviram[1] proposed the possible production of a molecular rectifier that this area received particular attention. In the late 1990s Mark Reed and Jim Tour[2] succeeded in demonstrating molecular circuitry in the laboratory. They showed that a monolayer of about 1000 molecules exhibited the phenomenon of negative differential resistance (NDR) – a current-voltage characteristic that differs from the normal in certain special systems. This property leads to the possibility of a molecular 'memory' being developed. As a result, molecular electronics is currently a very active research field, sometimes marked by controversy since many fundamental questions concerning both theory and experiments are left open. Much controversy remains regarding the fundamental events governing electron transfer through single molecules. Self-assembled monolayers, in particular redox-active molecules, provide an ideal platform to study such processes. To this end my Ph.D. has concentrated on the properties of redox active molecules, the complete understanding of which is essential to the development of molecular electronics.

There are five distinct areas in this work. The first four deal solely with theoretical studies of electron transfer mechanisms through electroactive self–assembled monolayers. The final section deals with the immobilisation of enzyme molecules atop of self-assembled monolayers with a view to developing a platform that can provide increased understanding of the electron properties of different enzymes. This section is intended to demonstrate a practical basis for the use of self-assembled monolayers.

Firstly the electron transfer properties of electroactive SAMs were investigated using CV, EQCM and Chronoamperometry (CA). Studies of the electron transport phenomenon in electroactive SAMs are usually complicated by interactions

between neighbouring electroactive moieties. These interactions were examined using a modified version of the Brown-Anson model[3] that has been used to treat the interactions between redox sites in electroactive polymers. An interaction parameter and the extent of deviation from ideality were determined. SAM mass changes during redox processes are monitored via quartz crystal microbalance.

Secondly the adsorption mechanism of SAMs was investigated. One of the most important aspects of SAM use in molecular electronics is their ability to spontaneously form in nanometer scale areas where direct manipulation would require complex techniques. The role that defects play in device functionality has not been addressed at all. For this reason a new technique is developed using an electrochemical quartz crystal microbalance (EQCM) and cyclic voltammetry (CV) to determine the quality of deposited monolayers as a function of time, concentration and temperature.

In the last section it was determined that interactions do exist between individual redox active molecules and that they cause a deviation from the ideal electroactive response necessary to fully understand electron transport phenomenon. To combat this problem 'mixed' monolayers are formed which theoretically can exhibit ideal surface electrochemistry. Some details regarding the exact mechanism of mixed monolayer formation remain unresolved[4-6]. This work utilizes EQCM and CV to improve and elucidate the process of mixed monolayer formation. Two complementary methods have been developed (place exchange and coadsorption).

The fourth section investigated the effects of an external magnetic field on the electron transport properties of redox active SAMs. Significantly reduced currents were observed during the SAM redox processes under the influence of a magnetic field. The current transient data provided by chronoamperometry showed an increased rate of electron transfer through the organic monolayer as a result of the application of the magnetic field. EQCM was used to investigate the mass change on the surfaces of the SAMs due to the formation of ion pairs between the redox active molecules and the electrolyte occurring during the SAM redox processes.

In the final section various self-assembled monolayers were used as a platform to anchor glucose oxidase and cytochrome c to the electrode surface. In this section cyclic voltammetry and amperometry are used to investigate the electron transport properties of the previously mentioned enzymes. In the case of the glucose oxidase system the use of a redox mediator system is demonstrated. Michaelis-Menten

analysis is also utilised in the case of the glucose oxidase system. In the case of the cytochrome c system an improvement in electron transfer reversibility of the cytochrome c enzyme is displayed using self-assembled monolayers as an electrode surface modifier.

References

1. A. Aviram, and M.A Ratner, *Chem. Phys. Lett.* **1974**, *29*, 277
2. M.A Reed, C Zhou, C.J Muller, T.P Burgin, and J.M Tour, *Science*, **1997**, *278*, 252
3. A.P. Brown and F.C Anson, *J Electroanal. Chem.* **1978**, *92*, 133.
4. C. E. D. Chidsey, C. R. Bertozzi, T. M. Putvinski, and A. M. Mujsce *J. Am. Chem. Soc.* **1990**, *112*, 4301
5. D. M. Collard and M. A. Fox, *Langmuir*, **1991**, *7*, 1192.
6. M. Lee and C. Chung, *Bull. Korean Chem. Soc.* **1999**, *Vol. 20*, No. 21

1. Introduction to Organosulfur Self-Assembled Monolayers

1.1 Introduction to Nanoscience based on Organosulfur Self-Assembled Monolayers 1

1.1.1 What is Nanoscience? 1
1.1.2 Surfaces and Interfaces in Nanoscience 2
1.1.3 SAMs as Components of Nanoscience 3

1.2 Introduction to Organosulfur Self-Assembled Monolayers 4

1.2.1 Definition of a Self-Assembled Monolayer 4
1.2.2 Types of Self Assembled Monolayer on Electrodes 7
1.2.3 Preparation of Self Assembled Monolayers 7
1.2.3.1 Substrate Choice 8
1.2.3.2 Solution Adsorption 10
1.2.3.3 Other Deposition Methods 13
1.2.4 Nature of the Gold-Thiolate Interface 14
1.2.4.1 Thermodynamic Analysis 14
1.2.4.2 Surface Structure of Alkanethiols on Gold 16
1.2.5 Organisation of the Organic Layer 18
1.2.5.1 Orientation of the Organic Layer in SAM 18
1.2.5.2 Multichain Model to Describe the Orientation of the Organic Layer 21
1.2.5.3 The Odd-Even Effect for Alkanethiols on Gold 21
1.2.5.4 Effect of the Organic Component on the Stability of the SAM 22
1.2.6 Defects in SAMs 23
1.2.6.1 Variations in the Surface of the Substrate 24
1.2.6.2 Reconstruction of the Surface During Assembly 24
1.2.6.3 Structural Dynamics Related Defects 25
1.2.6.4 Composition of SAMs 26
1.2.6.5 Pinholes 26
1.2.7 Blocked Electrodes 28
1.2.7.1 Monolayer Structure and Blocking Behaviour 28
1.2.7.2 Capacitance 33
1.2.7.3 Electrochemical Desorption 41

1.3 Applications of SAMs 44

1.3.1 SAMs as Etch Resists 45
1.3.2 SAMs as Barriers to Electron Transport 46
1.3.2.1 SAMs in Electrochemistry 47
1.3.2.2 SAMs in Organic/Molecular Electronics 49
1.3.3 SAMs in Biochemistry and Biology 54
1.3.3.1 SAMs as Model Biological Surfaces 56
1.3.3.2 SAMs for Cell Biology 58
1.3.3.3 Structure Considerations for SAMs used in Biology 59
1.3.4 SAMs for Sensing 61
1.3.4.1 Applications of SAMs in Biosensors 61
1.3.4.2 Applications of SAMs in pH Sensors 67

2. Experimental Theory and Methodology

2.1 The Electrochemical Cell **80**

2.1.1 Working Electrode 80
2.1.2 Reference Electrode 80
2.1.3 Auxiliary Electrode 81
2.1.4 Electrolyte Solutions 81
2.1.5 Materials 81

2.2 Instrumentation **82**

2.2.1 CHI Workstation 82

2.3 Electrode Modification Techniques **82**

2.3.1 Electrode Pre-Treatment 82
2.3.2 Monolayer Deposition 83

2.4 Experimental Techniques **84**

2.4.1 Cyclic Voltammetry 84
2.4.1.1 Reversible Systems 85
2.4.1.2 Irreversible Systems 89
2.4.1.3 Cyclic Voltammetry of Electroactive Monolayers 10
2.4.2 Chronoamperometry 93
2.4.2.1 Chronoamperometry of Electroactive Monolayers 95
2.4.3 Electrochemical Quartz Crystal Microbalance 96

2.5 Magnetic Field **98**

3. Characterisation of Electroactive Monolayers

3.1 Introduction 101

3.1.1 Ferrocene Terminated Organosulfur Monolayers 101
3.1.1.1 Surface Coverage 103
3.1.1.2 Peak Shape and Peak Potentials 104
3.1.1.3 Other Probe Techniques

3.2 Experimental 106

3.3 Results and Discussion 107

3.3.1 Effect of Chain Length 107
3.3.2 Molecular Interactions Within the Monolayer 109
3.3.3 Electrochemical Quartz Crystal Microbalance 114
3.3.3.1 Effect of Chain Length 114
3.3.4 Chronoamperometry 118

3.4 Conclusion 123

4. Adsorption Studies of Electroactive Monolayers

4.1 Introduction 125

4.1.1 Growth Mechanisms 125
4.1.2 Adsorption of Alkanethiols on Gold 129
4.1.3 Functional Form of Coverage Kinetics 133
4.1.4 Solvent Effects 135
4.1.5 Chain Length Effects 136
4.1.6 Submonolayer Islands 137

4.2 Experimental 138

4.3 Results and Discussion 140

4.3.1 Macroelectrode Cyclic Voltammetry 140
4.3.1.1 8Fc thiol – Discussion of 0.01mM, 0.1mM and 1mM Results 140
4.3.1.2 10Fc thiol – Discussion of 0.01mM, 0.1mM and 1mM Results 149
4.3.1.3 12Fc thiol – Discussion of 0.01mM, 0.1mM and 1mM Results 155
4.3.2 Electrochemical Quartz Crystal Microbalance Study 160
4.3.2.1 8Fc thiol – Discussion of 0.01mM, 0.1mM and 1mM Results 161
4.3.2.2 10Fc thiol - Discussion of 0.01mM, 0.1mM and 1mM Results 166
4.3.2.3 12Fc thiol - Discussion of 0.01mM, 0.1mM and 1mM Results 170

4.4 Conclusion 174

5. Formation of Electroactive Mixed Monolayers

5.1 Introduction 177

5.2 Experimental 182

5.3 Results and Discussion 183

5.3.1 Mixed Monolayer Formation via Coadsorption 183
5.3.2 Mixed Monolayer Formation via Place Exchange 195
5.3.3 Chain Length Comparisons 205
5.3.3.1 Coadsorption 205
5.3.3.2 Place Exchange 209

5.4 Conclusion 213

6. Magnetic Field Effects on Electroactive Monolayers

6.1 Introduction 216

6.2 Experimental 218

6.3 Results and Discussion 220

6.3.1 Effect of B-field on Redox Activity 220
6.3.1.1 Effect of Chain Length 221
6.3.1.2 Effect of Solvent 222
6.3.2 Chronoamperometry 224
6.3.3 Electrochemical Quartz Crystal Microbalance 228
6.3.4 Magnetic Field and Time Dependence 233
6.3.5 Effect of Magnetic Field Orientation 237
6.3.5.1 Magnetodynamic Considerations 241
6.3.6 Magnetic Field Forces in Aqueous Electrolytes 243

6.4 Conclusion 244

7. Self-Assembled Monolayers and Enzymes

7.1 Introduction **247**
7.1.1 Introduction to Self-Assembled Monolayers and Enzymes 247
7.1.2 Introduction of Glucose Oxidase 249
7.1.3 Introduction to Cytochrome c 250

7.2 Experimental **254**
7.2.1 Glucose Oxidase 254
7.2.2 Cytochrome c 255

7.3 Results and Discussion **256**
7.3.1 Glucose Oxidase 256
7.3.1.1 Inhibition of Interferers 256
7.3.1.2 SAM/Glucose Oxidase System 262
7.3.1.3 Michaelis-Menten Analysis of the SAM/Glucose Oxidase System 265
7.3.2 Cytochrome c 274
7.3.2.1 SAM/Cytochrome c System 276
7.3.2.2 Electron Transfer Rates 281

7.4 Conclusion **284**

8. General Conclusions and Future Recommendations

8.1 General Conclusions **287**

8.2 Future Recommendations **289**

APPENDIX **290**

To Mam and Dad

CHAPTER 1 –

INTRODUCTION TO ORGANOSULFUR SELF-ASSEMBLED MONOLAYERS

1. Introduction to Organosulfur Self-Assembled Monolayers

1.1 Introduction to Nanoscience based on Organosulfur Self-Assembled Monolayers

1.1.1 What is Nanoscience?

Nanoscience is the study of objects or systems that have at least one dimension in the range of 1-100nm. The important point about systems with dimensions in this range is that they are larger than atoms or small molecules but still smaller than the structures produced in modern microtechnologies using fabrication methods such as photolithography. Because the dimensions of the systems used in Nanoscience are normally smaller than or equal to the dimensions that define the physical properties of bulk materials they exhibit useful behaviour based on quantum phenomena such as electron confinement[1], near field optical effects[2], electron tunnelling[3] and ballistic transport[4].

New synthetic methods have made it possible to produce uniform nanostructures such as nanocrystals, nanowires, block copolymers and nanotubes. These new small-scale structures have applications as catalysts in materials science, in medicine for use in drug delivery in magnetic storage media and in electronic and optical devices.

The inspiration for nanotechnology comes from biology in the form of the cell. The cell is essentially an assembly of complex nanomachines. Nanoscale components such as DNA, RNA, enzymes, proteins and many more interact with one another to regulate their activities. They cooperatively self-assemble to form "soft" structures, together, they interpret the local surroundings and modify it, they also carry out collective functions such as motility, replication and metabolism.

The development of Nanoscience has, in a major way, been aided by developments in surface probe techniques such as STM, SEM and AFM. The ability to collect good quality images of nanostructures has lead to ideas for new nanotechnologies such as assemblers, nanorobots and 'grey goo'. Such technologies are somewhat far-fetched at present however there are some technologies based on Nanoscience which are more realisable in the foreseeable future. A good example of this is the drive for smaller and smaller electronic devices. This downscaling of the size of the devices has lead to a downscaling in the size of the microprocessors

driving them. There is an upper limit on the number of such devices that can be placed on silicon chips using current fabrication technology. This limit implies that eventually, should we want to increase the processing power of our devices we will need increase the size of the chip and hence of the device. To tackle this problem we look to the ability to fabricate nanoscale components for electronic devices. Such small-scale components would dramatically reduce the size of electronic devices. Another advantage of using nanoscale components in electronics is, as already mentioned, the ability to take advantage of electron tunnelling effects that occur in such devices. For example electron tunnelling between two conducting regions separated by an insulating medium can increase the speed of electron conduction relative to modern through-metal conduction methods thus increasing the speed of devices based on nanoscale components.

Other realisable applications of nanofabrication include areas such as tailoring the toughness and electrical conductivity of composite materials and new classes of biosensors.

1.1.2 Surfaces and Interfaces in Nanoscience

The most important characteristic of structures with nanometer sized dimensions is that they have an extraordinary percentage of their atoms at the surface whereas in ordinary bulk materials the majority of the atoms residing in the bulk of the material. As the size of an object diminishes so too does the volume in space it occupies and consequently so too does its surface area. However the rate at which the volume of an object and the surface area of an object diminish are not identical. Whereas the volume (V) of an object is related to its characteristic length (l) by $V \propto l^3$ the surface area (S) is related to the characteristic length by $S \propto l^2$. As the characteristic length get smaller and smaller (i.e. nanometer dimensions) this scaling behaviour leads can lead to a structure where almost all of the atoms present reside on the surface. What makes nanostructures interesting is that atoms on the surface of a material experience a different environment from those in the bulk of a material. They have different free energies, electronic states, relativities, mobilities and structures[5]. The physical properties of macroscopic materials such as electrical conductivity, hardness etc. are in general determined by the properties of the bulk material. In the case of nanostructured materials however the physical properties depend much more strongly on their surface and interfacial environment.

1.1.3 How do SAMs relate to Nanoscience and Nanotechnology?

Bare surfaces of metals and metal oxides adsorb organic materials readily because this process lowers the free energy of its surface and the surrounding environment[5]. However most organic materials that spontaneously adsorb onto metal surfaces, whilst they do have effects on the properties of the surface, are not well defined. SAMs take advantage of this phenomenon to spontaneously adsorb onto the surface of a metal. Such monolayers form in a well defined manner on the surface of a metal, metal oxide or semiconductors. They can be deposited from both the liquid and gas phase. The affinity for the SAM molecules can be tailored such that it is surface-specific (headgroup tailoring). The surface of the SAM that interacts with the ambient environment can also be specified such that it is appropriate for specific interfacial tasks (terminal group tailoring). By far the most common type of SAMs studied are those based on alkanethiol chains. These are effectively an alkane chain with a sulphur headgroup and various surface-specific terminal groups. The adsorption of such SAMs has been studied on gold[6-13], silver[12, 14, 15], copper[12] palladium[16,17], platinum[18] and mercury[19].

The thickness of one alkanethiol monolayer is typically in the range of 1-3nm depending on the length of the alkane chain. Because of this SAMs are themselves nanostructures. The composition of the alkane chains determines the orientation of the molecules in the SAM relative to the surface normal and as already mentioned it is possible to tailor both the head and terminal groups to suit a particular application or system. It is also possible to pattern SAMs on the surface of a metal. This can be done by microcontact printing (μCP)[20,21] destruction of certain areas of the SAM with energetic beams[22-27] or by their deliberate removal with scanning probe microscopes moving in a predetermined pattern[28,29]. Mixed monolayers consisting of two or more constituents which undergo phase separation to form domains of specific molecules can also be formed[30]. All in all SAMs are ideally suited to applications in Nanoscience for a number of reasons. Firstly they are very simple to prepare not requiring any specialised, expensive equipment. In the majority of cases the substrate to be modified is simply exposed to a solution containing a low concentration of the molecule in question. The same solution may be reused countless times. Secondly, because of their spontaneous assembly mechanism they have the ability to form on surfaces irrespective of their size. They can thus be used to modify or stabilise pre-

formed nanostructures such as thin films and nanoparticles. Because this occurs spontaneously no human interaction is necessary. Thus it is possible to modify nanoscale structures using SAMs with involved technology. Thirdly it is possible to couple the external environment to the properties of the system being studied. A good example of this regards a metallic film modified with a SAM and coupled to the external environment via electrochemistry using a technique such as cyclic voltammetry. Finally they have the ability to link molecular scale to macroscale properties. A good illustration of this is the ability of a SAM to modify the wettability of a surface. Such modifications can be easily detected using a macroscopic analysis technique such as water contact measurement.

1.2 Introduction to Organosulfur Self-Assembled Monolayers

1.2.1 Definition of a Self-Assembled Monolayer

Self-Assembled Monolayers are monomolecular layers which are spontaneously formed upon introducing a specific substrate to the adsorbate molecules. Such monolayers exhibit a high degree of orientation, molecular order and packing. Figure 1.1 below shows a schematic diagram of an alkane chain based self-assembled monolayer.

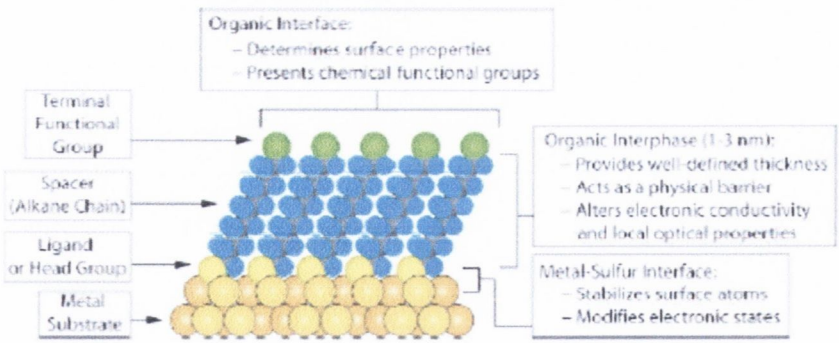


Figure 1.1 – Schematic showing the ideal orientation of an alkane chain based self-assembled monolayer adsorbed on a metallic substrate. Reproduced from Reference 31

Two main methods exist for depositing self-assembled monolayers. These are the Langmuir-Blodgett (LB) method and the self-assembly method. The LB method consists of transferring a compacted layer of molecules spread over an air water interface to the substrate in question. This is done by touching the substrate against the air-water interface of the compacted molecules[32-33]. Monolayer order is achieved

in two steps. The fist step is to orientate the molecules in before they are transferred to the substrate. This is achieved by having the head group hydrophilic and the terminal group hydrophobic such that all head groups will align along the surface of the water and all terminal groups will be repelled to stand straight up away from the water. The orientation of the molecules on the substrate is then determined by how hydrophilic/hydrophobic the substrate is.

The self-assembly method involves the assembly of molecules onto a substrate by the spontaneous adsorption of these molecules from a homogeneous solution. The assembly process is driven by the affinity of the headgroups of the adsorbate molecules for the substrate and favourable interactions between neighbouring molecules. The method preparing self-assembled monolayers was first described by Bigelow et al.[34] in 1946. This paper remarked that certain types of polar organic molecules are adsorbed from solutions of non-polar solvents to form well-oriented monolayers on a variety of metallic and non-metallic surfaces. It was found that such monolayers with a polar headgroup and one or more methyl terminal groups exhibited both hydrophobic and oleophobic properties. In 1978 Polymeropoulous et al.[35] revisited self-assembly. In this study a tunnelling junction was set up by sandwiching the monolayer of alkanesilanes of varying chain lengths between two layers of aluminium. Using this method the conduction properties of the SAMs were examined. In 1983 Allara and Nuzzo published a paper based on the adsorption of organic molecules with a sulphur headgroup onto a gold substrate[36]. Study of the self-assembly method came to the fore in 1987 and 1988 when a series of papers by various groups[37-44] were published relating to the adsorption of thiol-based organic molecules onto coinage metal surfaces. The popularity of sulphur based molecules, in particular alkanethiols, arises from their stability and the ease at which sulphur based molecules may be synthesised with respect to other molecules used for self assembly. When alkanethiol SAMs are deposited onto a gold substrate a bond of approximately 188kJmol^{-1} is thought to be formed[45]. This bond is strong enough that a wide range of functional groups can be incorporated both into and on the surface of the SAM. Furthermore the synthesis of molecules based on sulphur groups is much easier than using the hydrolytically active silane groups on which early monolayer studies were performed.

Due to the stability of sulfur-based alkanethiol molecules they have the ability to survive electrochemical experiments intact. These monolayers retain a high degree

of order and remain structurally intact over a range of electrode potentials. This is a result of both the strength of the gold-thiolate bond and the binding interactions between neighbouring molecules in the SAM. These binding interactions are particularly apparent in alkanethiol SAMs. These binding interactions ensure that such SAMs obtain a high packing density upon formation. This high packing density renders the SAM impermeable to both solvent and electrolyte ions whilst in solution. Given the qualities of stability over a range of potentials and the fact that they are impermeable to electrolyte/solvent ions alkanethiol SAMs become ideal for a number of experiments based on the theory of electron transfer phenomena. For example an alkanethiol SAM can be used as a spacing layer between a redox couple and an electrode. This redox couple may be either incorporated into the SAM as a specific terminal group or be freely diffusing in solution. Take the case of a gold electrode in contact with a freely diffusing, solvated redox couple such as the ferri-ferrocyanide couple. When the potential of the gold electrode is raised to the appropriate level there is an exchange of electrons between the gold surface and the redox couple in solution. Consider then the gold electrode coated with an alkanethiol SAM. Due to the close packed nature of the SAM the ferri-ferrocyanide redox couple are not permitted to approach the gold surface. The transfer of electrons between the gold surface and the redox couple must then proceed via a tunnelling mechanism. This tunnelling effect produces a large decrease in the rate of electron transfer in the SAM. The effect of chain length, chain composition, temperature and other factors on the rates of electron transfer can then be calculated. This type of experiment is useful for evaluating the results predicted by Marcus Theory. Marcus Theory was developed in a series of papers by R.A Marcus in 1965[46-63] and examines rates of electron transfers in from a donor to an acceptor state. It predicts that the rate of electron transfer depends on: (1) The distance between the donor and acceptor with electron transfer becoming more efficient as this distance decreases. In this discussion the distance between the donor and acceptor is the width of the SAM or the alkanethiol chain length. (2) The Gibbs energy of the reaction. The more energy released by the reaction the more efficient electron transfer becomes. (3) The reorganisation energy of the donor, acceptor and medium during electron transfer. Electron transfer becomes more efficient as this reorganisation energy marches the Gibbs energy of the reaction.

Imparting electron-transfer selectivity to the SAMs provides the ability to carry out further experiments regarding the nature of electron transfer through SAMs.

This can be done by incorporating so-called 'molecular gates'. These are certain sites in the SAM through which electron transfer can freely occur. Such sites can be introduced by incorporating a known fraction of certain molecules permeable to electron transfer.

1.2.2 Types of Self Assembled Monolayer on Electrodes

A vast number of compounds have been deposited as self-assembled monolayers on every electrode material. For this reason this sub-section will try to refer to the most commonly encountered SAMs. The most common electrodes are composed of gold, silver, copper, platinum and mercury. All of these materials are susceptible to passivation using thiol-based molecules. By far the most common sulfur-based molecules are alkanethiols. A typical alkanethiol molecule is shown below in Figure 1.2. Besides sulfur-based molecules the most common type of SAMs are those based on alkanesilane molecules[64,65], however sulfur-based aromatic molecules have been used[66]. SAMs based on isonitriles have also been examined[67,68]. Chlorosilanes have been used and it has been found that they will assemble on doped metal surfaces such as SnO_2[69] as well as silicon with an oxide coating[70]. Chlorosilanes were also found to form on gold electrodes[71,72]. It was observed by Linford et al.[73,74] that the generation of an alkane radical near an oxide free silicon surface resulted in the formation of a bond between the methylene carbon and the silicon surface. This process led to the formation of a densely packed SAM.

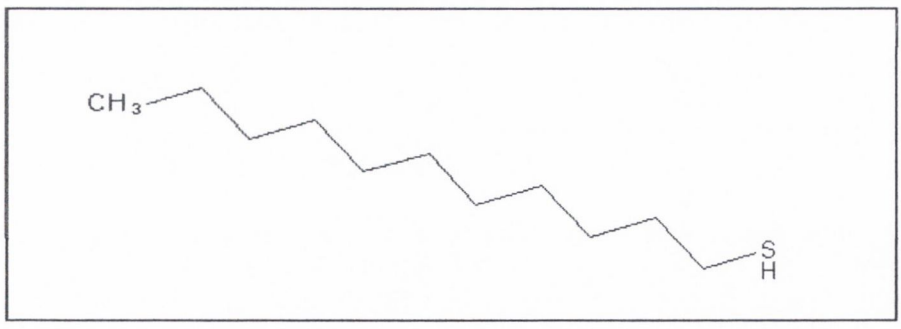


Figure 1.2 – Schematic diagram showing a $SH(CH_2)_{10}CH_3$ alkanethiol molecule.

1.2.3 Preparation of Self Assembled Monolayers

As already mentioned there are a wide variety of compounds that can be used to form self-assembled monolayers on various substrates. Because of this diversity this

section will limit its scope to the preparation of alkanethiol monolayers on a gold substrate. This section will therefore first look at why gold substrates have become the standard for alkanethiol adsorption. A detailed look at adsorption of alkanethiols from solution will be taken, as in most cases formation of alkanethiols from solution on a laboratory is sufficient. Finally the other methods of SAM formation such as adsorption from the gas phase will be dealt with.

1.2.3.1 Substrate Choice

As has already been discussed, alkanethiol monolayers will form on almost all modern electrode surfaces. By far the most common substrate used for SAM deposition is gold. There are five reasons cited for gold being the substrate of choice. (1) Gold is easy to obtain commercially although it is expensive. Thin films of gold can be formed via sputtering, vapour deposition and electro deposition. (2) Gold is an inert metal. This ensures that surface oxides, which can be detrimental to SAM structure, are not formed. Because of this experiments involving SAMs can be carried out in atmospheric laboratory conditions without the need for clean room or UHV conditions. (3) Gold bonds to thiol molecules with high affinity. As already mentioned a bond strength of ~188kJmol^{-1} is expected for the gold-thiolate bond. This high affinity is also likely to take precedence over any materials already on the gold surface leading to a well-ordered SAM. (4) A number of existing techniques such as ellipsometry and quartz crystal microbalance (QCM) utilise thin films of gold. Thus SAMs already formed on thin gold films can be easily coupled to these techniques. (5) It is known that cells do not show signs of toxicity on gold surfaces. Also because of the stability of SAMs on gold they are seen to be stable when placed in contact with the liquid media required for cell study for periods of days to weeks. This advantage relates to possible biological applications of SAMs.

An important aspect of SAM formation on gold relates to the morphology of the gold film. In particular, attention must be drawn to whether the gold is single crystal or polycrystalline. Single crystal gold surfaces are usually prepared by sputtering or evaporating gold on cleaved mica, single crystal silicon or on glass. Such films formed on silicon and glass usually exhibit a strong single crystal character whilst those prepared on mica have been shown to be essentially a complete single crystal[75, 76]. It must be noted at this point that there is no evidence to suggest that a single crystal gold surface is necessary for a defect free monolayer to form. It is

likely that the presence of impurities, grain boundaries and steps between atomically smooth planes will have more to do with SAM quality than the degree of crystallinity. It has actually been shown that better quality SAMs appear to be formed on polycrystalline gold surfaces than on single crystals. It has been shown by Creager et al. [77] that with substrate cleaning and annealing SAMs formed on polycrystalline gold surfaces are of better quality than those formed from single crystals. This was apparent from the blocking of the approach of redox couples to the electrode surface which was better in the case of SAMs formed on polycrystalline gold surfaces than SAMs formed on single crystal gold surfaces. The key to this apparent contradiction is thought to lie in the consideration of the microscopic roughness, of the order of the size of an adsorbate molecule. It is this microscopic roughness that is thought to introduce most of the defect sites into the monolayers. The microscopic roughness must be greater for the single crystal gold surfaces than it was for the polycrystalline surfaces. Macroscopic roughness was considered be only a minor factor in promoting defect formation in self-assembled monolayers. Creager also looked at the exchange of unsubstituted molecules in the SAM with electroactive molecules when the SAM was placed in contact with a solution of the electroactive thiol molecules. It was found that in the case of the SAM formed on the polycrystalline gold surface less exchange took place than did in the case of the single crystal gold surface. The fact that less exchange took place provides evidence that the SAMs formed from the polycrystalline gold surfaces are more stable than those formed on the single-crystal surface. Guo et al.[75] noted how the blocking behaviour of alkanethiol SAMs increased with increasing substrate roughness. This was done by annealing a gold substrate and examining the blocking behaviour of the SAM as the substrate became progressively smoother. It was determined that an atomically flat substrate was formed between 450-500°C and that SAMs formed on substrates that had been annealed at this temperature displayed the largest amount of permeation by the solvated redox couple. This led to the observation that the most poorly formed SAMs were formed on such substrates whilst the best blocking behaviour was found for SAMs prepared on substrates that had not undergone annealing.

It has also been noted that the roughness of the films is less important to SAM quality than other factors. Studies carried out by Steinberg et al. [78,79] on SAMs formed on evaporated and sputtered films were found to be free of defects even

though the grain sizes on these films was thought to be much smaller than in the case of evaporated films.

1.2.3.2 Solution Adsorption

Self Assembled Monolayers of thiol based molecules form spontaneously from solution and from the vapour phase onto gold surfaces. For all experimental procedures carried out in this report self assembly from solution was sufficient. Thus this section will discuss the main considerations regarding solution adsorption. Further discussion and experimental findings regarding the exact mechanisms of solution adsorption can be found in *Chapter 4*. For completeness the next section will provide a brief discussion regarding alternative methods of SAM deposition.

By far the most common method of SAM deposition is solution deposition. This is usually carried out from a dilute ethanolic solution (1-10mM) over a period of 12-24hrs at room temperature. This method results from studies carried out by Bain et al. [80] designed to optimise the deposition process. It is known that the majority of the thiol molecules are deposited onto the surface after a relatively short period of time (seconds) - however for a highly orientated SAM it is advisable to allow the deposition process to run for longer periods. In practice it is possible to successfully prepare SAMs from relatively 'dirty' conditions (i.e. a laboratory bench) without complication. However there are a number of experimental factors that can be taken into account when rigorously preparing well-formed SAMs from solution. These are solvent, solution temperature, solution concentration & deposition time, solution oxygen content, adsorbate purity, adsorbate structure, and substrate cleanliness. These factors will be dealt with in turn.

Solvent. The solvent most widely used when preparing SAMs is ethanol. The main reasons for the use of ethanol are: its easy availability, its low toxicity, its ability to solvate a wide range of alkanethiol molecules and the fact that it is inexpensive. Studies have been carried out comparing SAMs formed with ethanol to those formed with other solvents [80] and little difference has been found.

When regarding the impact of solvent on self-assembly the main considerations are the solvent-molecule interactions and the solvent-substrate interactions. The rate at which molecules are deposited is determined to some extent by their solubility. If a molecule has a high free energy in solution it is likely to

deposit more quickly than a molecule that is well solvated. The rate at which the molecules are deposited is also determined somewhat by the solvent substrate interactions. For a molecule to be deposited onto the substrate it must first displace solvent molecules residing there. If the interactions between the solvent and the substrate are attractive then it will be more difficult for the thiol molecules to displace them.

It has been suggested that the rates of formation of alkanethiol SAMs is faster from certain non-polar solvents[81,82] than from ethanol. These solvents are alkanes such as heptane, hexane etc. It was found however that as the chain length increased in these solvents the rates of formation reverted back to a rate comparable with that of ethanol. These hydrocarbon chains may, in some cases, increase the rates of SAM formation however it has been noted that the quality of the SAM is better when using ethanol than when using non-polar solvents[80]. This effect can be explained by large solvent-adsorbate molecule interactions in the case of alkanethiol molecules at least. It has been shown in studies by Schneider at al[83] and Ishida et al.[84] that polar liquids appear to reduce the quantity of certain defects in the fully formed SAM. This is most due to the poor solubility of the SAM molecules in these solvents as well as the low heat of interactions between the solvent molecules with the substrate surface serve to produce a more ordered layer.

Solution Temperature. Whist it is satisfactory in most cases to deposit SAMs from solutions at room temperature the temperature of the deposition solution temperature is likely to have an effect on both the kinetics and quality of SAM formation. Higher solution temperatures are likely to increase the rates of SAM formation as well as giving the adsorbed molecules enough energy to overcome imperfections in their orientation on the substrate surface such as coiled chains and lateral reorientation. Yamada et al.[85] utilised STM to monitor the formation of SAMs at various elevated temperatures. It was determined that the first 15 minutes of formation was most affected by the elevated temperature of the solution whilst the remainder of SAM formation (15mins-18hrs) was relatively unaffected.

Solution Concentration and Immersion Time. The concentration of the deposition solution and the time needed to produce a well-formed SAM are intrinsically related and are normally discussed in tandem. With regard to concentration and deposition

time the way in which a SAM forms is intuitive. Lower solution concentrations form SAMs more slowly due to mass transport considerations[86,87,88]. From simple geometry we can calculate that when a SAM is fully formed on an Au (111) surface that the coverage corresponds to 4.6 x 10^{14} moleculescm^{-2}. This coverage required for a fully formed SAM places a limit on the solution concentration of 1μM where there will be ~6 X 10^{14} cm^{-3}.(*See Section 1.2.4.2).* It was determined that SAMs formed from micromolar solutions or below do not exhibit the same characteristics as SAMs formed from higher concentrations[80]. For most experimental needs 1mM solutions are adequate. The normal immersion time for solutions is between 12-24hrs and it is noted that in general the overall properties of SAMs prepared as such do not vary from experiment to experiment. However is it noted that the properties of SAMs can change when subjected to prolonged immersions for up to 10 days. Chidsey et al.[89] found the kinetics of electron transfers through alkanethiol SAM to be more monodisperse if SAMs were allowed to assemble over as long as a week. Sun and Crooks[90] decorated pinhole defects in an HDT SAM with Cu and imaged them with STM and observed a steady loss of pinhole defects over a period of 7 days.

Solution Oxygen Content. It has been suggested that the degassing of thiol solutions using an inert gas such as argon or nitrogen prior to deposition may improve the reproducibility of monolayers formed[10, 13]. It is thought that this is because limiting the amount of oxygen in the deposition solution limits the degree to which the thiol moieties can become oxidised to sulfonates which are detrimental to SAM quality. Nothing appears to be known regarding the degree to which oxygen content in deposition solutions affects SAM formation rates.

Adsorbate Purity. In the case of thiol molecules the most common type of impurity encountered are disulfides. However such impurities are not thought to impede the formation or alter the structure of the SAMs formed. Love et al.[16] cites factors 'other than chain organisation' contributing to defective SAMs being produced and also suggests that percolating the thiols over neutral alumina as a method of removing oxidised contaminants such as sulfonates. Normally contaminants are not a problem in SAM formation when the thiol is subjected to the normal purification techniques such as recrystallisation, distillation or column chromatography.

Adsorbate Structure. In the case of alkanethiols any discussion regarding adsorbate structure is essentially based on the alkane chain length. Chidsey et al.[91] formed mixed monolayers of alkanethiols comprised of varying chain lengths. It was determined that longer chain alkanethiols adsorb more quickly from ethanolic solutions than do shorter chains. This is due to the higher free energy possessed by longer chains in solution making them less soluble than shorter chains.

Longer chain length alkanethiols are also expected to show better packing density than shorter chains as there are a greater amount of attractive Van der Waals interactions between the neighbouring chains. Needless to say many thiol-based molecules have been used to form SAMs and the packing mechanism of such SAMs is specific to the molecule used.

Substrate Cleanliness. Because of the strong affinity of the thiol based moieties towards gold substrates it is likely that any physisorbed impurities residing on the surface will be displaced by the adsorbing molecules. For this reason an argument exists that a substrate cleaning step is not necessary prior to SAM deposition [9, 92]. In most cases however some attempt is made to clean the substrate of impurities before it is introduced to the thiol molecules. Cleaning procedures include electrochemical cycling of the substrate in a solution of dilute acid, exposure of the substrate to a 'piranha' solution, strong heating of the substrate or exposure of the substrate to ozone or UV radiation. In the case of gold substrates a check for cleanliness is to electrochemically cycle the substrate between 0.5 and 1.4V in dilute sulphuric acid. This cycle should produce the characteristic anodic peak at 1.1V and an oxide stripping peak near 0.9V vs Ag/AgCl. Such a scan should be reproducible. Terminating the scan at a potential negative to the oxide stripping peak at 0.9V ensures that the gold is free of surface oxides.

1.2.3.3 Other Deposition Methods

Of the methods other than solution adsorption used to prepare SAMs by far the most utilised is the method of assembly from the gas phase. Vapour phase deposition may be carried out when the thiol is sufficiently volatile. It can be carried out in a vacuum [93] or at ambient pressures[94]. It was shown by Chailapakul et al.[94] using FTIR and ellipsometry that a range of alkanethiol SAMs formed from the vapour phase were

virtually identical to those formed from solution. Common practice when forming SAMs from the gas phase is to purge the substrate with a stream of nitrogen after deposition. This ensures that any loosely bound molecules are removed from the surface. The major way in which assembly from the vapour phase falls down is that many SAMs of interest may not be volatile enough to form a vapour phase. Another effect that limits this methods usefulness is the finite time spent by molecules at the surface when diffusing in the vapour phase this may impede the formation of a densely packed SAM.

Other methods involve the substrate being electrochemically held at a potential that assists SAM formation[95] and spreading a mixture of alkanethiol and alkanol molecules on a LB trough and applying to a gold substrate[96-98].

1.2.4 Nature of the Gold-Thiolate Interface

The formation of a SAM on a metal surface intrinsically demands that a reactive interface is formed. This reactive interface implies that both the substrate and the adsorbate molecules are transformed to some degree upon formation of the SAM. Gold unlike most other common electrodes used as substrates to deposit SAMs does not form a surface oxide. Hence the chemistry involved with the gold-thiolate bond is expected to be straightforward. There remains however a degree of ambiguity as to the exact nature regarding the gold-thiolate bond. For this reason a discussion is presented here regarding what is known about the chemistry between thiol molecules and the gold surface. Following this the overall structure adopted by alkanethiols on the gold surface is detailed.

1.2.4.1 Thermodynamic Analysis

The formation of an alkanethiol SAM on a gold surface requires the activation the S-H bond in the alkanethiol molecule. Studies were carried out regarding the nature of this bond by Nuzzo et al.[45] in 1987. It was determined for the case of methanethiol that during SAM formation there was no evidence of S-H cleavage although this finding is disputed. This implied that a gold(I)-thiolate bond was formed with a bond strength of 40-50kJmol^{-1}. This study also evaluated the adsorption energy of a disulfide compound as methyl thiolate as 117kJmol^{-1} yielding the expected result that a disulfide compound binds to the gold surface more strongly than in the case of a

single sulfur atom. Temperature-programmed desorption (TPD) studies regarding the thermodynamics of the gold-thiolate interface were carried out by Lavrich et al.[99]. This study determined that alkanethiols physisorb onto gold surfaces through van der Waals interactions. It was determined that the physisorption entalphy per CH_2 group in an alkanethiol molecule was 6.1kJmol^{-1}. The physisorption entalphy associated with the thiol group was determined to be of the order of 33kJmol^{-1} with 24kJmol^{-1} of this contributed by the sulfur atom. When in the bulk it was determined that the molecules were bound more strongly to the gold surface than to one another by a factor of 1.15. Alkanethiols showed a chemisorption energy of 126kJmol^{-1}. This would imply that once the length of the carbon chain in the alkanethiol molecules exceeds 14 CH_2 units the energy of physisorption of the molecule would be greater than the energy of chemisorption. This observation manifested itself in the fact that for chains of 14 CH_2 units or more only a single desorption peak is observed and accounts for the energy of physisorptin of all the molecules on the surface. In the case of chains shorter than 14 CH_2 units two peaks were observed. The first peak accounted for all physisorbed molecule whilst the second peak, at higher energies, accounted for chemisorbed molecules. As has already been noted the fate of the hydrogen atom in the S-H bond after SAM formation has not been definitively explained. As already discussed, Nuzzo et al.[45] described the S-H bond remaining intact after SAM formation. This theory was backed by Hasan et al.[100] using ^{1}H NMR studies. Using silver as a substrate for deposition Lee et al.[101] also determined that the S-H bond was retained during self assembly via a combination of Auger Electron Spectroscopy (AES), Low Energy Electron Diffraction (LEED) and Temperature Programmed Desorption (TPD). However these studies were countered by Widrig et al.[102] who reported the loss of the hydrogen group and the resulting oxidation of the sulfur group upon SAM formation.

Attention is now focused upon the fate of the hydrogen atom should it be dissociated into solution during SAM formation. It is likely that SAM formation in a vacuum would lead to the formation of H_2. In solution it is thought that the presence of oxygen atoms may cause the hydrogen to combine with them to form water. However whether or not the S-H bond is retained at the surface is of little consequence for most experimental procedures.

1.2.4.2 Surface Structure of Alkanethiols on Gold

Attention now turns to the structure of the alkanethiol monolayer on the gold surface. When considering the structure of the monolayer it is necessary to take into consideration the three interactions that determine the overlayer structure. These are: (1) The interactions between the terminal thiol groups and the atoms in the gold lattice. (2) The interactions between neighbouring alkane chains. (3) The interactions between the head groups of a particular SAM molecule. Early electron diffraction studies carried out by Strong et al.[43] determined that alkanethiol chains formed a incommensurate (7 x 7) overlayer structure on Au(111) The results of this study were re-evaluated by Chidsey et al.[103] and it was determined that a commensurate ($\sqrt{3}$ a x $\sqrt{3}$ a)R30° (where a = 2.884Å, the Au lattice constant, and R means rotated and refers to the fact that this new structure is a 30° rotation of the initial (7 x7) suggestion) overlayer structure was the correct interpretation. In this structure the thiol head groups would bond to threefold hollow sites on the gold surface. Further work carried out by Nuzzo et al.[104] determined, via IR, that the alkane chains were tilted at an angle of 30° to the surface normal and that the molecules in the SAM existed in two distinct twist azimuths. The structure of an alkanethiol SAM on Au(111) is shown in Figure 1.3. Some studies have called into question the structure described above by suggesting a structure that involves some degree of disulfide formation between adjacent sulfur atoms[105,106]. At this time however the structure described above is the one generally accepted as that adopted by alkanethiol SAMs on Au(111).

A secondary ordering of the chains is also suggested by Camillone et al.[107]. This study reported an orthorhombic unit cell with dimensions of 3a x $2\sqrt{3}$ a. This structure may equally be described as a c(4 x 2) superlattice.

The final feature of the surface structure of SAMs that must be dealt with is the issue of surface coverage. Collard and Fox[108] reported that the maximum surface coverage of alkanethiol molecules in a hexagonally packed ($\sqrt{3}$ a x $\sqrt{3}$ a)R30° structure is 4.6 x 10^{14} moleculescm^{-2}. It must be asked how such a value was arrived at? To do this we consider Figure 1.4 below. This shows, as in Figure 1.3(a), the packing of the sulfur molecules on the gold surface. The hexagonal packing of the sulfur atoms is also included in red. From electron diffraction studies[43] it is known that the distance between neighbouring sulfur atoms is 5Å.

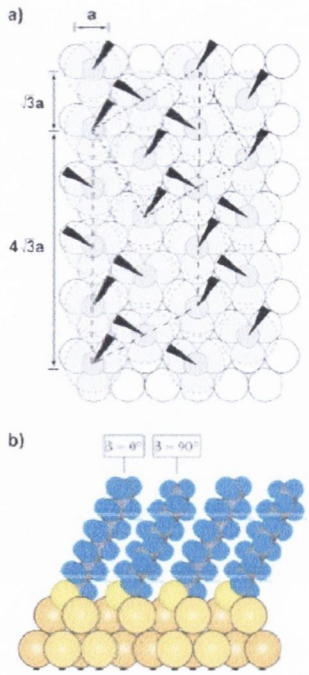


Figure 1.3. Schematic diagram depicting the arrangement of a fully formed monolayer of alkanethiol molecules on an Au(111) lattice. (a) Structural model showing the accepted ($\sqrt{3}$ x $\sqrt{3}$)R30° structure. In this structure the sulfur atoms (represented by grey circles) are positioned in threefold hollow sites on the gold lattice. (The underlying white circles represent the gold lattice). Surrounding each sulfur atom is a dashed circle. This circle represents the area each alkanethiol molecule is expected to take up. The black wedges represent the azimuthal twist of the alkanethiol molecules. The parallelogram traced by the long dashes traces the c(4 x2) superlattice. Note that this c(4x2) structure is defined by the azimuthal twist of the molecules. The square traced by the short dashes traces the equivalent $2\sqrt{3}$ x 3 unit cell. (b) Cross section of the alkanethiol SAM. The blue circles represent the hydrogen atoms of the alkane chain. Note the differing orientations of these hydrogen atoms which correspond to the differing orientations of the carbon atoms in the molecules. The value β indicates the relative twists of neighbouring chains. Reproduced from Reference 31

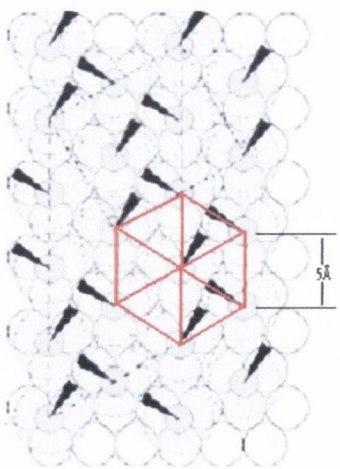


Figure 1.4. An alkanethiol monolayer on A(111). The hexagonal packing of alkanethiol molecules on Au(111) is traced in red. Partly Reproduced from Reference 31.

We now consider the hexagon that is formed by six alkanethiol molecules. This hexagon may be split into six identical triangles as shown. The area of one triangle may be calculated using $\frac{1}{2}ab\sin C$, where a and b are both 5 x 10^{-10}m and the angle with C is 60°. This yields an area for a single triangle of 10.8 x 10^{-20}cm^2. The overall area of the hexagon may be calculated as 6.5 x 10^{-19}m^2. Each hexagon is comprised of three full alkanethiol molecules. Thus the surface coverage can be determined as 4.6 x 10^{18} molecules/m^2 or 4.6 x 10^{14} molecules/cm^2 which corresponds to that quoted by Collard and Fox[108]. Often surface coverage values will we quoted in moles.cm^{-2}. Thus using N_A the surface coverage may also be represented as 7.6 x 10^{-10}moles/cm^2.

1.2.5 Organisation of the Organic Layer

The previous section described how the density of alkanethiol molecules on the surface of a gold surface has an upper limit of 4.6 x 10^{14} molecules/cm^2. This upper limit is based on the geometric arrangement of the sulfur moieties on the surface and the size of the lattice constant for the gold substrate. It is thought however that this arrangement may not minimise the free energy of the alkanethiol layer and that the two-dimensional density of molecules predicted in the previous section may not correspond to the density that the alkanethiol molecules achieved in the crystalline form. This is due to the fact that the alkanethiol molecules may adopt conformations in which there are high degrees of van der Waals interactions with neighbouring molecules[109] or in the case of certain molecules hydrogen bonding[110, 111]. Such arrangements can lead to a secondary level of organisation in alkanethiol monolayers that is important in determining macroscopic properties such as wetting and lubrication.

1.2.5.1 Single Chain Model to describe the Orientation of the Organic Layer in the SAM

In this section a simple single chain model of the SAM is used to describe the orientation adopted by linear alkanethiol molecules on metal surfaces. Two parameters can be used to describe the orientation of linear alkanethiols. These are α and β and can be seen in Figure 1.5 below. α is the angle of tilt of the alkanethiol chain away from the surface normal and, as already discussed, is taken to be 30° in the case of alkanethiol molecules on gold. We note that α can assume both positive and

negative values. β describes the angle of rotation of the carbon chain in the alkanethiol molecule relative to the plane of the surface normal. β can adopt values between 0° and 90°.

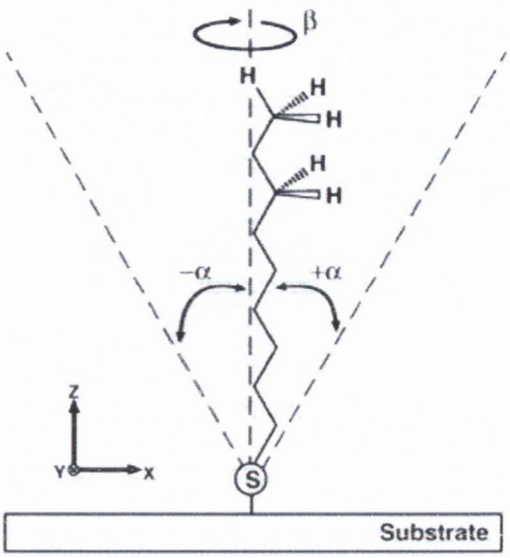


Figure 1.5. Schematic view of a long chain alkanethiol molecule adsorbed on a metal substrate. This diagram shows the tilt angle, α, which defines the tilt of the chain relative to the surface normal. Also shown is the twist angle, β, that describes the twist of the carbon chain relative to the plane of the surface normal. Reproduced from Reference 31.

Table 1.1 shows the orientations adopted by fully formed alkanethiol SAMs formed on gold, silver, copper, mercury and platinum.

Substrate	Cant Angle, α	Chain Rotation, β	Reference
Au	28°	53°	12
Ag	13°	44° ±6°	14
	15°	45°	112
Cu	12°	45°	12
Hg	0°	n.a	113
Pt	<15°	n.a	18

Table 1.1. Values of α and β for alkanethiols on various substrates.

Alkanethiol SAMs on the various metals are seen to adopt a quasi-crystalline structure with the alkane chains fully extended in a trans conformation. The tilts of the alkane chains vary depending on the substrate. Note that the highest tilt occurs on gold whist alkanethiols deposited on mercury are seen to stand perpendicular to the substrate. The chains in general are rotated by 45° relative to the surface normal. The data

presented above are based on space filling models similar to that presented by Labinis et al.[12] and involve the chain tilts lying in the direction of the next-nearest neighbour. Simply put these models involve the hexagonal arrangement of the molecules on the specific substrate similar to that previously described. The validity of such a model has been confirmed (at least in the case of gold) using grazing x-ray diffraction measurements[114].

A large body of work exists also on sulfur-based self-assembled monolayers based on structures other than linear chain alkanes. Of particular interest are aromatic based molecules. Examples of such molecules are shown in Figure 1.6. When dealing with aromatic molecules steric interactions between neighbouring must be taken into account. Many aromatic bulky aromatic molecules can make it impossible for other such molecules to adsorb onto the metal lattice site that would permit best packing. It is thought though that when limiting mass coverage is achieved that aromatic based molecules may adopt a $(\sqrt{3} \times \sqrt{3})R30^{\circ}$ orientation. In general the ordering of aromatic molecules is an interplay between the contributions from the substrate-molecule interactions and the molecule-molecule interactions. It is thought that as the length of a thioaromatic molecule increases so too does the contribution from molecule-molecule interactions.

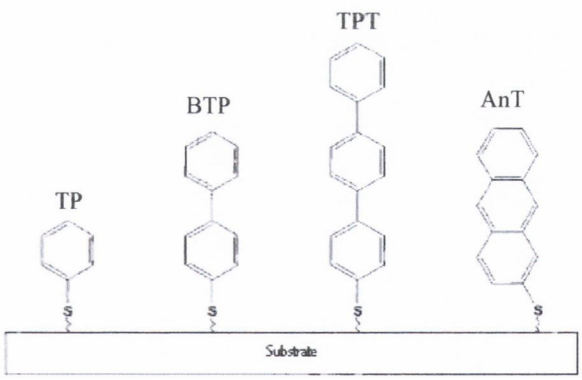


Figure 1.6. Examples of four different sulfur-based aromatic molecules used for the formation of self-assembled monolayers[115]. In this diagram: TP = thiophenol, (BTP) = 1,1'-biphenyl-4-thiol, TPT = 1,1;4',1''-terphenyl- 4-thiol, and AnT = anthracene-2-thiol.

This is borne out by the fact that as the chain length increases the value of α decreases corresponding to the molecules adopting a more perpendicular conformation on the surface[115]. This observation is due to the fact that as the chain length increases so too do the interactions between neighbouring chains. The influence of the substrate-molecule interactions should not be neglected although it is thought that the

interactions between the substrate and thioaromatic molecules is not as important as in the case of alkanethiols. It is determined that the average α value of the thioaromatic molecules is ~22° on Au whereas the corresponding value for alkanethiols is ~30° which again points to the importance of intermolecular interactions straightening the thioaromatic molecules on the Au surface.

1.2.5.2 Multichain Model to Describe the Orientation of the Organic Layer.

The previous section described how the structure of the organic layer could be described for thiols of different types on different substrates and provided a means by which comparisons could be made between them. Inherent to this method however is a lack of detail regarding the actual orientation of the SAMs. This is because the single chain model only describes average values of cant, (α) and rotation, (β), over the entire monolayer. We have already described how the c(4 x 2) superlattice structure is defined by alkanethiol molecules having orthogonal cants. However the single chain theory simply describes an average molecular cant value that is clearly oversimplified for the system in question. Similarly when we describe values of the carbon chain rotation, (β) the model becomes oversimplified. If we look at an orthorhombic sublattice of chains as seen in Figure 1.3(b) we note the carbon chains in adjacent alkanethiol molecules would be rotated 90° with respect to one another. However the single chain model would simply quote an average value of ~45° for β which would not tell the full story. In general the multichain model for describing molecular orientation is simply an extension of the single chain model. It takes into account the fact that chain orientations can be quite different in a unit cell and not simply described by an averaged value. This technique is very rarely, if ever, alluded to in literature as a method to describe cell conformation.

1.2.5.3 The Odd-Even Effect for Alkanethiols on Gold

We have already noted that alkanethiol SAMs formed on Au(111) adopt a ($\sqrt{3}$ x$\sqrt{3}$)R30° structure with a 30° angle of tilt towards the plane. This structure is formed irrespective of the length of the alkane chain. This feature of the assembly can lead to different surface orientations of the alkanethiol molecules depending on whether the number of methylene units is odd or even. For this reason it is known as the 'Odd-Even' effect. It is thought that 'Odd-Even' effects can lead to different surface free-

energies for odd and even numbered chains. This effect is thought to arise mainly from the different orientations adopted by terminal groups in odd and even numbered chains. IR studies have shown that the orientation of the methyl group orientation arises from the tilt angle of the alkane chain[116-120]. Due to this the permanent dipole moment of the methyl groups is forms a greater angle with the surface normal than it does when the chain is even[121]. This can lead to subtle differences in the wettability and lubrication properties of alkanethiol monolayers depending on whether the chain has an odd or even number of carbons,

The 'Odd-Even' effect was examined for alkanethiol SAMs with a phenyl headgroup by Lee et al.[122]. Here the 'Odd-Even' effect was apparent and indicated that SAMs with an even number of methylene units exhibited a greater chain twist than the SAMs with an odd number of methylene units. This difference in chain twist can led to differences in separation between the headgroups. This in turn led to different degrees of terminal group interactions that which affects the free energy of the surface.

It is also thought that the 'Odd-Even' effect has an effect on the value of the chain tilt angle, α[123, 124]. This is because the odd or even character of the chain has an effect on the van der Waals interactions between neighboring chains. The strength of these van der Waals interaction in turn have an effect on the angle of tilt of the alkane chains.

1.2.5.4 Effect of the Organic Component on the Stability of SAMs

The stability of self-assembled monolayers does show sensitivity to the structure of the organic component. Considering the case of alkanethiol molecules it would be expected that longer chains would be more robust than shorter chains as the lateral interactions between the alkane chains are increased leading to increased stability. As a general rule the stability of any SAM would be expected to increase as substrate-molecule and molecule-molecule interactions are increased. For example the 'melting' of an alkanethiol SAM which corresponds to its phase transition when heated to a high enough temperature is dependent on the length of the alkanethiol chain. Monolayers formed from molecules with an aromatic organic group are likely to be quite stable again because intermolecular interactions are likely to be maximised in such cases. Schreiber[125] has discussed the aspects of SAM stability in a review with particular attention drawn to thermal stability.

1.2.6 Defects in SAMs

As already discussed alkanethiol and related molecules form spontaneously on gold and other metal substrates through a thermodynamically driven process. For this reason they have been identified as a building block for future nanoscale design. The structure of SAMs has been thoroughly described in the previous section which has theoretically described not only the position but also the tilt angle and chain twist of individual alkanethiol molecules on a nanoscale level. However this treatment is a long way from dealing with the reality of SAM formation. SAMs formed from alkanethiol or other molecules are far more complex than the above treatment suggest and contain a host of defects which must be considered in order to obtain a realistic notion of the nature of self-assembled monolayers. Shown in Figure 1.7 are many of the common defect types.

The causes of defects in SAMs can be both intrinsic and extrinsic. Intrinsic factors result from the very nature of the SAMs in that they are dynamic systems with complicated phase behaviours. External factors such as the purity of adsorbate, purity of solvent, crystallinity of substrate, cleanliness of substrate, atmospheric conditions etc. can all have an effect on the quality of the monolayer produced.

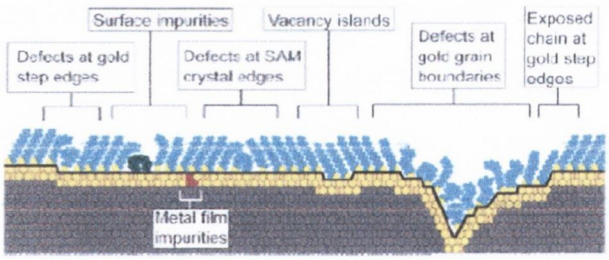


Figure 1.7. Schematic illustration of some of the intrinsic and extrinsic defects found in SAMs formed on metal substrates. The dark line at the metal-molecule interface indicates the topography of the surface in an attempt to elucidate some defect types. Reproduced from Reference 31.

As the drive for technology based on nanostructured materials increases so too will the need to isolate and eliminate any defects present in self-assembled monolayers. The issue of defects will be dealt with in this section focusing on the causes of defects such as those illustrated in Figure 1.7. As well as the causes of defects particular attention will be paid to defects known as 'pinholes', which are essentially molecular vacancies in the SAM, as a large body of work has been created on such defects.

1.2.6.1 Variations in the Surface of the Substrate

Even the most highly crystalline metal substrates are likely to involve some degree of defect. Many studies have been carried out, mainly via STM, regarding the nature of the metal substrate. It has been found that Au(111), the most widely used substrate, is likely to have many surface defects such as grain boundaries, faceting occlusions, twins, etc. Metal substrates are also likely to have a varying density of atomic steps. The degree to which defects occur in a fully formed SAM is likely to be governed by the amount of defects present at the surface[126, 127, 128, 306].

1.2.6.2 Reconstruction of the Surface During Assembly

One type of defect inherent to SAM formation on Au(111) are monatomic vacancies . This type of defect arises from the formation of Au vacancies during SAM formation. Such Au vacancies are manifested in a fully formed monolayer by regions in that monolayer that are offset by one gold atomic diameter from the surrounding regions. Such Au vacancy islands were first observed by Haussling et al.[130]. This was followed by a study by Edinger et al.[131] that examined the offsets in heights in an alkanethiol monolayer and determined that their depth was 2.5Å or one gold atomic step height. This measurement then attributed the decrease in heights to a vacancy in the underlying gold lattice. The monolayers in this study were deposited from solution. The deposition solutions were then subjected to atomic adsorption spectroscopy and it was found that they contained dissolved Au species. It was then proposed that such vacancy islands were formed by the etching of the Au substrate during monolayer formation. This model has been brought into question however by experiments showing that Au vacancy island formation occurred during monolayer adsorption from the gas phase[132, 93]. The mechanism for their formation has been described by Yang et al.[133] and can be explained thus: An Au(111) surface exhibits a surface morphology of (23 x $\sqrt{3}$) reconstruction. This can be understood as one extra gold atom per unit cell that corresponds to a slight compression of the gold surface relative to the bulk. During the formation of an alkanethiol monolayer the reconstruction of the Au lattice is lifted and two gold atoms per (23 x $\sqrt{3}$) unit cell are released on the surface terraces. Because the atoms are released on the terraces this corresponds to one net vacancy per unit cell. The released Au atoms diffuse rapidly and merge at neighbouring step edges while the vacancies that they have

produced coalesce into vacancy islands, which form at the terraces. Such vacancy islands have been observed in STM studies by both Poirer[126] and Yang et al.[133].
It has been proposed that vacancy islands such as those described may undergo Ostwald ripening which is in essence the growth of larger particles at the expense of smaller ones. In the case of highly dispersed vacancy islands a large perimeter to area ratio is observed. This means that there is a large step edge area to vacancy area ratio which is energetically unfavourable. Thus the Otswald ripening of the vacancies is driven by the reduction in the total step edge energy. This process is thought to occur by the detachment of single atom vacancies from a certain island edge followed by the migration of this vacancy to the step edge of another, larger, vacancy island. It has been determined in a study by Poirer and Tarlov[134] that the rate of ripening is most rapid when alkanethiol monolayers are in their initial disordered formation stage. It is also thought that elevated temperatures may increase the ripening effect as high temperatures above 350K[134, 135, 114] melt the monolayer and produce a disordered effect such as that seen in the initial stages of monolayer formation.

1.2.6.3 Structural Dynamics Related Defects

This section deals with defects in SAMs that are intrinsic to the nature of the SAM itself. Defects intrinsic to SAMs are generally considered to arise from two sources. The first arises from the thermodynamic stability of the SAM and the second arises from intrinsic structural dynamics in the SAM. We have already discussed that SAM formation is thermodynamically driven by interactions between the adsorbate molecules and the substrate. It is expected that the molecules with the most favourable interactions with the surface will be deposited onto the surface. In the case of the deposition of a SAM from solution it is likely that there will be continual competitive adsorption between various molecules causing molecules to be continually desorbed and adsorbed at the surface. It is expected that this phenomenon is likely to give rise to an intrinsic thermodynamic instability in the SAM and that only in the case where there is a complete absence of desorption processes would the SAM be expected to remain in an unchanged, stable state for an indefinite period.

Another type of thermodynamic instability encountered is the ability of a fully formed SAM to resist competitive binding from impurities and their ability to survive in the ambient conditions (exposure to high temperatures or competing chemical

species). Bhatia and Garrison[136] performed molecular dynamics simulations to examine the effect of elevated temperatures on the packing of the chains in an alkanethiol monolayer. It was determined, as would be expected, that elevated temperatures gave rise to orientationally disordered states. The stability to such conditions depends mainly on the strength of the bond between the adsorbate molecule and the surface.

The second type of intrinsic defect that exists in alkanethiol monolayers is related to the inherent disorder associated with the orientation of the alkane chain. Because the alkanethiol chains of the SAM are canted this gives rise to complex phase transitions including the chains being thermally driven to gauche conformers and tilt-order phase transitions.

1.2.6.4 Composition of SAMs

This form of defect arises from the fact that the formation of alkanethiol monolayers involves a thermodynamic equilibrium between molecules that have been adsorbed onto the surface and those that remain in solution. Due to this the composition of the fully formed monolayer will reflect only those molecules that interact most strongly with the substrate. Impurities in the synthesis of the adsorbate molecules or impurities in the solvent used are likely to complicate such effects and lead to defects in the final structure of the SAM. If proper care is taken in experimental procedure such defects can be minimised.

1.2.6.5 Pinholes

Pinholes are defects that have been found to occur widely in SAMs and this discussion will begin by defining what a pinhole is. A pinhole is a site in a self-assembled monolayer at which the electrode surface is exposed to the electrolyte. Not only is an adsorbed molecule absent at a pinhole but the tails of nearby adsorbed molecules do not block the site. In more simplistic terms we can view pinholes as simply a molecular vacancy in the SAM.

The effect of pinholes is most apparent in blocking SAMs (which will be discussed in the next section). A blocking alkanethiol SAM is one which prevents any Faradaic processes occurring between the electrolyte and the electrode. Such SAMs are typically formed from simple methyl terminated alkanethiol molecules. The effect

of pinholes manifests itself in a departure from ideal blocking behaviour in such SAMs. Consider the case of a bare gold electrode immersed in a dilute aqueous acid electrolyte. If the potential of the electrode is swept to positive potentials the surface oxidation of the gold is achieved and a well defined anodic peak is seen. The oxidation of the gold surface typically forms 1-3 monolayers of gold oxide depending on the crystallinity and cleanliness of the surface. When the potential of the electrode is subsequently swept in the negative direction a cathodic peak is observed corresponding to the stripping of the gold oxide. When a blocking alkanethiol monolayer is present the oxidation of the gold surface and hence the stripping of the gold oxide is suppressed[39-41]. In reality the immersion of a bare gold electrode into a solution of blocking alkanethiol molecules for a period of 12 hours yields a gold surface completely bereft of any Faradaic processes which is manifested by a completely featureless CV response. Pinholes are most evident in such experiments should they occur. This is because it is possible to oxidise/reduce the electrode surface at the site of a pinhole due to presence of water molecules at the surface. When a pinhole is present in the SAM water molecules are allowed close approach to the SAM at this point and oxidation may occur. The oxidation of this point on the CV is evident as a small anodic and corresponding cathodic current. It is possible to estimate the area fraction of pinholes by the area of these peaks.

Another major manifestation of pinholes occurs when dealing with the Faradaic processes involved with a solvated redox couple. Again the presence of a blocking SAM generally inhibits the approach of the redox couple to the gold surface. Pinholes can be observed when the SAM is not strongly blocking to the redox couple and a certain amount of redox activity is seen to occur.

The extent to which pinholes are present on the surface of the SAM can be determined in various ways. Pinholes on the surface can be treated as an array of microelectrodes and using microelectrode parameters a simple equation can be drawn up to describe the coverage of pinholes. Also the oxide stripping current can be used. By taking the ratio of the coated and clean oxide stripping peaks on a gold CV it is possible to determine $1 - \theta$ (where θ is the coverage of the monolayer). Typical values for $1 - \theta$ range from 0.01 – 0.0001. It is noteworthy that the formation of gold oxide at pinhole sites perturbs the order of the SAM if it is subjected to repeated oxide formation. It is thought that the oxide formation and subsequent stripping may remove

more weakly bound molecules nearby. This effect is manifested by a small increase in the oxide formation and stripping peaks in subsequent scans. Other methods for determining the amount of pinhole sites present have utilised chronoamperometry, linear sweep voltammetry, AC impedance spectroscopy, metal decoration and the oxidation of adsorbed iodine.

1.2.7 Blocked Electrodes

The scope of this thesis will mainly focus on electroactive self-assembled monolayers however a major class of SAMs exist in the form of blocking monolayers and for this reason they will be reviewed here.

One of the most desirable features of monolayers on electrodes is their ability to block the access of solution phase molecules to the electrode surface. The presence of a hydrocarbon layer between the electrode surface and the electrolyte ions leads to a substantial decrease in the observed interfacial capacitance. In the case of the voltammetric response of an electrode this phenomenon leads to a dramatic decrease in the charging current. This results in the Faradaic current response being magnified to the observer provided it is not blocked by the monolayer. This phenomenon has been shown to be advantageous in the area of biosensor design[137]. Alternatively should the monolayer be completely impermeable to a redox couple in solution measurements can be made regarding the tunnelling of electrons through a well-defined medium of controllable distance (i.e. length of the alkane chain). This effect produces a greatly reduced electron transfer rate and using this property theories regarding electron transfer such as Marcus Theory can be tested.

It is necessary for blocking SAMs to be stable for use in any application which requires them to be resistant within large limits of electrode potential, temperature and chemical treatments. In general alkanethiol SAMs are very resistant to this type of treatment. The first topic in this section will focus on the blocking behaviour of SAMs as a function of various parameters. The blocking alkanethiol monolayer will be taken as the reference SAM.

1.2.7.1 Monolayer Structure and Blocking Behaviour

Temperature and Electrolyte Effects. The first topic of interest is how the blocking behaviour of SAMs depends on the temperature and solvent. Many possible uses of

blocking SAMs may require them to be subjected to elevated temperatures. Of particular interest to studies at higher temperatures is the possible existence of phase transitions in the monolayer such as the melting of the monolayer (this occurs when the SAM passes from the crystalline to the liquid phase). Nuzzo et al.[104] carried out Surface IR Spectroscopy on blocking alkanethiol chains over a temperature range of 80 – 420K and succeeded only in identifying an increasing number of alkane chains adopting a gauche conformation. Fenter et al.[114] carried out X-Ray Diffraction measurements on alkane chains of varying length and found that in general a 2D liquid-like structure was formed at ~60°C which corresponds to the melting of the monolayer. Thus it is reasonable to say that in general a monolayer will become unstable at temperatures above 60°C.

Relatively little work has been carried out regarding the effect of different electrolytes on the structure of the SAM. This is due to the fact that the vast majority of the work carried out is in aqueous electrolytes thus neglecting nonaqueous types. IR studies carried out by various groups indicate that SAMs undergo a only a slight degree of disorder when in contact with the more polar liquids typical of voltammetry [138 – 142].

Chain Composition. When discussing self-assembled monolayers the majority of blocking layers are based on alkane chains with either a thiol or disulfide headgroup. Such molecules form a commensurate structure on an Au(111) surface and are well understood. There are however reports on the blocking behaviour of other sulfur based molecules. Zhang et al.[143] carried out IR studies on unsymmetrical dialkyl sulphide monolayers. It was expected that because such monolayers would possess a greater degree of disorder they would have poorer blocking properties than straight chain alkanethiol molecules. It was determined via electrochemical studies that solution permeation did not occur in such dialkyl SAMs and that the charge transport properties were indistinguishable from straight chain alkanethiol molecules. In dialkyl molecules such as those discussed form on electrodes the monolayers they produce can be described as possessing a liquid-like structure. This is due to the degree of disorder that they possess. Another group of molecules that are thought to form a liquid-like structure are the calixarenes. Thoden van Velzen et al.[144] carried out studies on a SAM formed using resorcin[4]arene – such molecules are a form of calixarenes. It was determined from capacitance measurements of the SAM effective

thickness that such a monolayer was impermeable towards electrolyte intrusion. This study provided another example of the fact that a completely commensurate, well ordered, layer is not necessarily paramount to forming a SAM with good blocking behaviour.

As well as the orientation of the alkane chains on the surface the structure of the chains themselves has also been subject to investigation. Alves and Porter[145] studied the orientation of fluorinated alkanethiol SAMs on Au(111). In the case of normal alkanethiol monolayers packed in a commensurate manner on Au(111) the alkane chains do not fully fill the area around them. This phenomenon causes the alkanethiol molecules to tilt in order to maximise interchain interactions. When the bulkier CF_2 groups replaced the CH_2 groups it was found that the fluorinated alkane chains filled the space around them more completely. This led to a decrease in the molecular tilt and thus a decrease in the disorder of the layer which is expected to lead to better blocking behaviour than in the case of normal alkanethiol molecules. This observation was proved correct by Chidsey et al.[103] who carried out electrochemical capacitance measurements on SAMs formed from $CF_3(CF_2)_7(CH_2)_2SH$. It was determined that such SAMs exhibited a grater degree of impermeability to solvent molecules than a range of other alkanethiol molecules. The reason that fluorinated chains possess superior blocking properties than alkanethiol molecules is as follows: In the case of all alkanethiol monolayers formed on gold various domains will form side by side in which the tilts of the alkanethiol molecules will differ. The boundary at such a domain interface can result in a locally thin region of the SAM where electrolyte permeation or defect formation is more likely. Because of the reduced molecular tilt in SAMs formed from fluorinated alkanethiols this effect is minimised leading to the superior blocking behavior exhibited by SAMs formed from fluorinated alkane chains.

Another type of blocking molecule is based on staffanes. Obeng et al.[146] carried out a cyclic voltammetry and chronoamperometry studies of staffane molecules with differing chain compositions and terminal groups. It was determined that staffane molecules with thiol molecules at both the terminal and head groups exhibited poor blocking behaviour whereas molecules with acetate or ruthenium head groups exhibited excellent blocking behaviour with the molecules determined to be standing perpendicular to the surface of the electrode.

Other types of blocking SAM to be discussed are those based on oligoimides with four repeating units[147], which were shown to exhibit excellent stability on the electrode surface but poor blocking properties, and mixed monolayers comprised of alkanethiol molecules and anthraquinone[148]. Such mixed monolayers exhibited excellent blocking behaviour towards ferrocyanide oxidation.

Terminal Groups. Much work has been carried out regarding the dependence of the blocking behaviour of SAMs on the type of headgroup present. It is generally agreed that the blocking ability of SAMs scale approximately with the degree of crystallinity they exhibit rather than the nature of the head group. Chidsey and Loiacono[103] demonstrated this by showing that the more hydrophobic headgroup, CN, was more prone to defect and pinhole currents than was the more hydrophilic CH_2OH headgroup. It is pointed out in this study that it would be expected that a monolayer whose surface is wet by aqueous electrolytes would be more prone to permeation than in the case of a hydrophilic surface. This is not the case however due to the superior packing of molecules terminated with CH_2OH groups. It was also suggested that alkanethiol SAMs terminated with COOH groups form a quasi-liquid type structure indicating again that the nature of the headgroup does affect the packing of the SAM. This would appear to be an intuitive observation as bulkier headgroups are likely to undergo steric interactions with their neighbors which can lead to less than ideal packing. As well as the size of the headgroup the position of the headgroup with respect to the electrolyte interface must also be taken into account. This is not an issue when dealing with straight chain alkanethiols however it was found in the case of asymmetric disulfides monolayers that the position of the carboxyl headgroup was relevant[143]. It was determined that the permeability of such monolayers was greatest when the carboxyl group was closest to the interface. The above case is only one example of many regarding alkanethiol SAMs with different headgroups and is meant as an illustration to the fact that the effect of certain terminal groups must be examined on a case-to-case basis.

In general however it can be noted that electrostatic attraction or repulsion between surface moieties with their neighbors and with solution redox couples have a powerful effect on the blocking behavior of the alkanethiol SAMs.

Polymerisable SAMs. Very little work has been carried out regarding Polymerisable SAMs however in theory this is a method by which the permeability of SAMs could be tailored to a specific value. Batchelder et al.[149] showed how dialkyl disulfide molecules could spontaneously adsorb onto gold to form a well ordered monolayer. When subjected to UV radiation for a short period of time the monomeric molecules were readily converted to their polymeric form on the surface identifiable by its blue colour. It was determined from a combination of Raman and FTIR spectroscopies that the polymer growth proceeded via the formation of islands. It is thought that the size of the polymer islands increased at the expense of the intermediate monomeric phases. Finally it is thought that large areas of polymerised SAM was formed, which however was interspersed with small areas of monomeric material.

As well as polymerising entire SAM molecules the headgroups of SAMs may also be polymerised. Willicut et al.[150] showed how a pyrrolyl-alkanethiol SAM deposited on gold could be polymerised by electrochemical cycling in propylene carbonate past +1V vs SCE. Wang et al.[151] hydrolysed monolayers of (3-mercaptopropyl)-trimethoxysilane ($HS(CH_2)_3Si(OMe)_3$) to produce a siloxane polymer. Fox et al.[152] showed how alkanethiol SAMs with anthracene headgroups undergo a photochemical change to form dimers when irradiated with UV radiation. Similarly Li et al.[153] showed how SAMs with a 7-(10-thiodecoxy)coumarin headgroup undergo photodimerisartion. Finally Paul et al.[154] showed how polyacrylonitrile could be formed from alkanethiol SAMs which contained a dithiol-AIBN initiator which was activated by irradiation at 400nm.

Polymer SAMs. When dealing with self-assembled monolayers formed from polymers on gold the most common method of assembly is achieved via pendant thiols, disulfides or sulfides[155, 156, 157, 158, 159]. Lenk et al.[155] showed how poly(methyl methacrylate) with sulfur derivatised side chains spontaneously adsorb onto a gold substrate. It was shown that both the thickness of the adsorbed chains and their resistance to displacement depended on the concentration of the sulfur containing side-chains. As would be expected a shorter spacing between sulfur side- groups along the chain leads to a more compact and stable film. It was also found that thinner monolayers form at higher concentrations of sulfur side-groups. Erdelen et al.[156] formed methacrylic copolymers using a disulfide anchoring group to stabilise the polymer on a gold support and a self-organising surface unit side chain of 2-

hydroxyethyl acrylate (HEA). This side chain improved the ability of the polymer to organise into an ordered layer. It was found however from cyclic voltammogram analysis that such polymers did not form a particularly blocking film due, most probably, to the coil formation occurring in such a complex polymer. Niwa et al.[157] examined the deposition of polymeric amphiphiles containing poly(methacrylic acid) (PMA) segments connected to alkane chains with a pendant disulfide group. It was found that such polymers spontaneously adsorbed onto a gold surface. The dependence of solution pH on film formation was also examined. It was determined that as the acidity of the deposition solution increased so too did the packing density of the film. This behaviour is consistent with the tendency of PMA films to adopt a tightly coiled conformation at low pH and a more stabilised form at higher pH. Thus when the polymer is more stretched more disulfide groups are available to bind to the gold surface leading to better packing density. Sun et al.[158] deposited alkyl disulfide polyacrylated onto a gold surface from a chloroform solution. Again it was determined that such films form via multipoint attachment to the gold substrate. In further work by Sun et al.[159] the binding properties of poly[methyl(mercaoptopropyl)siloxane] on a gold surface was examined. Such monolayers were again tethered to the gold surface via a gold-thiolate bond. It was determined however that only ~35% of the thiol groups present in the siloxane film were engaged in gold-thiolate bonds with the remaining 65% of the anchors unbound and dispersed throughout the film. Measurements utilising cyclic voltammetry indicated that the monolayer blocked electron transfer through the film to a considerable extent although defects in the film did exist.

It is accepted generally that thin coatings formed by the adsorption of polymers on gold anchored using sulfur groups are more stable than the average alkanethiol monolayer. However the blocking properties of such polymer SAMs to solvent and redox species is inferior. This is due to the fact that most polymers have a much greater ability to be structurally disordered than alkanethiol monolayers leading to an increased amount of disorder in such layers and poorer packing.

1.2.7.2 Capacitance

When a metal electrode comes into contact with an ionic electrolyte the interface between the two exhibits a capacitance the magnitude of which reflects the distribution of ions in the electrolyte relative to the electrode. In relatively

concentrated electrolytes the capacitance of the electrode/electrolyte interface is dominated by the Helmholtz layer which is a layer of ions directly in contact with the electrode. When a long chain, blocking, alkanethiol SAM is deposited onto the surface of an electrode the layer of ions and solvent that make up the Helmholtz layer is replaced by an ion-free hydrocarbon layer. This results in a dramatic change in the interfacial capacitance observed. When quantitatively dealing with the interfacial capacitance associated with a deposited alkanethiol SAM the simplest approach is known as the Helmholtz Model. As well as this model other more detailed models that take into account the potential drop across the monolayer exist. This review will initially describe the Helmholtz treatment of the interfacial capacitance. This will be followed by a description of the more advanced treatment.

Helmholtz Model. It has been previously mentioned that when a long chain alkanethiol monolayer of low dielectric constant is deposited on the surface of a metal electrode replacing a layer of solvent and ions with a high dielectric constant the interfacial capacitance is dramatically reduced and becomes virtually independent of potential. The total interfacial capacitance associated with the hydrocarbon layer can be obtained easily utilising cyclic voltammetry by dividing the charging current by the scan rate. The interfacial capacitance of a typical alkanethiol monolayer lies between 1-3μFcm^{-2}[103]. This represents a dramatic decrease in the interfacial capacitance considering that the typical value for a bare metal lies between 10-100μFcm^{-2}.

The interfacial capacitance is comprised of two distinct individual capacitances. These are the monolayer capacitance (C_M) and the double layer capacitance (C_D). For electrolyte concentrations above 0.1M the interfacial capacitance is dominated by the capacitance associated with the SAM. The simplest expression for the capacitance of a SAM is shown in Equation 1.1 below.

$$C_M = \frac{\varepsilon_M \varepsilon_0}{d} \tag{1.1}$$

Where d is the thickness of the dielectric layer, ε_M is the dielectric constant of the SAM and ε_0 is the permittivity of free space. From the above expression it can also be noted that the thickness of the alkane layer is linear with respect to the reciprocal

of C_M. This observation has been confirmed for alkanethiol monolayer chains with 10 or more methylene units by various groups[8, 102, 160, 161]. Porter et al.[8] plotted the reciprocal of capacitance vs. the number of methylene units over a range of electrolytes. The slope of this graph yielded an effective dielectric constant of 2.5 for an alkane chain standing perpendicular to the electrode surface. The thickness of the alkane chains was then modified to take into account for the 30° tilt associated with alkanethiol monolayers on gold surfaces. This modification yielded an effective dielectric constant of 2.3. This value can be favourably compared with the known value of 2.3 for polyethylene. This excellent degree of agreement also suggests that the monolayers are purely hydrocarbon and not permeated by solvent molecules.

Although the above results would seem to demonstrate that the Helmholtz Model describes the capacitive behaviour of alkanethiol monolayers extremely well other differing results have been arrived at. Widrig et al.[102] carried out capacitance tests on alkanethiol SAMs with chain lengths between 2 and 17 methylene units deposited on extremely well ordered gold surfaces. Although a plot of reciprocal capacitance vs. chain length yielded a straight-line characteristic of the Helmholtz Model a value of 6 for the dielectric constant of the alkanethiol layer was arrived at. A possible explanation for this increased value is that the electrochemical measurements used in the study were carried out in 0.5M KOH. This strongly basic electrolyte may have caused defects in the SAM leading to its permeation with ions of high dielectric constant and thus increasing the overall value of dielectric constant measured. As well as the normal methyl terminated SAMs capacitance measurements have also been carried out on hydroxyl-terminated alkanethiol SAMs in a study carried out by Miller et al.[160]. This study yielded a dielectric constant of 3.0 for such SAMs.

Thus far only capacitance measurements for long chain alkanethiols have been discussed. Porter et al. (8) found that shorter chain lengths exhibited larger capacitances than longer chains. This observation is again likely to be caused by solvent ions being able to permeate more easily into shorter chain SAMs which are not likely to pack as well as longer chains

As well as the chain length another factor that must be taken into account when dealing with the Helmholtz capacitance measurements is the effect of the variations of the headgroup from the usual CH_3 terminated alkanethiol SAMs. Miller et al.[160] determined the capacitance of alkanethiol SAMs with OH headgroups. Chidsey and Loiacono[103] carried out capacitance measurements on alkanethiol

SAMs with OH, COOH, CH_3 and CN headgroups. It was determined in this study that the capacitances were found to increase in the order CH_3 < OH < CN < COOH. It is thought that the polar carboxyl group exhibits the highest capacitance due to the fact that monolayers with such headgroups do not pack well leading to extensive permeation of the monolayer with solution redox species. The effect is not thought to be due to the expected increase in wettability attained by adding polar surface functionality. This observation is substantiated by the fact that monolayers with the hydrophobic CN exhibit the next highest capacitance measurement which is close to that observed for the carboxyl terminated monolayer. This is again due to the fact that the CN terminated monolayers do not pack well. The results of this capacitance study suggests the importance of steric and electrostatic interactions between appended functional groups in determining the packing of the chains.

Thus far it has been described how the Helmholtz model of capacitance has been used in a number of cases to describe the interfacial properties of alkanethiol SAMs. Most descriptions utilised a plot of reciprocal capacitance vs. chain length. From the slope of such a graph the dielectric constant of the layer may be determined and compared with the relevant literature values. However the linearity of such a plot may not be definitive evidence that the Helmholtz Model provides an accurate description of layer capacitance. This is due to the fact that the Helmholtz Model assumes that the dielectric constant of the hydrocarbon layer is independent of its thickness. Evans and Ulman[162] determined via surface potential measurements that the dielectric constant may decrease as the length of the chain increases. This observation would lead to the plot of reciprocal capacitance vs. chain length becoming steeper with respect to that expected for a chain with a constant dielectric value. Such an observation as that made by Evans and Ulman points towards the fact that a more advanced model to describe the alkanethiol monolayer capacitance may be necessary.

More advanced Models. To fully understand the nature of the capacitance of an alkanethiol SAM it is necessary to consider the potential drop within the monolayer. To do this Equation 1.2 below may be used.

$$\frac{\varphi_M - \varphi_S}{\varphi_M} = \frac{C_T}{C_M} \qquad (1.2)$$

Here φ_M is the potential at the surface of the metal, φ_S is the potential at the external surface of the SAM, C_T is the total interfacial capacitance and C_M is the capacitance of the monolayer. Equation 1.2 thus describes how the ratio of the potential drop between the electrode and the solution phase is inversely proportional to the relevant capacitances.

Such an analysis can be extended into a more detailed model by taking into account the potential drop across the diffuse layer. In order to carry out such an analysis it is necessary to have knowledge of the externally applied potential corresponding to the zero surface potential (E_{ZSP}). At E_{ZSP} there is neither an excess of cations nor anions in the diffuse layer. The value of E_{ZSP} can be obtained by taking the minimum value in a plot of diffuse layer capacitance (C_d) vs. electrode potential. In order to observe such a minimum value of C_d the value of C_M must be of roughly equal magnitude. It is notable that if the capacitance of a typical alkanethiol monolayer lies between 1-3μFcm^{-2} it has been calculated that the concentration of the electrolyte should be of millimolar levels in order to successfully observe a minimum C_d value. Steinberg et al.[78] made a plot of capacitance vs. electrode potential for self assembled monolayers of thiobis(ethylacetoacetate) (TBEA). It was determined that the potential of minimum ion binding (E_{ZSP}) for such a SAM was 0.15V vs. SCE which lead to a capacitance of 5.6μFcm^{-2} being determined for such SAMs using this advanced model. Becka and Miller[163] utilised this advanced approach to evaluate the capacitances of methyl and hydroxyl terminated alkanethiol monolayers. It was determined from a plot of capacitance vs. electrode potential that the capacitance minimum for the methyl terminated SAM occurred at a much more negative potential than did the minimum in the case of the hydroxyl terminated SAM. Both SAMs are relatively similar in structure with regards to their packing and the fact that large differences in E_{ZSP} values observed from this advanced method can be viewed as an indication of its sensitivity. It is thought that the difference in E_{ZSP} values could be attributed to one or a combination of three different factors. The first is the difference in hydrophobicity between the two monolayers. In the study by Becka and Miller electrochemical measurements were carried out in CF_3COONa and it is expected that the highly hydrophobic methyl terminated SAM may allow the larger CF_3COO^- ions a closer approach than the more solvated and hence more aqueous Na^+ ions. The

concentration of anions could push the potential of zero charge in a more negative potential for the methyl terminated SAMs. The second theory is that the methyl terminated SAMs contained a greater amount of defects than did the hydroxyl terminated SAMs which allowed a greater amount of anions to permeate their structure. This effect may have pushed E_{ZSP} in a negative direction. The third theory is that the adsorption of an alkanethiol SAM on a gold electrode creates a positive surface potential relative to the bare gold. This is due to the fact that the adsorption of an alkanethiol molecule produces a dipole moment at the electrode surface between the thiolate headgroup and the alkane radical. To compensate for this positive surface potential the capacitance minimum will be shifted to a more negative E_{ZSP} value. The incorporation of an OH headgroup which has a negative charge on the surface of the SAM creates another dipole whose orientation would cause the surface potential to be less positive than in the case of the methyl terminated SAM. This in turn causes the E_{ZSP} value of the OH terminated SAM to be shifted a more positive potential with respect to the methyl terminated SAM. It has thus been shown how the more complex model of capacitance can be utilised to draw a number of observations regarding the nature of different alkanethiol SAMs even if the differences in their structure are quite subtle.

A slightly altered method to the one described above was described in a study carried out by Sondag-Huethorst et al.[164] who utilised simultaneous contact angle and electrochemical measurements to determine E_{ZSP} for a long chain alkanethiol SAM. Contact angle measurements were utilised due to the fact that the interfacial capacitance measurements between –0.8V and +0.8V vs. SCE were found to be constant. Thus no minimum could be observed in a plot of capacitance vs. potential and attributed to E_{ZSP}. Instead of this the wetting contact angle was measured as a function of potential. It was noted that the contact angle measurements exhibited a broad maximum between –0.2V and –0.6V vs SCE. The centre of this broad maximum was taken as the value of E_{ZSP}.

As well as the various studies taking into account the bearing of the diffuse layer on the capacitance the role of certain functional groups must also be taken into account. If a SAM contains functional groups whose charge can be modified either by oxidation/reduction or acid-base reactions this can have a marked effect on the potential at the external surface of the SAM, φ_S. The value of φ_S can be very

sensitive to both electrode potential and electrolyte pH. These two situations have been investigated in two papers by Smith and White[165,166]. The first paper considered a model where the redox centre was situated at the surface of the SAM or at some well defined distance away from the metal electrode[165]. The idea of situating the redox centres at a defined distance away from the metal electrode introduces the notion of the plane of electron transfer (PET) which is commonly used when dealing with electroactive SAMs and related to the distance of the redox group away from the surface of the metal. Smith and White related the potential drop across the monolayer, $\varphi_M - \varphi_S$, and the charge density at the PET to the fraction of redox centres in each of the two oxidation states. It was determined that although the diffuse layer capacitance is, as expected, much larger than the film capacitance it is not constant. The large variation of the charge at the PET amplifies the variation in the diffuse layer capacitance especially when close to the redox potential of the electroactive groups. An even more detailed model dealing with the capacitance associated with the charging of pendant redox species was developed by Fawcett[167] which introduces an inner Helmholtz layer between the PET and the edge of the diffuse layer. This takes into account the discreteness of charge associated with the individual pendant groups as opposed to treating the charge at the PET as delocalised as did Smith and White.

The second study by Smith and White[166] considered the case of an electroactive film with an acid group (HA) confined to the surface of a monolayer film with $HA \rightarrow H^+ + A^-$. It was assumed that this film is irreversibly adsorbed and that all acid/base groups lie in a common place known as the plane of acid dissociation (PAD). The study defines an expression relating the interfacial capacitance to the fraction of deprotonated acid groups. This expression is shown in Equation 1.3 below.

$$\frac{1}{C_T} = \frac{1}{C_M} + \frac{1}{C_d + C(f)} \tag{1.3}$$

Again C_T is the total interfacial capacitance, C_M is the capacitance associated with the SAM and C_d is the capacitance associated with the diffuse layer. C(f) is the effective capacitance associated with the fraction ionised acid groups. It is noted in this study that at pH values far from the monolayer surface pK_a value the film will become

either fully protonated ($pK_a >> pH$) or fully deprotonated ($pK_a << pH$). In each of these cases $C(f) \rightarrow 0$ and the total capacitance is equal to that expected for a totally inert film and the total interfacial capacitance is given by Equation 1.4.

$$\frac{1}{C_T} = \frac{1}{C_M} + \frac{1}{C_d} \tag{1.4}$$

At less extreme values of pH the value of C(f) remains finite and varies in response to the electrostatic potential at the PAD reaching a maximum value when the film is half ionised.

Although this model is instructive with regard to dealing with ionisable acid groups it is thought that it does not fully take into account all of the necessary considerations. Fawcett et al.[168] considered the same situation of an acidic headgroup tethered to an organic film as did Smith and White but included in the study the treatment of the effects of charge discreteness and well as the phenomenon of inner and outer Helmholtz planes. Discreteness of charge effects take into account the fact that ionised headgroups such as those that occur in acid terminated SAMs undergo a number of electrostatic interactions with the surroundings. These include influences from image charges in the metal electrode, influences from other ionised headgroups or influences from image charges of other ionised headgroups. The inner Helmholtz plane (IHP) described in this study can be thought of as the equivalent of the PAD defined by Smith and White. The outer Helmholtz plane (OHP) is defined as the closest approach of solvated counterions. The diffuse layer starts at the OHP and extends into the bulk solution. The area between the IHP and OHP is considered to consist of water molecules of a lower dielectric constant than bulk water whose dielectric constant is taken to be identical to the hydrocarbon layer.

Although the Fawcett model represents an improvement on the Smith and White model it is still thought that further improvements could be made such as a unique value of the dielectric constant of the layer between the IHP and OHP as well as changes in the dielectric constant of this layer with respect to potential.

Apart from its many complexities electrochemical capacitance studies remain an excellent method for examining the structure of alkanethiol SAMs.

1.2.7.3 Electrochemical Desorption

One of the most important aspects of alkanethiol SAMs deposited on gold substrates is their ability to withstand a wide range of electrode potentials and aqueous electrolyte compositions with only subtle changes in their structure. However in a strong base and at certain potentials alkanethiol monolayers can be quantitatively desorbed from the electrode surface.

It has been demonstrated by various groups that alkanethiol SAMs deposited on Au(111) can be electrochemically desorbed by immersion in 0.5M KOH and sweeping the potential of the electrode to –1.5V vs. Ag/AgCl[169, 170, 171].

The mechanism for the electrochemical desorption of alkanethiol SAMs was first fully described in a study carried out by Widrig et al. in 1991[102]. This study showed that alkanethiol SAMs could be reductively desorbed in alkaline solutions (pH >11) through respective three electron and one-electron paths as shown in reactions I and II below.

$$Au\text{-}S(CH_2)_nCH_3 + 2H_2O \rightarrow Au(0) + {}^-O_2S(CH_2)_nCH_3 + 4H^+ + 3e^- \quad (I)$$

$$Au\text{-}S(CH_2)_nCH_3 + e^- \rightarrow Au(0) + {}^-S(CH_2)_nCH_3 \quad (II)$$

It was also importantly determined in the course of this study that the charge consumed by each desorption experiment can translated to a charge consistent with the predictions of a $(\sqrt{3} \times \sqrt{3})R30^\circ$ overlayer model.

Weisshaar et al.[170] also carried out electrochemical desorption experiments on alkanethiol SAMs and determined that the potential at which the desorption occurs is linearly dependent on the number of methylene groups (n) in the alkane chain. The potential was found to shift to more negative values as n increases. This dependence can be related to a two-capacitor model assumed for the alkanethiol layer. In this model the SAM is treated as two capacitors connected in series where one capacitor corresponds to the thiolate head group and the other to the hydrocarbon phase. The dependence of the desorption potential is then related to the potential induced penetration of ions through the polymethylene chains. Thus the less densely packed chains desorb at less negative potentials. It is expected that shorter chain alkanethiols will be less densely packed than longer chain thiols and hence desorb at more positive potentials as already observed. Also noted in this study was the effect of the structure

morphology of the gold surface on the reproducibility of the desorption experiments. It was determined that on well orientated, annealed, Au(111) surfaces there were well defined, single wave, voltammetry characteristic of the desorption of SAM molecules from a terraced gold surface. Desorption form a non-annealed gold surface leads to a multiple wave desorption process characteristic of the desorption of SAM molecules from a number of different binding sites of different binding energies.

Zhong and Porter[169] characterised the electrochemical desorption of butanethiol, (BT), and butyl sulphide, (BS), SAMs on gold-surfaces. It was noted that BT desorbed at –0.77V vs. Ag/AgCl with a charging current of 75μCcm^{-2} and that BS desorbed at –0.78V vs. Ag/AgCl with a charge of 70μCcm^{-2}. The fact that the desorption characteristics of both molecules were almost identical argues that the interaction between the gold and the binding molecule was identical irrespective of the type of molecule.

Walczak et al.[171] carried out electrochemical desorption experiments on the now widely utilised, electroactive, ferrocene terminated alkanethiol SAMs. The study was carried out on $FcCO_2(CH_2)_nSH$ where n = 8 and 11. It was determined from cyclic voltammetry experiments that the surface coverages for the n = 8 and n = 11 layers were 3.8 x 10^{-10}mol.cm^{-2} and 5.3 x 10^{-10}mol.cm^{-2} respectively. These surface coverage values were then compared to the surface coverages calculated from desorption experiments. It was found from such experiments that coverages for the n = 8 and n = 11 ferrocene terminated layers were 7.6 x 10^{-10}mol.cm^{-2} and 10 x 10^{-10}mol.cm^{-2} respectively. These values were much larger than those obtained from CV experiments. It was proposed that the reason for such high values was the possible electroactivity of the ferrocene moieties at the high negative potentials needed for the reductive desorption of the SAM. This electroactivity is thought to add to the observed cathodic current in the stripping experiments. To factor out such effects the ferrocene terminated SAMs were electrolysed in 0.1M NaCl which resulted in the loss of the ferrocene moiety from the surface. When this was complete the desorption experiments were repeated and showed a marked decrease in the cathodic currents. It was found that the surface coverages for the n = 8 and n =11 chain lengths were 4.9 x 10^{-10}mol.cm^{-2} and 5.7 x 10^{-10}mol.cm^{-2} respectively. These values were much closer to those observed from CV experiments and demonstrate well the one electron model of

desorption may be used to describe the removal of alkanethiol SAMs from gold electrodes.

Schneider and Buttry[83] carried out desorption experiments utilising an Electrochemical Quartz Crystal Microbalance (EQCM) and CV. This study again tackled the issue of discrepancies between values of alkanethiol surface coverage obtained from CV and that obtained from desorption experiments. In this case such discrepancies were attributed to the considerable double layer charging associated with reductive desorption experiments. As the SAM is removed from the metal electrode surface during a desorption experiment the capacitance of the interface rises from that associated with the SAM to that of the bare electrode. This charging is likely to be manifested in the desorption charging current rendering it an inaccurate reading. It is thought that such an effect could make up around 20% of the overall stripping charge observed in such experiments.

It has also been shown by various groups that the thiolate product of the stripping can be readsorbed form solution onto the gold surface by rescanning the potential of the electrode to more positive values[171, 172]. The readsorption pathway is the reverse of Scheme I. The reversal of the electrode potential generates an anodic peak on the return scan of the CV.

A study carried out by Weisshaar et al.[172] noted three important features of this readsorption process. (1) As already mentioned, the reverse of Scheme I is used. (2) The readsorbed monolayers have structures and interfacial properties similar to their self-assembled analogs. (3) The extent of the deposition can be controlled by the reaction thermodynamics – this essentially means that the coverage of the SAMs can be controlled by halting the electrode potential at some point during the readsorption process. It was also noted in this study that the charge under the anodic redoposition wave was slightly less than the coverage under the cathodic desorption wave. This indicates that that there is incomplete readsorption of the alkanethiol molecules. This effect is probably due to a limiting factor caused by the alkanethiol molecule desorption kinetics.

Pan et al.[173] utilised AFM measurements on long chain alkanethiol SAMs to verify the $(\sqrt{3} \times \sqrt{3})R30^{\circ}$ overlayer model adopted by alkanethiol SAMs on Au(111). This study found that the SAMs were destroyed when subjected to potentials more positive than 1.59V and more negative than –0.3V. Comparison of images before and

after the stripping of the SAM from the gold surface were used to confirm the ($\sqrt{3}$ x $\sqrt{3}$)R30° structure.

Finally Abbott et al.[174] carried out contact angle measurements during the desorption of $CH_3(CH_2)_nSH$ where n = 2 and n = 15. It was determined that at neutral potentials SAMs formed from both molecules were hydrophobic with contact angles between 80° and 110°. However as the electrode potential was swept to more negative values (~-1.3V vs Ag wire) the contact angle measured was observed to drop to ~10° corresponding to the desorption of the SAM from the surface. It was found that if the potential was returned to its neutral value a rise in the contact angle value back to ~80° was observed corresponding to the readsorption of the thiol molecules from the electrolyte solution.

1.3 Applications of SAMs

The modification of an interface on a molecular level with more than one building block is essentially an example of 'bottom-up' fabrication of nanoscale systems. The development of such systems has seen rapid progress in recent years due to the emergence of self-assembled monolayers. SAMs are important to the development of nanoscale systems for two main reasons. (1) They are intrinsically an easily prepared nanostructured system sensitive to the local environment on a nanoscale level. (2) They can be used to fabricate micro- and nanoscale architecture using patterning techniques such as microcontact printing and photolithography. The use of SAMs is expanding into an ever widening range of systems and for this reason this discussion of SAM applications will focus exclusively on SAMs deposited on metal films. SAMs deposited on metal films can be used to specifically tailor the interfacial properties of a surface. Two simple examples of how SAMs can effect the macroscopic properties a surface can be demonstrated by their effect on wetting[86] and corrosion[175]. Whitesides and Labinis[86] utilised contact angle titration, a technique in which contact angles are measured as a function of drop pH, to determine the interfacial wetting properties of a range of alkanethiol SAMs. As a general rule when the most simple, CH_3 terminated, alkanethiol SAM is deposited on a metal surface it will impart a strongly hydrophobic character to the surface. Jennings et al.[175] showed how long chain alkanethiol molecules could be used to protect copper substrates from corrosion by prohibiting the metal from undergoing oxidation. Such corrosion protection on

copper has large applications in integrated circuit technology. Copper has the potential to replace aluminium as the interconnect of choice due to its superior bulk electrical resistance (1.7 vs. 2.7μΩcm for Al). SAMs on metal films also provide model surfaces for the study of charge transfer processes through molecules[176] as well as biochemistry and cell biology [177, 178].

The use of SAMs for a particular application is often device specific and therein lies the major advantage of SAMs as the almost unlimited variety available means that they can be tailored to suit almost all applications. For example when studying electron transfer processes through organic molecules the rate of electron transfer is extremely dependent on the length of the molecule through which the electron must travel. This factor being considered it is possible to control the distance through which the electron travels during experiments simply by varying the number of CH_2 linker units in the alkane chain of the deposited SAM. Other applications such as the continued development of biosensors rely more on the ability of the SAM to allow the electron transfer of a specific redox mediator[137]. This ability to discriminate between specific redox mediators is dependent on the structure and packing of the SAM. This is because a densely packed SAM may be permeated only by small redox molecules and not by larger ones. Thus by choosing the appropriate molecule to form a SAM it is possible to be specific regarding which redox mediator may permeate the monolayer and which mediator will be blocked. Such properties can provide the ability to block common interferers in the blood which can complicate some biosensor designs whilst retaining the ability to detect the reqired substance.

The following section will focus on the major areas of interest and development to which SAMs have been applied. It will begin with a description of how SAMs can be used as etch resists and be followed by regarding the utilisation of SAMs in the study of electron transport and in particular their possible role in future electronic devices. The use of SAMs in biological systems is then addressed. This will be followed finally by a review of the advances in SAMs as sensors which has also become an area of great interest recently.

1.3.1 SAMs as Etch Resists

The ability of SAMs to withstand harsh chemical treatments makes it possible to utilise them to fabricate micro- and nanostructures on the surface of many metal films

including gold, silver, copper, platinum, palladium and some alloys. It has been shown that SAMs formed from long chain alkanethiol molecules have the ability to protect metal surfaces from corrosion by wet chemical etchants[179]. Combining this property with the ability to deposit defined patterns of SAMs on the surface of a metal utilising microcontact printing (μCP) makes it possible to develop a well-defined nanoarchitecture on the surface of a metal. Scaling limits on such nanostructures are imposed by the density of defects in the SAM, SAM composition and the type of etchant used. The areas of the metal that have not been passivated with SAM molecules using the above patterning technique may then be chemically etched to a desired depth profile. It has been shown for the case of a gold film that such etching may be achieved using a complex etchant solution described by Xia et al.[180]. Such etchants have also been developed for the case of silver[180], copper[181], palladium[17] and platinum[182] films. This method of selective metal etching again has certain drawbacks – pinholes are known to occur in SAMs and at such pinholes the etchant solution is free to perform unwanted dissolution of the underlying metal film. It was determined by Zhao et al.[183] when etching with an aqueous ferricyanide solution that the number of pinhole defects in long chain alkanethiol SAMs was 500pits/cm^2. Fabrication techniques in modern microelectronics demands that there are less than 0.003defects/cm^2. Also a degree of uncertainty regarding the roughness of the edges of the etched metal exists. Due to such limitations it is thought that such etching applications using SAMs are limited to architecture of lateral dimension 500nm or greater in the case of gold surfaces. It is thought that the use of palladium or a gold-palladium alloy as the underling metal substrate may improve the problem of edge roughness due to the smaller grain size of palladium (15-30nm) with respect to gold (35-75nm). This smaller grain size is more suitable for etching thin lines in the metal. As well as this palladium is compatible with the current CMOS processing techniques [184]. Despite this there is still much progress to be made before SAMs as etch resists can be fully integrated into industrial fabrication techniques.

1.3.2 SAMs as Barriers to Electron Transport

The transport of electrons from one point to another over very small distances is fundamental to a wide range of processes both in modern device electronics and in natural biological functions such as photosynthesis and respiration. The mechanisms

of electron transfer in metals and semiconductors as well as solutions of coupled redox species are well understood. Less well understood however is the theory of electron transport through organic materials. It is thought that future technology could utilise a hybrid of molecular and solid-state technology and for this reason it is necessary to fully understand charge transfer processes in organic molecules. Preliminary experiments regarding the electronic properties of metal-molecule-metal junctions has been carried out by Beebe et al.[185] who measured the resistance of alkanethiols and alkyl isonitriles sandwiched between Au, Ag, Pl and Pt contacts. Much work however remains to be carried out.

There are a number of fundamental questions underlying the transport of electrons through organic materials. (1) What is the fundamental electron transport mechanism? (2) What are the potential barriers? (3) At what rate are the electrons transported? (4) How does the structure of the molecule affect the electron transfer process (length and composition effects)? Such questions are far from trivial however SAMs do provide an extremely convenient system on which intrinsic studies can be based. Again there are a number of reasons for this. (1) They are well ordered, contain relatively few defects and their composition can be tailored very using appropriate synthetic strategies. (2) They can be formed reproducibly. (3) They are relatively resistant to most common chemical species that are likely to be used in experimental procedures particularly with regard to electrochemical experiments which are described in the following section.

1.3.2.1 SAMs in Electrochemistry

Using SAMs it is possible to chemically modify an electrode in a desired manner. Of particular interest to electrochemical experiments is their ability to form barrier layers that prevent the diffusion of electroactive species in solution to the electrode. It is also possible using suitable SAMs to immobilise an electroactive species on the electrode itself. SAMs are ideally suited to electrochemistry due to the fact that they are easily deposited onto the electrode surface and can withstand the conditions of most electrochemical experiments.

In electrochemical studies, as already mentioned, there are two types of experimental set-up that are generally utilised when studying electron transfer processes in SAM modified electrodes. The first involves modifying the electrode surface with a blocking, hydrophobic monolayer of known thickness (usually about 1-

2nm) to block solution redox species diffusing to the electrode surface. A typical experiment of this type was carried out by Porter et al.[38]. In this study measurements of electron transfer rates at a gold electrode modified with a CH_3 terminated alkanethiol SAMs with varying chain lengths were carried out. It was determined using $Fe(CN)_6^{3-}$ and $Fe(H_2O_2)_6^{3+}$ redox probes that the variations in the reduction currents of the electroactive species in solution with overpotential and with chain length agreed with the predictions of simple electron transfer theory i.e. the currents were found to decrease rapidly with chain length. The second type of experimental setup utilises SAMs with an electroactive component, usually positioned at the top of the SAM. Such monolayers have the effect of minimising the effects of diffusion on the current response. A typical experiment of this type was carried out by Chidsey et al.[91]. In this study the electron transfer kinetics at monolayers containing varying amounts of alkanethiols terminated with CH_3 group and alkanethiols terminated with a ferrocene group linked with a polar ester group were carried out. It was determined that monolayers containing a low enough coverage of ferrocene exhibit ideal surface electrochemistry with the electron transfer sites non-interacting. Utilising such a setup it is possible to measure the rates of electron transfer without the complication of diffusion currents.

Using electrodes modified with self-assembled monolayers a number of charge transport phenomena have been studied. These include: (1) How parameters such as distance from surface, electrolyte, temperature, type of electrode effect electron transfer through the alkane chain. Many studies of this type have been carried out. One of the earliest of this type was carried out in 1993 by Finklea et al.[186] who examined the kinetics of electron transfer as a function of aqueous electrolyte and temperature. (2) Coupled electron transfer reactions[187]. (3) The effect of solvation of electroactive species in hydrodynamic environments on redox reactivities. Cannes et al.[188] determined that a $CH_3(CH_2)_{17}SH$ SAM acted as a better barrier towards the transport of ferrocyanide than it did towards the transport of menodione . This is due to the fact that menadione is more hydrophobic than ferrocyanide and thus can permeate the monolayer more easily. (4) The effect of counterion concentration motion on the rates of electron transfer[189]. (5) The effect of orientation and conformation of electroactive proteins on the rate of electron transport across a SAM. Such studies are important in the development of electrochemical sensors that can detect enzyme activity. Pilloud et al.[190] studied the electron-transfer characteristics of

iron(III)-protoporphyrin and iron(III)-hematoporphyrin covalently attached to dimercaptoalkane modified electrodes. It was determined that the redox processes occurred by electron tunnelling through the alkane spacer with the rate of transfer decreasing exponentially with the length of the chain.

In general when studying the electron transfer processes that can occur when an electrode has been modified with a SAM there are three main ways by which electron transfer may occur. (1) The electron may transfer through the film via a tunnelling mechanism. (2) The electroactive species in solution could permeate the through the monolayer and react with the electrode surface. (3) The electroactive species could diffuse to a bare spot (pinhole) on the electrode surface. In general one can rule out mechanisms (2) and (3) by electrochemical tests as if these pathways were dominant a current-voltage response would exhibit diffusion limited characteristics which they should not do in a well-formed blocking layer. Because of this the electron transfer is likely to occur via (1) the mechanism of which is well described by Marcus Theory and is the subject of many studies.

1.3.2.2 SAMs in Organic/Molecular Electronics

The use of molecules as the active components of electronic devices in place of traditional semiconductors is an area that has received much interest in the last decade. Theoretical studies have suggested that it may be possible to tailor molecules that mimic common circuit elements that are found in modern microelectronics. To this end study has concentrated on metal-molecule-metal junctions because of their proposed use as elements in molecular scale electronic components. Such junctions can exhibit non-linear current-voltage characteristics. Of particular interest is the phenomenon of negative differential resistance (NDR) - a property of electrical circuit elements composed of certain materials. In such circuits over certain voltages, the current is seen to be a decreasing function of voltage. It is proposed that metal-molecule-metal junctions could serve as nanoscale electronic switches. A good introduction to this area is provided in a study by Wasrel et al.[191] who attenuated the NDR peak currents in ferrocene labelled alkanethiol SAMs by capping them with β-cyclodextrin.

The area of molecular electronics is still in its infancy and some reviews have been drawn up to describe the state of the field[192, 193, 194, 195]. This section will attempt

to describe some of the main concepts behind molecular electronics and address some of the challenges faced in this area.

Metal-Molecule-Metal Junctions. The basis of metal-molecule-metal (M-M-M) junctions arises from the fact that when a molecular layer with a large HOMO-LUMO gap is sandwiched between two metal contacts tunnelling is expected. The normal configuration consists of a single molecule or an entire SAM formed between two metals. Self-assembled monolayers thus lend themselves extremely well to such a system. The charge transport through alkanethiol SAMs is expected to be tunnelling because the Fermi level of the metal contacts lie within the large (~8eV) HOMO-LUMO gap of the alkanethiol molecules.

When fabricating M-M-M junctions which utilise alkanethiol SAMs there are two main mechanisms that are commonly used. (1) The first mechanism involves using a metal film as one contact upon which the SAM is deposited with the second metal film deposited on top of this as the second contact. The second contact has been generated in a number of ways. Examples of such methods include depositing the metal film by evaporation or thermal annealing[196, 197]. It is also possible to position a conducting probe such as an STM tip in contact with the top of the SAM as a second contact[191]. (2) The second method of constructing the M-M-M junction involves the formation of a pair of nanoelectrodes mounted on a planar surface with a SAM positioned in the space between them. This gap has been fabricated in a number of ways including breaking a single wire mechanically or electrochemically[198], narrowing a gap to a very small distance by electrodeposition of a metal[197] or by techniques such as e-beam or focused ion beam lithography[199]. A third type of junction has been postulated and involves a nanoparticle coated with an alkanethiol SAM deposited onto a metal surface[200] with the second contact being made using a conducting probe.

Interesting I-V characteristics such as NDR responses have been observed in such junctions utilising alkanethiol SAMs but there remains a degree of uncertainty due to discrepancies between results. The most consistent data has been produced on alkanethiol SAMs however. It had been shown that the current through devices containing SAMs of these molecules depends exponentially upon the thickness of the SAM. The exponential dependence of the current response to the thickness of the

deposited SAM again indicates that the mechanism through which electrons are transported through the SAMs is via tunnelling[196, 197].

Challenges for Molecular Electronics. When studying the electron processes occurring through organic molecules and particularly when utilising M-M-M junctions a number of new factors come into consideration which would otherwise not pose a problem when dealing with electron transfer studies in the normal three electrode electrochemical experiment. These challenges can relate to the orientation, structure or identity of the species bridging a junction after a M-M-M junction has been formed. Other problems relate to the nature of the interface between the bridging molecule and the metal supports[201]. Other problems relate to the formation of metal films as the second contact that has been described in method (1) of M-M-M junction film formation in the previous section. This problem was addressed by deBoer et al. [202] who examined the effect of Au, Al and Ti vapour-deposited films onto SAMs of conjugated mono- and dithiols with sulfur groups at either end such that one end of the molecule bonded with a metal support with the other sulfur free to bind with the deposited metal. It was determined that Au and Al vapour-deposited films did not react with the conjugated backbone of the dithiol SAM but did react with the sulfur groups at the SAM/vacuum interface. The evaporation of Ti films was found to destroy the conjugated dithiol SAMs. In the case of monothiols it was found that Au did bind with the surface sulfur atoms but penetration of the Au atoms into the monolayer could not be ruled out. Al deposition was found to clearly permeate the SAM structure whilst again Ti deposition destroyed the layer. Because of the problems such as those that have been described a lot of work remains before a full understanding of molecular electronics can be achieved. The following six topics in this section will describe the areas that require development. Following this discussion the possible future direction of molecular electronics will be addressed.

Structure of Complex SAMs. This problem relates to the fact that much of the work carried out relating to the electronic characteristics of single molecules has been carried out using molecules that are more complex than the simple long chain alkanethiol molecules. An example of this is a recent study carried out by Ulrich et al. [203] studying the conductance of four different bridging molecules in a molecular

junction. Only one of the molecules studied was a straight chain alkanethiol molecule; the others were more complex possessing aromatic groups. The problem with such complex molecules is that they have the propensity to structural disorder and less is known about their order than common long chain alkanethiol SAMs. Another complication may arise from the type of metal used to form the junctions as the molecules may order themselves differently on the surface depending on the type of metal used. This leads to the next topic.

Nature of the Interface between SAMs and their Electrical Contact. As already explained, in M-M-M junctions two contacts are present. At least one of these contacts (and many times both) involves the formation of a metal-thiolate bond. How this interface affects the electrical characteristics of the junctions remains unclear. For example Beebe et al.[185] examined the contact resistance, R_0, when Au and Ag were used to contact a SAM whilst the contact was formed using an AFM tip. A large difference in R_0 values between Au (62kΩ) and Ag (234kΩ) was observed. Further work needs to be carried out in this area as a variety of metals are available to form junctions. The complexity of junction contact effects can be extended even further by taking into account the fact that in a M-M-M junction different metals can be used to form either contact in a two-metal junction.

Ambiguity also exists regarding the second contact in the M-M-M junction. This junction is normally formed by the vapour-deposition of a metal or by bringing a scanning probe tip into contact with the surface of the SAM. The effects of metal vapour-deposition onto the surface of the SAM has already been discussed[202] and it has been determined that such deposition can have detrimental effects on SAM structure. Scanning probe techniques are known to be less damaging but they do introduce additional problems due to interfaces such as SAM/vacuum/tip or SAM/electrolyte/tip that must be taken into consideration.

Mechanism of Electron transport in Metal-Molecule-Metal Junctions. A degree of discussion remains regarding the exact mechanism of electron transport through bridging organic molecules in M-M-M junctions. The vast majority of reports agree that the mechanism by which electrons travel through the molecule is via tunnelling. This is a process by which the organic molecule mediates the electron transfer but the

electron transfer does not reside on the molecule for a significant period of time. Difficulties arise when contemplating the electron tunnelling processes that occur in some of the more complex molecules used to bridge M-M-M junctions.

Complications also arise due to the possibility of other conductions such as thermionic emission (the flow of electrons from a metal surface due to thermal vibration energy) and electron hopping in which the electron being transported through the organic molecule does localise at specific sites in the molecule. Both thermionic and hopping conductivity have been observed for 4-thioacetyl-biphenyl[204] ad 1,4 phenelyene diisocyanide SAMs[205].

Perturbations to the Electronic and Vibrational States of Bridging Molecules. The effect of the electric fields applied to molecules in M-M-M junction experiments is not well understood. One of the very few studies carried out to examine this effect was undertaken by Wang et al.[206]. In this study Inelastic Tunnelling Spectroscopy (ITES) was used to determine the vibrational modes of alkanethiol SAMs in a nanometer scale device. ITES spectroscopy may also be used to confirm the exclusive presence of specific molecules at the junction.

Identification of I-V Curves for Two-Terminal Devices. It has been found that experimentally observed I-V curves for two terminal devices such as M-M-M junctions are very difficult to interpret due to the fact that subtle changes in the electrostatic environment near the junction and in the electronic and physical couplings at the junction contacts affects the measured I-V response.

Defects in Junctions. When considering systems as sensitive as two-terminal devices the presence of defects plays an important role in device functionality. There are as yet no methods available to characterise defects in M-M-M junctions. The types of defects that are thought to exist are shown in Figure 1.8 below.

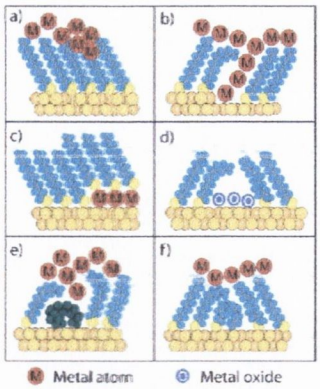


Figure 1.8. Illustration of the type of defects that can occur in SAMs when forming two- or three-terminal devices. (a) Metal atoms being chemically bound to the organic component of the SAM. (b) Formation of metallic filaments. (c) Deposition of metal adlayers onto the underlying metal support. (d) Formation of oxide impurities on the underlying metal support. (e) Organic impurities in the SAM. (f) Defects in the SAM structure resulting from alkane chain disorder. Reproduced from Reference 31.

The Future of Molecular Electronics. The area of microelectronics is still in its infancy and the question of how electrons move through single molecules remains fascinating yet poorly understood. It is likely that self-assembled monolayers will continue to be an integral part of the development of molecular electronics. This is due mainly to two reasons. The first relates to the practicalities of the experiments being carried out – SAMs are readily deposited spontaneously in nanometer scale areas where direct manipulation would require complex techniques. SAMs form on a wide range of metals and their structure and composition can be readily tailored. The second reason relates to the fact that research up to the present has concentrated on SAMs and thus any new research efforts are likely to be based upon previously described theory.

In the short term it is necessary to develop M-M-M junctions based on alkanethiols that can be readily reproduced in a manufacturing sense and yield a reproducible electronic response. Slowinski and Majda[207] have recently developed one particular type of junction that has generated interest based on mercury-drops. In this case the junction is formed by contacting two hanging mercury drops each coated with an alkanethiol layer. Mercury as a liquid metal offers atomically smooth, defect free surfaces that are likely to be less destructive to the SAM layer when the mercury drops contact the alkanethiol molecules. A variation on this type of junction has been described by Galperin et al.[208]. In this study a Au/alkanethiol/Hg junction was formed by carefully bringing an alkanethiol coated gold substrate into contact with a mercury drop. Such systems may form the basis of future junction devices although, again, as yet they are poorly developed.

It is thought that the combination of a well defined reproducible junction system and modern spectroscopic techniques will provide sufficient data to establish general guidelines relating to electron transfer processes through single organic molecules.

1.3.3 SAMs in Biochemistry and Biology

As has already been discussed self-assembled monolayers are examples of ordered nanostructures. With relation to biological systems it is notable that the membranes that define the boundaries of individual cells area examples of naturally occurring nanostructures. A biological membrane is one that acts as a barrier within or around a cell. It is normally a lipid bilayer, specifically a phospholipid. Such membranes typically define an enclosed space or compartment in which cells can maintain a chemical environment that differs from the external environment. Such membranes can have dimensions ranging from a hundreds to tens of nanometers. One example of a nanoscale membrane are integrins. Integrins have the role of attaching a cell to the extracellular (ECM) matrix as well as signal transduction to the ECM. Such integrins typically have a width of 10nm.

In biological assemblies there is a very broad range of membrane-bound assemblies. The interactions between single ligand-receptor pairs enable individual cells to sense their local environment, communicate with other cells and regulate intracellular. Probably the most important feature of a biomembrane is that it is selectively permeable. That is the membrane has the ability to determine whether other molecules attempting to cross it are allowed to based on their size, charge and other chemical properties.

Certain fundamental aspects of cell biology are difficult to study due to the extremely complex nature of biological systems. In order to further develop an understanding of such systems model surfaces such as those imparted using SAMs could be used. Processes which could be, in theory, much better understood include the physical-organic chemistry of biomolecular recognition, determining the effect of individual recognition events on the functional behaviour of cells and investigating the structural factors that enable surfaces to resist the adsorption of proteins. Such simplified systems may also be used in the advancement of applications in biotechnology such as biosensors. This is because developing model surfaces allows precise control of the structure and composition of the surface. It also allows the

exclusive study of single or a few types of interaction. This simplification with respect to the realistic and complex biological environment means it could theoretically be possible to treat individual processes and combine the understanding of them in a meaningful way.

SAMs are useful model surfaces on which to base model biological systems for a number of reasons. Firstly then have dimensions on a nanometer scale, as do biological surfaces (membranes). Secondly They possess a wide range of structural functionality. Thirdly it is possible to deposit SAMs with certain ligands that are required for biological studies either by developing such a molecule synthetically and then depositing it or attaching the ligands to the surface of a previously deposited, reactive SAM.

The major disadvantage of using SAMs as a system to study biological interfaces is that their structure is essentially static in contrast to biological membranes that are fluid and rearrange dynamically.

1.3.3.1 SAMs as Model Biological Surfaces

If SAMs are to be successfully used to model biological surfaces it is thought that they should possess three main features. Firstly they should resist non-specific adsorption of proteins or other biomolecules on the surface, i.e. they should only allow interactions between certain molecules and ligands so that meaningful analysis can be made regarding such processes. Second, it should be possible to modify the structure of the immobilised ligands or biomolecules. Finally the ligands of interest should be orientated in a manner that minimises the influence of the surface, e.g. mass transport problems, blocked binding sites. This discussion will now focus on the three main areas to which SAMs have been applied as model biological surfaces in biological studies.

Protein Resistant Surfaces. Protein resistant surfaces are ones with the capability to resist the non-specific binding of other biomolecules and cells. They are often commonly referred to as 'inert' surfaces. Common protein resistant surfaces developed using SAMs are based on alkanethiol molecules with headgroup of poly(ethylene glycol). Pal-Grosdemage et al.[209] examined this property by exposing electrodes modified with a common CH_3 terminated alkanethiol SAM and an oligo(ethylene glycol) (OEG) terminated SAM to a protein solution. Using

ellipsometry to determine the thickness of the layers before and after exposure to a protein solution it was determined that the OEG terminated SAM resisted protein adsorption and remained the same thickness whilst the CH_3 terminated SAM exhibited an increase in thickness corresponding to protein adsorption.

Because SAMs terminated with ethylene glycol groups form the basis of synthetic protein-resistance surfaces a number of studies have been carried out regarding their orientation.

Harder et al.[210] carried out FTIR and XPS studies to determine the molecular conformation of OEG terminated alkanethiol SAMs. The study revealed the presence of a crystallographic helical OEG phase coexisting with amorphous OEG moieties. These findings were verified in a study by Zwahlen snd coworkers[211] who studied SAMs terminated with poly(ethylene glycol) groups of differing length using NEXFAS. This study confirmed that only a certain fraction of the monolayer was in the second helical conformation, aligned perpendicular to the surface, whilst the remainder were in the amorphous phase.

Mixed SAMs as Model Biological Surfaces. Mixed monolayers containing two or more constituients have the ability to provide a model system to study the fundamental aspects of surface-molecule interactions in biological systems. The reason why mixed monolayers are used as model biological systems is due to the fact that they can combine the selectivity of certain SAMs of appropriate end groups with the protein resistant properties of others. By tailoring the amount of such species it is possible to develop a surface upon which to carry out more specific studies.

A typical example of a mixed monolayer used in biological studies has been demonstrated in a study by Frederix et al.[212]. In this case mixed SAMs with carboxylic and poly(ethylene glycol) were deposited onto the surface of an electrode. This study showed the ability of mixed SAMs to selectively recognise and immobilise human serum albunium (HSA).

Another typical study using mixed monolayers as mimics for biological studies was carried out by Ostuni et al.[213]. In this work mixed SAMs composed of components with a hydrophobic end group and a blocking end group were used to study the hydrophobic interactions that can occur during protein adsorption. It was shown in this study that the amounts of adsorbed protein could be controlled by the extent of hydrophobic groups in the mixed monolayer.

Finally Lahiri et al.[214] examined the steric interactions between carbonic anhydrase (CA) in mixed monolayers if benzenesulforamide and tri(ethylene glycol) terminated SAMs.

SAMs as Components for Arrays of Biomolecules. Any substrates that support arrays of biological molecules are becoming a more important technology for examining the biology of ligand-receptor and enzymatic activities. Many studies have focused on immobilising molecules of interest onto such substrates. These studies have included DNA[215], proteins[216], carbohydrates[217] and antibodies[218]. SAMs are becoming an increasingly important method for tethering such molecules because their chemistry, especially when deposited onto gold substrates, is very well understood. The planar format used in such studies is ideal for electrochemical experiments looking at biological activity. Again the electrochemical properties of adsorbed alkanethiol SAMs are very well understood.

1.3.3.2 SAMs for Cell Biology

The main advantage of SAMs when used to study cell biology is again their ability to modify their structure to a system specific composition. When dealing with studies regarding cells in living organisms we note that cells are surrounded by a complex matrix of proteins and other biomolecules. Due to the wide variety of SAMs available it is possible to generate model organic surfaces to which cells can attach and interact. Processes such as cell attachment and intracellular signalling can then be examined in a simplified manner due to the wide understanding of the chemistry of organic SAMs that has already been developed.

One particular application to which SAMs are employed regarding cell biology is the area of ligand-receptor interactions. Such interactions lead to a structural rearrangement of the molecules in question therefore altering their susceptibility to other chemical reactions. Mixed SAMs composed of a ligand presenting molecule and a protein resisting molecule make it possible to vary the accessibility of ligands to a surface and aid in the study of ligand-receptor interactions. One such study was carried out by Roberts et al.[219]. In this work mixed SAMs composed of arginine-glycine-asparate (RGD), which promotes cell adhesion by binding to the cell integrin receptors, and the previously described OEG molecules were used to measure the adsorption of carbonic anhydrase and fibrinogen to the

RGD groups. Thus by using a substrate system that presented RGD groups in an interface that would be otherwise inert to the attachment of biological entities, it was demonstrated that integrin-RGD interactions were sufficient for the attachment and survival of cells over a period of 24 hours.

Another more technologically advanced method for selectively attaching cells to surfaces has been demonstrated using μCp. In this mechanism hydrophobic SAM molecules can be deposited in a defined manner onto an electrode. Subsequent immersion of this substrate into a solution of protein resistant molecules provides a method of forming mixed SAMs to defined dimensions. The profile of adherent cells on the surface of the electrode can thus be controlled due to the fact that their adsorption is not permitted at protein resistant sites. Jiang et al.[220] used a combination of μCp monolayer patterning and electrochemistry to demonstrate that bovine capillary endothelial (BGE) cells confined to microislands could be released from their confinements by electrochemical desorption of the SAMs which allowed the proteins to adsorb onto the electrode surface. This work was an attempt to dynamically control the cell-substrate interactions.

1.3.3.3 Structure Considerations for SAMs used in Biology

The types of molecule that are used to form SAMs used in biological studies are generally different from the simple alkanethiol molecules that have been described earlier in this work. Three main factors account for this difference. Firstly the size and shape of the ligands immobilised onto the surface of the SAM must be taken into account. Secondly the composition and dynamics of the functional groups presented at the surface of the SAM that resist protein adsorption must be taken into account. Finally the interactions of the SAM with the aqueous medium, which normally consists of dissolved proteins and other biomolecules must be taken into account. These three factors will now be dealt with in turn.

Influence of Biological Ligands on SAM Structure. The ligands and biomolecules tethered to SAMs that are required to study biological systems are normally much larger than the alkane chain by which they are tethered. Because of the steric interactions between large pendant biomolecules it is not possible to pack them in tethered arrays with the order and density associated with simple alkanethiol systems.

In domains of ordered biomolecules tethered via alkanethiol linkers it has been found by Yeo et al.[221] that a large amount of pinholes and defects are present.

A number of presumptions are commonly made regarding systems where ligands are tethered to a substrate via an alkanethiol chain. (1) The ligand molecule does not interact with the surface of the substrate. Given the high degree of pinholes and defects found in domains of alkane-linked ligands this may not hold true, particularly in the case of a ligand sitting next to a pinhole site where the electrode surface is exposed. (2) The ligand is well solvated and presented at a well defined distance from the surface of the electrode. Again this may not necessarily be true as alkane chains in many SAM systems have shown the propensity to coil and kink which may leave the ligand at an ill-defined distance from the substrate. (3) In mixed SAMs the ligands are evenly dispersed throughout the SAM film and do not phase segregate. Although there is no experimental evidence to confirm or deny this phase segregation it is widely understood to occur in mixed SAMs where the molecules have differing headgroups. The same situation may occur with ligand-linked molecules.

Due to the lack of experimental data regarding these assumptions much work remains to be carried out regarding the structural properties of SAMs used in biological studies.

Composition of Surfaces that Resist Protein Adsorption. As already discussed many mixed monolayer systems have been developed to study biological processes. An integral part of such systems is a section of the monolayer that resists protein adsorption thus increasing the selectivity of the monolayer. The structural conformation of these protein resistant sections are poorly understood.

The best understood class of protein resistant molecules are the oligo(ethylene glycol) molecules. Valiokas et al.[222] carried out contact angle, ellipsometry and IR studies of OEG terminated alkanethiols. Both contact angle and ellipsometry measurements indicated excellent packing and ordering properties of the OEG layers. IR spectroscopy confirmed these findings indicating a well-ordered, crystalline, helical OEG layer. Schwendel et al.[223] examined the properties of OEG layers as a function of temperature. It was determined from this study that such layers remain protein resistant up to 85°C. Deng et al.[224] examined the ability of a specifically tailored alkanethiol molecule presenting a tri-(propylene sulfoxide) protein resistant

group. This work demonstrated that OEG presenting SAMs were not alone in their ability to serve as an inert surface. In general the factors that would appear to correlate with the ability of molecules to resist protein adsorption include polarity, electrostatic neutrality, absence of H-bond donors and conformational flexibility.

Behaviour of SAMs in Solvents of Biomolecules. The use of self-assembled monolayers as models for biological surfaces requires, experimentally, that they come into contact with high concentrations (~200mM) of salts as well as various biomolecules. Because of this it is necessary to have a full understanding of the properties of the SAM-electrolyte interface to fully develop a well-ordered SAM system to mimic a biological surface. Much less is known regarding the SAM-electrolyte interface in the case of biological systems then in the case of typical ionic electrolytes. It is postulated however that the nature of the electrolyte can have a profound effect on the structure of SAMs tethered to ligands.

An example of such conformational changes were demonstrated in a report carried out by Fick et al.[225] that showed swelling of poly(ethylene glycol) terminated monolayers when placed in contact with water. The main point of note in this study was that the amount of electrolyte interference was directly dependent on how well such systems were packed with amorphous films showing much greater swelling than crystalline films.

Flynn et al.[215] used several analytical techniques to characterise the effect of immobilising EGO presenting SAMs in phosphate buffer and calf serum. It was determined that over a period of 35 days there was a substantial loss of integrity of the SAM. The most likely origin of the observed SAM disintegration was the oxidation of the thiolate headgroup and its subsequent desorption from the gold surface. Valioleas and coworkers[226] studied the phase behaviour of seven different OEG based SAMs. This report determined that intermolecular interactions between ester and amide linker groups substituted into the OEG chains could be used to partly control the order and conformation of the OEG portion of the SAM. It was also noted that it was likely that the interchain hydrogen bonding helps to stabilise the OEG layer, as is the case when dealing with simple alkanethiol systems.

1.3.4 SAMs for Sensing

Probably the most frequent present application of self-assembled monolayers is in the area of sensing. For this reason this section will focus on the common areas that SAMs are used to impart selectivity onto the electrode towards a particular species.

This section will attempt to provide an insight to some of the present applications of SAMs in the area of sensing. Particular attention will be paid to biosensors as this is by far the most widely used commercial application of SAMs to date. Following this a brief discussion of the application of SAMs to another type of sensor, the pH sensor, will be discussed.

1.3.4.1 Applications of SAMs in Biosensors

The most frequent application of SAM modified electrodes to date has been in the detection of organic and biochemical species in systems known as biosensors. A biosensor is usually defined as a sensing device consisting of a biological recognition element in intimate contact with a suitable transducer that has the ability to convert a biological recognition event or biocatalytic process into a measurable signal. Such devices have a wide commercial potential due to their selectivity, stability, portability, speed, low cost and potential for miniaturisation.

In electrochemical biosensors the most common analyte are enzymes and electrochemical transduction is the most popular method of sensing. The two most established methods in electrochemical transduction are potentiometric and amperometric. In potentiometric devices the analytical information is generated by converting the biorecognition process into a potential signal. In amperometric devices the electrode potential is used to drive an interfacial redox reaction and the resulting current is measured. The current flowing in this case is directly proportional to the analyte concentration. It is generally agreed that amperometric biosensors are the more attractive of the two methods. This is due to their higher sensitivity and wider range. Such devices have the ability to combine the selectivity of an enzyme for a specific target analyte with direct transduction of the rate of the biocatalytic reaction into a current signal.

Thus far biosensor development can be broadly classified into three generations. The first generation of biosensors that have been developed are based on the electrochemistry of the enzyme substrate or product. The second generation are based on the use of redox mediators which can be freely diffusing in solution or

immobilised with the biomolecule. Third generation biosensors involve direct electron transfer between the redox active biomolecules and the electrode surface. These three biosensor types are shown below in Figure 1.9.

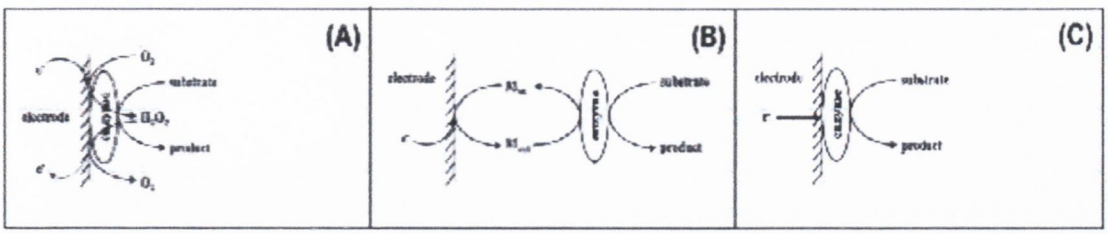


Figure 1.9. Schematic reperesentation of the three generation of biosensors. (A) First generation, (B) Second generation, (C) Third generation. Reproduced from Reference (227).

Both first and second generation biosensors have problems associated with them. First generation devices require, at times, quite high applied potentials to generate an adequate signal and thus may not be of practical use commercially. Second generation devices involve the use of redox active mediators to facilitate electron transfer between the enzyme and the electrode surface. Such mediators may also facilitate the electron transfer of various interferer species. These problems turn attention towards third generation biosensors. In such sensors the electron transfer is associated with, or occurs during, the catalytic transformation of a substrate into a product at a target enzyme site. The redox enzyme then acts as an electrocatalyst facilitating the electron transfer between the electrode and the substrate molecule. This type of biosensor would appear to offer ideal selectivity towards specific molecules. Also such a biosensor is able to operate in a potential range closer to the redox potential of the enzyme. Lastly and importantly the simplicity of such devices make them good systems for commercial construction.

It has been shown thus far that third generation biosensors have large advantages over earlier models. The question must be then asked as to how self-assembled monolayers are relevant to such systems? SAMs are relevant because one of the major obstacles still to be overcome in the construction of these devices is how to optimise the electron transfer between the enzyme and electrode surface. Unfortunately the distance between the electrode surface and the prosthetic group can be quite long because of protein shell shielding. Because of Marcus Theory considerations the amount of current detectable in this system can be far from optimum. Thus a problem exists regarding the design of enzyme based devices to optimise the electron transfer between the enzyme and the substrate. The immobilised

biomolecule must have an appropriate orientation to facilitate electron transfer between itself and the electrode surface. Several methods have been used to immobilise enzymes on substrate surfaces including physical adsorption, entrapment between a dialysis membrane and entrapment within a polymer film to name but a few. However such methods have been found to produce an enzyme film that remains randomly orientated on the surface. This problem leads to the use of SAMs. By linking SAMs of the appropriate composition to a desired enzyme it is possible to produce an electrode modified with a highly orientated layer of enzyme molecules with the organic SAM as the electron transfer mediator. SAMs retain all of their advantages such as convenient assembly, high order, etc. in this area and thus provide an excellent basis upon which to base new, improved biosensor design. Many of the important issues regarding the fabrication of enzyme electrodes have been previously discussed[228, 229, 230, 231] and for this reason the remaining discussion will focus on some common examples of integrated SAM-enzyme biosensor systems.

Lotzbeyer et al.[232] carried out a study on common monolayer immobilised enzymes that catalyse the reduction of H_2O_2 such as cytochrome c, microperoxidase and horseradish peroxidase. It was determined that their catalytic activity in solution was not correlated with their abilities for direct electrochemical communication with the electrode when immobilised at thiol monolayers. The most important factor is the distance between the active site in the enzyme and the electrode surface. Because of this factor it was found that using microperoxidase instead of horseradish peroxidase gave better access to the enzyme active site because of its smaller molecular weight. The detected current associated with microperoxidase was found to increase by a factor of 1,800 relative to the much larger horseradish.

Jiang et al.[233] studied the electrochemistry of glucose oxidase (GuOx) at an electrode modified with an organic DTSSP monolayer. It was determined that the Au-DTSSP-GuOx system readily underwent reversible charge transfer and that the peak currents were found to be directly dependent on the potential scan rate in phosphate buffer. Enhancement of the oxidation current upon addition of glucose to the phosphate buffer was observed. As an increased amount of glucose was added to the phosphate buffer the recorded catalytic current was seen to increase. Unsurprisingly the current response of this system was found to be quite poor due to the fact that the electroactive FAD site was deeply buried within the enzyme.

To combat this problem Willner et al.[234] constructed an artificial GuOx environment by directly attaching a FAD site to the electrode surface via a cystamine monolayer. The FAD site was then treated with apo-glucose oxidise which produced the reconstituted and densely packed GuOx unit. This system yielded much faster electron transfer kinetics between the immobilised enzyme and the electrode than relative to those observed by Jiang and coworkers.

Even faster electron transfer kinetics have been observed through conjugated molecular bridges by Creager et al.[235] with respect to the aliphatic bridges used by Wilner at al. However such systems have not been studied with regard to sensor applications. Similarly O'Kelley et al.[236] have demonstrated faster electron transfer kinetics through DNA molecules.

Lisdat and Scheller[237] investigated the electrochemical behaviour of cytochrome c. In this study a short, double stranded oligonucleotide (short sequence of DAM) was tethered to a gold electrode using a $-(CH_2)_3SH$ group. When the oligonucleotide modified electrode was exposed to a solution containing cytochrome c a reversible CV was recorded. The electron transfer between cytochrome c and the electrode was rather fast. It was shown that the immobilised electroactive cytochrome c is accessible to small analyte molecules.

An excellent example of a self-powered biosensor based on self-assembled monolayers was demonstrated in a report by Katz et al.[238]. In this device a two-electrode cell is used. The setup consists of an anode consisting of an artificial glucose oxidase unit constructed as described previously[234] and cathode comprised of layered cross-linked cytochrome c/cytochrome oxidase functionalised electrode. The biocatalysed oxidation of the anode by O_2 yields electrical power (fuel) which essentially makes the anode a power source for the device. The open circuit potential of the system is sensitive to the concentration of fuel. This type of device offers key advantages over other biosensors in that the open circuit potential operation removes the problem of electrochemical interferers. Also the absence of an external power supply makes it ideal as an implantible device. Katz et al. also discuss a variation on this device in the study. This second configuration is capable of detecting lactate whilst the first configuration detects glucose.

SAMs are very useful in systems such as those described above due to the fact that they have the ability to mediate electron transfer which is easily detectable. However they have been much less used in affinity sensing due to the absence of any

redox active product. In the case of affinity sensing, when an antibody is used, the biospecific recognition events and interactions take place without any analyte conversion.

Some reports in the area of antibody detection utilising SAMs have been carried out however. One such study was carried out by Spinke and coworkers[239] who investigated a self-assembled multiplayer system capable of sensing the presence of human chorionic gonadotrophin (HCG) the detection of which is of interest to pregnancy testing. It was found in this system that the binding of the antibody was limited by steric hindrance and a detection limit of $1x10^{-8}$M was observed. Such a system requires modification if it is to be applied to commercial pregnancy testing as a marketable system requires a sensitivity of $5x10^{-11}$M. The basis of such antibody is essentially the ability of antigen binding to reduce the accessibility of the electrode to redox species in solution. As a consequence many of the antibody sensors are based on a mixed monolayer platform with certain constituents coupling to the biorecognisable molecule and the others only present to passivate the electrode surface. In general a change in the capacitance or impedance of the layer is monitored in order to detect the presence of an immunoreaction

A final and extremely important class of modern biosensor to which SAMs have been have been applied are in the area of detecting specific DNA sequences. In such electrodes a single strand of probe DNA is attached to the electrode surface. Exposure of such an electrode to the complimentary strand results in strand hybridisation that can be detected electrochemically. Self-assembled monolayers are particularly useful in such systems for two main reasons. Firstly, in order for hybridisation to occur efficiently between the DNA strands it is necessary to have a well defined end point of the immobilised strand. Tethering a strand to the electrode using an alkanethiol linker achieves this. Secondly it has been shown by Levicky et al.[240] that the formation of a mixed monolayer of alkanethiol-tethered DNA strands and alkanethiol molecules with an alcohol group results in the single strand DNA being orientated away from the electrode and thus making hybridisation with its complimentary strand more facile.

As well as the electrochemical detection of DNA the hybridisation process can also be detected, as discussed in the case of antibody detection, by a change in the interfacial capacitance of the electrode. This is because DNA is a polyanion and hybridisation results in an increase in the negative charge at the electrode. Willner et

al.[241] have used this increase in negative charge to monitor the hybridisation of DNA by an increase in the Faradaic impedance where ferricyanide was used as the redox label in solution.

Another method for DNA sensing was developed by Takenaka et al.[242]. In this study an electroactive naphthalene dimide derivative was found to bind 4 times more strongly to an intact DNA sequence than it did to the corresponding denatured sequence. Using this mechanism it was possible to detect the presence of a particular type DNA strand. This was done by firstly immobilising a thiol linked single strand of DNA on the surface of the electrode. This electrode was then treated with a solution of the complimentary DNA sequence. Finally the electrode was soaked in the naphthalene dimide derivative. Cyclic voltammetry and differential pulse voltammetry were then used to determine an electrochemical signal due to the reaction of the redox active derivative with the double stranded DNA.

Other methods of DNA sensing rely on the ability of a double stranded DNA molecule to mediate long range electron transfer. O'Kelley and coworkers[236] studied this phenomenon by firstly tethering 15 base-pair DNA molecules to a gold electrode via self-assembled monolayers. A redox active intercolatir, daunomycon (DM) was then crosslinked into the DNA strand at various positions. Remarkably efficient reduction of DM was observed regardless of its position in the base-pair sequence. Such good electron transfer properties through the DNA molecules was found that it became evident that the rate determining factor was the transfer through the alkanethiol linker. This report showed the ability to correlate the electron transport rate with single base mismatches and in theory provides an alternative means to hybridisation to detect genetic mutations in a DNA sequence.

Many methods have been discussed here to detect DNA using SAMs. However the currently used DNA sensor of this type has been developed by Clinical Microsystems the design of which was proposed in a study by Umek et al.[243] in 1991. This sensor utilises a multi-component SAM consisting of a DNA thiolated section, a polyethylene glycol terminated section and an alkanethiol segment to resist non-specific binding of DNA. Oligophenylethynyl thiols are also present which act as molecular wires to allow communication to the electrode surface. In this setup unlabeled nucleic acid targets are immobilised on the surface of the SAM through sequence specific hybridisation with the DNA capture probe. A separate signalling probe, containing ferrocene modified nucleotides and complementary to the target

region adjoining the capture probe binding site is held in close proximity to the SAM in a sandwich complex. The SAM allows electron transfer between the immobilised ferrocenes and the electrode whilst insulating the electrode from redox species. Recognition of the target strand is transduced by the occurrence of a current signal. Another system currently being commercialised by AMBRI based on SAMs is the ion-channel biosensor, however at present the system developed by Umek et al. is the standard DNA sensor.

1.3.4.2 Applications of SAMs in pH Sensors

Hickman et al.[244] first used SAMs as a method to determine solution pH by voltammetric means in a study in 1999. In this report a two terminal pH sensor was developed with a monolayer of quinines as the pH sensitive electrode and a pH-independent electroactive ferrocene terminated SAM as a reference electrode. The oxidation and reduction peaks of the quinine terminated SAM was found to vary linearly with the pH of the electrolyte allowing measurements between pH 1-11.

Another example of pH sensing using SAMs was carried out by Beulen et al.[245]. Here a mixed monolayer of alkanethiols with both carboxylic acid and ferrocene end groups to give a bifunctional monolayer. It was determined that the electrochemical response of the bifunctional monolayer is strongly influenced by the pH of the electrolyte solution. This is due to the fact that as the pH of the solution changed so too did the extent of deprotonation of the carboxylic groups. It was shown that the redox active ferrocene groups sensed the deprotonation of the carboxylic acid and hence sensed the pH of the solution. This is because the carboxylates in the oxidised state of the ferrocene groups were stabilised and as a consequence of this the redox potential of the ferrocene group shifted cathodically. By this means it was possible by voltammetric means to sense the pH of the electrolyte solution.

A final example of a pH sensor utilising SAMs has been developed by Wilner et al.[246]. In this system a cystamine monolayer is covalently attached to a pH sensitive probe, in this case pyrrolquinoline quinone (PQQ). This probe in turn was covalently attached to a specific enzyme. In the case of this study the reaction the enzyme urease with urea caused a change in the local pH. This pH change was then registered by the PQQ group and the signal transduced to the electrode via the cystamine monolayer. It was determined using such a system that the increase in the amount of enzyme reacting increased so too did the pH. This increase in pH caused a

decrease in the registered peak potential. This study again demonstrated how it was possible to determine pH by voltammetric means using SAMs as a system component.

References

(1) S. A Empedocles, R. Neuhauser, K Shimizu, and M.G. Bawendi,. *Adv. Mater.* **1999**, *11*, 1243.

(2) J. Jiang, K. Bosnick, M. Maillard and L. Brus, *J. Phys. Chem. B* **2003**, *107*, 9964.

(3) J.A. Stroscio, and D.M. Eigler, *Science,* **1991**, *254*, 1319.

(4) T.V. Torchynska, *J. Appl. Phys.* **2002**, *92*, 4019.

(5) A.W. Adamson and A.P. Gast, *Physical Chemistry of Surfaces*, 6th ed.; Wiley-Interscience: New York, 1997.

(6) G.E. Poirier and E.D. Pylant, *Science,* **1996**, *272*, 1145.

(7) R.G. Nuzzo and D.L. Allara, *J. Am. Chem. Soc.* **1983**, *105*, 4481.

(8) M.D. Porter, T.B Bright, D.L. Allara and C. E. D. Chidsey,. *J. Am. Chem. Soc.* **1987**, *109*, 3559.

(9) C.D. Bain, J. Evall and G.M. Whitesides, *J. Am. Chem. Soc.* **1989**, *111*, 7155.

(10) C.D. Bain and G.M. Whitesides, *Science* **1988**, *240*, 62.

(11) H.A. Biebuyck, C.D. Bain, and G.M. Whitesides, *Langmuir* **1994**, *10*, 1825.

(12) P.E. Laibinis, G.M. Whitesides, D.L. Allara, Y.T. Tao, A.N. Parikh, and R,G, Nuzzo, *J. Am. Chem. Soc.* **1991**, *113*, 7152.

(13) L.H. Dubois, B.R. Zegarski and R.G. Nuzzo, *J. Chem. Phys.* **1993**, *98*, 678.

(14) M.M. Walczak, C. Chung, S.M. Stole, C.A. Widrig, and M.D. Porter, *J. Am. Chem. Soc.* **1991**, *113*, 2370.

(15) P. Fenter, P.Eisenberger, J. Li, N. Camillone, S. Bernasek, G. Scoles, T.A. Ramanarayanan, and K.S. Liang, *Langmuir* **1991**, *7*, 2013.

(16) J.C Love, D.B. Wolfe, R. Haasch, M.L. Chabinyc, K.E. Paul, G.M. Whitesides, and R.G. Nuzzo, *J. Am. Chem. Soc.* **2003**, *125*, 2597.

(17) A. Carvalho, M. Geissler, H. Schmid, B. Micel and E. Delamarche, *Langmuir* **2002**, *18*, 2406.

(18) Z. Li, S.-C. Chang, and R.S. Williams, *Langmuir* **2003**, *19*, 6744.

(19) N. Muskal, I. Turyan and D.J. Mandler, *Electroanal. Chem.* **1996**, *409*, 131.

(20) Y. Xia and G.M. Whitesides, *Angew. Chem., Int. Ed. Engl.* **1998**, *37*, 550.

(21) B. Michel, A. Bernard, A. Bietsch, E. Delamarche, M. Geissler, D.Juncker, H. Kind, J.P. Renault, H. Rothuizen, H.Schmid, P. Schmidt-Winkel, R. Stutz, and H. Wolf, *IBM J. Res. Dev.***2001**, *45*, 697.

(22) M.R. Shadnam, S.E. Kirkwood, R. Fedosejevs and A. Amirfazli, *Langmuir* **2004**, *20*, 2667.

(23) R. Klauser, I.H. Hong, S.C. Wang, M. Zharnikov, A. Paul, A. Goelzhaeuser, A.Terfort and T.J. Chuang, *J. Phys. Chem. B* **2003**, *107*, 13133.

(24) S. Sun, K.S.L. Chong, and G.J. Leggett, *J. Am. Chem. Soc.* **2002**, *124*, 2414.

(25) J.M. Behm, K.R. Lykke, M.J. Pellin, J.C. Hemminger, *Langmuir* **1996**, *12*, 2121.

(26) K.K. Berggren, A. Bard, J.L. Wilbur, J.D Gillaspy, A.G. Helg, J.J. McClelland, S.L. Rolston, W.D. Phillips and M. Prentiss, *Science*, 1995, *269*, 1255.

(27) M.L. Chabinyc, J.C.Love, J.H. Thywissen, F. Cervelli, M.G. Prentiss and G.M. Whitesides, *Langmuir* **2003**, *19*, 2201.

(28) G.-Y Liu, S. Xu and Y. Qian, *Acc. Chem. Res.* **2000**, *33*, 457.

(29) S. Kraemer, R.R. Fuierer and C.B. Gorman, *Chem. Rev.* **2003**, *103*, 4367.

(30) S.J. Stranick, A.N. Parikh, Y.T. Tao, D.L. Allara and P.S. Weiss, *J. Phys. Chem.* **1994**, *98*, 7636.

(31) J. C. Love, L. A. Estroff, J. K. Kriebel, R. G. Nuzzo, and G. M. Whitesides, Chem. Rev. **2005,** 105, 1103-1169

(32) K. B. Blodgett, *J. Am. Chem,. Soc*, **1935**, *57*, 1007

(33) K.B. Blodgett and I. Langmuir, *Phys Rev*, **1937**, *51*, 964

(34) W.C. Bigelow, D.L. Pickett and W.A. Zisman, *J. Colloid Sci.* **1946**, *1*, 513

(35) E.E. Polymeropolous and J. Sagiv, J. Chem Phys, **1978** , 69, 1836

(36) R.G. Nuzzo and D.L. Allara, *J Am. Chem. Soc,* **1983**, *105*, 4481

(37) R.G. Nuzzo, F.A. Fusco and D.L. Allara, *J. Am. Chem. Soc*, **1987**, *109*, 2358

(38) M.D. Porter, T.B. Bright, D. Allara and C.E.D. Chidsey, *J. Am. Chem. Soc*, **1987**, *109*, 3559

(39) H.O. Finklea, S. Avery, M. Lynch, and T. Furtsch, *Langmuir*, **1987**, *3*, 409

(40) E. Sabatani, .I. Rubenstien, R. Maoz and J. Sagiv, *J. Electroanal Chem,* **1987,** *219,* 365

(41) E. Sabatani and .I. Rubenstien, *J. Phys. Chem,* **1987,** *91,* 6663

(42) E.B. Troughton, C.D. Bain, G.M. Whitesides, R.G. Nuzzo, D.L. Allara and M.D. Porter, *Langmuir*, **1988,** *4,* 365

(43) L. Strong and G.M. Whitesides, *Langmuir,* **1988,** *4,* 546

(44) C.D. Bain and G.M. Whitesides, *J. Am. Chem. Soc,* **1988,** *110,* 3665

(45) R.G. Nuzzo, B.R. Zegarski and L.H. Dubois, *J. Am. Chem. Soc,* **1987,** *109,* 733

(46) R. A. Marcus, *J. Chem. Phys.* **1956**, *24*, 966

(47) R. A. Marcus *J. Chem. Phys.* **1957,** *26*, 867

(48) R. A. Marcus *J. Chem. Phys.* **1957,** *26*, 872

(49) R. A. Marcus *Trans. N. Y. Acad. Sci.* **1957.** *19*, 423

(50) R. A. Marcus *Can. J. Chem.* **1958**, *36*, 102

(51) R. A. Marcus *Can. J. Chem.* **1959**, *37*, 155

(52) R. A. Marcus *Discussions Faraday Soc.* **1960**, *29*, 21

(53) R. A. Marcus *Transactions of the Symposium on Electrode Processes,* E. Yeager, ed. (Wiley, New York, 1961) p. 239.

(54) R. A. Marcus *J. Phys. Chem.* **1963**, *67*, 853

(55) R. A. Marcus *Ann. Rev. Phys. Chem.* **1964,** *15*, 155

(56) R. A. Marcus *J. Chem. Phys.* **1964**, *41*, 2614

(57) R. A. Marcus *J. Chem. Phys.* **1964**, *41*, 2624

(58) R. A. Marcus *Encyclopedia of Electrochemistry*, C. A. Hampel, ed. (Reinhold, New York, 1964) p. 529.

(59) R. A. Marcus *J. Chem. Phys.* **1965**, *43*, 679

(60) R. A. Marcus *Fundamental Questions of Contemporary Theoretical Electrochemistry* (Mir Publishing, Moscow, 1965)

(61) R. A. Marcus *Advan. Chem. Ser.* **1965**, *50*, 138

(62) R. A. Marcus *J. Chem. Phys.* **1965**, *43*, 3477

(63) R. A. Marcus *Proc. Symp. Exchange Reactions* (Atomic Energy Agency 1965) p. 1.

(64) H.O. Finklea, L.R. Robinson, A. Blackburn, B. Richter, D. Allara and T. Bright, *Langmuir,* **1986**, *2*, 239.

(65) Y. Okahata, M. Yokobori, Y. Ebara, H. Ebato and K. Ariga, *Langmuir,* **1990,** *6,* 1148

(66) S. E. Creager and K. G. Olsen, Analytica Chimica Acta 307 (1995) 277-289

(67) U.B. Steiner, W.R. Caseri and U.W. Suter, *Langmuir*, **1992,** *8*, 2771

(68) J.J. Hickman, C. Zou, D. Ofer, P.D. Harvey, M.S. Wrighton,P.E. Laibinis, C.D. Bain and G.M. Whitesides, , *J. Am.Chem. Soc.*, **1989,** *111*, 7271

(69) I. Tabushi, K. Kurihara, K. Naka, K. Yamamura and H. Hatakeyama, *Tetrahedron Lett.*, **1987,** *28*, 4299

(70) Z.H. Jin, D.V. Vezenov,Y.W. Lee, J.E. Zull, C.N. Sukenik and R.F. Savinell, , *Langmuir*, **1994,** *10*, 2662.

(71) H.O. Finklea, L.R. Robinson, A. Blackburn, B. Richter, D. Allara and T. Bright, *Langmuir*, **1986** *2*, 239.

(72) D.L. Allara, A.N. Parikh and F. Rondelez, *Langmuir*, **1995**, *11*, 2357.

(73) M.R. Linford and C.E.D. Chidsey , *J. Am. Chem. Soc.*, **1993,** *115*, 12631.

(74) M.R. Linford, P. Fenter, P.M. Eisenberger and C.E.D. Chidsey, *J. Am.Chem. Soc.*, **1995,** *117*, 3145

(75) S.D. Evans, K.E. Goppert-Bearducci, E. Urankar, L.J. Gerenser and A. Ulman, *Langmuir,* **1991,** *7*, 2700

(76) L.-H. Guo, J.S. Facci, G. McLendon and R. Mosher, *Langmuir,* **1994,** *10*, 4588

(77) S.E. Creager, L.A. Hockett and G.K. Rowe, *Langmuir,* **1992,** *8*, 854

(78) S. Steinberg, Y. Tor, E. Sabatini and I. Rubenstien, *J. Am. Chem. Soc.* **1991,** *113,* 5176

(79) S. Steinberg and I. Rubenstien, *Langmuir,* **1992,** *8,* 1183

(80) C. D Bain, E. B Troughton, Y. T Tao, J Evall, G. M Whitesides, and R. G Nuzzo,. *J. Am. Chem. Soc.* **1989**, *111*, 321.

(81) K. A Peterlinz and R. Georgiadis, *Langmuir* **1996**, *12*, 4731.

(82) O. Dannenberger, J.J. Wolff and M. Buck, *Langmuir* **1998**, *14*, 4679.

(83) T. W. Schneider and D. A. Buttry. *J. Am. Chem. Soc.* **1993**, *115*, 12391.

(84) T. Ishida, W. Mizutani, H. Azehara, F. Sato, N. Choi, U. Akiba, M. Fujihira and H. Tokumoto. *Langmuir* **2001**, *17*, 7459.

(85) R. Yamada, H. Wano and K. Uosaki, *Langmuir* **2000**, *16*, 5523

(86) G.M. Whitesides and P.E Labinis, *Langmuir,* **1990,** *6,* 87

(87) C.D. Bain, E.B. Troughton, Y.-T. Tao, J. Evall, G.M. Whitesides and R.G. Nuzzo, *J. Am. Chem. Soc,* **1989,** *111,* 321

(88) H.A. Biebuyck, C.D. Bain and G.M. Whitesies, *Langmuir,* **1994,** *10,* 1825

(89) C. E. D Chidsey. *Science,* **1991**, *251*, 919.

(90) L. Sun and R.M. Crooks, *J. Electrochem. Soc.* **1991**, *138*, L23-L25

(91) C.E.D. Chidsey, C.R. Bertozzi, T.M. Putvinski and A.M. Mujsce, *J. Am. Chem. Soc.* **1990**, *112*, 4301

(92) N. Muskal and D. Mandler, *Electrochim. Acta* **1999**, *45*, 537.

(93) G.E. Poirier and E.D. Pylant, *Science*, **1996,** *272,* 1145

(94) O. Chailapakul, L. Sun, C. Xu, R.M. Crooks, *J. Am. Chem. Soc*, **1993,** *115*, 12459

(95) F. Ma and R. B, Lennox, *Langmuir* **2000,** *16,* 6188

(96) R. Bilewicz and M. Majda, *Langmuir*, **1991,** *7*, 2794

(97) P. Krysinski, R.V. Chamberlain and M. Majda, *Langmuir*, **1994,** *10*, 4286

(98) R. Bilewicz, T. Sawaguchi, R.V. Chamberlain and M. Majda, *Langmuir*, **1995,** *11*, 2256

(99) D.J. Lavrich, S.M. Wetter, S.L. Bernasek and G.J. Scholes, *J. Phys. Chem. B,* **1998,** *102,* 3456

(100) M. Hasan, D. Bethel and M. Brust, *J. Am. Chem. Soc,* **2002,** *124,* 1132

(101) J.-G. Lee, J. Lee and J.T. Yates, *J. Am. Chem. Soc,* **2004,** *126,* 440

(102) C.A. Widrig, C. Chung, and M.D. Porter, *J. Electroanal. Chem. Interfacial Electrochem.* **1991,** *310,* 335

(103) C.E.D Chidsey and D.N. Loiacono, *Langmuir* **1990**, *6*, 682.

(104) R.G Nuzzo, E.M Korenic and L. H Dubois,. *J. Chem. Phys.* **1990**, *93*, 767.

(105) L.-J Wan. Y. Hara, H Noda and M. Osawa,. *J. Phys. Chem. B,* **1998**, *102*, 5943.

(106) M.F. Danisman, L. Casalis, G. Bracco and G. Scoles, *J. Phys. Chem. B,* **2002**, *106*, 11771.

(107) N. Camillone, C.E.D Chidsey, G.-Y. Liu and G. Scoles,. *J. Chem. Phys.* **1993**, *98*, 3503.

(108) D.M. Collard and M.A. Fox, *Langmuir,* **1991,** *7,* 1192

(109) J.P. Bareman and M.L. Klein,. *J. Phys. Chem.* **1990**, *94*, 5202.

(110) M.K. Ferguson, E.R. Low and J.R. Morris, *Langmuir,* **2004,** *20,* 3319

(111) J.H. Kim, H. S. Shin, S.B. Kim and Takeshi Hasegawa, *Langmuir,* **2004,** *20,* 1674

(112) M.A Bryant and J.E Pemberton. *J. Am. Chem. Soc.* **1991**, *113*, 8284.

(113) K. Slowinski, R. V Chamberlain, C. J Miller and M. Majda, *J. Am. Chem. Soc.* **1997**, *119*, 11910.

(114) P. Fenter, P. Eisenberger and K.S. Liang, *Phys. Rev. Lett.* **1993**, *70*, 2447.

(115) S. Frey, V. Stadler, K Heister, W. Eck, M. Zharnikov, M. Grunze, B. Zeysing, and A. Terfort, *Langmuir* **2001**, *17*, 2408.

(116) R.G Nuzzo, L.H Dubois and D.L Allara,. *J. Am. Chem. Soc.* **1990**, *112*, 558

(117) P.E Laibinis, G.M Whitesides, D.L Allara, Y.-T Tao, A.N Parikh and R.G Nuzzo,. *J. Am. Chem. Soc.* **1991**, *113*, 7152

(118) T.-W Li, I. Chao and Y.-T. Tao,. *J. Phys. Chem. B,* **1998**, *102*, 2935

(119) M.M. Walczak, C. Chung, S.M Stole, C.A Widrig and M.D Porter,. *J. Am. Chem. Soc.* **1991**, *113*, 2370

(120) A.N. Parikh and D.L Allara,. *J. Chem. Phys.* **1992**, *96*, 927

(121) S.-S Wong,. H. Takano and M.D Porter, *Anal. Chem.* **1998**, *70*, 5209

(122). A. Lee, M. Puck, M. Graupe, R. Colorado, Y.-S. Shon, T. R. Lee, and S. S. Perry, *Langmuir* **2001,** *17*, 7364-7370

(123) I. Wenzl, C.M. Yam, D. Barriet and T. R Lee, *Langmuir* **2003**, *19*, 10217.

(124) S. Lee, A Puck, M Graupe, R Colorado, Y.-S. Shon, T.R Lee and S.S Perry, *Langmuir* **2001**, *17*, 7364.

(125) F. Schreiber, *Prog. Surf. Sci,* **2000,** *65,* 151.

(126) G.E. Poirer, *Chem. Rev.***1997,** *97,* 1117.

(126) G.E. Poirier, *Langmuir* **1997**, *13*, 2019.

(128) L. Sun and R.M. Crooks, *Langmuir* **1993**, *9*, 1951.

(129) C. O'Dwyer, G. Gay, B.V. de Lesegno, and J. Weiner, *Langmuir* **2004**, *20*, 8172.

(130) L. Haussling, B. Michel, H. Ringsdorf, and H.Rohrer, *Angew. Chem., Int. Ed. Engl.* **1991**, *30*, 569.

(131) K. Edinger, A. Golzhauser, K. Demota, C. Woll and M. Grunze,. *Langmuir* **1993**, *9*, 4.

(132) O. Chailapakul, L. Sun, C. Xu and R.M. Crooks, *J. Am. Chem.Soc.* **1993**, *115*, 12459.

(133) G. Yang and G.-Y. Liu, *J. Phys. Chem. B* **2003**, *107*, 8746.

(134) G. E Poirier and M.J. Tarlov, *J. Phys. Chem.* **1995**, *99*, 10966.

(135) N. Camillone, *J. Chem. Phys.* **1994**, *101*, 11031.

(136) R. Bhatia and B. J. Garrison, *Langmuir* **1997**, *13*, 765.

(137) S.E. Creager and K.G. Olsen, *Analytica Chimica Acta*, **1995**, *307*, 277.

(138) M.A. Hines, J.A. Todd and P. Guyot-Sionnest, *Langmuir*, **1995**, *11*, 493

(139) S.M. Stole and M.D. Porter, *Langmuir*, **1990**, *6*, 1199.

(140) M.R. Anderson and M. Gatin, *Langmuir*, **1994**, *10*, 1638

(141) T.H. Ong, R.N. Ward, P.B. Davis and C.D. Bain, *J. Am. Chem. Soc*, **1992**, *114*, 6432

(142) T.H. Ong, P.B. Davis and C.D. Bain, *Langmuir*, **1993**, *9*, 1836

(143) M. Zhang and R.M. Anderson, *Langmuir*, **1994**, *10*, 2807

(144) E.U. Thoden van Velzen, J. F. J. Engbersen, and D. N. Reinhoudt, *J. Am. Chem. Soc.* **1994**,*116*, 3597

(145) C.A. Alves and M.D. Porter, *Langmuir*, **1993**, *9*, 3507

(146) Y.S. Obeng, M.E. Lang, A.C. Freidli, H.C. Yang, D.N. Wang, E.W. Thulstrup, A.J. Bard and J. Michl., *J.Am. Chem. Soc*, **1992**, *114*, 9943.

(147) W.S.V. Kwan, L. Atanasoska and L.L. Miller, *Langmuir*, **1991**, *7*, 1419.

(148) L. Zhang, T. Lu, G.W. Gokel, and Angel E. Kaifer, *Langmuir*, **1993**, *9*, 786

(149) D.N. Batchelder, S.D. Evans, T.L. Freeman, L.Haussling, H. Ringsdorf and H. Wolf, *J. Am. Chem. Soc*, **1994**, *116*, 1050

(150) R. J. Willicut and R. L. McCarley, *J. Am. Chem. Soc.* **1994**,***116***, 10823.

(151) J. Wang, P.V.A. Pamidi, and D.R. Zanette, *J. Am. Chem. Soc.* **1998**, *120*, 5852

(152) M. A. Fox and M. D. Wooten, *Langmuir* **1997**, *13*, 7099-7105

(153) W. Li, V. Lynch, H. Thompson, and M. A. Fox, *J. Am. Chem. Soc.* **1997**, *119*, 7211

(154) R. Paul, R. Schmidt, and D. J. Dyer, *Langmuir* **2002**, *18*, 23

(155) T. J. Lenk, V. M. Hallmark, J. F. Rabolt, L. Hlussling and H. Ringsdorf, *Macromolecules* **1993**, *26*, 1230

(156) C. Erdelen, L. Haussling, R. Naumann, H. Ringsdorf, H. Wolf, J. Yang, M. Liley, J. Spinke, and W. Knoll, *Langmuir* **1994**,*10*, 1246

(157) M. Niwa, T. Mori, and N.Higashi, *Macromolecules*, **1993**, *26*, 1936

(158) F. Sun, D.G. Castner, and D. W. Grainger, *Langmuir* **1993**,*9*, 3200

(159) F. Sun, D. W. Grainger, D. G. Castner, and D. K. Leach-Scampavia, *Macromolecules* **1994**, *27*, 3053.

(160) C. Miller, P. Cuendet, and M. Gratzel, *J. Phys. Chem.* **1991**, *95*, 877

(161) A. L. Plant, *Langmuir* **1993**, *9*, 2764

(162) S.D. Evans and A. Ulman, *Chem Phys Lett*, **1990**, *170*, 462

(163) A.M. Becka and C.J. Miller, *J. Phys. Chem*, **1993**, *97*, 6233

(164) J.A. M. Sondag-Huethorst and L.G.J. Fokkink, *Langmuir*, **1992**, *8*, 2560

(165) C.P. Smith and H.S. White, *Anal. Chem*, **1992**, *64*, 2398

(166) C.P. Smith and H.S. White, *Langmui*, **1993**, *9*, 1

(167) W.R. Fawcett, *J. Electroanal. Chem.* **1994**, *378*, 117

(168) W.R. Fawcett and R. Andrew, *J. Phys. Chem.* **1994**, *98*, 12753

(169) C. -J. Zhong and M.D. Porter, *J. Am. Chem. Soc.***1994**, *116*, 11616

(170) D.E. Weisshaar, M.M. Walczak and M.D. Porter, *Langmuir*, **1993**, *9*, 323

(171) M.M. Walczak, D.D. popenoe, R.S. Deinhammer, B.D. Lamp, C.Chung and M.D. Porterm *Langmuir*, **1991**, *7*, 2687

(172) D.E. Weisshaar, B.D. Lamp and M.D. Porter, *J. Am. Chem. Soc*, **1992**, *114*, 5860.

(173) J. Pan, N. Tao and S.M. Lyndsay, *Langmuir*, **1993**, *9*, 1556

(174) N.L. Abbott, C.B. Gorman and G.M. Whitesides, *Langmuir*, **1995**, *11*, 16

(175) G. K Jennings, T.-H Yong, J. C Munro and P. E Laibinis,. *J. Am. Chem. Soc.* **2003**, *125*, 2950.

(176) D. M Adams, L Brus, C. E. D Chidsey, S Creager, C Creutz, C. R Kagan, P.V Kamat, M Lieberman, S Lindsay, R. A Marcus, R. M Metzger, M. E Michel-Beyerle, J. R Miller, M.D Newton, D. R Rolison, O. Sankey, K. S Schanze, J Yardley and X. Zhu, *J. Phys. Chem. B* **2003**, *107*, 6668.

(177) E. Ostuni, L. Yan and G. M. Whitesides *Colloids Surf. B*, **1999**,*15*, 3.

(178) M. Mrksich. *Curr. Opin. Chem. Biol.* **2002**, *6*, 794.

(179) Y. Xia, X.-M Zhao and G. M. Whitesides, *Microelectron. Eng.* **1996**,*32*, 255.

(180) Y. Xia, X.-M. Zhao, E. Kim and G. M Whitesides. *Chem. Mater.***1995**, *7*, 2332.

(181) Y. Xia, E. Kim, M. Mrksich and G. M. Whitesides *Chem. Mater.***1996**, *8*, 601.

(182) M. Geissler, J.Chen and Y. Xia, *Langmuir* **2004**, *20*, 6993.

(183) X.-M Zhao, J.L. Wilbur and G. M. Whitesides *Langmuir* **1996**,*12*, 3257.

(184) S. Wolf, *Silicon Processing for the VLSI Era*; Lattice Press: Sunset Beach, **1990**.

(185) J. M. Beebe, V. B. Engelkes, L. L Miller and C. D. Frisbie. *J. Am.Chem. Soc.* **2002**, *124*, 11268.

(186) H.O Finklea, M.S. Ravenscroft and D.A. Snider, *Langmuir* **1993**,*9*, 223.

(187) H.O. Finklea, *J. Phys. Chem. B* **2001**, *105*, 8685

(188) C. Cannes, F Kanoufi, A. J. Bard, *Langmuir* **2002**, *18*, 8134.

(189) G.K. Rowe, S. E. Creager *J. Phys. Chem.* **1994**, *98*, 5500

(190) D.L. Pilloud, X. Chen, P. L Dutton, C.C Moser, *J. Phys. Chem. B*, **2000**, *104*, 2868.

(191) R.A, Wassel, G.M. Credo, R.R. Fuierer, D.L. Feldheim and C. B. Gorman *J. Am. Chem. Soc.* **2004**, *126*, 295

(192) A. Salomon, D. Cahen S.Lindsay, J. Tomfohr, V.B Engelkes and C. D. Frisbie, *Adv. Mater.* **2003**, *15*, 1881.

(193) A. Nitzan and M.A. Ratner, *Science (Washington, D.C.)* **2003**, *300*,1384. Reed, M. A. *Nat. Mater.* **2004**, *3*, 286.

(194) M. A. Rampi and G. M. Whitesides, *Chem. Phys.* **2002**, *281*, 373.

(195) T Lee. W. Wang, J. F.Klemic, J. J. Zhang, J. Su and M.A. Reed *J. Phys. Chem. B.* **2004**, *108*, 8742.

(196) W. Wang, T. Lee and M. A Reed. *Phys. Rev. B: Condens. Matter* **2003**, *68*, 035416/1.

(197) L.T. Cai, H. Skulason, J.G. Kushmerick, S.K. Pollack, J. Naciri, R. Shashidhar, D.L. Allara, T.E. Mallouk and T. S. Mayer, *J. Phys. Chem. B* **2004**, *108*, 2827.

(198) M. A Reed, C. Zhou, C. J. Muller, T. P Burgin and J. M Tour,. *Science (Washington,D.C.)* **1997**, *278*, 252

(199) W. Liang, M.P. Shores, M. Bockrath, J. R Long. and H. Park *Nature (London)* **2002**, *417*, 725.

(200) S Chen and R. W. Murray, *J. Phys. Chem. B* **1999**, *103*, 9996.

(201) N.B. Zhitenev, A. Erbe and Z. Bao. *Phys. Rev. Lett.* **2004**, *92*.

(202) B de Boer, M. M Frank, Y. J Chabal,, W. Jiang, E Garfunkel and Z Bao, *Langmuir* **2004**, *20*, 1539.

(203) J. Ulrich, D. Esrail, W. Pontius, L. Venkataraman, D. Millar and L. H. Doerrer, **2006,** *110*, 2462.

(204) C. Zhou, M.R. Deshpande, M.A. Reed, L. Jones and J. M Tour. *Appl. Phys. Lett.* **1997**, *71*,611

(205) J. Chen, L.C. Calvet, M.A. Reed, D.W. Carr, D.S. Grubisha and D.W. Bennett. *Chem. Phys. Lett.* **1999**, *313*, 741.

(206) W. Wang, T. Lee and M.A Reed, *J. Phys. Chem. B.* **2004**, *108*,18398.

(207) K. Slowinski and M. Majda. *J. Electroanal. Chem.* **2000**, *491*, 139.

(208) M. Galperin, A. Nitzan, S. Sek, and M. Majda. *J. Electroanal.Chem.* **2003**, *337*. 550

(209) C. Pale-Grosdemange, E.S. Simon, K.L. Prime and G.M. Whitesides,. *J. Am. Chem. Soc.* **1991**, *113*, 12

(210) P. Harder, M. Grunze, R. Dahint, G.M Whitesides and P.E. Laibinis, *J. Phys. Chem. B*, **1998**, *102*, 426.

(211) M. Zwahlen, S. Herrwerth, W. Eck, M. Grunze and G. Haehner, *Langmuir* **2003**, *19*, 9305.

(212) F. Frederix, K. Bonroy, W. Laureyn, G. Reekmans, A. Campitelli, W. Dehaen and G. Maes, *Langmuir* **2003**, *19*, 4351

(213) E. Ostuni, B.A. Grzybowski, M. Mrksich, C.S. Roberts and G.M. Whitesides, G. M. *Langmuir* **2003**, *19*, 1861.

(214) J. Lahiri, L. Isaacs, B. Grzybowski, J.D. Carbeck and G.M. Whitesides,. *Langmuir* **1999**, *15*, 7186.

(215) N.T. Flynn, T.N.T. Tran, M.J. Cima and R.Langer, *Langmuir*, **2003**, *19*, 10909.

(216) Y.-S. Lee and M. Mrksich,. *Trends Biotechnol.* **2002**, *20*, S14

(217) K.R. Love and P.H. Seeberger, *Angew. Chem., Int. Ed. Engl.* **2002**,*41*, 3583.

(218) D.M. Jones and W.T.S. Huck, *Adv. Mater.* **2001**, *13*, 1256.

(219) C. Roberts, C.S. Chen, M. Mrksich, V. Martichonok, D.E. Ingber, and G.M. Whitesides, *J. Am. Chem. Soc.* **1998**, *120*, 6548.

(220) X. Jiang, R. Ferrigno, M. Mrksich and G.M. Whitesides, *J. Am.Chem. Soc.* **2003**, *125*, 2366.

(221) W.-S. Yeo and M. Mrksich, *Angew. Chem., Int. Ed. Engl.* **2003**, *42*,3121.

(222) R. Valiokas, S. Svedhem, S.C.T. Svensson and B. Liedberg, *Langmuir* **1999**, *15*, 3390

(223) D. Schwendel, R. Dahint, S. Herrwerth, M. Schloerholz, W. Eck and M. Grunze, *Langmuir***2001**, *17*, 5717

(224) L. Deng, M. Mrksich and G.M. Whitesides, *J. Am. Chem. Soc.***1996**, *118*, 5136.

(225) J. Fick, R. Steitz, V. Leiner, S. Tokumitsu, M. Himmelhaus and M. Grunze, *Langmuir* **2004**, *20*, 3848.

(226) R. Valiokas, S. Svedhem, M. Oestblom, S.C.T. Svensson and B. Liedberg, *J. Phys. Chem. B* **2001**, *105*, 5459.

(227) R. S. Freire, C. A. Pessoa, L. D. Mello and L. T. Kubota, *J. Braz. Chem. Soc.*, **2003**, *14*, 230).

(228) J. J. Gooding and D. B. Hibbert, *Trends Anal. Chem.***1999**, *18*, 525.

(229) I. Willner and E. Katz, *Angew. Chem.-Int. Edit.* **2000**, *39*, 1181.

(230) J. J. Gooding, P. Erokhin, D. Losic, W. R. Yang, V.Policarpio, J. Q. Liu, F. M. Ho, M. Situmorang, D. B.Hibbert, and J. G. Shapter, *Anal. Sci.* **2001**, *17*, 3.

(231) J. J. Gooding, P. Erokhin and D. B. Hibbert, *Biosensors Bioelectronics*, **2000**, *15*, 229.

(232) T. Lotzbeyer, W. Schuhmann and H.-L. Schmidt, *Sensors Actuators* **1996**, *B33*, 50.

(233) L. Jiang, C. J. McNeil and J. M. Cooper, *Chem. Commun.* **1995**,1293.

(234) I. Willner, V. Heleg Shabtai, R. Blonder, E. Katz and G. L. Tao, *J. Am. Chem. Soc.* **1996**, *118*, 10321.

(235) S. Creager, C. J. Yu, C. Bamdad, S. O7Connor, T. MacLean, E. Lam, Y. Chong, G. T. Olsen, J. Luo, M. Gozin and J. F.Kayyem, *J. Am. Chem. Soc.* **1999**, *121*, 1059.

(236) S. O. Kelley, N. M. Jackson, M. G. Hill and J. K. Barton, *Angew.Chem. Int. Ed.* **1999**, *38*, 941.

(237) F. Lisdat, B. Ge and F.W. Scheller, *Electrochem. Commun.***1999**, *1*, 65.

(238) E. Katz, A. F. Buckmann and I. Willner, *J. Am. Chem. Soc.* **2001**, *123*, 10752.

(239) J. Spinke, M. Liley, H. J. Guder, L. Angermaier and W. Knoll, *Langmuir* **1993**, *9*, 1821.

(240) R. Levicky, T. M. Herne, M. J. Tarlov and S. K. Satija, *J. Am.Chem. Soc.* **1998**, *120*, 9787.

(241) A. Bardea, F. Patolsky, A. Dagan andI. Willner, *Chem.Commun.* **1999**, 21.

(242) S.Takenaka, K. Yamashita, M. Takagi, Y. Uto and H. Kondo, *Anal. Chem.* **2000**, *72*, 1334.

(243) R. M. Umek, S.W. Lin, J. Vielmetter, R. H. Terbrueggen, B.Irvine, C. J. Yu, J. F. Kayyem, H. Yowanto, G. F. Blackburn,D. H. Farkas and Y. P. Chen, *J. Mol. Diagn.* **2001**, *3*, 74.

(244) J. J. Hickman, D. Ofer, P. E. Laibinis and M. S. Wrighton, *Science 1991*, *252*, 688.

(245) M. W. J. Beulen, F. C. J. M. van Veggel and D. N. Reinhoudt, *Chem. Commun.* **1999**, 503.

(246) I. Willner, A. Bardea and E. Katz, *Electroanalysis*, **2000**, *12*, 731.

CHAPTER 2 –

EXPERIMENTAL THEORY AND METHODOLOGY

2. General Theory and Experimental Methodologies

2.1 The Electrochemical Cell

The electrochemical cell consists primarily of a working vessel, electrodes and an electrolyte solution. A cell top with inlets for the electrodes and a gas purger sealed the working vessel at all times. Solutions were degassed with inert nitrogen gas for approximately 15 minutes before experimentation to remove any dissolved atmospheric gasses. The dissolved atmospheric gases, particularly oxygen, are replaced with nitrogen, which is inert over the potential range of the experiments.

2.1.1 Working Electrode

In electrochemical cells the experimental data observed is determined by the reaction occurring at the working electrode. Designs of working electrodes are diverse. Preferentially they will be smooth, symmetrical and importantly they will be chemically inert with respect to the solvent or solution components. The useful working range of working electrodes is difficult to define as it can be complicated by oxygen and hydrogen evolution or solvent decomposition. It also depends on the reactants and products being studied.

Gold macroelectrodes supplied by IJ Cambria with a substrate area of $0.0314cm^2$ were used to carry out electrochemical measurements that did not require EQCM data. Experiments requiring EQCM were carried out on a gold working electrode with an area of $0.196cm^2$.

2.1.2 Reference Electrode

The purpose of the reference electrode is to provide a fixed potential which is invariant with respect to time during the experiment. Thus any change in potential appears at the working electrode/solution interface. Common reference electrodes are the saturated calomel electrode, the normal hydrogen electrode (NHE) and the silver/silver chloride electrode. An Ag/AgCl reference electrode supplied by IJ Cambria was used in this report. The electrode was stored in a 3M solution of KCl when not in use.

2.1.3 Auxiliary Electrode

The purpose of the auxiliary/counter electrode is to supply the current required by the working electrode without in any way limiting the measured response of the cell. The counter electrode should not impose any characteristics on the measured data. In this work a platinum wire supplied by IJ Cambria was used as the counter electrode.

2.1.4 Electrolyte Solutions

The electrolyte solution is the medium between the electrodes in the cell. It consists of a solvent and a high concentration of ionised salt. The supporting electrolyte is present for three reasons. Firstly it increases the conductivity of the solution and hence reduces the resistance between the working and the counter electrode as well as reducing potential error because of uncompensated solution resistance. Secondly it minimises the potential of the outer Helmholtz plane hence reducing the amount of charge transfer occurring due to the potential difference between the metal surface and the outer Helmholtz plane. Thirdly it eliminates migration as a mode of mass transport for the electroactive species. If the ions of the supporting electrolyte are present in large excess over the electroactive species they will transport the majority of charge through the solution.

Unless otherwise stated 0.1M solutions of perchloric acid (70%, Merck) were used as the electrolyte in this work.

2.1.5 Materials

Ferrocenylcarbonyloxy-hexanethiol, Ferrocenylcarbonyloxy-octanethiol, Ferrocenylcarbonyloxy-decanethiol, Ferrocenylcarbonyloxy-undecanethiol and Ferrocenylcarbonyloxy-dodecanethiol were synthesised by Ray O'Brien and Conchiur MacGloinn according to the method described by Napper et al.[1]. Dr. John O'Brien verified the structures via ^{1}H NMR.

2.2 Instrumentation

2.2.1 CHI Workstation

A CH Instruments Model 440 Electrochemical Quartz Crystal Microbalance was used to gather all electrochemical data. The system contains a quartz crystal oscillator, fast digital function generator, high speed data acquisition circuitry, a potentiostat and a galvanostat. The potential control range of the instrument is ±10V and the current range is ±250mA. Data was processed using an Advent 3036A Model W0311 Pentium 3 processor PC.

2.3 Electrode Modification Techniques

2.3.1 Electrode Pre-Treatment

In this work the surface of gold macroelectrodes were renewed by carrying out a standard polishing procedure prior to experiments to produce a reproducible surface morphology and freedom from adsorbed impurities as verified by CV

The polishing kit used in this surface renewal contained a range of alumina polishing powders and a range of polishing pads composed of different material. The polishing powders used were: 1.0 micron Alpha alumina powder, 0.3 micron Alpha alumina powder and 0.05 micron Alpha alumina powder. Three polishing pads were used. These were composed of: 1200 grit Carbimet disks, Nylon and Microcloth. All pads were discs and were 73mm in diameter.

In order to polish the gold macroelectrodes they were first rotated in a figure of eight motion on bare Carbimet pads for 1minute in order to remove any visible scratches if they existed. Such scratches were rare and normally occurred only if an electrode was accidentally dropped. If no scratches were visible this polishing stage was not carried out. Following this the electrodes were polished in a figure of eight motion for one minute on the Nylon polishing pads covered with a paste made from 1.0 micron alumina powder and Milllipore water. The electrodes were then thoroughly rinsed with Millipore water and transferred to a separate Nylon polishing pad covered with a paste made from 0.3 micron alumina powder and Milllipore water. Again they a figure of eight motion for 1 minute was used for polishing. The electrodes were again thoroughly rinsed in Millipore water. Finally the electrodes

were transferred to a Microcloth polishing pad covered with a paste made from 0.05 micron alumina powder and Milllipore water. Again a figure of eight motion for 1 minute was used for polishing. This completed the electrode surface renewal. Normally the electrodes were rinsed again with Millipore before being inserted into the electrochemical cell.

Due to the nature of the EQCM gold electrodes it was not possible to use this polishing step. The EQCM electrodes are delicate and only a thin film of gold is deposited on the surface. Any polishing step would certainly have stripped the gold layer from the crystal. The EQCM crystals were instead placed in 3.6% HCl for 5 minutes then rinsed with copious amounts of millipore water and finally rinsed with copious amounts of the solvent chosen to deposit the monolayer. This approach yielded reproducible surface morphology as verified by CV.

2.3.2 Monolayer Deposition

Following the cleaning steps described in *Section 2.3.1* the electrodes were ready for the deposition of alkanethiol monolayers. There are numerous methods of depositing alkanethiol monolayers. As well as solution adsorption alkanethiols may be deposited form the vapour phase both in vacuum[2] and at ambient pressures[3] providing the thiol is sufficiently volatile. The resulting SAMs appear identical to those formed from the solution phase. Lennox et al.[4] reported that alkanethiols could be quickly and reliably assembled onto gold surfaces by holding the potential of the working electrode in thiol solution for a period of as little as 15 minutes. This method was attempted but as yet failed to give reproducible monolayer formations.

The method used in this work was solution adsorption. Firstly the electrodes were rinsed with copious amounts of the solvent of choice. The gold electrodes were then immersed in a 1mM solution of alkanethiol for a period of 48 hours. Upon removal from the thiol solution the electrodes were again rinsed with copious amounts of solvent to remove any physisorbed species. Thiols were prepared using ethanol, methanol, hexane, toluene and acetonitrile. The most common solvent used was ethanol due to its faint odour, low toxicity and ready availability. The typical experimental setup for solution adsorption is shown in Figure 2.1.

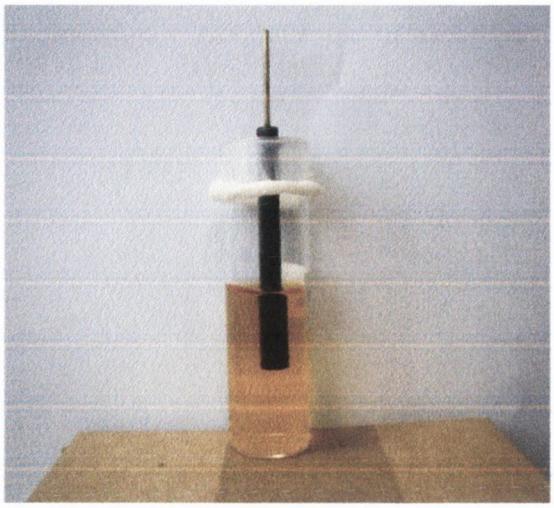


Figure 2.1. Typical Adsorption of a self-assembled monolayer onto a gold macroelectrode.

2.4 Experimental Techniques

The experimental techniques that are widely used in this work are Cyclic Voltammetry (CV), Chronoamperometry (CA) and Electrochemical Quartz Crystal Microbalance (EQCM). For this reason an introduction to the theory behind each of the techniques will now be given.

2.4.1 Cyclic Voltammetry

Cyclic voltammetry is a type of potentiodynamic electrochemical measurement. A specific type of voltammetry, it is used to normally used in studies of the redox properties of chemicals as well as in the study of interfacial structures.

Cyclic voltammetry essentially involves applying a time dependant potential between two limits (E_1 and E_2) to the working electrode and measuring the resulting current response. The rate at which the potential is swept between these two limits is defined by the scan rate, ν. The shape of this waveform is sometimes known as a 'sawtooth' waveform and is shown in Figure 2.2.

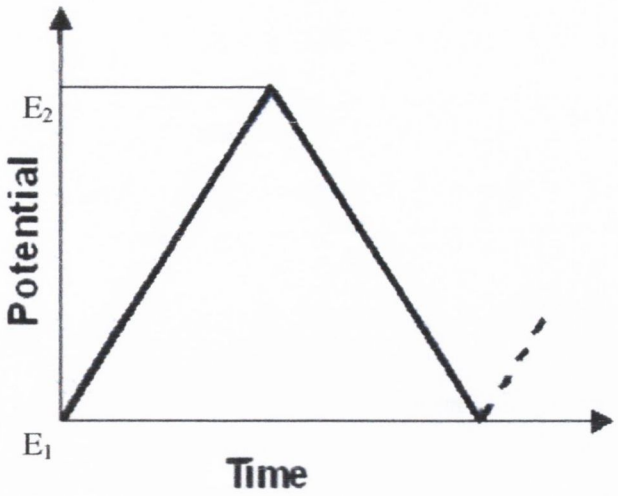


Figure 2.2. Illustration of the potential sweep waveform associated with cyclic voltammetry between two voltage limits E1 and E2

Data from cyclic voltammetry experiments are usually plotted as current against voltage and from such plots it is possible to derive a wealth of information regarding the exact nature of redox couples in solution or in special cases surface bound redox centres. A wide array of literature is available to detail the theory of cyclic voltammetry. A particularly good review is given in a text by Southampton[5] and for this reason the following discussion of cyclic voltammetry will present a summary of this work.

When considering cyclic voltammetry experiments electrochemical systems may be broadly classified into three specific categories. These are reversible, irreversible and quasi-reversible. Reversible and irreversible systems will now be discussed in turn and the obvious extension to quasi-reversible systems will be outlined.

2.4.1.1 Reversible Systems

Inn order to describe both reversible and irreversible systems using cyclic voltammetry it is first necessary to describe how the shape of a typical cyclic voltammogram is achieved. This will be based on the simple reversible reaction in Equation 2.1 below.

$$R + ne^- \Phi P \qquad (2.1)$$

Consider the case of linear diffusion of either R or P to a planar electrode driven by a change in potential of the electrode which catalyses Equation 2.1. Changes in the

concentration of R and P are assumed to occur perpendicular to the electrode only. This being the case the diffusion of either R or P to the surface can be described by Fick's Law that states that the flux through any plane parallel to the electrode surface is directly proportional to the concentration gradient at that plane. This is described in Equation 2.2.

$$Flux = -D_i \frac{dc_i}{dx} \tag{2.2}$$

Where D_i is the diffusion coefficient of a species i, c_i is the concentration of species i and x, to all intents and purposes, is the distance from the electrode. Fick's Law can be used to relate the current to the chemical change at the electrode by relating the flux of R and P to the flux of electrons. This is shown in Figure 2.3 below.

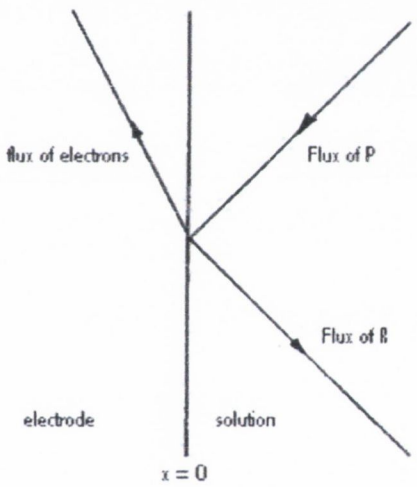


Figure 2.3. Schematic illustration of the flux of product (P) and reactant (R) to the surface of an electrode leading to the flow of electrons.

The resulting currents attributed to the product and the reactant can be simply derived and are given in Equation 2.3. Thus it has been determined that the current that is registered at the electrode is directly proportional to the concentration gradient of either the product or reactant described in Equation 2.1 at the electrode surface.

$$\frac{I}{nF} = -D_R \left(\frac{\partial c_R}{\partial x} \right)_{x=0} \quad \text{and} \quad \frac{I}{nF} = D_P \left(\frac{\partial c_P}{\partial x} \right)_{x=0} \tag{2.3}$$

This treatment will now be used to describe the cyclic voltammetry of a reversible system. Imagine at first the steady state response. In this case the ratio of the reactant, (R) and product, (P), are determined by the Nernst equation and are said to be in Nernstian Equilibrium. Should the potential at the electrode surface be made more negative slowly (slow potential sweep rate) R will be reduced and thus its surface concentration will be decreased. Due to this a concentration gradient will be established between the reactant at the electrode surface and the reactant in the diffusion layer. This gradient will cause a current increase to be recorded. When the diffusion has alleviated this gradient the current will cease to rise and plateau. Imagine the case now where the potential sweep in much larger. Now the diffusion layer is not given sufficient time to relax as it did at slow sweep rates. When the electrode potential is such that it can reduce the reactant, (R), a concentration gradient is again established. A current proportional to the gradient will flow. As the sweep rate is increased the concentration gradient established rises and increasing peak heights are observed in the CV response. At a certain stage in the voltammetric sweep the concentration gradient will begin to decrease due to diffusion and the recorded current will fall. This effect is slightly offset however by the fact that the electrode potential is continuing to change and reduce R. This effect explains the gradual diminishing of the current response after the peak until eventually the concentration of R at the surface reaches zero and the current plateaus. In a cyclic voltammetry experiment the voltage will be now swept in the reverse direction after the cathodic peak of interest has been observed. This reverse scan is interpreted in a similar way. At slow sweep rates the current response is expected to directly track the forward sweep. At higher sweep rates a different trace is observed normally exhibiting an opposite, anodic, peak to the cathodic one already observed. This is due to the fact that after the initial reduction of R the concentration of P is now in excess at the electrode. As the electrode potential is made more positive the product (P) at the surface is reoxidised back to R. Again this sets up a concentration gradient and results in a current, the reverse of the one that was initially observed. The form of the cathodic peaks for a typical reversible cyclic voltammograms is shown in Figure 2.4.

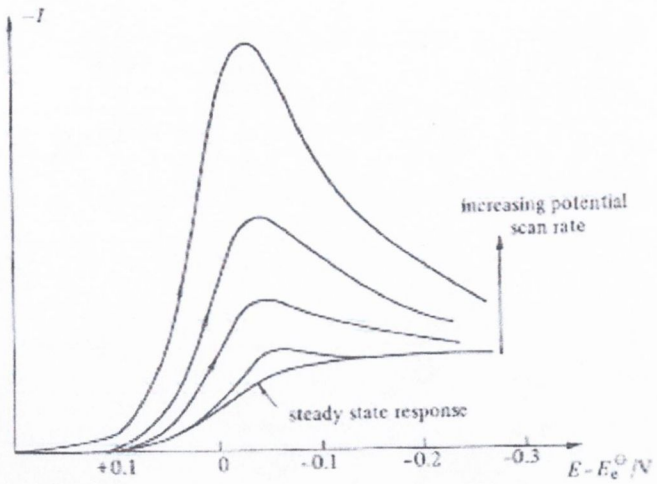


Figure 2.4. A series of linear sweep voltammograms showing how the peak current varies with increasing scan rate in a reversible system. Reproduced from Reference (4).

The exact mathematical form of a cyclic voltammogram can be described by the *Randles-Sevcik* Equation described in Equation 2.4.

$$i_p = -(2.69x10^5)n^{3/2}c_0^{3/2}D^{1/2}\nu^{1/2} \qquad (2.4)$$

Here i_p is the peak current density, n is the number of electrons transferred, c_0 is the bulk electrolyte concentration, D is the diffusion coefficient and ν is the potential sweep rate.

A direct test of whether or not a system is reversible is to plot peak current vs sweep rate. Should this plot be linear it is a good indication that the system is reversible however a number of other diagnostic tests can also be carried out. These are: (1) The potential difference between the anodic and cathodic peaks is 59/n mV. (2) The ratio of the anodic and cathodic peak currents is unity. (3) The voltage at which the anodic and cathodic peaks appear is independent of the sweep rate. (4) At potentials beyond the peak potentials Γ^2 is proportional to time.

It is important to note at this time that a reversible cyclic voltammogram is observed only if both R and P are stable and the kinetics of electron transfer are fast enough that at all potential and sweep rates the surface concentrations of R and P in solution can be calculated from the Nernst Equation, i.e. it is assumed that any R or P at the electrode surface has the ability to immediately transfer their electrons.

2.4.1.2 Irreversible Systems

In the case of reversible systems such as those described above the electron transfer rates are much greater than the rates of species diffusion and for this reason the Nernstian equilibrium is always maintained. In the case of irreversible systems the rate of electron transfer is too slow to maintain such equilibrium. Due to this the current response in reversible systems differs from that in irreversible systems.

At low potential sweep rates the rate of electron transfer is great enough that a reversible voltammetric response may be recorded. As the sweep rate is increased however and the rate of mass transport is increased the electron transfer processes are unable to keep up. The most notable effect this has on the CV response is to increase the separation between the peaks.

It is also noted that as well as an increase in peak separation a peak height decrease is also normally observed. The reason the peak height is diminished to related to the fact that in an irreversible process the peak is more drawn out. This is because the surface concentration of R changes more slowly with potential in irreversible systems.

The most marked feature of a cyclic voltammogram in totally irreversible systems is the total absence of any reverse peak. This feature however does not necessarily imply total irreversibility but may be due to a fast chemical reaction occurring upon the reduction of R. Typical cyclic voltammograms associated with irreversible systems are shown in Figure 2.5

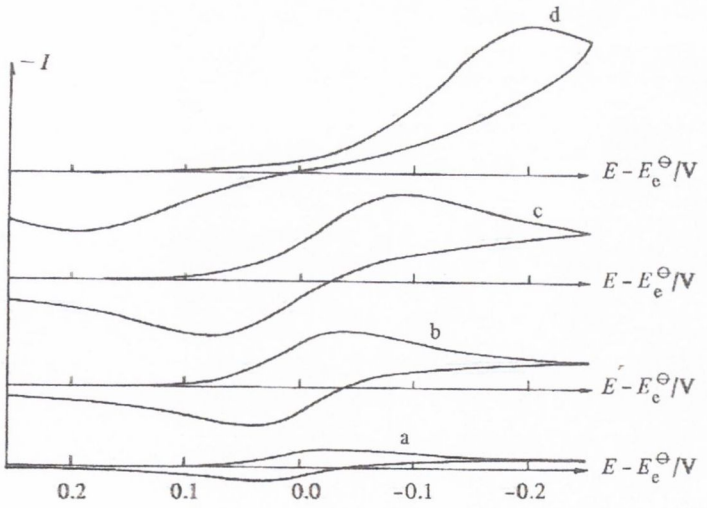


Figure 2.5. A series of cyclic voltammograms showing the change associated with an increasing scan rate in an irreversible system. (a) $0.13Vs^{-1}$, (b) $1.3Vs^{-1}$, (c) $4Vs^{-1}$and (d) $13Vs^{-1}$. Reproduced from Reference (4).

As well as an increase in peak splitting, peak broadening and the absence of a reverse peak there are three other tests for irreversibility. These are: (1) The cathodic peak current is proportional to the square root of the sweep rate. (2) The cathodic peak potential shifts $30/\alpha_c n_\alpha$ mV with each decade increase in ν. Here α_c is the cathodic electron transfer coefficient and n_α is the number of electrons transferred. (3) The difference between the average peak potential (E_p) and the average half peak potential ($E_{p/2}$) is $48/\alpha_c n_\alpha$ mV.

At this point it is necessary to also mention quasi-reversible systems. Such systems generally exhibit reversible electron transfer at low sweep rates whilst exhibiting irreversible behaviour at high sweep rates. Quasi-reversibility is essentially a middle ground between reversible and irreversible systems.

2.1.4.3 Cyclic Voltammetry of Electroactive Monolayers

Due to the fact that this work is based primarily on self-assembled monolayers with an electroactive headgroup an introduction will now be given to the response of such a monolayer to a cyclic voltammetry experiment. Particular attention will be paid to the CV response of monolayers with electroactive ferrocene headgroups. A typical CV for an electroactive monolayer is shown in Figure 2.6

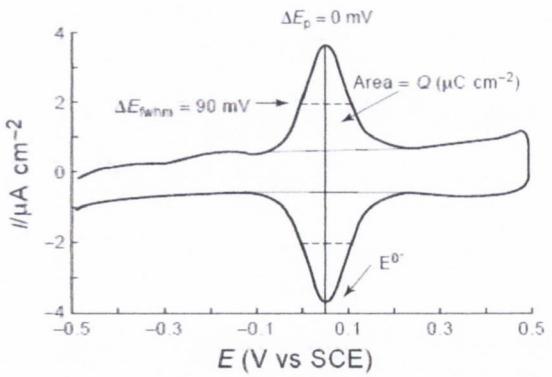


Figure 2.6. Reversible CV of an electroactive SAM. The redox thiol is $HS(CH_2)_{11}CONHCH_2pyRu(NH_3)_5^{2+/+3}$ and the diluent thiol is $HS(CH_2)_{11}COOH$. The electrolyte is 1M Na_2SO_4 at pH4. Reproduced from Reference (6).

A CV for an electroactive SAM usually exhibits matching anodic and cathodic peaks. The coverage of the redox centre, Γ, on the electrode surface may be obtained by current integration after extrapolating and subtracting the charging current baseline

underneath either the anodic or cathodic peak. The surface coverage of redox active sites on the electrode may be calculated using Equation 2.5.

$$\Gamma = \frac{Q}{nFA} \tag{2.5}$$

Where Q is the peak area in coulombs, n is the number of electrons transferred in the redox centre half reaction, F is Faradays constant and A is the electrode area. Chidsey et al.[7] reported that the maximum coverage of ferrocene alkanethiol molecules should be 2.4 x 10^{14} molecules/cm^2 or 3.9 x 10^{-10} mol/cm^2 assuming a diameter of 6.6 angstrons for the ferrocene group[8].

The CV for an electroactive SAM is reversible if its shape and the peak positions do not change with scan rate. The peak current, i_p, is proportional to the scan rate, ν, according to Equation (2.6).

$$i_p = \frac{n^2 F^2 A \Gamma \nu}{4RT} \tag{2.6}$$

where n, F, A and Γ retain their value from Equation 2.5, R is the gas constant and T is the temperature. For an ideally shaped CV the current obeys Equation (2.7).

$$i = \frac{4 i_p e^{\theta}}{(1+e^{\theta})^2} \tag{2.7}$$

where θ is given by Equation (2.8),

$$\theta = \frac{nF(E-E^0)}{RT} \tag{2.8}$$

where E^0 is the peak potential of the redox species which are assumed for the moment to be equal. The peak half width, ΔE_{fwhm} is expected to be 90.6/n mV.

The above represents ideal CV diagnostics for an electroactive monolayer. Deviations from ideality are common in ferrocene alkane thiol monolayers. Such deviations reveal molecular detail about the redox centre and/or the SAM. Differences in the peak potentials of the oxidation and reduction waves (non-zero peak splitting

indicates possible intermolecular interactions between the redox centres or a change in the SAM structure with respect to the oxidation state of the redox centres (eg. structure may change due to ion pairing). Another parameter of interest is the Peak Width a Half Maximum (ΔE_{pwhm}). ΔE_{pwhm} may be larger or smaller than the theoretical 90.6/n mV.

Larger than theoretical values can indicate a wide spread of formal potentials, possibly indicating a disorganised SAM with a range of local environments, intermolecular interactions between redox centres or double layer effects. Double layer effects occur when the charge density on the SAM surface causes a change in the local electrostatic potential[9, 10]. Such distortions are reduced when the fraction of redox active sites on the surface is reduced.

Smaller than theoretical values are manifested by a sharp CV are obtained if the redox centres tend to form a solid like phase. This occurs in the most densely packed electroactive SAMs.

A typical CV for a 100% ferrocene alkanethiol monolayer is shown in Figure 2.7. A small pre-peak just occurring at a slightly lower potential and on the shoulder of the main oxidation peak is observed. This pre-peak is characteristic of domains of SAM molecules arranged in a slightly different manner to the rest of the SAM. Such domains can have oxidation potentials slightly different to the main oxidation potential of the SAM. The main sharp peaks observed may be attributed to a very densely packed monolayer[11]. Labinis et al.[12] postulated that these sharp peaks are due to a change in structure of the monolayer upon oxidation/reduction of the ferrocene groups. This work would disagree with the work of Labinis and coworkers and cite a later study by Sato et al.[13] which notes that the terminal group of the ferrocene labelled SAM is neutral in the reduced form and has a positive charge in the oxidised form. As the terminal ferrocene group is oxidised to the ferriecenium cation an ion pair between the positively charged ferrocene group and an electrolyte ion is formed. Since the distance between the ferrocene group and the positively charged gold electrode is smaller than the distance between the electrolyte ion and the gold electrode there will be an electrostatic repulsion between the gold and the ferricenium cation. This causes the SAM to rotate to a more perpendicular position relative to the electrode surface in order to increase the distance between the two positively charged surfaces. Upon reduction the pendant ferrocene molecules become neutral and the ion

pairing is lost as is the repulsion between the ferrocene molecules and the electrode. This causes the SAM to relax into a less perpendicular position relative to the electrode. This structure change is more likely to manifest itself in a nonzero peak splitting rather than sharp peaks, as different orientations of the SAM are likely to have different redox potentials.

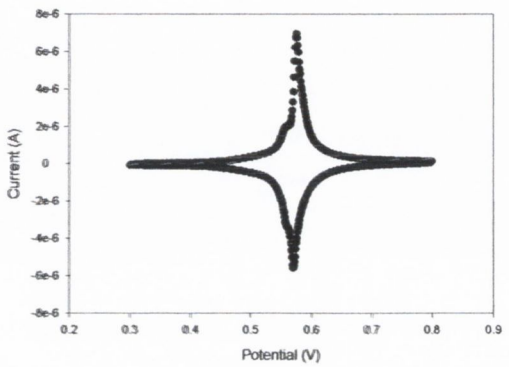


Figure 2.7. Reversible CV of an electroactive SAM. The redox thiol is $HS(CH2)_{10}COOHFc$ in 0.1M $HClO_4$ formed from a 1mM ethanolic solution. Scan rate 0.02V/s.

2.4.2 Chronoamperometry

In this work some chronoamperometry experiments are described. For this reason a general description of the technique is now given. Following this the treatment will be extended to the case of redox active monolayers as it was in the previous section.

Chronoamperometry is an example of a potential step technique. In such techniques the potential of the working electrode is changed instantaneously and either the current-time or charge-time response is recorded. In chronoamperometry the current-time response is recorded. The current-time profile of a typical chronoamperometry experiment is shown in Figure 2.6.

In order to describe this technique it is necessary to again assume an electrode reaction of the form of Equation 2.9.

$$R + ne^- \Phi P \qquad (2.9)$$

A potential-time profile of the form of Figure 2.6 is then applied to the electrode. The values of E_1 and E_2 are chosen such that the reduction of R takes place within this limit. The current transient at a planar electrode is then described by the Cottrell Equation given in Equation 2.10.

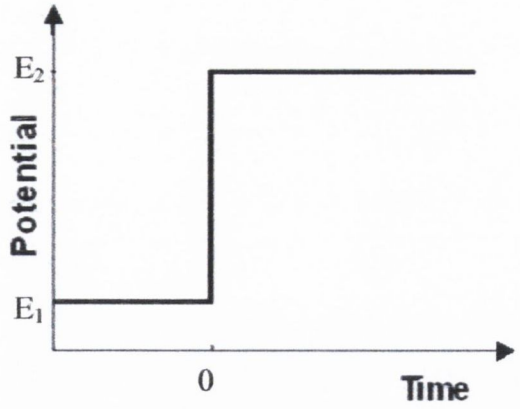


Figure 2.6. The potential-time profile for a potential step chronoamperometric experiment.

$$I = \frac{nFD^{1/2}c_0^{\infty}}{\pi^{1/2}t^{1/2}} \tag{2.10}$$

That is the current decays at $t^{-1/2}$ when the potential-step in Figure 2.6 is applied. The normal method of plotting a chronoamperometric response is given in Figure 2.7 with current plotted against time.

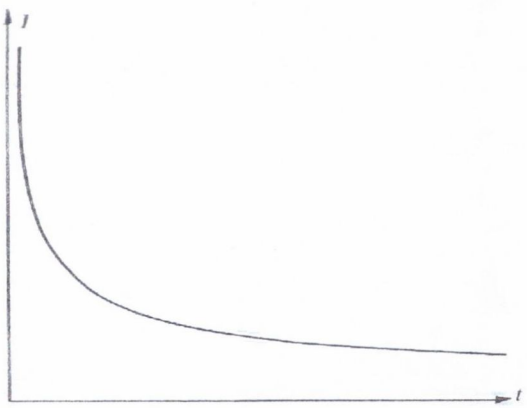


Figure 2.7. The current-time profile for a diffusion controlled potential step chronoamperometric experiment. Reproduced from Reference (4).

However it is possible also to plot current against $t^{-1/2}$ which is expected to be linear. Such a plot is normally used as a test for diffusion control. When applying such tests for diffusion control and evaluating diffusion coefficients it is important to set the correct time scale to ensure reliability of results. The shortest possible time for a chronoamperometry experiment is set by the time taken to charge the cell. The longest

possible time is taken as the time where natural convection has time to come into effect. Normally a value anywhere between 1ms and 10s may be used.

2.4.2.1 Chronoamperometry of Electroactive Monolayers

The expected chronoamperometry of a redox active monolayer has been previously treated by Lyons[14] and it is from this work that the following discussion is based.

Consider potential step such as that described in Figure 2.6 applied to a redox couple A/B immobilised on a surface. Let Γ_A and Γ_B represent the surface coverage of either component on the surface. The total surface coverage can then be described by Equation 11.

$$\Gamma_\varepsilon = \Gamma_A + \Gamma_B \tag{2.11}$$

In the simplest case we can treat the reaction as irreversible and thus write Equation 2.12.

$$\frac{-d\Gamma_A}{dt} = \frac{d\Gamma_B}{dt} = k_E^{'}\Gamma_A \tag{2.12}$$

Where $k_E^{'}$ is the heterogeneous electrochemical rate constant of the form given in Equation 2.13.

$$k_E^{'} = k^0 \exp[\beta\xi] \tag{2.13}$$

Where k^0 denotes the standard rate constant, β is the symmetry factor and ξ denotes a normalised potential given by $\xi = \frac{F}{RT}(E - E^0_{A/B})$. The current response to the applied potential step can then be written in the form of Equation 2.14.

$$i(t) = nFAf_\varepsilon(t) = nFAk_E^{'}\Gamma_A(t) \tag{2.14}$$

Where f_ε denotes the net flux, n denotes the number of electrons transferred in the surface redox process, A denotes the geometric area of the electrode and F is the Faraday constant. The variation of surface coverage with time is obtained by

integration of Equation 2.7 assuming that t=0 and that all the redox active sites at the surface are in the form of A. This treatment gives Equation 2.15.

$$\Gamma_A = \Gamma_\varepsilon \exp(-k_E t) \tag{2.15}$$

The surface redox process can then be written as:

$$i(t) = k_E' Q \exp(-k_E t) \tag{2.16}$$

Where the charge Q is related to the surface coverage of the electroactive groups by Equation 5. Taking natural logarithms of Equation 16 gives Equation 2.17 below.

$$\ln i = \ln(k_E' Q) - k_E t \tag{2.17}$$

Thus a plot of ln(i) versus t is expected to be linear with a slope that yields the heterogeneous rate constant. This approach has been used by many groups to examine the dynamics of self assembled monolayers[15-28] with particular reference to testing the theories of long range electron transfer. Such plots can be used to test the quality of self assembled monolayers. For example if a plot of ln(i) versus time is non-linear this shows that there is a spread of electron transfer rate constants throughout the monolayer indicating redox headgroups in different orientations[19-22].

2.4.3 Electrochemical Quartz Crystal Microbalance

The electrochemical quartz crystal microbalance is a variant of acoustic wave microsensors that are capable of ultrasensitive mass measurements. Under favourable conditions a typical EQCM can measure a mass change of 0.1-1ng/cm^2. The QCM technique was first identified by Sauerbrey[23]. QCM oscillates in a mechanically resonant shear mode under the influence of a high frequency AC electric field applied across the thickness of a quartz crystal. The top and bottom sides of the quartz crystal are coated with a layer of gold that act as the working electrode.

QCM and the combination of QCM and electrochemistry (EQCM) have been widely employed for studies of ion transport processes in polymer films[24], biosensor

developments[25] and investigations of the kinetics of the adsorption of adsorbate molecules[26, 27].

The mass sensitivity of EQCM originates from the relationship between the oscillation frequency of the total mass of the crystal and the oscillation frequency of the crystal with adlayers of material residing on the metal coated crystal. This relationship is shown in Equation 2.18 and is known as the Sauerbrey Equation.

$$\Delta f = -\frac{2f_0^2}{A\sqrt{\mu\rho}}\Delta m \qquad (2.18)$$

Here f_0 is the resonant frequency fundamental to the crystal, A is the area of the gold electrode coated onto the crystal, ρ is the density of the crystal and μ is the shear modulus of quartz. In the CH Instruments Model 440 system these values are, f_0 = 8MHz, A = 0.196cm^2, ρ = 2.648g.cm^{-3}, μ = 2.947 x 10^{11} g.cm^{-1}.s^{-2}. Using these values it is seen that a frequency change of 1Hz corresponds to a mass change of 14ng using the CH Instruments Model 440 EQCM. The minus sign in Equation 2.18 determines that a frequency decrease corresponds to a mass increase. The EQCM cell used for this work is shown in Figure 2.7.

The EQCM cell consists of three round Teflon pieces. The total height of the cell is 37mm and its diameter is 35mm. The top piece is the cell top that holds the counter and reference electrodes. There are also two 2mm holes for degassing solutions. The centre piece is the cell body used for holding solution. The bottom piece is for mounting the quartz crystals. Four screws are used to seal the bottom and centre pieces together. The quartz crystal is located between the bottom and centre pieces. The top piece may be pressed into the centre piece to complete the cell.

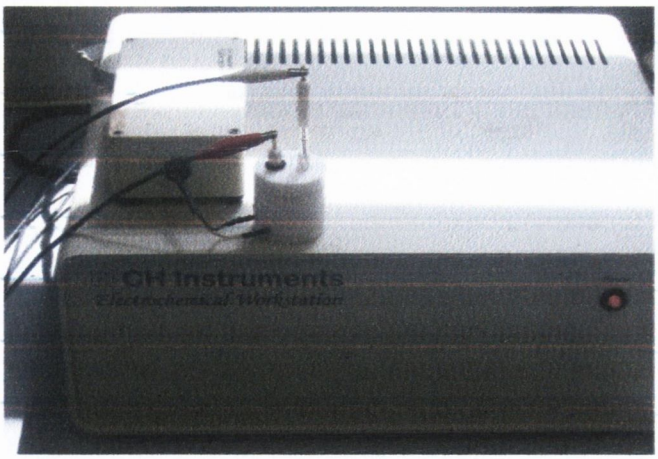


Figure 2.7. Photograph of the CH Instruments Model 440 Workstation as well as the EQCM cell with counter (red) and reference (white) electrode inserted.

2.5 Magnetic Field

In this work magnetic fields were applied using a cylindrical magnet, the Halbach Cylinder, supplied by Prof. J.M.D. Coey of Magnetic Solutions Ltd. The magnet had a field strength of 0.5 Tesla. The magnet was formed from sintered Nd-Fe-B and consisted of twelve segments providing a homogeneous magnetic field in the circular bore (diameter of 5.4 cm).

Macroelectrode experiments involving the magnetic field involved firstly coating the electrode with a SAM from a dilute solution of thiol (See *Section 2.3.2*). Cyclic voltammetry was then performed in the absence of a magnetic field to ensure monolayer quality. The electrochemical cell was then placed in the bore of the magnet with the direction of the magnetic field running parallel to the surface of the working electrode and hence perpendicular to the direction of the alkane chains on the surface of the monolayer. Cyclic voltammograms were then run continuously between the upper and lower voltage limits and scans performed after defined time intervals in the bore of the magnet were selected for analysis. Certain experiments involved analysis of the SAM redox activity when the field was removed. In this case the electrochemical cell was removed from the bore of the magnet after analysis and subsequent cyclic voltammetry was performed in the absence of the magnetic field

During EQCM experiments the entire Teflon cell was carefully placed into the bore. Because of the design of the EQCM cell little could be done to ensure that the orientation of the B-field relative to the electrodes was exactly the same during

different experiments. However the technique for voltammetric analysis in the presence of the magnetic field was identical to that used in the case of macroelectrodes.

References

(1) A.M. Napper, H. Lui and D.H. Waldeck, *J. Phys. Chem. B.* **2001**, *105*, 7699

(2) G.E. Poirier and E.D. Pylant, *Science*, **1996**, *272*,1145.

(3) O. Chailapakul, L. Sun, C. Xu, and R.M. Crooks, *J. Am. Chem. Soc.*, **1993**, *115*, 12459.

(4) R.B. Lennox and F. Ma, *Langmuir* **2000**, *16*, 6188.

(5) Southampton Electrochemistry Group, *Instrumental Methods in Electrochemistry*, First Edition, Wiley **1985**.

(6) H. O'Finklea *Electroanalytical Chemistry*, Marcel Dekker, New York, **1996**, Vol. 19, 109, 335.

(7) C.E.D. Chidsey, C.R. Bertozzi, T.M. Putvinski and A.M Mujsce, *J. Am Chem. Soc*, **1988**, *112*, 4301

(8) P.E. Labinis, G.M. Whitesides, D.L. Allara, Y.T. Tao, A.N. Parikh and R.G Nuzzo, *J. Am. Chem. Soc*, **1991**, *113*, 7152

(9) C.P. Smith and H.S. White, *Anal Chem*, **1992**, *64*, 2398.

(10) R. Andreu, J.J. Calvente, W.R. Fawcett and M. Molero, *J. Phys. Chem. B*, **1997**, *101*, 2884.

(11) K. Sato, K.Uosaki, *The Electrochemical Society, Pennington, NJ*, **1993**, 299.

(12) K. Uosaki H. Kita and Y. Sato, *Langmuir*, **1991**, *7*, 1510.

(13) Y.Sato, S.Ye, and K. Uosaki, *Langmuir*, **1997**, *13*, 3157.

(14) M.E.G. Lyons, *Sensors* **2002**, *2*, 314.

(15) Finklea, H.O.. *J.Electroanal. Chem*. **2001**, *495*, 79-86

(16) Chidsey, C.E.D. *Science* **1991**, *251*, 919

(17) Becka, A.M.; Miller, C.J. *J. Phys. Chem*. **1992**, *96*, 2657-2668.

(18) Forster, R.J.; Faulkner, L.R. *J. Am. Chem. Soc.* **1994**, *116*, 5444

(19) Nahir, T.M.; Bowden, E.F. *J. Electroanal. Chem*. **1996**, *410*, 9

(20) Gosavi, S.; Gao, Y.Q.; Marcus, R.A. *J. Electroanal. Chem*. **2001**, *500*, 71

(21) Xu, J.; Li, H-L.; Zhang, Y.. *J. Phys.Chem*. **1993**, *97*, 11497-11500.

(22) Sumner, J.J.; Creager, S.E. *J. Phys. Chem. B*. **2001**, *105*, 8739-8745.

(23) E. Sabatani, I. Rubenstien, R. Maoz and J. Sagiv, *J. Electroanal Chem*, **1987**, *219*, 365

(24) E. Sabatini, I. Rubenstien, *J. Phys. Chem*, **1987**, *91*, 6663

(25) E.B. Troughton, C.D. Bain, G.M. Whitesides, R.G. Nuzzo, D.L. Allara and M.D. Porter, *Langmuir*, **1988**, *4*, 365.

(26) L. Strong and G.M. Whitesides, *Langmuir*, **1988**, *4*, 546

(27) C.D. Bain and G.M Whitesides, *J. Am. Chem. Soc*, **1988**, *110*, 3665

CHAPTER 3 –

CHARACTERISATION OF ELECTROACTIVE MONOLAYERS

3. Characterisation of Electroactive Monolayers

3.1 Introduction

Self-assembled monolayers provide a convenient method to anchor redox centres at a well defined distance from the electrode surface. The length of the alkane chain determines the distance between the redox centre and the electrode surface. Using such redox active systems it is possible it is possible to probe the characteristics of self-assembled monolayers as well as test some of the current theories relating to electron transfer through organic materials.

The body of this thesis relates to redox active self-assembled monolayers and in particular those based on a pendant ferrocene redox group. Consequently the following chapter will provide an introduction to previous work that has been carried out on the ferrocene/alkanethiol/Au system. The topics of surface coverage, shape of cyclic voltammograms and finally non-electrochemical probes will be discussed here. Following this, experimental results will be presented to characterise the redox system in question.

3.1.1 Ferrocene Terminated Organosulfur Monolayers

As already indicated this work will focus on ferrocene terminated, redox active, alkanethiol monolayers. Such systems are by far the most popular type of electroactive monolayer due to the fact that a variety of methods are available for their synthesis. The particular system used here is shown in Figure 3.1 and for clarity the particular molecule used is shown in Figure 3.2

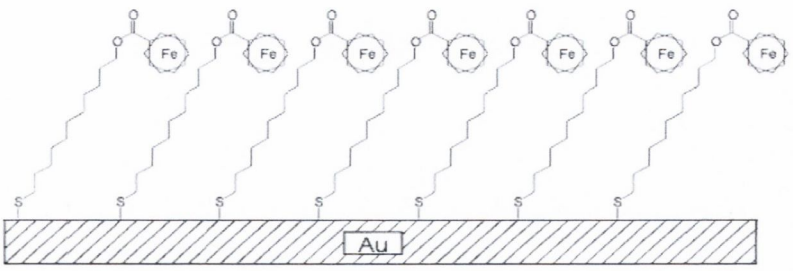


Figure 3.1. Schematic illustration of a self-assembled monolayer of $HS(CH2)_{11}CO_2HFc$. Such a SAM system is used throughout this thesis.

It is notable in this case that the ferrocene group is linked to the alkane spacer by a carboxylic ester group. A number of different linkers for the ferrocene group have

been synthesised. These include a direct connection of the ferrocene to the alkanethiol molecule, an amide group (Fc-CONH) and a ketone group (FcCO). The terminal group that links the alkane chain to the gold surface is almost always a thiol group but disulfides, thiocarbamates and isonitriles have been used.

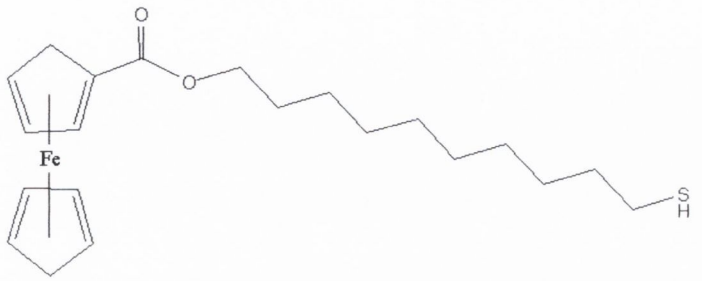


Figure 3.2. Illustration of the $HS(CH2)_nCO_2HFc$ molecule used to form redox active self-assembled monolayers in the study.

Such SAMs are deposited in the normal manner described in *Section 2.3.2* where an electrode is soaked in a dilute solution of the molecule.

3.1.1.1 Surface Coverage

The maximum theoretical surface coverage of ferrocene-terminated alkanethiol molecules on a Au(111) surface has been calculated by Chidsey and coworkers[1] as $4.5x10^{-10}mol.cm^{-2}$. In this study the pendant ferrocene molecules are taken to have a diameter of $6.6Å^2$. In general a larger value than this is determined experimentally. Two factors account for these higher readings. The first is due to the fact that alkane chains have the ability to kink and coil leaving the ferrocene moieties buried in the layer. The maximum coverage of ferrocene-based SAMs is based on the steric interactions that occur between the pendant ferrocene molecules residing on the surface of the monolayer. When ferrocene molecules are buried in the layer they are no longer subject to these steric interactions and thus more of them may be present on the surface. The second factor is simply due to the inherent surface roughness of the gold surface. Steps, terraces, etc, increase the effective surface on a gold substrate leading to an increase in the surface available for molecular adsorption. This leads to an increase in the observed surface coverage. Slightly lower values of surface coverage may also be observed, normally in the case of ferrocene molecules linked by shorter chain alkanethiols. This is due to the reduction of interchain interactions in

shorter chain alkanethiols which may prohibit them from packing as densely as the longer chain molecules.

Walczak et al.[2] calculated the coverage of ferrocene-terminated alkanethiol molecules of two different chain lengths by reductive desorption (*see Section 1.2.7.3*) and compared this value with that attained by cyclic voltammetry experiments. The values of surface coverage from CV experiments were $5.3x10^{-10}$mol.cm^{-2} for an $FcC_{11}SH$ layer and $3.8x10^{-10}$mol.cm^{-2} for an FcC_8SH layer. Both values were within reasonable experimental error compared to the theoretical value. These values were then compared to those calculated from reductive desorption experiments. The comparison was found to be unfavourable - yielding a surface coverage value almost twice that derived from CV experiments in the case of each SAM. The $FcC_{11}SH$ desorption gave a surface coverage of 11.1 x 10^{-10}mol.cm^{-2} and the FcC_8SH desorption gave a surface coverage of 8.4 x 10^{-10}mol.cm^{-2}. It was postulated in this report that the lower CV calculated coverages were due to cycling in a neutral chloride electrolyte leading to the desorption of the redox centres.

Kondo et al.[3] examined the adsorption characteristics of ferrocene terminated alkanethiol molecules. It was determined that the kinetics of adsorption of such molecules could be described by the simple Langmuir rate expression. Acyl and alkyl groups were introduced into the ferrocene ring in complimentary studies and the redox potentials of monolayers formed from such molecules were examined. Introduction of an acyl group into the ferrocene ring caused the redox potential of the SAM to shift positive by approximately 300mV. Introduction of a butyl group into the ring shifted the redox potential of the SAM by approximately 15mV positive.

The above is a basic introduction into the surface coverage characteristics of ferrocene terminated SAMs. The main point to be taken from this discussion however is that the maximum theoretical surface coverage of ferrocene terminated SAMs is 4.5 x 10^{-10}mol.cm^{-2} and that deviations are almost certain to occur experimentally due to disorder in the layer and surface roughness.

3.1.1.2 Peak Shape and Peak Potentials

This section will focus on the cyclic voltammetry of ferrocene terminated alkanethiol SAMs.

A reversible cyclic voltammogram for a ferrocene terminated alkanethiol monolayer is likely to exhibit a number of deviations from the ideal shape. As is

expected with such electroactive systems the shape of the CV response is likely to differ between experiments. However a number of characteristics in these CVs are normally evident when run in $0.1HClO_4$ which is the standard electrolyte used in this study. These characteristics will now be discussed in turn. (1) The peak potential always occurs between 0.5 and 0.7V vs. Ag/AgCl. Some peak splitting is normally observed. The magnitude of this splitting is normally small (a few mV). This usually implies a square scheme such as that shown below.

$$\begin{array}{ccc} O + ne^- & \leftrightharpoons & R \\ \uparrow & & \downarrow \\ O' + ne^- & \leftrightharpoons & R' \end{array}$$

Reasons for this peak splitting can include the formation of a strong ion pair between the oxidised state of the redox active moiety and electrolyte ions (this happens between Fc^+ and ClO_4^- ions in the system being considered in this work) and a major change in the hydrophobicity/hydrophilicity of the redox centre as a function of its oxidised state. (2) The peak width half maximum (E_{PWHM}) is almost always significantly smaller than the ideal 91/n mV. CV waves can be either smaller or larger than this ideal value. A smaller value implies a high surface concentration of redox active molecules with attractive interactions between them. Such interactions can be eliminated by the formation of mixed monolayers (See *Chapter 5*). (3) At times some shoulders normally occur prior to the oxidation and after the reduction peak. These are characteristic of certain phases of ferrocene molecules in a different orientation to the bulk phase. Such orientations have a redox potential that is slightly different to the bulk and this appears as a shoulder on the main peak.

3.1.1.3 Other Probe Techniques

A limited amount of non-electrochemical techniques have been applied to study the ferrocene/alkanethiol/gold system. These will be discussed as follows.

Ohtuska et al.[4] carried out dynamic ellipsometry studies of 11-ferroceneyl-1-undecanethiol monolayers in 1M $HClO_4$ formed on a gold electrode. The thickness of the monolayer was determined to be 2.91nm. This thickness was found to increase by 0.3nm upon oxidation of the layer corresponding to the formation of an ion pair between the ferricenium cation and perchlorate ions.

Abbott and Whitesides[5] utilised contact angle measurements to study the potential dependant wetting of a self assembled monolayer of $FcCO(CH_2)_{15}SH$ deposited on Au. It was determined that the contact angles decreased from 71° to 43° when the potential of the SAM was increased from 0.3 to 0.5V and was subsequently increased from 43° to 58° when the SAM potential was returned to 0.2V. It is postulated in this study that the decrease in contact angle during the oxidation of the SAM (0.3-0.5V) arises from the formation of the more polar and consequently more wettable Fc^+ groups.

Another probe that has been applied to examine the structure of ferrocene-terminated monolayers is the Electrochemical Quartz Crystal Microbalance (EQCM). During the oxidation of the ferrocene redox centres an ion pair is formed between the positively charged ferricenium group and an anion in the electrolyte. This leads to an increase in the mass of the layer. A corresponding decrease in the mass of the layer is expected when the ferricenium group is reversibly reduced to the neutral ferrocene and the ion pairs are no longer required to retain charge neutrality. EQCM has been used to study SAMs deposited on both gold[6] and platinum[7].

De Long et al.[8] carried out EQCM studies on loosely packed monolayers of FcCONH-benzylmercaptain where the mass change ($50gmol^{-1}$) was much lower than that expected for a densely packed SAM ($160gmol^{-1}$)[9]. This is due to the fact that in more loosely packed SAM the number of ion pairs formed will be diminished and thus the observed mass change will also be diminished. An excessive mass change in an EQCM scan can point towards the ingress of aqueous molecules into a self-assembled monolayer. In turn this can point to a loosely packed layer. Yao et al.[10] calculated that up to 13 water molecules can be incorporated into the free volume between the alkane chains in ferrocene terminated SAM.

3.2 Experimental

Electrochemical Measurements. All electrochemical measurements were carried out on a CH Instruments Model 440 potentiostat as described in *Section 2.2.1.*

Gold Substrate. The gold substrate used whether it be a standard macroelectrode or an EQCM electrode is as described in *Section 2.1.1.*

Electrode Pre-Treatment. **Electrode Pre-Treatment**. The method used for electrode pre-treatment is described in *Section 2.3.1.*

Monolayer Deposition. All monolayers were deposited using solution deposition. The method used is described in *Section 2.3.2.*

Electrolyte Solutions. The electrolyte solutions used in all experiments were 0.1M Perchloric Acid with the exception of *Section 3.3.2* where the electrolyte concentration was varied as stated. *Section 2.1.4* provides further details.

3.3 Results and Discussion

3.3.1 Effect of Chain Length

Figure 3.3 shows typical cyclic voltammograms (CV) performed on the monolayers formed from the electroactive alkanethiol molecules of the form shown in Figure 3.2. All scans were carried out in 0.1M $HClO_4$ at 0.02V/s scan rate.

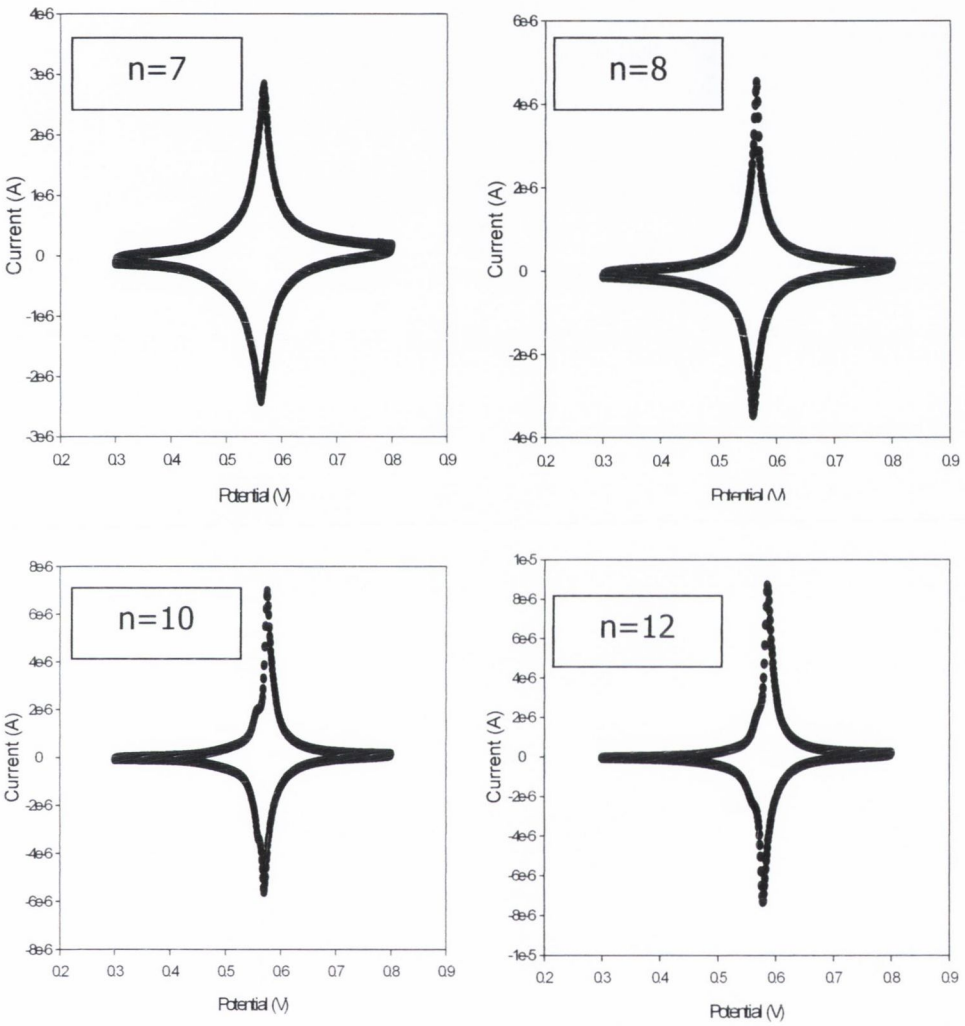


Figure 3.3 Cyclic voltammogram of a gold electrode modified with 1mM $S(CH_2)_nCO_2HFc$ (n=7,8,10,12). The modification was carried out by immersing the electrode in the thiol solution for 48 hrs.

Table 3.1 shows the monolayer surface coverages calculated for modified electrodes of varying chain length calculated using Equation 2.5.

n	Surface Coverage (Γ) ($x10^{-10}$ mol.cm^{-2})
7	8.3 ± 2.0 (m=3)
8	10.7 ± 5.3 (m=5)
10	13.9 ± 3.0 (m=7)
12	16.9 ± 3.0 (m=6)

Table 3.1. Surface coverages calculated for gold electrodes modified with $S(CH_2)_nCO_2HFc$. In this table m denotes the number of electrodes that were used to calculate the surface coverages and associated error.

It is evident that as the chain length of the thiol molecule increases so does the surface coverage. Van der Waals interactions occur between the alkane chains in the monolayer and aid in the formation of a compact monolayer. As the length of the chain increases so do the interactions between the chains enabling longer chains to pack more densely than do shorter chains. This effect explains the trend observed in Table 3.1.

It is also worth noting that as the chain length increases so too does the height of the peaks. The reason the peak height increases is again due to the Van der Waals interactions between chains. At longer chain lengths Van der Waals interactions are greater causing the molecules to pack in a more ordered manner. Different orientations of the ferrocene molecules on the surface are likely to have slightly different oxidation potentials. This accounts for the more densely packed monolayer having a thinner window of oxidation potentials because the ferrocene molecules will be mainly orientated in the same direction. This also accounts for the smaller peak currents and slightly broader peaks observed at lower chain lengths. The peak width half maximum (PWHM) for $S(CH_2)_7CO_2HFc$ is 34.7mV whereas the PWHM for $S(CH_2)_{12}CO_2HFc$ is 17mV indicating the increase in ordering of the monolayer as the chain length increases. Table 3.2 shows this data.

n	E_{Pa} (mV)	E_{Pc} (mV)	E^0 (mV)	PWHM (mV)
7	568	562	565	35
8	568	560	564	18
10	575	570	573	15
12	586	578	582	17

Table 3.2. Showing data relating to the cyclic voltammograms for the $S(CH_2)_nCO_2HFc$ (n=7,8,10,12) modified electrodes in Figure 3.3.

In a typical voltammogram the PWHM has a value of 90mV/n where n is the number of electrons involved in the redox process. It is generally accepted that the redox process involving the ferrocene moiety involves a sole electron and hence the PWHM values above for the $S(CH_2)_7CO_2HFc$ and $S(CH_2)_{12}CO_2HFc$ modified electrodes would seem to be incorrect. *Section 3.2.2* examines the interactions between the ferrocene molecules in the monolayer.

3.3.2 Molecular Interactions Within the Monolayer

Upon oxidation, the ferrocene group of the electroactive monolayer immobilised on the surface of the electrode becomes the ferrocenium cation (Fc^+). When this oxidation occurs an anion (X) is incorporated onto the surface of the monolayer from the electrolyte in order to maintain charge neutrality. The redox process in this case is expressed as follows,

$$Fc \rightarrow Fc^+ + e^-$$

$$Fc^+ + X^- \rightarrow Fc^+X^-$$

where Fc^+X^- represent the ion pair formed.

This can be represented by the simple Nernst equation:

$$E = E^0 + \frac{RT}{F}\ln(\frac{Fc^+}{Fc}) \qquad (3.1)$$

By considering the ion pair equilibrium:

$$K = \frac{[Fc^+X]}{[Fc^+][X^-]} \tag{3.2}$$

It is noted that:

$$[Fc^+] = \frac{[Fc^+X^-]}{K[X^-]} \tag{3.3}$$

The Nernst equation then becomes:

$$E = E^0 + \frac{RT}{F}\ln(\frac{[Fc^+X^-]}{[Fc]}) - \frac{RT}{F}\ln K - \frac{RT}{F}\ln[X^-] \tag{3.4}$$

Hence it is expected that a plot of E against $\log_{10}[X^-]$ will produce a slope of 2.303RT/F where 2.303RT/F = 60mV/decade.

However the basic version of the Nernst equation is unlikely to hold true in the case where interactions occur between the ferrocene alkanethiol molecules. When the CV in Fig. 3.4 is examined a non-zero peak splitting between the oxidation and reduction peaks is noted. It is widely accepted that this peak splitting occurs due to interactions between adjacent redox centres in the monolayer. In the ideal case where interactions do not occur between the molecules no splitting would be evident.

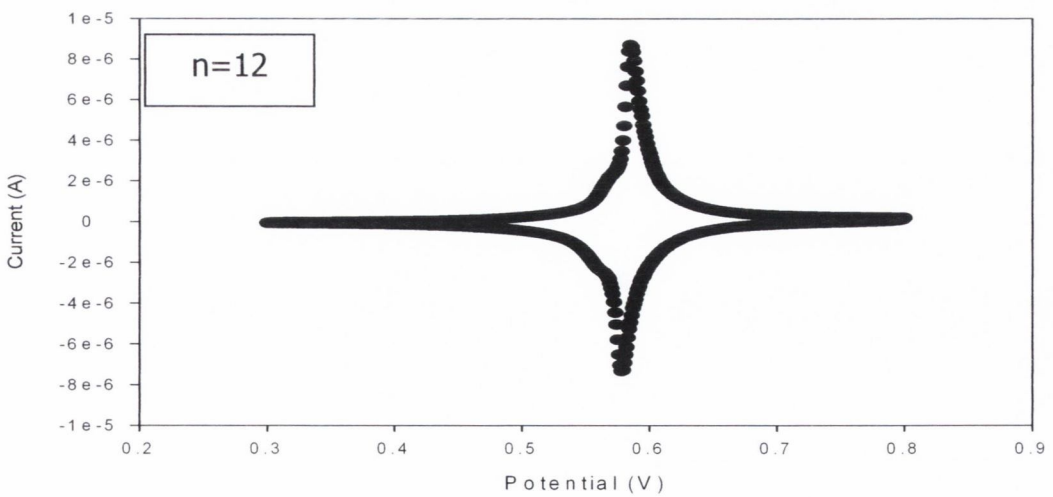


Figure 3.4. Cyclic voltammogram of a gold electrode modified with 1mM $S(CH_2)_{12}CO_2HFc$. The non-zero peak splitting is attributed to interactions between ferrocene molecules.

Returning to the Nernst equation it is possible to represent these interactions by the dimensionless interaction factor α. Equation. 3.4 may then be written to include this factor as:

$$E = E^0 + \frac{RT}{\alpha F}\ln(\frac{[Fc^+X^-]}{[Fc]}) - \frac{RT}{\alpha F}\ln K - \frac{RT}{\alpha F}\ln[X^-] \qquad (3.5)$$

Hence it would be expected that a plot of E against $\log_{10}[X^-]$ to produce a slope of $2.303RT/\alpha F$. Thus by varying the concentration of X^- and making such a plot it is possible to quantify α. In this case the CVs were run in varying concentrations of the perchloric acid electrolyte ($HClO_4$).

Such plots have been carried out for $S(CH_2)_nCO_2HFc$ (n = 7, 8, 10, 12). They are shown in Figure 3.5.

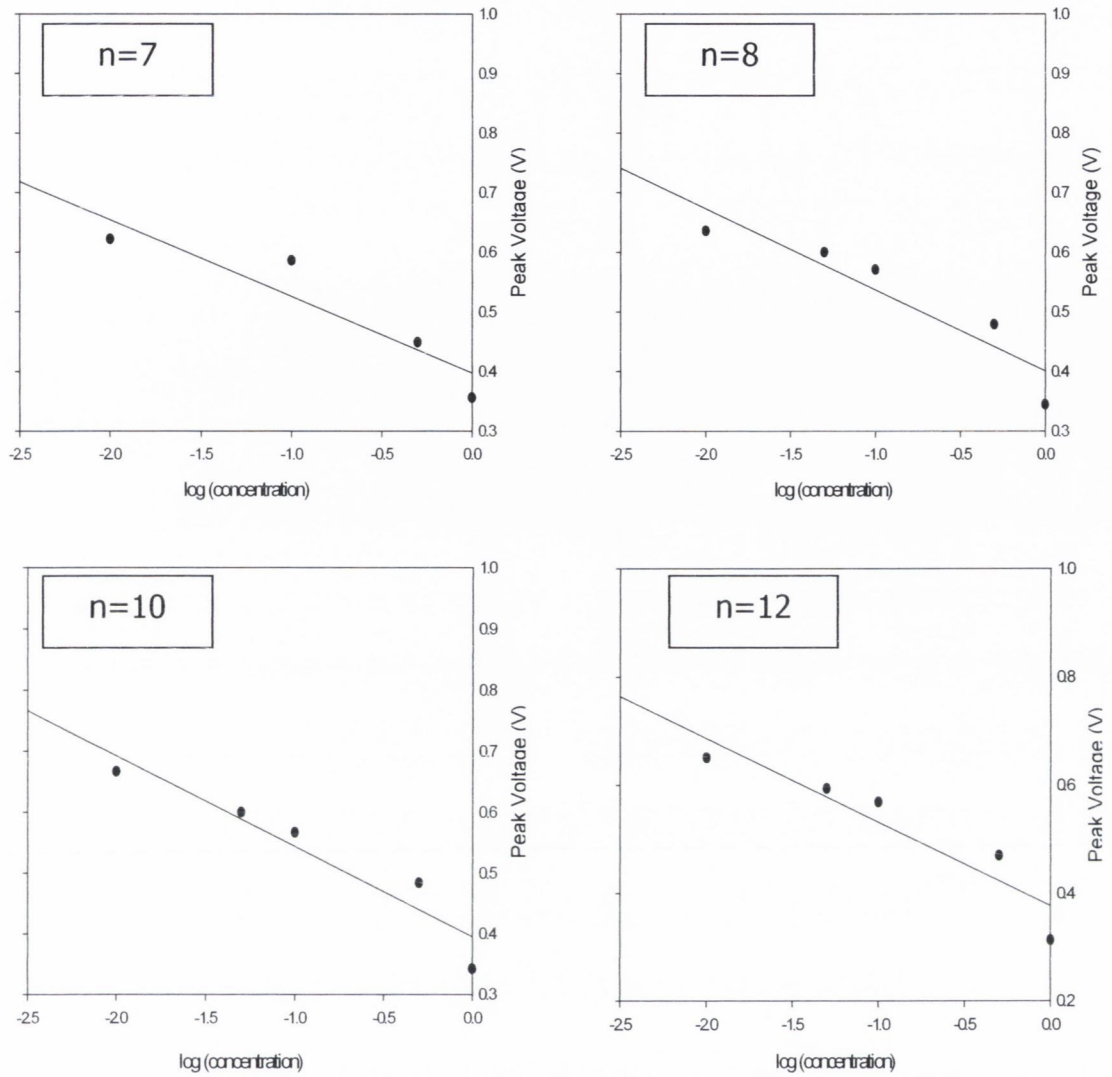


Figure 3.5. Effect of anion concentration on the peak voltage of a gold electrode modified with 1mM $S(CH_2)_nCO_2HFc$. The perchloric acid concentrations were 0.01M, 0.05M, 0.1M, 0.5M and 1M.

The slopes of these graphs were then calculated and the interaction parameters between the redox centres for the various chain lengths can be calculated. These are shown below in Table 3.3.

n	Slope (mV/decade)	α (see text)
7	128.4	0.46
8	136.1	0.44
10	148.6	0.40
12	155.0	0.38

Table 3.3. Slopes calculated for graphs of peak voltage vs. anion concentration on gold electrodes modified with $S(CH_2)_nCO_2HFc$ (n = 7, 8, 10, 12). Interaction parameters are also shown.

The interactions in Table 3.3 were calculated from the modified Nernst equation (Equation 3.5). The slope of peak voltage vs. $\log_{10}(X^-)$ is given by $2.303RT/\alpha F$. Hence values of α can be calculated for each of the SAMs.

From the calculations of α the examination of the interactions between redox sites can be extended using the *Brown-Anson* model. This model was originally developed to examine interactions between adjacent redox sites in an electroactive polymer film but is extended here to consider interactions between the redox sites in an electroactive SAM. When interactions are absent the Nernst Equation for our system can be written as:

$$\frac{[Fc^+]}{[Fc]} = e^{[\frac{F}{RT}(E-E^0)]} \tag{3.6}$$

This can be simplified to:

$$y = \theta \tag{3.7}$$

where $y = \ln\{[Fc^+]/[Fc]\}$ and as in Equation (9) is given by $\theta = F/RT(E - E^0)$. If interactions are present then the Nernst equation can be modified to read:

$$y = \xi.\theta \tag{3.8}$$

Where we have now introduced the parameter ξ, a measure of the departure from the ideal. The fundamental expression for ξ in the *Brown-Anson* model is:

$$\xi = [1 - \frac{\alpha}{2}(\frac{\tanh(\frac{y}{2})}{\frac{y}{2}})]^{-1} \tag{3.9}$$

For small values of y Equation (3.9) reduces to:

$$\xi = \{1 - \alpha/2\}^{-1} \tag{3.10}$$

$$\boxed{\xi = 2/\alpha - 2} \tag{3.11}$$

Table 3.4 below shows values of ξ (the deviation from ideality) for the different chain lengths using values of α calculated in Table 3.3.

n	α	ξ
7	0.46	2.3
8	0.44	2.5
10	0.40	3.0
12	0.38	3.2

Table 3.4. The deviation from ideality, ξ, calculated for $S(CH_2)_nCO_2HFc$ (n = 7, 8, 10, 12). Interaction parameters are also shown.

Table 3.4 shows the departure from the ideal increasing as the length of the alkane chain increases. As the chain length of the SAM increases so too does the packing between the molecules in the SAM. The more compact the SAM the closer the redox centres are likely to be to one another. Hence the redox centres are likely to interact to a greater extent and cause a larger deviation from the ideal.

3.3.3 Electrochemical Quartz Crystal Microbalance

3.3.3.1 Effect of Chain Length

An electrochemical quartz crystal microbalance (EQCM) was employed to investigate the mass changes on the surface of the monolayer during the redox processes of the ferrocenylalkanethiol SAM. As already described $S(CH_2)_nCO_2HFc$ monolayers allow electron transfer between the gold electrode and the electrolyte. During the redox oxidation of the ferrocenylalkanethiol SAM the normally neutral terminal ferrocene group is transformed to the positive ferrocenium cation (Fc^+). As the terminal group becomes positively charged, anions from the perchloric acid solution (ClO_4^-) are attracted towards the surface of the SAM. An ion pair is then formed between the terminal Fc^+ ion and the ClO_4^- molecule. The incorporation of the ClO_4^- anion onto the surface results in a mass change which may be measured via EQCM. An increase in the loading on the surface of the quartz crystal corresponds to a damping in its resonance frequency. The formation of the ion pair on the SAM surface will cause such a damping and thus a decrease in the recorded frequency corresponds to an increase in the mass of the monolayer.

Figure 3.6 shows the frequency changes over the oxidation potentials of $S(CH_2)_nFc$ for (n = 7, 8, 10, 11, 12). It is now necessary to relate the mass changes

determined to the process occurring. From Table 3.1 it is possible to calculate the average surface coverage for $S(CH_2)_nCO_2HFc$ (n = 7, 8, 10, 12) as $\Gamma = 3.3 \times 10^{-10}$ $mol.cm^{-2}$. This value is within a reasonable experimental error limit of the theoretical surface coverage of 4.5×10^{-10} $mol.cm^{-2}$ as determined by Chidsey at al[(1)]. The average mass increase for the various chain lengths can be calculated as $\Delta m = 26ng$.

From the surface coverage value it is possible to calculate the number of molecules per cm^2 as follows,

$$\#\ Molecules/cm^2 = \Gamma.N_a \qquad (3.12)$$

$$\Rightarrow\ \#\ Molecules/cm^2 = (3.3 \times 10^{-10}\ mol.cm^{-2})(6.023 \times 10^{23} molecules.mol^{-1})$$

$$\Rightarrow\ \#\ Molecules/cm^2 = 1.9 \times 10^{14}$$

Thus the number of ferrocene alkanethiol molecules on the surface of the gold electrode has been determined. There will be the same number of ferrocene molecules on the surface forming ion pairs with ClO_4^- molecules, i.e. 1.9×10^{14} ion pairs will be formed on the surface of the SAM and thus 1.9×10^{14} ClO_4^- will be incorporated onto the surface of the SAM.

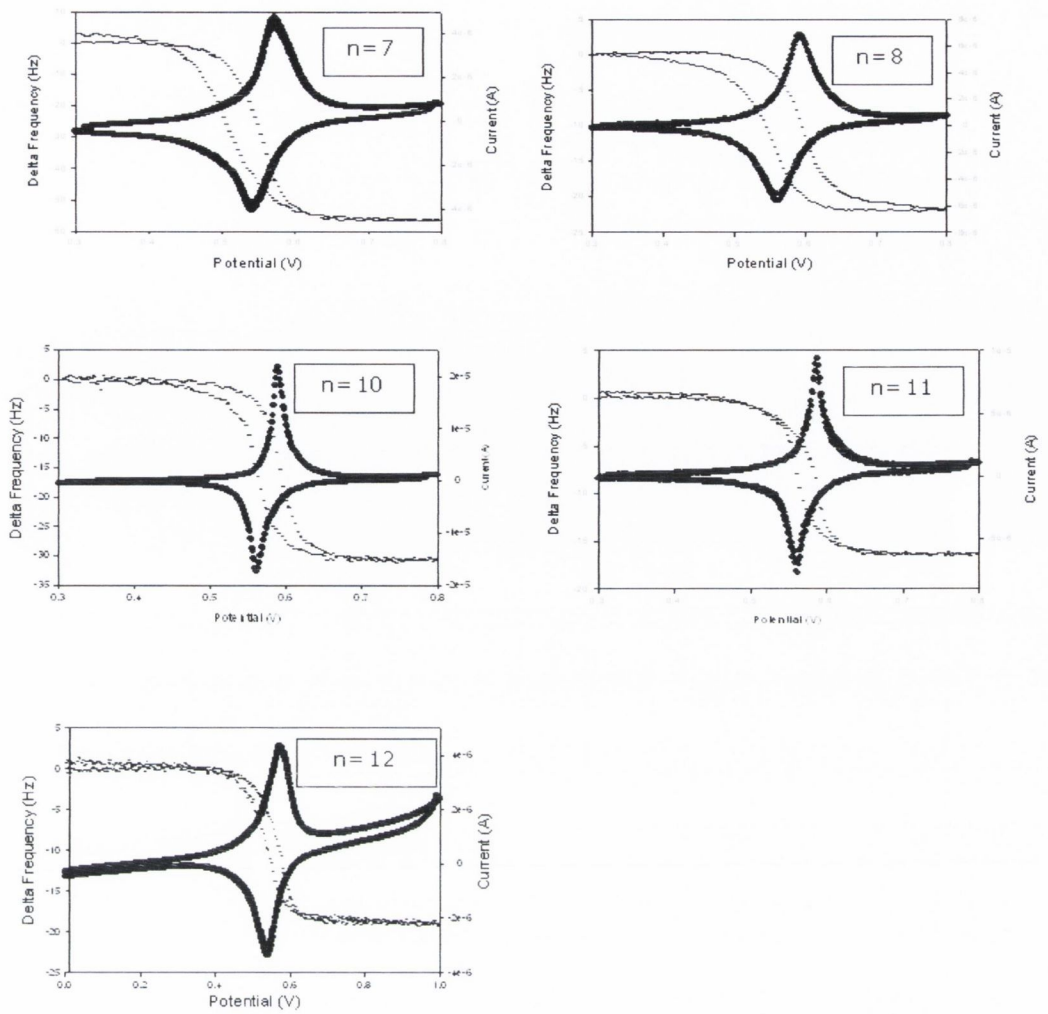


Figure 3.6. CV (dark trace) and frequency change (light trace) corresponding to the oxidation of $S(CH_2)_nCO_2HFc(n=7,8,10,11,12)$ SAM. The ferrocene moiety is oxidised to ferricenium and there is the subsequent formation of an ion pair at the surface of the SAM.

One ClO_4^- molecule weighs 99.45g.mol^{-1} and using Avogadro's number the weight per molecule can be determined as 1.6 x 10^{-22}grams.molecule^{-1}. 1.9 x 10^{14} molecules are incorporated onto the surface of the SAM. The mass change expected due to the incorporation of these molecules is:

$$\Delta m = (1.6 \times 10^{-22} \text{g.molecule}^{-1})(1.9 \times 10^{14} \text{ molecules})$$

$$\Rightarrow \Delta m = 31 \text{ng}$$

The average mass change calculated for the different chain length thiols SAMs in Table 3.5 is $\Delta m = 29ng$. Discrepancies between the expected and the observed values can be attributed to imperfections in the monolayers resulting perhaps in pinholes or sites which for some reason may not form a ion pair with the ClO_4^- anion.

Table 3.5 shows frequency changes accompanying the oxidation of the different chain length SAMs over their oxidation potentials as determined from Figure 3.6.

n	Oxidation Potential range	Frequency Change (Hz)	Mass Change (Δm) (ng)
7	0.45V – 0.65V	19.6	27
8	0.45V – 0.65V	18.2	26
10	0.5V – 0.7V	29.2	42
11	0.5V – 0.7V	16.6	23
12	0.5V – 0.7V	18.5	26

Table 3.5. EQCM frequency changes due to the oxidation of Fc to Fc^+ and the corresponding formation of an ion pair on the SAM surface. Frequency changes are shown for $S(CH_2)_nCO_2HFc$ where n = 7, 8,10,11, 12.

Inspection of Table 3.5 reveals that the monolayer formed from $S(CH_2)_{10}CO_2Fc$ undergoes a considerably larger mass increase than any of the other chain length thiols. This result provides information regarding this particular monolayer undetectable by cyclic voltammetry. The large increase in mass can be attributed to the incorporation of electrolyte molecules into the monolayer during the redox processes. When the charge compensation electrolyte molecules are drawn to the surface of the SAM it is likely that they will find pinholes or other such defects in this particular SAM structure and permeate the surface of the SAM. This leads to an increase in mass that is larger than expected. Observation of the CV response of $S(CH_2)_{10}CO_2HFc$ in Figure 3.5 alone would give no clue to the disordered structure of the monolayer.

This study has shown that ion pairing between oxidised ferrocene molecules and electrolyte counter ions does occur and that a monolayer of anions are present on the surface of the SAM during oxidation. It is also noted that a corresponding decrease in the surface mass of the SAM occurs upon reduction. This corresponds to the ferricenium cation returning to the neutral ferrocene and the ClO_4^- anions returning to solution.

3.3.4 Chronoamperometry

In order to gain further insights into the nature of electron transfer processes through self assembled monolayers chronoamperometry was employed. The details of the chronoamperometry experiments involving electroactive monolayers are explained in *Section 2.4.2*. Figure 3.7 below shows the current response for a potential step across the oxidation potential of ferrocene-terminated monolayers of varying chain length.

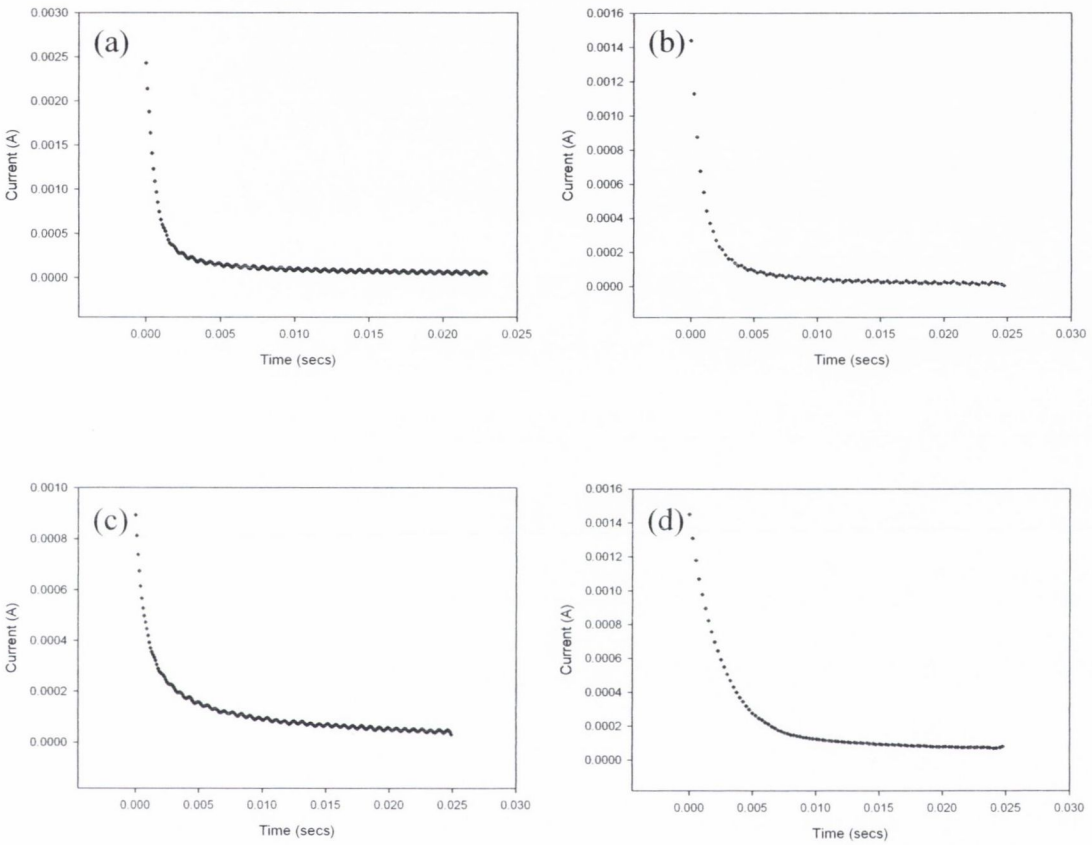


Figure 3.7. Chronoamperometry response over the oxidation processes of $S(CH_2)_{11}FcCO_2H$ (n=6,8,10,l2). (a) n=6, (b) n=8, (c) n=10, (d) n=12

From the current transients shown in Figure 3.7 it is possible to extract electron transfer rate constants. Again this method is described extensively in *Section 2.4.2.* Plots can be made of the natural logarithm of current versus time. This graph is expected to be linear the slope of which yields the electron transfer rate constant. Generally two rate constants may be obtained from plots such as those shown in Figure 3.7. The first, a faster rate constant, occurs at shorter timescales and may be attributed to a combination of the charging of the electrode surface (associated with chronoamperometry experiments) and electron transfer between the redox moiety and the electrode surface. The second, slower rate constant, occurs at longer timescales

and is attributed to arise from solely from the transfer of electrons. A sample of such natural logarithm of current versus time plot is shown in Figure 3.8 and the how the two rate constants are extracted in shown in Figure 3.9 below.

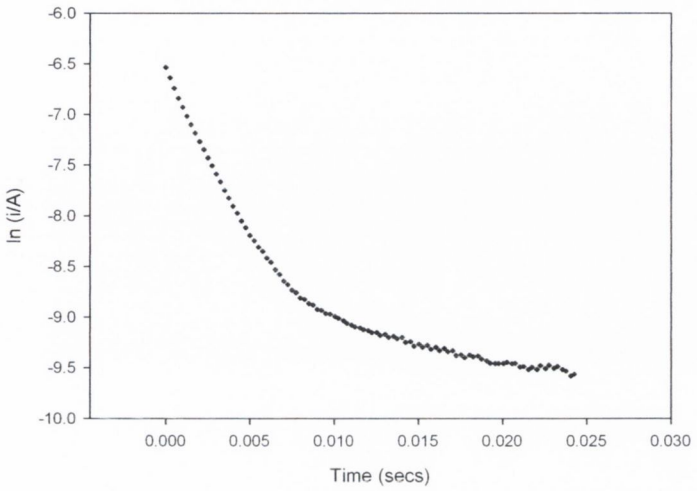


Figure 3.8. Natural logarithm of current vs. time for the oxidation process of $SH(CH_2)_{10}CO_2HFc$. The non-linearity of the plot indicates a dispersion of electron transfer rate constants.

Figure 3.9 below shows how the two rate constants described above may be extracted from the plot in Figure 3.8. The two separate regions are then subjected to least squares linear fitting. It is using this method that two distinct rate constants may be determined from each chronoamperometric response. It is noteworthy at this point to make reference to work carried out by Albrey et al.[11] who have described a complimentary method of measuring rate constants based on the assumption that there is a Gaussian spread of the rate constants throughout the system. This method has not been used in this work however.

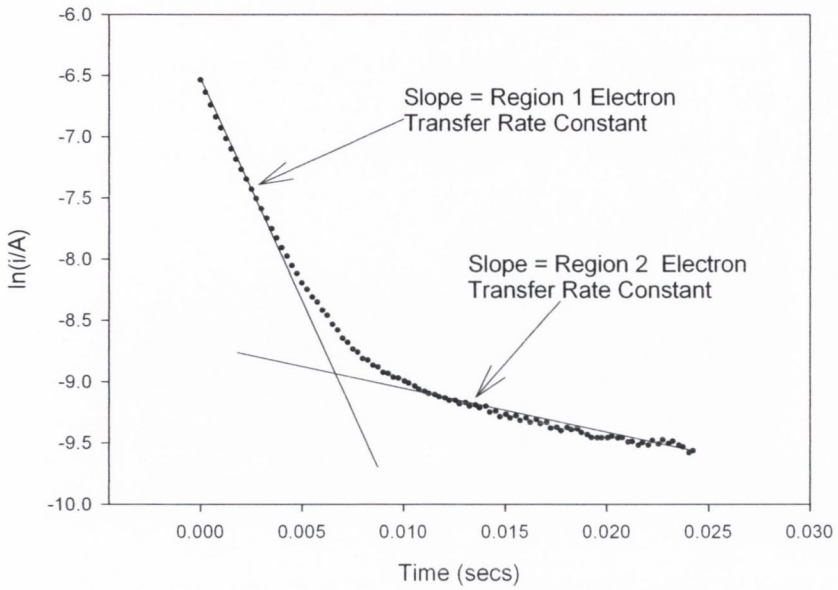


Figure 3.9. The two regions of linearity that may be used to extract electron transfer rate constants from a plot such as that presented in Figure 3.8.

As shown in Figure 3.7 chronoamperometry studies were carried out on electroactive monolayers of varying alkane chain length. For each chain length the two electron transfer rate constants were extracted. These are shown in Table 3.6 below.

Electron Transfer Rate Constant (s^{-1})			
n	**Chain Length* (Å)**	**Region 1**	**Region 2**
6	10.2	1024	51
8	12.7	838	82
10	15.2	577	62
12	17.7	365	42

Table 3.6. The electron transfer rate constants extracted from the oxidative chronoamperometry response of an $FcCO_2H(CH_2)_nSH$ (n=6,8,10,12) monolayer. Two values of electron transfer rate constant for each chain length are calculated. The origin of these two rate constants is described above in the text *The chain length (l) is defined as the distance between the carbon linked to the sulfur and the linked carbon of the cyclopentadiene ring. Thus l=0 when the cyclopentadiene carbon is directly linked to the sulfur. Chain lengths are calculated using standard values of CH_2 and ester linker lengths as described by Smalley et al.[12].

Using the results shown in Table 3.6 it is possible to test one of the fundamental predictions of Marcus Theory which governs electron transport phenomena which is

that the probability of electron transfer depends directly on the distance over which the electron must travel. This is described in Equation 3.13 below.

$$k_{et} = \exp(-\beta x) \tag{3.13}$$

Rearranging this yields Equation 3.14.

$$\ln(k_{et}) = \beta.x \tag{3.14}$$

Where k_{et} is the electron transfer rate constant, β is the probability of electron transfer and x is the distance over which the electron must travel (effectively the length of the alkane chain. Thus a plot of $\ln(k_{et})$ vs. the chain length is expected to be linear. Figure 3.10 shows a plot of $\ln(k_{et})$ vs. the number of CH_2 units comprising the alkane linker to the ferrocene carboxylic acid redox moiety. Electron transfer rate constants of the Region 1 and Region 2 type were plotted. From such a graph it is possible to determine how the probability of electron transfer changes as a function of the number of CH_2 groups in the alkane chain. The first thing that may be noted from Figure 3.10 is that the plot of electron transfer rate constant against the number of CH_2 groups is only linear in the case of Region 1 rate constants and not in the case of Region 2. Considering Region 1 rate constants (Figure 3.10(a)) it is determined that β, the probability of tunnelling, is 0.17. This indicates that the probability of tunnelling decreases by 0.17 or 17% as each CH_2 unit is added. However it has already been noted that the Region 1 response in chronoamperometry is mainly due to the charging of the electrode surface and thus this plot should not be considered particularly instructive. The Region 2 rate constants provide a much better indication of the actual rate of electron transfer occurring between the electrode surface and the redox moiety. The plot in Figure 3.10(b) however is not linear as would be predicted by Marcus Theory. It is instructive to consider the values of the Region 2 rate constants though. The average value of k_{et} in Region 2 is ~$60s^{-1}$. Typical values for the rate of electron transfer in ferrocene based electroactive alkanethiol systems lie in the range of $1x10^3$ s^{-1} to $1x10^4$ s^{-1} [13, 14]. The electron transfer rate constants determined in Region 2 are dramatically lower than these expected values. The fact that the rate constants measured in Region 2 for each of the chain lengths are so much lower than this

expected value would indicate that the rate of electron transfer in the system is very much affected by the ability of the pendant ferrocene molecules to form ion pairs with the perchlorate molecules. Thus the formation of ion pairs at the surface of the electroactive SAM is likely to be the rate determining step in the electron transfer.

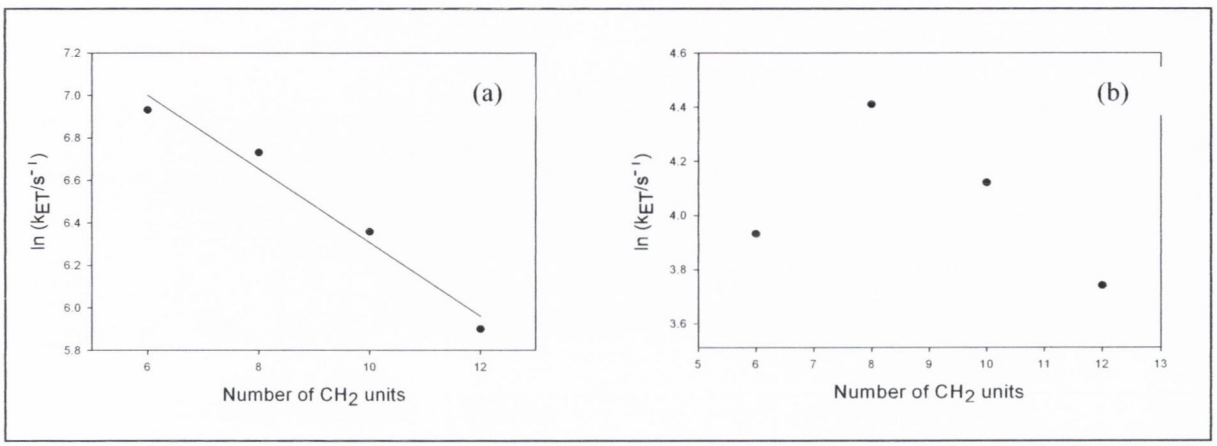


Figure 3.10. Plot of ln(k_{et}) vs. number of CH_2 alkane linker units for (a) Region 1 and (b) Region 2 electron transfer rate constants as a test of the predictions of Marcus Theory.

3.4 Conclusion

In this chapter self-assembled monolayers of ferrocene terminated alkane thiols were extensively characterised via the use of cyclic voltammetry (CV) an electrochemical quartz crystal microbalance (EQCM) and chronoamperometry.

Firstly monolayers with a range of linker sizes ($S(CH_2)_nCO_2HFc$ n = 7, 8, 10, 11) were investigated via cyclic voltammetry. It was determined that as the length of the alkane linker to the pendant ferrocene molecules increased so too did the surface coverage due to increased packing between the alkane chains.

Molecular interactions between adjacent redox pairs in the monolayer were then calculated using an extension of the Brown-Anson model. The deviation from an ideal electroactive monolayer was calculated and it was found that the deviation increased as the chain length increased. Again this is due to the increased packing between longer chain alkanethiols leading to increased interactions between adjacent ferrocene molecules. EQCM was then employed to investigate ion pairing between the ferrocene molecules and electrolyte ions. In general it was found that SAMs incorporated one monolayer of ions upon oxidation that were subsequently discarded back into solution upon reduction.

Finally chronoamperometry was used as a tool to investigate the nature of electron transfer through the electroactive monolayers and to test one of the fundamental aspects of Marcus Theory. Two electron transfer rate constants were measured one the first was due to the charging of the electrode surface and the second due to electron transfer. From slower than expected electron transfer rate constants in the second region it was proposed that the rate determining step in electron transfer events in ferrocene terminated SAMs was ion pairing.

References

(1) C.E.C Chidsey, C.R. Bertozzi, T.M. Putvinski and A.M. Mujsce, *J. Am. Chem. Soc.* **1991,** *112,* 4301.

(2) M.M. Walczak, D.D. Popenoem R.S. Deinhammer, B.D. Lamp, C. Chung and M.D. Porter, *Langmui,* **1991,** *7,* 2687

(3) T. Kondo, M. Takechi, Y. Sato and K. Uosaki, *J. Electroana.l Chem.* **1995**, *381,* 203

(4) T. Othsuka, Y. Sato and K. Uosaki, *Langmuir,* **1994**, *10,* 3658.

(5) N.L. Abbott and G.M. Whitesides, *Langmuir,* **1994**, *10,* 1493.

(6) K. Shimazu, I. Yagi, Y. Sato and K. Uosaki, *J. Electroanal. Chem.* **1994**, *372*, 117

(7) K. Shimazu, Y. Sato, I. Yagi and K. Uosaki, *Bull. Chem. Soc. Jpn.* **1994**, *67,* 863

(8) H.C. DeLong, J.J. Donohue and D.A. Buttry, *Langmuir,* **1991**, *7*, 2196

(9) K. Shimazu, I. Yagi, Y. Sato and K. Uosaki, *Langmuit,* **1992**, *8,* 1385.

(10) X. Yao, J. Wang, F. Zhou, J. Wang and N. Tao, *J. Phys. Chem B,* **2004,** *108*, 7206

(11) W.J. Albrey, P.N. Bartlett, C.P. Wilde, J.R. Darwent, *J. Am. Chem. Soc.* **1985,** *107,* 1854.

(12) J. F. Smalley, H. O. Finklea, C. E. D. Chidsey, M. R. Linford, S. E. Creager, J. P. Ferraris, K. Chalfant, T. Zawodzinsk, S. W. Feldberg, and M. D. Newton, *J. Am. Chem. Soc.* **2003,** *125,* 2004.

(13) J. J. Sumner, K. S. Weber, L. A. Hockett, and S. E. Creager, *J. Phys. Chem. B* **2000,** *104,* 7449.

(14) K. Weber, L. Hockett, and S. Creager, *J. Phys. Chem. B* **1997,** *101,* 8286

CHAPTER 4 –

ADSORPTION STUDIES OF ELECTROACTIVE MONOLAYERS

4. Adsorption Studies of Electroactive Monolayers

4.1 Introduction

This aim of this section is to provide a full understanding of the processes involved in the formation of self-assembled monolayers. This work will be structured as follows. Firstly there will be an introduction to the area of SAM adsorption where the processes thought to be involved in SAM formation are detailed. An introduction to work that has been carried out previously will also be given.

This will be followed by results focusing on the adsorption of alkanethiol molecules. The basis of the study involves using electroactive molecules as the adsorbate. This gives the opportunity to not only examine the kinetics of SAM formation but also to examine the quality of the layers deposited as will be discussed. The adsorption mechanisms will be studied as a function of chain length, deposition solution concentration and temperature. Following this a combination of cyclic voltammetry and EQCM will be combined in a unique way to investigate the nature of monolayer formation.

4.1.1 Growth Mechanisms

This section will address the two main process involved in the formation of self assembled monolayers (SAMs) of alkanethiols. The first process is bulk transport and adsorption which deals with the transport of alkanethiol molecules to the surface of the electrode and the likelihood of it sticking to the surface. The second, self-organisation, deals with the most important aspect of alkanethiol SAMs that being the ability of the molecules to orientate themselves in a ordered manner.

Bulk Transport and Adsorption

The first step in the formation of a SAM is the transport of the alkanethiol molecules from the solution to the electrode surface. This transport can be a combination of diffusive and convective transport. Once the species has been transported to the surface of the electrode it is required to adsorb to the surface. This process occurs with a certain adsorption rate which is governed by the ease at which molecules can bind to the electrode surface. This is commonly known as the sticking probability. A number of factors determine the sticking probability among the most prominent are

the electrode-molecule tail group interactions, electrode surface morphology and the amount of molecules already bound to the electrode surface.
The overall SAM formation kinetics are likely to be determined by a mixture of bulk transport control and adsorption control.

Self Organisation

The second and certainly most complex area regarding the formation of alkanethiol SAMs is related to the mechamism by which the molecules order themselves in an ordered manner when they have successfully adsorbed onto the surface of the electrode. In SAM formation there must be an evolution of molecular order as adsorption progresses and surface coverage increases. To demonstrate what is meant by the increase in molecular order as adsorption increases we imagine at the beginning of the SAM formation isolated alkanethiol molecules sitting on the surface of an electrode. The chains are conformationally disordered and randomly distributed around the surface. As the adsorption reaches its end the alkane chains are standing upright and densely packed on the electrode surface with a common conformational orientation. However there it is postulated that there does not exist a continuous path between these initial and final states. Experiments show that there is a stepwise path between the initial and final states. Possible states are identified as (1) a low density phase where the mobile alkanethiol molecules are randomly deposited on the surface of the electrode and the chains are conformationally disordered. (2) A mixed phase involving alkanethiol molecules adsorbed on the electrode surface which may be either conformationally disordered or lying flat on the surface of the electrode. (3) A final high-density phase involving the molecules being conformationally ordered, close packed and standing (in the case of close packed alkanethiol molecules) with a tilt angle of approximately 30^{O} to the surface normal[1]. The formation of the monolayer system can be represented by isothermal path through a 2D-phase diagram such as that shown in Figure 4.1.

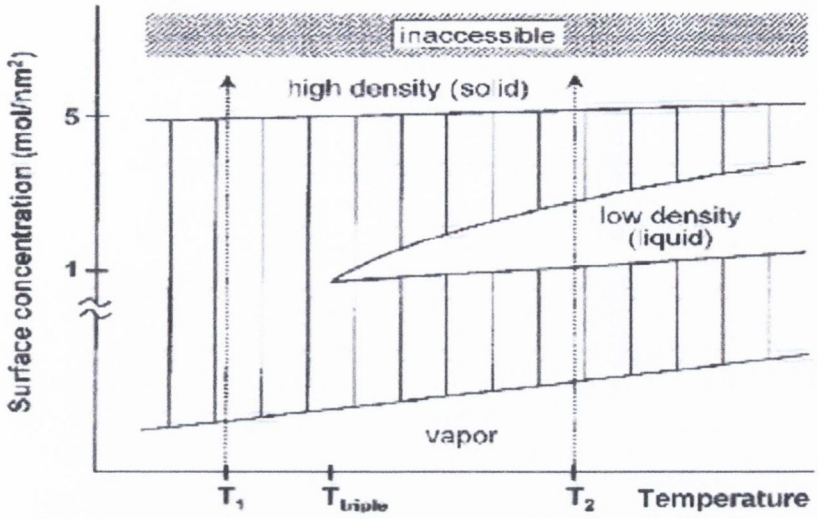


Figure 4.1. 2D-phase diagram for showing proposed paths for the formation of alkanethiol SAMs. The dotted lines represent proposed paths for the growth of SAMs at two different temperatures T_1 and T_2 above and below the triple point temperature, T_{triple}, respectively. Reproduced from reference (2).

Two different monolayer formation mechanisms are postulated. These mechanisms occur at T_1 and T_2. If the temperature of the system is T_1, which is lower than the triple point temperature, then the adsorption mechanism is thought to be as follows. Firstly the molecules will form a 2D-vapor phase. At a relatively low surface concentration the molecules will form an intermediate region between the disordered vapour phase and the ordered solid phase. It is thought that these intermediate islands of solid phase will nucleate and grow surrounded by regions of the disordered vapour phase. These ordered regions will eventually grow to encompass the entire substrate. This mechanism is similar to the formation mechanism for epitaxial films from the vapour phase[3]. If the temperature of the system is T_2 we see that the surface concentration of the vapour phase increases as well as this the formation of islands of intermediate structure will form. Such phases are known as 2D-liquid phases. These intermediate, 2D, regions may consist of either a disordered solid phase where the alkanethiol molecules are observed to be orientated parallel to the surface or effectively lying down on the surface or a low density solid phase. Eventually the growth will involve islands of the high density solid films surrounded by the low density regions. These regions eventually coalesce to form one high density film.

A schematic representation of the two mechanisms postulated above is shown in Figure 4.2.

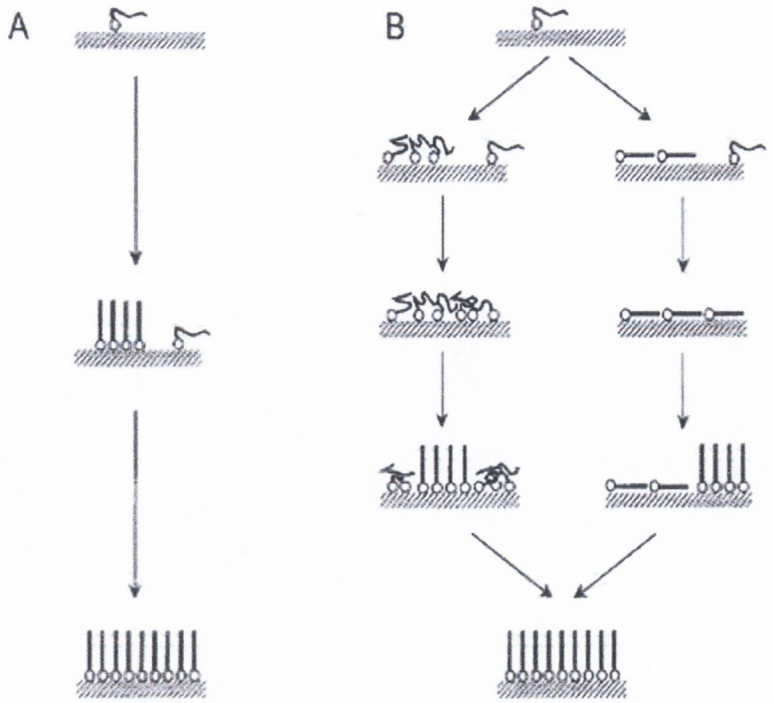


Figure 4.2. Showing the mechanisms described for the formation of alkanethiol SAMs. (A) Showing the growth mechanism below the triple point (T_1). This depicts the initial formation of a 2D vapour phase followed by the formation of a solid-vapour coexistence region and finally the formation of an ordered film. (B) Showing the two mechanisms thought to be responsible for the formation of a SAM above the triple point temperature (T_2). In this case the SAM formation must pass between three distinct phases before it reaches the ordered phase. Reproduced from reference (2).

At this point we must mention that the descriptions of the various mechanisms of SAM formation have been somewhat oversimplified. There are two main simplifications made. The first involves the fact that the entire above description hinges on the fact the adsorption rate of alkanethiol molecules on the surface of the electrode is much slower than other processes that happen on the electrode surface. This essentially means that as soon as the molecules are adsorbed onto the surface of the electrode the SAM molecules proceed through the various conformational changes before much more adsorption occurs on the surface of the electrode. This is not necessarily a correct assumption. The ramifications of this can be described by imagining the nucleation of the condensed phases on the electrode surface. If the growth of these condensed phases do not keep up with the adsorption rate of the alkanethiol molecules it is likely that further molecules impacting upon the surface will not be bound to the growing condensed phases as expected but be adsorbed at less condensed phase sites. The less condensed phase then becomes extremely

concentrated and will have a density greater than the equilibrium coexistence concentration. Thus the density of the so-called "less dense" or "vapour" regions are likely to fluctuate much more than was expected by using the simplified model discussed.

A second simplification of the above adsorption model is that the 2D-liquid phase which appears at temperatures above the liquid phase is likely to be much more complicated than is depicted in Figure 4.1 where the condensed phase consists of only one region. In the case of alkanethiol molecules that have numerous degrees of freedom there is likely to be more than one condensed phase into which the molecules orientate themselves which is not depicted in the phase diagram of Figure 4.1. Kaganer et al.[4] showed for the case of long chain fatty acids that there are a number of different orientations that the alkane chains could adopt in the liquid phase and determined that such different phases showed differences in compressibility when using the Langmuir method to deposit SAMs. Indeed it was suggested by the author that the term "liquid-condensed" corresponding to the 2D-liquid phase in the alkanethiol system be abandoned completely due to the ambiguity associated with it's description.

However, although the above description is certainly oversimplified it will still be used as an outline to attempt to describe how the self assembled monolayers are formed.

4.1.2 Adsorption of Alkanethiols on Gold

A vast amount of literature has been published regarding the formation mechanisms of alkanethiols on gold. For this reason this section will attempt to summarise recent work regarding the nature of alkanethiol adsorption.

In 1989 Whitesides et al.[5] utilised contact angle and ellipsometry experiments to monitor the rate of growth of alkanethiols on gold. This study determined that the growth of alkanethiol monolayers reached 90% of their final value after one minute adsorption time. After the first minute a second step was identified which lasted a number of hours.

Shimazu et al.[6] utilised EQCM to monitor the mass change on the surface of a gold electrode as a function of time. In this case the molecules concerned were ferrocene substituted alkanethiols. Again in this case an initial rapid adsorption step

was observed lasting approximately 10 seconds followed by a slower orientation period lasting 800 seconds in the case of this study where the mass of the film seemed relatively constant indicating that no further adsorption onto the surface was taking place. Kim et al.[7] also utilised EQCM to observe the formation of alkanethiol SAMs. This study observed the change in mass of a gold electrode when exposed to differing concentrations of octadecanethiol. Again an initial rapid adsorption step was observed after a few seconds followed by a longer orientation period lasting 2000 seconds. Strangely the final mass of alkanethiol deposited on the surface of the electrode was not identical in the case of all concentrations. Lower concentrations of alkanethiols deposited a lower mass onto the electrode surface than in the case of higher concentration. This may indicate that the experiment was not run long enough for the films to be fully formed. Frubose et al.[8] also utilised EQCM to study SAM formation and noted that two distinct timescales were involved, the first lasting a period of about 120 seconds whilst the second occurred over a period approximately 1 hour. Schneider et al.[9] utilised EQCM to study SAM formation they proposed multiplayer formation as a possibility when alkanethiols are deposited on gold from acetonitrile whilst no multiplayer formation is observed in the case of adsorption from a DMF solution. Karpovich et al.[10] as well as Schessler et al.[11] performed EQCM studies on the adsorption of octanethiol (C_8) and octadecanethiol (C_{18}) as a function of concentration. They noted that the adsorption kinetics exhibited concentration dependence with the rates of adsorption increasing with thiol concentration.

De Bono at al (12) utilised surface plasmon resonance (SPR). This study again observed a two-step mechanism for the formation of the mechanism and quotes a difference in timescales as differing by a factor of approximately 100 which is consistent with what has been described already utilising EQCM. The study states that the initial fast process results in around 80% of the SAM being formed for longer chain alkanethiols (C_{12} and C_{16}) wheras only 50% coverage is achieved during this step for shorter chain alkanethiols (C_6). It was also noted that the rate constant for the adsorption of the longer chain alkanethiols is greater than that of the shorter chain alkane thiols. These studies both used Langmuir adsorption kinetics to model the adsorption process.

The findings of De Bono et al. were contradicted by Peterlinz et al.[13] who cited a three-step process for SAM formation. An initial adsorption step was identified as lasting approximately 30-60 mins. However this study observed that as

the mass of the alkanethiol molecule used to form the SAM increased the rate constant for the formation of the SAM decreased during this first phase. It was determined that for shorter chain alkanethiols about 80% of the SAM was formed whereas for the longer chains only 40%-50% was observed. During a second step lasting several hours the reverse process is observed during which the longer chain alkanethiols are seen to adsorb more quickly than the shorter chains. The onset of the third step is observed after ~4hrs for C_{18} and 18hrs for C_{16} SAMs. The thickness of the C_{16} and C_{18} films appears to become stable after 72hrs.

Buck et al.[14] utilised in-situ simple harmonic generation (SHG) to observe the adsorption of alkanethiols. In this case only one timescale for the adsorption was observed which lasted less than one minute. Dannenberger et al.[15] also used SHG to look at the adsorption of alkanethiols of the form $CH_3(CH_2)_{n-1}SH$ where for n = 4 to n = 22. This study also looked at the effect of varying the concentration of the alkanethiols from 0.5 to 20 μmol. Again this study stated that the Langmuir adsorption model correctly explained their observations.

Kawasaki et al.[16] examined the initial 2 hrs of growth of alkanethiol SAMs as a function of concentration and temperature. This study noted that complete monolayer coverage was achieved at room temperature after 0.2-60 mins incubation in 0.1, 0.01 and 0.001mM ethanolic solutions of alkanethiols. They noted a single step process in the case of 0.1 and 0.01mM concentrations and a two step process in the case of the 0.001mM deposition solutions. By increasing the temperature of the deposition solution to 35^{O}C a single step adsorption was also observed for the 0.001mM solution.

Truong et al.[17] utilized infrared spectroscopy (IR) to monitor the decreased intensity of the CH_2 bands as the adsorbed film was permitted to equilibrate and assemble. The band intensities suggested that after 15 mins of immersion the alkane chains were orientated close to the surface normal. They also showed that molecules in less than full coverage SAMs tend to aggregate into islands which have identical properties to that of a fully formed SAM. Terrill et al.[18] used Fourier Transform Infrared Spectroscopy (FTIR) to monitor the assembly of hexadecanethiol (C_{16}) from 0.001, 0.1, 1, or 10 mM ethanolic solutions. The study identified an increase in SAM crystallinity and, in some cases, a decrease in average chain tilt angle with respect to the surface normal during a long assembly time. The main conclusion of this work

was that SAM crystallinity continued to evolve after for up to a period of as long as 10^6 seconds. It was found that smooth electrode surfaces and higher thiol concentration favored a more rapid SAM formation. Bensebaa et al.[19] studied the adsorption mechanism of docosanethiolate (C22) using reflection/absorption infrared spectroscopy (RAIRS). This study reported that well ordered and densely packed SAMs were formed after a period of 45 seconds and identified a two-step process for the formation of the SAM. The first step identified is expected to take ~1 second and involves the formation of disordered clusters on distant sites. The second step involves the formation of ordered domains that increase in size with immersion time. Himmelhaus et al.[20] performed sum frequency generation spectroscopy studies on docosanethiol (C_{22}) SAMs. In this case three distinct growth stages were identified. The first stage involved the formation of a bond with the thiol molecule and the gold surface. This process lasted approximately 5 minutes and was responsible for 80-90% of the surface coverage. The second stage lasting about 10 minutes involved the reorientation of the hydrocarbon chains from randomly ordered to a more densely packed orientation. The third and final stage lasting to about 2 hours immersion time involved the orientation of the terminal CH_3 groups in an ordered manner relative to one another.

Yamada et al.[21, 22] performed in-situ, real time STM studies of alkanethiols from heptane solutions. The alkanethiol systems studied were C_{10}, C_{15} and C_{18}. This study determined three basic steps for the adsorption mechanism. Firstly disordered islands of alkanethiol molecules were observed. The second step involved the formation of striped phases which were attributed to alkanethiols lying flat on the surface in a disordered manner. The third step involved the coalescence of these disordered islands to form an ordered monolayer. Xu et al.[23] carried out an AFM study which agreed with Yamada and coworkers STM description of the adsorption mechanism as well as providing information on the height profiles of the alkanethiol molecules. It determined a height of 0.5nm on the surface of the gold electrode after short immersion times consistent with alkanethiol molecules lying flat on the surface. After longer immersion times a height of 23nm was observed on the surface pointing to the alkanethiol molecules standing upright on the surface of the gold.

4.1.3 Functional Form of Coverage Kinetics

When a clean gold surface is immersed in an alkanethiol solution the following net chemical reaction occurs:

$$\text{Au} + \text{R-SH} \rightarrow \text{Au-SR} + \frac{1}{2}\text{H}_2$$

This is a chemisorption reaction which self-terminates when one monolayer has been formed. Langmuir adsorption kinetics may be used to describe this reaction. The model assumes that adsorption is limited to one monolayer, all surface sites are equivalent and that adsorption on one site is independent of occupancy of adjacent sites. The Langmuir isotherm was originally derived for physisorption but the alkanethiol – gold bond strengths are weak enough that the condition is not violated. Assuming Langmuir adsorption kinetics the rate of formation of the monolayers can be expressed in Equation 4.1.

$$\frac{d\theta}{dt} = k_a(1-\theta)C - k_d\theta \tag{4.1}$$

Where θ is a unitless quantity expressing the fraction of available sites upon which alkanethiol molecules have adsorbed, k_a and k_d are the adsorption and desorption rate constants respectively. Integration of Equation 4.1 yields Equation 4.2 where C is the thiol concentration in solution.

$$\theta(t) = \frac{C}{(C + \frac{k_d}{k_a})}(1 - e^{-(k_a C + k_d)t}) \tag{4.2}$$

We can set the observed rate constant as:

$$k_{obs} = k_a C + k_d \tag{4.3}$$

and for convenience:

$$k' = \frac{C}{(C + \frac{k_d}{k_a})} \tag{4.4}$$

resulting in Equation 4.5.

$$\theta(t) = k'(1 - e^{-k_{obs}t}) \tag{4.5}$$

Equation 4.5 has frequently been used to fit kinetic data for SAM growth. In fact in most cases the simple Langmuir model can be used to describe the adsorption process. In two papers by Dannenberger at al[15, 24] the early stages of alkanethiol adsorption were studied using SHG and found to agree quantitatively with the Langmuir adsorption model. These studies also considered a modified Langmuir adsorption model considering different pathways for the molecules to chemisorb called the Kisluik Model[25,26]. Himmelhaus et al.[20] used SFG and also found that early adsorption data was consistent with Langmuir kinetics. Peterlinz et al.[13] showed that the adsorption kinetics of alkanethiol molecules from an ethanol solution was a three step process. The first, most rapid, adsorption step and the third, slowest, step could be described well with the Langmuir adsorption model. The kinetics of the second step were shown to be zeroth order and dependant on alkanethiol chain length, concentration, and partial film thickness. The formation kinetics from a heptane solution were shown to be described by a simgle step Langmuir adsorption model.

Shao et al.[27] observed that the kinetics of SAM formation could be based on the Frumkin shown in Equation 4.6.

$$\frac{\theta}{1-\theta} = ce^{-(\frac{\Delta G_0}{kT})}e^{-g\theta} \tag{4.6}$$

Where we say that

$$\Delta G = \Delta G_0 + \gamma\theta \tag{4.7}$$

If the adsorbates attract then $\gamma > 0$ and if they repel then $\gamma < 0$. When $\gamma = 0$ we return to the Langmuir equation. Also $g = \gamma/kT$.

We have already shown with the aid of a number of examples that the processes involved in SAM formation have been observed to be far from simple as demonstrated by the difference in experimental observations. This being the case it is somewhat surprising that the simple Langmuir model effectively describes SAM formation involving island nucleation and growth, multiple 2D-phase transitions etc.

There are limitations to the Langmuir model however at the very early and very late formation stages. At early times a discrepancy is often found in the observed alkanethiol surface coverage and that expected from the Langmuir model. This difference is thought to be attributed to an induction time observed before the growth starts. At late formation times (final 10-20%) the SAM growth is generally found to evolve much slower than the earlier regimes. However the Langmuir model for all its simplicity remains remarkably robust and is well worth considering as the model for SAM formation kinetics.

4.1.4 Solvent Effects

Although the effect of solvent on SAM formation kinetics or quality will not be studied in this section it is felt necessary to provide a brief discussion of this area as a number of studies have been produced on the topic. Peterlinz[13] et al. utilised *in situ* SPR to monitor the growth of alkanethiol SAMs from ethanolic and heptane solutions. The study reports that the initial stage of SAM growth is ~35% faster using a heptane solution than from an ethanolic solution. Moreover their results indicate that the growth processes vary between the two solvents. Growth from heptane solutions proceeded via a single relatively rapid step whereas growth from ethanol solution involved three distinct growth steps. Karpovich et al. did not determine any significant difference in monolayer formation between hexane and cyclohexane[10]. Formation of multilayers in acetonitrile[9] and layers with 20% higher surface coverage than a single SAM[28] have also been reported. Dannenberger et al.[25] utilising SHG found that solvents affected the growth kinetics in the order hexane<ethanol<dodecane<hexadecane. This order corresponds to solvent viscosity and it is proposed that higher viscosity solvents impede the diffusion of the alkanethiol molecules through solution slowing down adsorption kinetics. It has also been suggested however that the rate of adsorption is limited by the ability of the SAM molecules to displace solvent molecules from the electrode surface, thus solvents with a greater affinity to the electrode surface would lead to slower deposition times.

4.1.5 Chain Length Effects

The effect of chain length on adsorption time is discussed in this section and thus a review of reports regarding chain length is presented here. There are two completely conflicting views on chain length effects the first stating that longer chain alkanethiols will form an ordered SAM more quickly than shorter chains and the second stating exactly the opposite.

The argument for longer chains forming a SAM more quickly is that the longer chains have a greater ability to be conformationally disordered in solution (bending stretching etc.) leading to them having a higher free energy in solution and thus being less soluble than shorter chains meaning that they will adsorb onto the electrode more quickly. This argument effectively assumes that diffusion controls the rate of SAM formation. This theory has confirmed experimentally by Bain et al.[5] who determined that C_{18} SAMs formed faster than C_{10} SAMs from ethanolic solutions and Xu et al.[23] who reported that C_{22} formed faster than C_{18} from 2-butanol solution. Jung at al[29] performed SPR studies on C_2 to C_{18} alkanethiols. It was determined the sticking probabilities of alkanethiol molecules increase as a function of chain length from $\sim 10^{-8}$ to $\sim 10^{-6}$.

The second, conflicting theory is that shorter chain alkanethiol molecules will form an ordered SAM more quickly than longer chains. This theory argues that the rate-limiting factor for SAM formation is determined by the time taken for the molecules to align themselves in an ordered fashion on the electrode surface. In this regard shorter chain molecules are likely to orientate themselves more quickly on the surface of the electrode since they have less propensity to be bent and coiled as the longer chains have. This theory has been reported by Peterlinz et al.[13] who found that the initial growth rate from ethanolic solution proceeded in the order $C_8 > C_{12} > C_{16} > C_{18}$. Dannenberger et al.[15] found that the growth rate went as $C_4 > C_{12} > C_{22}$.

Further to these studies De Bono et al.[12] found that the initial stages of growth for C_{16} and C_6 proceeded at the same rate both of which were faster than that of C_{12}. Karpovich et al.[10] found that the growth rate of C_8 and C_{18} were approximately equal.

Thus all of the above serves only to produce a more confused picture of the exact growth mechanism. What is most likely is that the mechanism of alkanethiol

adsorption is a complicated mechanism of solvent, chain length, temperature and electrode surface morphology effects.

4.1.6 Submonolayer Islands

As has been mentioned in *Section 4.1.1* the formation of an ordered SAM is usually preceded by the formation of islands of ordered areas. Because of the importance of this process in the overall formation mechanism this section will describe some studies regarding the nature of submonolayer islands. Doudevski et al.[30] utilised in-situ AFM to determine the time dependence of the island number density. Three main growth stages were identified regarding the islands. The first step (growth) occurred at times less than 600s formation of an increasing number of islands. The second step (aggregation) occurred between 600-3000s and involved the growth of the existing islands. The third growth step (coalescence) involved a rapid decrease in the number of observed islands due to the coalescence of existing islands to form one ordered SAM. It was also determined in this study that the critical nucleus for island formation consisted of only 2 molecules.

Further work by Doudevski & Schwartz[31] involved focusing on the aggregation regime of SAM growth, again using AFM. They found, as expected, that as growth proceeded the average island size increased within this regime. They used these results to test the dynamic scaling assumption, which is a fundamental assumption of cluster growth. The dynamic scaling concept assumes that at any given growth stage there will only be a single characteristic island size which is a function of the fractional island coverage. This study also identified the ratio R, where,

$$R = \frac{4D}{F} \tag{4.8}$$

Here F is the rate at which molecules are impinging on the surface from the bulk phase. When the molecules reach the surface they undergo a random 2D diffusion with diffusion constant, D. We note that when F is large the resulting high concentration of monomers makes collisions between monomers more likely and hence island nucleation more probable. When D is large molecules on the surface are more likely to collide and attach with existing islands also making island formation more probable. It has been shown that at a given stage of growth the number of islands typically scales as $R^{-1/3}$ [32].

4.2 Experimental

Electrochemical Measurements. All electrochemical measurements were carried out on a CH Instruments Model 440 potentiostat as described in *Section 2.2.1.*

Gold Substrate. The gold substrate used whether it be a standard macroelectrode or an EQCM electrode is as described in *Section 2.1.1.*

Electrode Pre-Treatment. The method used for electrode pre-treatment is described in *Section 2.3.1.*

Deposition of the ferrocenyl alkanethiol SAMs onto the gold substrates.
In the case of experiments performed using the macroelectrodes monolayers were allowed to form for a certain period of time and subsequently removed from their deposition solutions for cyclic voltammetry analysis. This process of halting the growth a monolayer for analysis is known as quenching. The formation intervals at which the monolayer was examined were after 5 secs, 10 secs, 20 secs, 30 secs, 1 min, 2.5 mins, 5 mins, 7.5 mins, 10 mins, 15 mins, 30 mins, 60 mins and 120 mins of growth time. The process involved thoroughly rinsing the electrode in ethanol and dipping it into the deposition solution of alkanethiol. When the required time period had elapsed the electrode was removed from the deposition solution, rinsed in ethanol and deionised water and placed in the electrochemical cell as the working electrode for cyclic voltammetry. When cyclic voltammetry had been carried out the electrode was removed from the electrochemical cell, rinsed in deionised water and ethanol and reintroduced into the deposition solution for the next period of time. The process of quenching was then repeated when this growth time had elapsed. For temperature measurements deposition solutions were heated to 40°C and 60°C using an IKA Labortecknik heater/thermostat.

In the case of EQCM measurements a similar mechanism of quenching was performed. In this case the deposition solution was introduced to the EQCM cell for a certain period of time and then removed from the cell via Pasteur pipette. The gold crystal was then rinsed with ethanol and deionised water and the aqueous perchloric acid electrolyte introduced in order to carry out combined cyclic voltammetry and quartz crystal microbalance measurements. The adsorption periods after which

monolayer formation was examined were 2.5 mins, 5 mins, 10 mins, 15 mins, 30 mins, 60 mins and 120 mins. When the measurement for a certain growth period was carried out the electrolyte was removed again by Pasteur pipette the gold crystal rinsed with deionised water and ethanol and the deposition solution again introduced to the EQCM cell for the required period of time.

Electrolyte Solutions. The electrolyte solutions used in all experiments were 0.1M Perchloric Acid unless otherwise stated. *Section 2.1.4* provides further details.

4.3 Results and Discussion

4.3.1 Macroelectrode Cyclic Voltammetry Investigation

In this section the cyclic voltammetry (CV) responses of a gold macroelectrode modified with quenched monolayers of ferrocene-terminated alkanethiols will be discussed.

As well as examining time dependence effects on monolayer growth the effect of deposition solution temperature and concentration will also be studied. These studies will be carried out for alkanethiols of three different chain lengths these being ferrocenylcarbonyloxy-octanethiol (8Fc), ferrocenylcarbonyloxy-decanethiol (10Fc) and ferrocenylcarbonyloxy-dodecanethiol (12Fc). Thus in effect the chain length dependence of monolayer deposition will also be studied.

The appendix at the end of this thesis gives pictures of all CVs recorded during this section of experiments as well as tables describing the voltammetry diagnostics.

4.3.1.1 8Fc thiol – Discussion of 0.01mM, 0.1mM and 1mM Results

8Fc 0.01mM Results. Figure 4.3 shows a plot of surface coverage vs. deposition time calculated from CVs recorded for the deposition of 8Fc thiol at 0.01mM concentration at room temperature (RT). Immediately at this point it is noted that no surface coverage data is presented for the depositions at 40°C and 60°C. This is because no electroactive ferrocene thiol is deposited at these particular concentrations and temperatures. The CVs corresponding to all depositions may be viewed in the appendix. The surface coverage values for the RT deposition (Figure 4.3) are seen to increase with increased deposition time however they remain well below the theoretical value of a full ferrocene-terminated monolayer, which is 4.5 x 10^{-10}mol.cm^{-2} [35], throughout the deposition. Again this would be is to be expected due to the low concentration of the deposition solution.

The voltammetry diagnostics for monolayer deposition can now be considered. Values for the voltammetry diagnostics are presented in the appendix. Firstly it is observed that the oxidation and reduction formal potentials, represented by E^0 where ($E^0 = (E_{ox} + E_{red})/2$), increase steadily towards a stable value of ~0.6V after 120mins deposition time. Whilst an increase in the E^0 is not necessarily expected a

stabilisation in its value is. This is due to the observation that as monolayer formation progresses the molecules will tend to align themselves in an ordered manner with respect to one another. This will lead to the formal potentials of the tethered ferrocene molecules tending to equality at longer deposition times, to the convergence of the overall monolayer formal potential at a particular value.

Secondly the oxidation and reduction peak currents are seen to increase as the deposition progresses indicating either an increased amount of alkanethiol molecules being deposited on the electrode surface or an ordering of the existing alkanethiol molecules which allows them to become electroactive.

Thirdly the peak separation, which is the voltage difference between the oxidation and reduction peaks, is seen to drop as monolayer formation progresses. A drop in peak separation is to be expected as in an ideally reversible monolayer no peak splitting would be observed. This nonzero peak splitting can usually be attributed to the fact that the solvation of the redox centres or the structure of the monolayer may change with the oxidation state of the redox centre. It has already been shown that the orientation of the alkanethiol molecules changes, relative to the electrode surface, upon oxidation[34].

Next the Peak Width Half Maximum (PWHM) values are examined. The PWHM values are effectively a measure of how well packed the SAM is. The ideal PWHM value for an electroactive monolayer with a one electron transfer reaction is 91mV. In this case however the PWHM value is well above the ideal value. These high values indicate a monolayer which is not densely packed or the existence of redox centres in a number of different redox environments. This manifests itself in wide peaks due to the fact that the molecules bound to the electrode become electroactive over a range of different potentials. This poor packing is to be expected for a monolayer formed from such a low concentration.

Attention is now turned to the monolayer depositions from solution with temperatures of 40°C and 60°C. It has been agreed that the deposition of monolayers from high temperature solutions is likely to lead to an increase in the quality of the SAM relative to that deposited at room temperature[36]. This is because when a monolayer is formed at room temperature alkanethiol molecules may order themselves in non-ideal conformations (e.g. chain entanglement). It is thought that the presence of a solution with an elevated temperature can provide enough energy to help the monolayer free itself from metastable disordered states. It has been

determined however that no electroactive thiol is deposited at these temperatures. Two possibilities could account for this observation. The first is that at higher temperatures the adsorption and desorption rate constants are in equilibrium such that it is not thermodynamically feasible for the molecules to remain on the surface of the electrode. The second is that at higher temperatures the molecules are forced to deposit in a certain manner such that they do not become electroactive over the potential range of this voltammetric analysis.

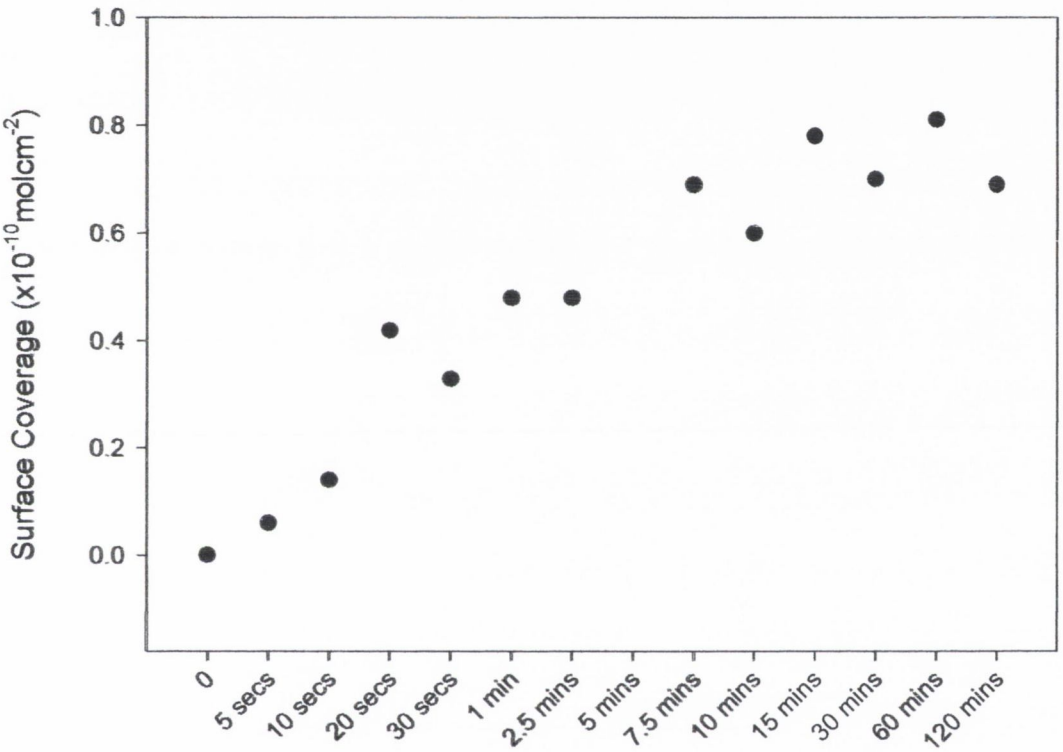


Figure 4.3. Surface Coverage as a function of deposition time calculated from cyclic voltammetry showing the deposition of 8Fc thiol from a 0.01mM solution at room temperature. All scans were carried out in 0.1M $HClO_4$ at 0.02Vs^{-1} scan rate.

8Fc 0.1mM Results. Figures 4.4, 4.5 and 4.6 show plots of surface coverage vs. deposition time calculated from CVs recorded for the deposition of 8Fc thiol at 0.1mM concentration at RT, 40°C and 60°C. Pictures of these CVs as well as voltammetry diagnostics are presented in the appendix.

Again for the 8Fc, 0.1mM, RT deposition the surface coverage values are far less than the theoretical value for a fully formed monolayer but are in general slightly higher than that of the 8Fc, 0.01, RT values especially in the initial stages of growth indicating faster bulk diffusion of the molecules in the case of higher concentrations.

Next the deposition of 8Fc, 0.1mM, 40°C is examined (Figure 4.5). In this case there is a definite deposition of the alkanethiol as opposed to the case of 8Fc, 0.01mM, 40°C. This would indicate that the formation of the monolayer is determined by a combination of temperature and concentration factors. At low concentrations and elevated temperatures the molecules may not be able to form the critical nucleus required for the formation of islands which signals the start of monolayer growth. This may be because the system has enough thermal energy to desorb what small amount of molecules deposit on the surface before they can form islands.

Interestingly in the case of 8Fc, 0.1mM, 40°C as the growth progresses to the longer deposition times of 60 mins and 120 mins the monolayer quality begins to drop. It is noted at these long times the surface coverage falls dramatically when it would be expected to increase and the PWHM values increase and in the case of 120 mins deposition becomes indeterminate. This would indicate that a monolayer will begin to degrade at this concentration after prolonged exposure to elevated temperatures.

Next the deposition of 8Fc, 0.1mM, 60°C is examined. In this case we encounter the same phenomenon as was seen for the 8Fc, 0.01mM elevated temperatures that being that no molecules appear to be deposited. Interestingly though this observation is only seen for 0.1mM concentration at 60°C deposition solution. In the case of the lower concentration (0.01mM) it occurred for 40°C and 60°C. Monolayer degradation only begins after 60 mins for 0.1mM at 40°C.

The voltammetry diagnostics for the deposition of 8Fc, 0.1mM at RT is now examined. Again these diagnostics are presented in the appendix. When this is compared to the 8Fc, 0.01mM, RT deposition it is noted that as the concentration increases so too do the peak currents for the oxidation and reduction currents. This would indicate that a greater amount of thiol is deposited onto the electrode surface at

a given time higher concentrations. The peak separations are similar in both cases indicating that there is a similar relationship between the oxidised and reduced forms of the electroactive species in both cases.

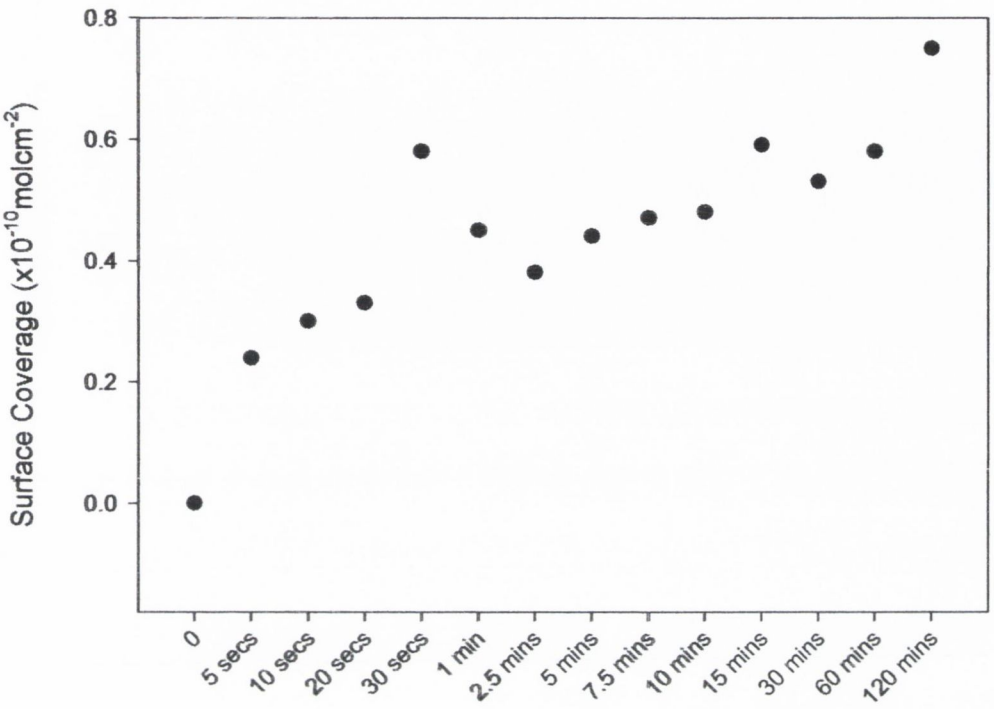


Figure 4.4. Surface Coverage as a function of deposition time calculated from cyclic voltammetry showing the deposition of 8Fc thiol from a 0.1mM solution at room temperature. All scans were carried out in 0.1M $HClO_4$ at 0.02Vs^{-1} scan rate.

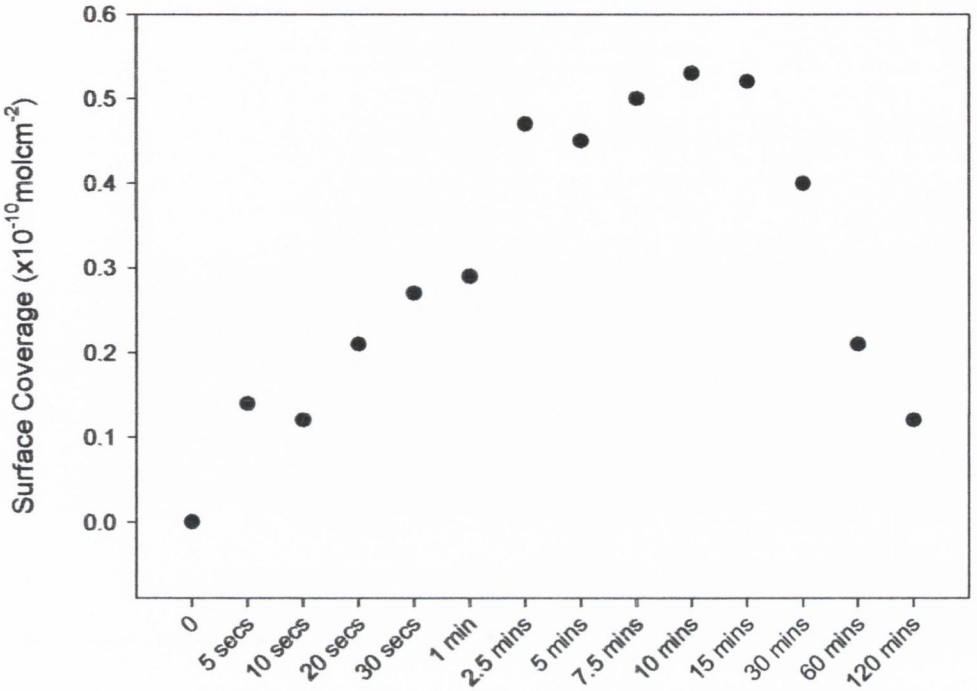


Figure 4.5. Surface Coverage as a function of deposition time calculated from cyclic voltammetry showing the deposition of 8Fc thiol from a 0.1mM solution at 40°C. All scans were carried out in 0.1M $HClO_4$ at 0.02Vs^{-1} scan rate.

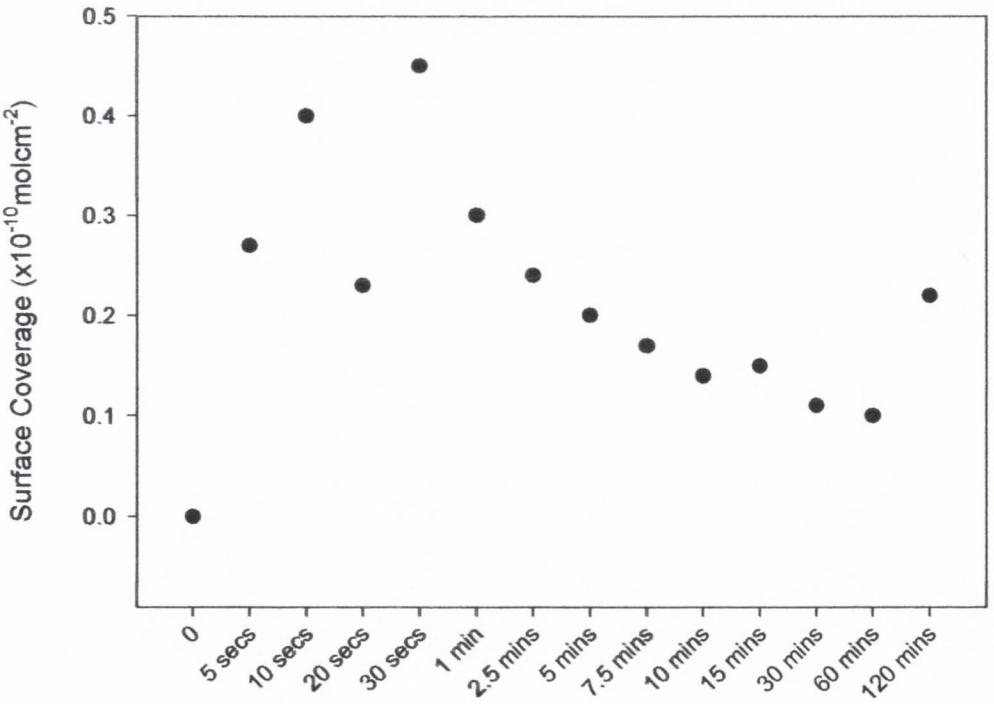


Figure 4.6. Surface Coverage as a function of deposition time calculated from cyclic voltammetry showing the deposition of 8Fc thiol from a 0.1mM solution at 60°C. All scans were carried out in 0.1M $HClO_4$ at 0.02Vs^{-1} scan rate.

8Fc 1mM Results. Figures 4.7, 4.8 and 4.9 show plots of surface coverage vs. deposition time calculated from CVs recorded for the deposition of 8Fc thiol at 1mM concentration at RT, 40°C and 60°C

Firstly the deposition of 1mM 8Fc at RT is examined. Surface coverage values are much higher than in the case of lower concentrations. Also the oxidation and reduction peak potentials, and hence the E^0 value, reach approximately their final value at very early deposition times. This suggests that at higher concentrations a well ordered monolayer is formed more quickly. This stability is also reflected in the peak current values that remain constant throughout the deposition apart from the values after 5 secs deposition.

Next the deposition of 8Fc, 1mM, 40°C is examined. Again in this case E^0 values reach an approximately constant value at very short deposition times. Oxidation and reduction currents are seen to grow only slightly throughout the monolayer growth with their final value being quite close to that achieved for 8Fc, 1mM, RT. Surface converge values grow steadily throughout the deposition again with the final value being relatively quite close to that achieved at RT. The major difference that was observed for growth at this elevated temperature was in the peak separation values which were much smaller than at RT indicating that less of a difference in conformation existed in between the oxidised and reduced form of the monolayer. An explanation for this is that differences between the oxidised and reduced states occur from defects in the monolayer (chain entanglement etc.). As stated before it is possible that elevated temperature growth removes such defects thus lowering the difference between oxidised and reduced states hence lowering peak separation values. Another interesting observation is that the PWHM values, which are essentially a measure of how well ordered the monolayer is, are lower than in the case of RT growth. The average value in this case is ~57mV compared to 75mV at RT. This observation adds weight to the theory that elevated temperature deposition removes defects during monolayer formation leading to a more ordered monolayer however this value is still not close to the ideal value of 90mV.

Finally the deposition of 8Fc, 1mM, 60°C is examined. Again in this case the value of E^0 reached a relatively constant value early in the deposition process. The values of the oxidation and reduction currents grow steadily throughout the growth process. The peak separation is small again indicating that higher temperatures

discourage the formation of defects. The average value of the PWHM is ~80mV which is the closest to the ideal 90mV obtained from any of the deposition conditions examined. Surface coverage increases steadily throughout growth and reaches a final value comparable to those obtained at RT and 40°C at this concentration but higher than anything obtained at lower concentrations.

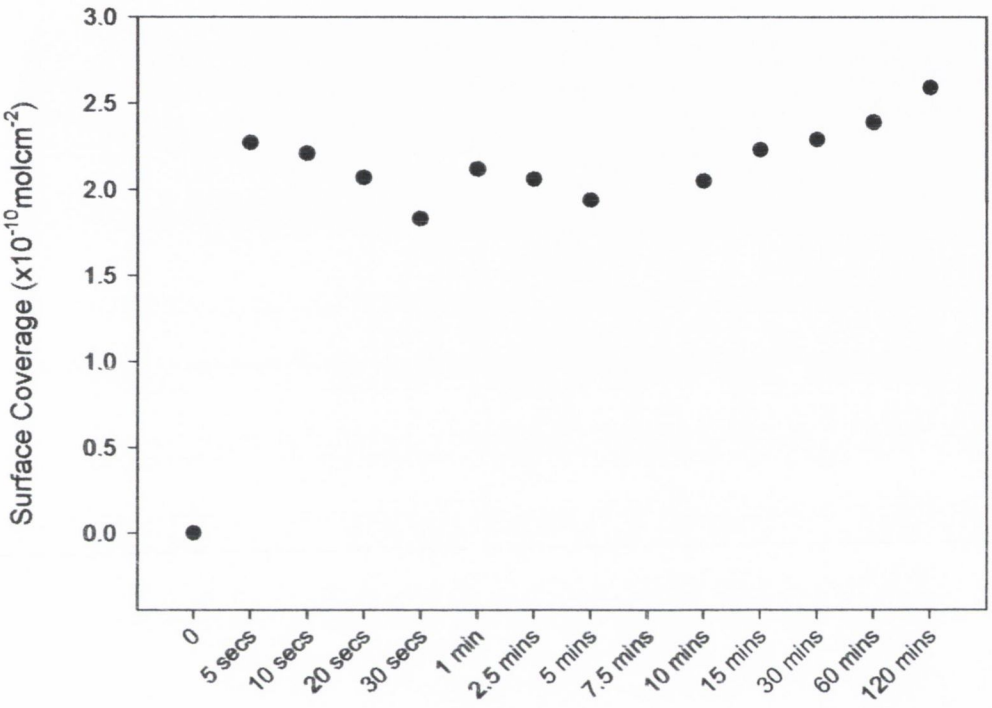


Figure 4.7. Surface Coverage as a function of deposition time calculated from cyclic voltammetry showing the deposition of 8Fc thiol from a 1mM solution at room Temperature. All scans were carried out in 0.1M $HClO_4$ at 0.02Vs^{-1} scan rate.

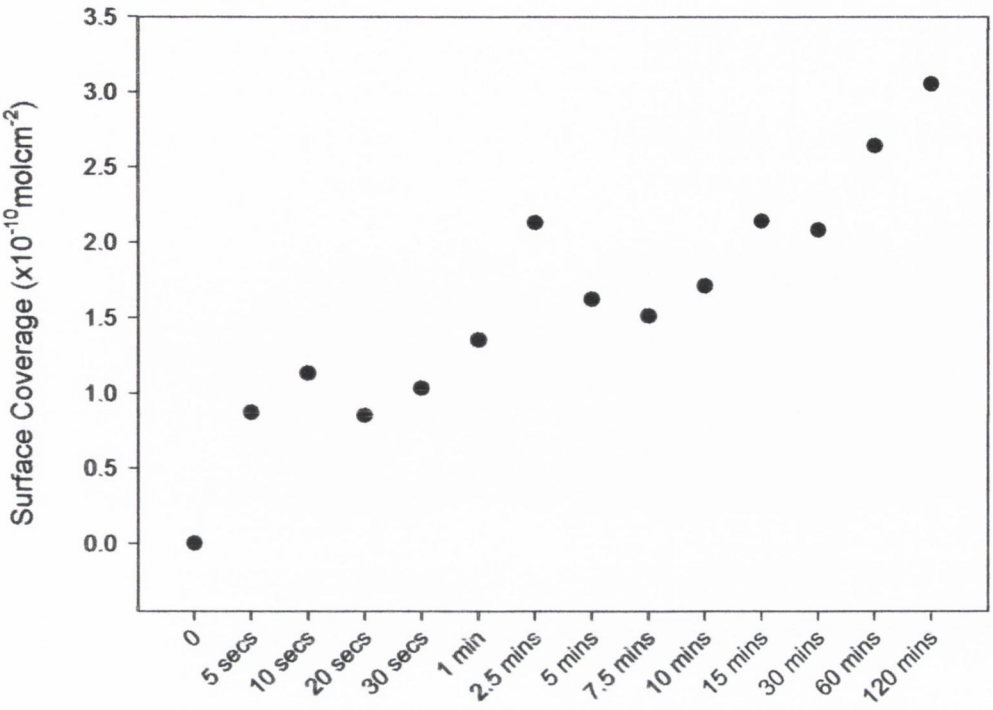


Figure 4.8. Surface Coverage as a function of deposition time calculated from cyclic voltammetry showing the deposition of 8Fc thiol from a 1mM solution at 40°C. All scans were carried out in 0.1M $HClO_4$ at 0.02Vs^{-1} scan rate.

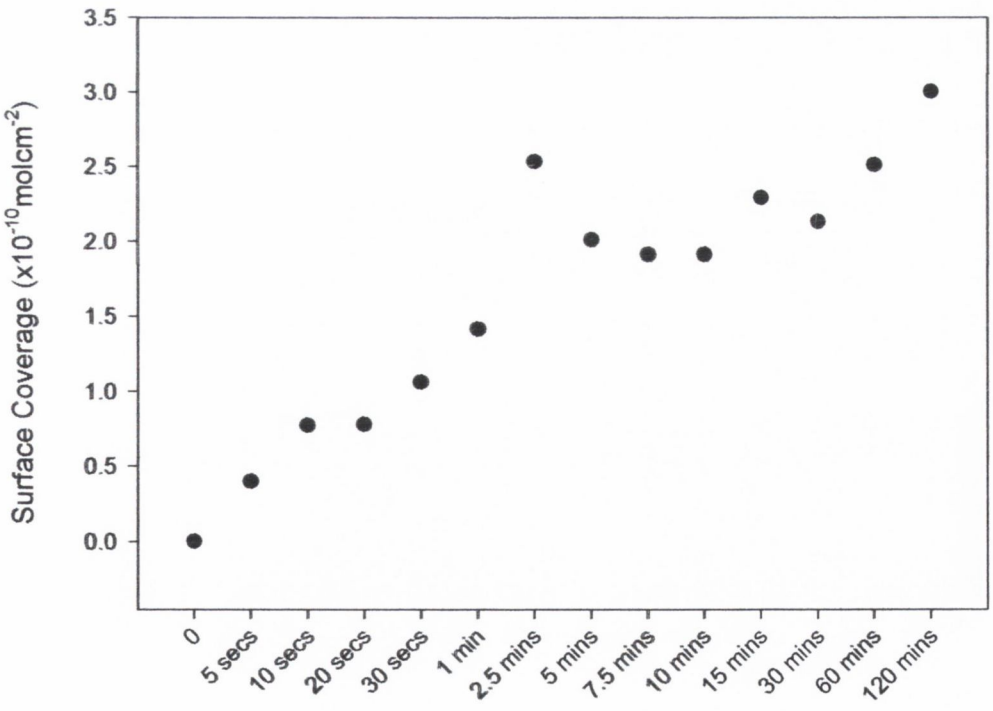


Figure 4.9. Surface Coverage as a function of deposition time calculated from cyclic voltammetry showing the deposition of 8Fc thiol from a 1mM solution at 60°C. All scans were carried out in 0.1M $HClO_4$ at 0.02Vs^{-1} scan rate.

4.3.1.2 10Fc thiol – Discussion of 0.01mM, 0.1mM and 1mM Results

10Fc 0.01mM Results. Figure 4.10 shows a plot of surface coverage vs. deposition time calculated from CVs recorded for the deposition of 10Fc thiol at 0.01mM concentration at RT. No data is presented for the 40°C and 60°C depositions as no thiol appears to be deposited at these temperatures.

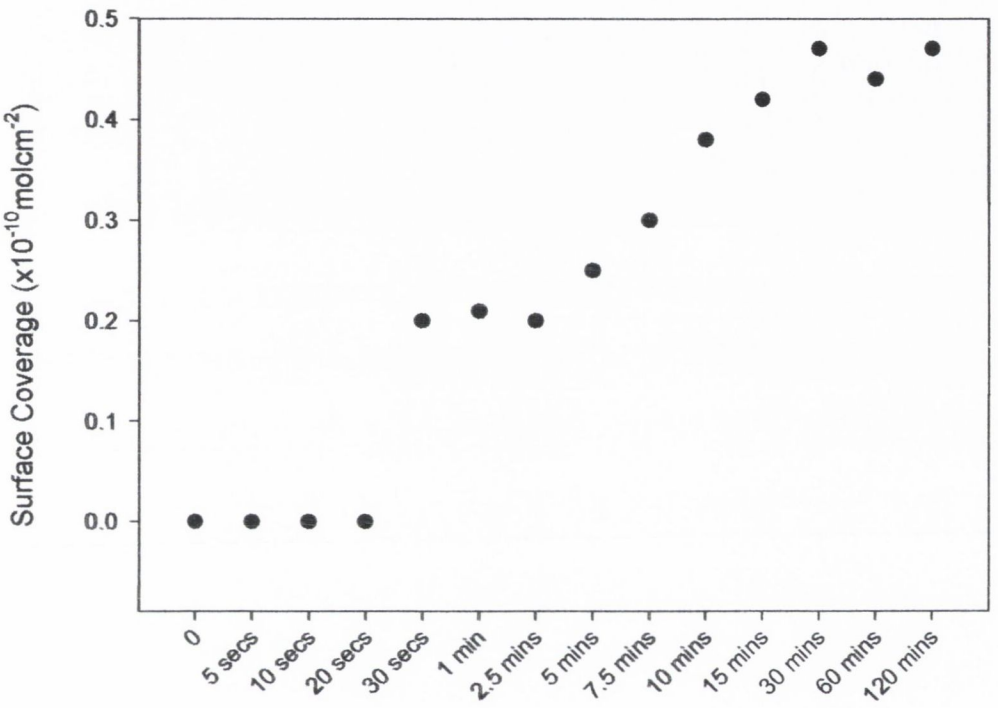


Figure 4.10. Surface Coverage as a function of deposition time calculated from cyclic voltammetry showing the deposition of 10Fc thiol from a 0.01mM solution at room temperature. All scans were carried out in 0.1M $HClO_4$ at 0.02Vs^{-1} scan rate.

The meaning of the parameters in the cyclic voltammetry diagnostics tables and their ramifications regarding monolayer formation has been explained thoroughly in the preceding section. For this reason it is not considered necessary to provide such a thorough explanation of the results in this section as the same conclusions may be drawn by the reader from the following results as from those which came before.

Firstly the deposition of 10Fc, 0.01mM at RT is examined. Again it is noted that the formation of the monolayer is rather slow and reference to Figure 4.10 the voltammograms in the appendix show that a densely packed, well orientated monolayer is not formed. It is also noted that the surface coverages remain low

throughout growth. This observation is typical for growth from low concentration solutions.

For growth at 10Fc, 0.01mM, 40°C/60°C (i.e. the growth from elevated temperature solutions at this concentration) the same situation is noted as in the case of 8Fc, 0.01mM, 40°C/60°C where no monolayer was deposited at these higher temperatures.

10Fc 0.1mM Results. Figures 4.11 and 4.12 show plots of surface coverage vs. deposition time calculated from CVs recorded for the deposition of 10Fc thiol at 0.1mM concentration at RT and 40°C. No data is presented for the 60°C deposition as no thiol appears to be deposited at this temperature.

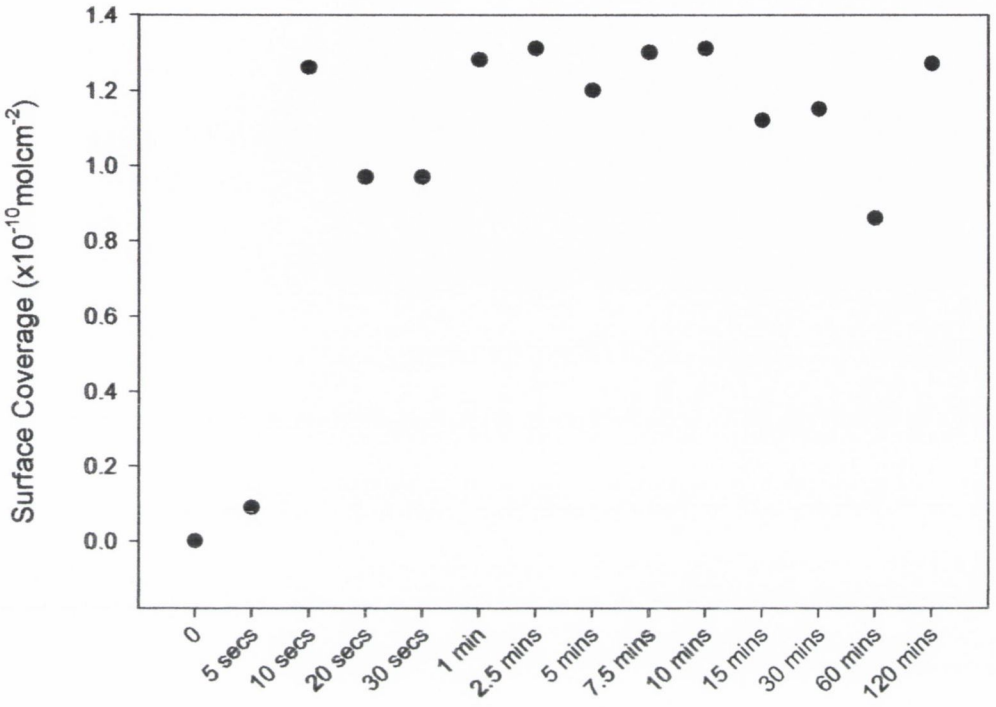


Figure 4.11. Surface Coverage as a function of deposition time calculated from cyclic voltammetry showing the deposition of 10Fc thiol from a 0.1mM solution at room temperature. All scans were carried out in 0.1M $HClO_4$ at 0.02Vs^{-1} scan rate.

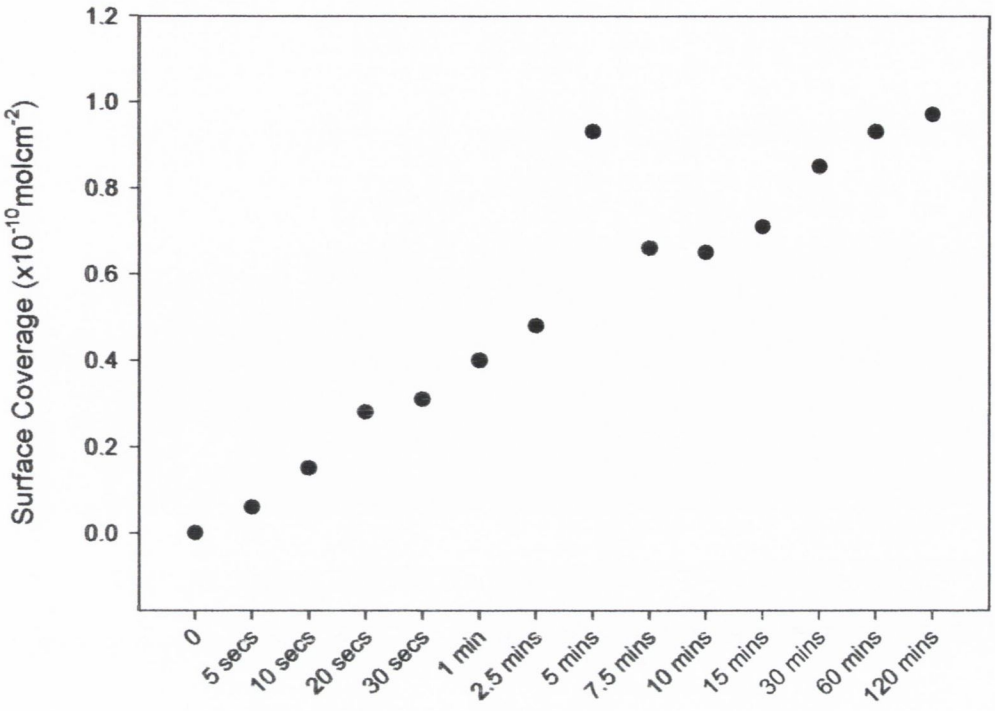


Figure 4.12. Surface Coverage as a function of deposition time calculated from cyclic voltammetry showing the deposition of 10Fc thiol from a 0.1mM solution at 40°C. All scans were carried out in 0.1M $HClO_4$ at 0.02Vs^{-1} scan rate.

Again at this concentration we see a similar phenomenon to that which occurred for 8Fc. Monolayer growth is feasible at RT and 40°C but does not occur at 60°C.

10Fc 1mM Results. Finally the deposition of 10Fc, 1mM, at RT, 40°C and 60°C is examined. Figures 4.13, 4.14 and 4.15 show plots of surface coverage vs. deposition time calculated from CVs recorded for the deposition of 10Fc thiol at 1mM concentration at RT, 40°C.and 60°C. Again a similar patter to that observed for 8Fc thiol emerges with good quality monolayers being formed from all solutions of all temperatures.

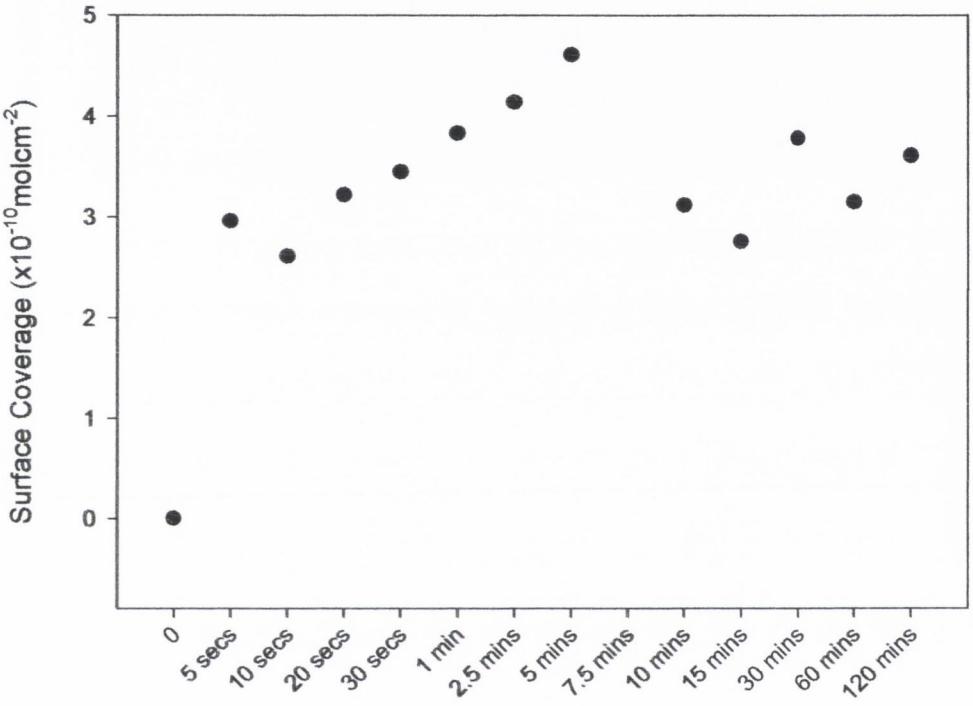


Figure 4.13. Surface Coverage as a function of deposition time calculated from cyclic voltammetry showing the deposition of 10Fc thiol from a 1mM solution at room temperature. All scans were carried out in 0.1M $HClO_4$ at 0.02Vs^{-1} scan rate.

It is noted for 10Fc deposition at 1mM solution concentration well ordered monolayers are formed at all deposition solution temperatures as was the case with 8Fc at this concentration. It is noted that at elevated temperatures no peak splitting is observed especially at a temperature of 60°C. This indicates as stated before that well ordered monolayers are formed at higher temperatures and high concentrations.

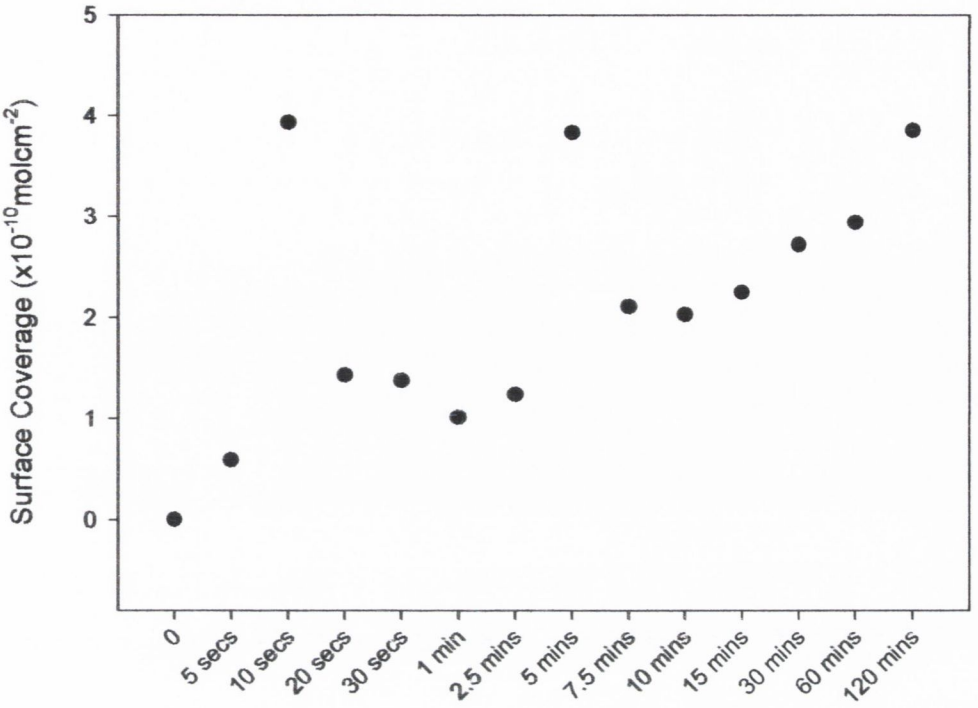


Figure 4.14. Surface Coverage as a function of deposition time calculated from cyclic voltammetry showing the deposition of 10Fc thiol from a 0.1mM solution at 40°C. All scans were carried out in 0.1M $HClO_4$ at 0.02Vs^{-1} scan rate.

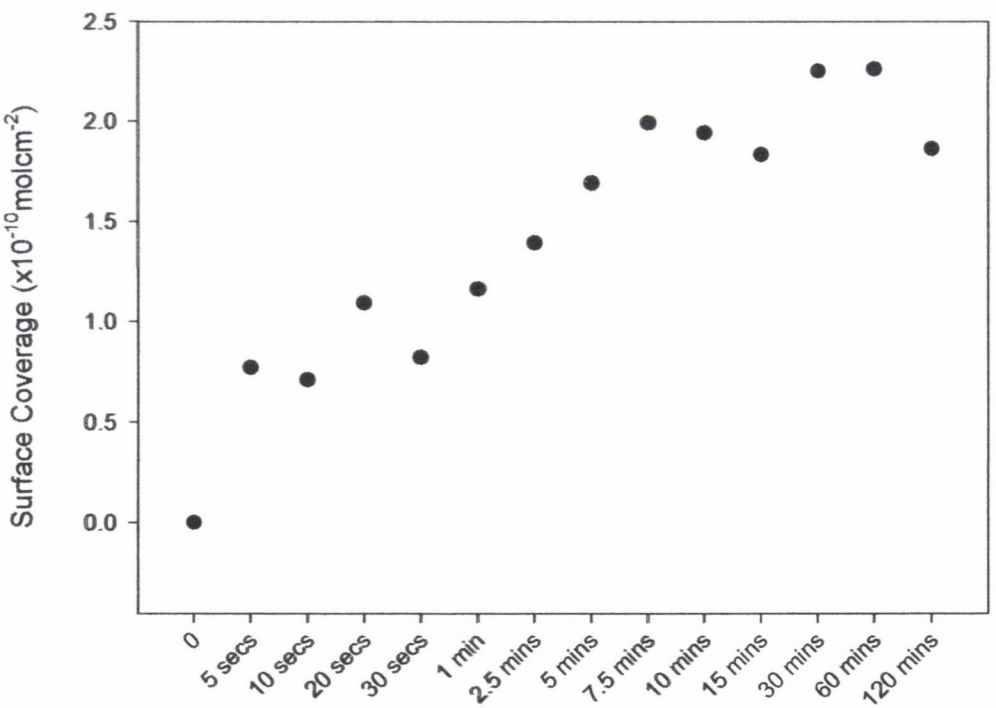


Figure 4.15. Surface Coverage as a function of deposition time calculated from cyclic voltammetry showing the deposition of 10Fc thiol from a 0.1mM solution at 60°C. All scans were carried out in 0.1M $HClO_4$ at 0.02Vs^{-1} scan rate.

4.3.1.3 12Fc thiol – Discussion of 0.01mM, 0.1mM and 1mM Results

12Fc 0.01mM Results. Figure 4.16 shows a plot of surface coverage vs. deposition time calculated from CVs recorded for the deposition of 12Fc thiol at 0.01mM concentration at RT. It is noted that no data is presented for the depositions at 40°C and 60°C because monolayer formation was not observed at these temperatures.

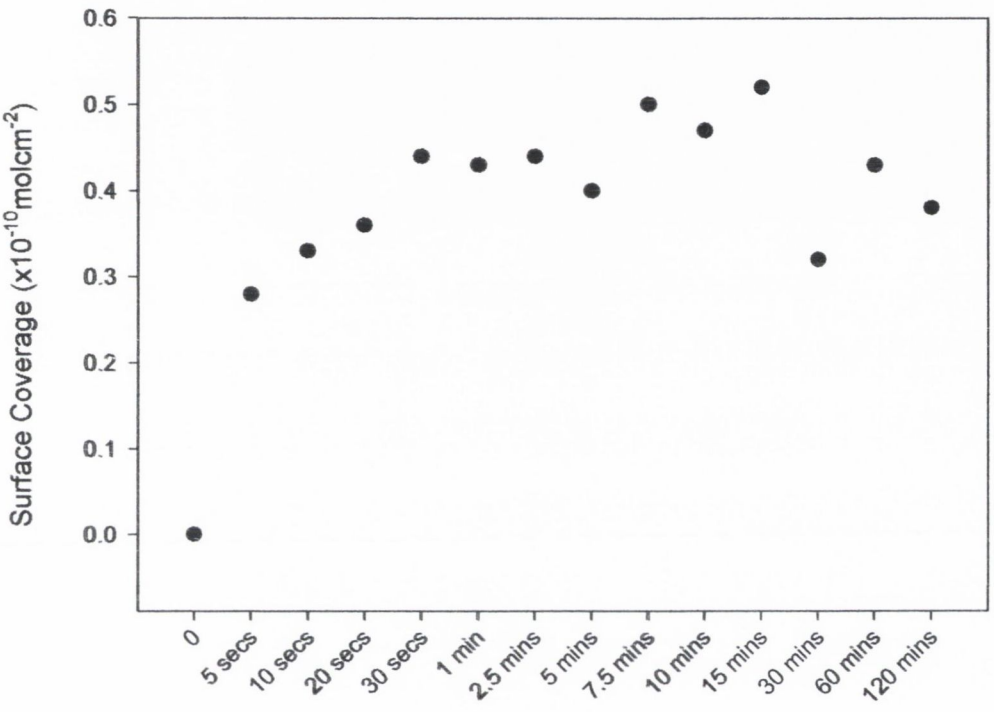


Figure 4.16 Surface Coverage as a function of deposition time calculated from cyclic voltammetry showing the deposition of 12Fc thiol from a 0.01mM solution at room temperature. All scans were carried out in 0.1M $HClO_4$ at 0.02Vs^{-1} scan rate.

12Fc 0.1mM Results. Figures 4.17, 4.18 and 4.19 show plots of surface coverage vs. deposition time calculated from CVs recorded for the deposition of 12Fc thiol at 0.1mM concentration at RT, 40°C.and 60°C.

The most interesting point to note at this deposition concentration is that monolayer growth is achieved at 60°C. In the case of 8Fc and 10Fc deposition at 0.1mM growth does not seem feasible at this temperature. The longer chain length of the 12Fc and hence the greater amount of attractive Van der Waals interactions between the chains may enable the chains to retain enough energy to form a critical island nucleus at this temperature. However it is notable that the surface coverages observed at 60°C remain lower than those for RT and 40°C and in many cases it is not possible to obtain a PWHM value due to high charging currents all of which indicates that although it may be possible to deposit a monolayer at this temperature and concentration for 12Fc the quality of that monolayer is unlikely to be high.

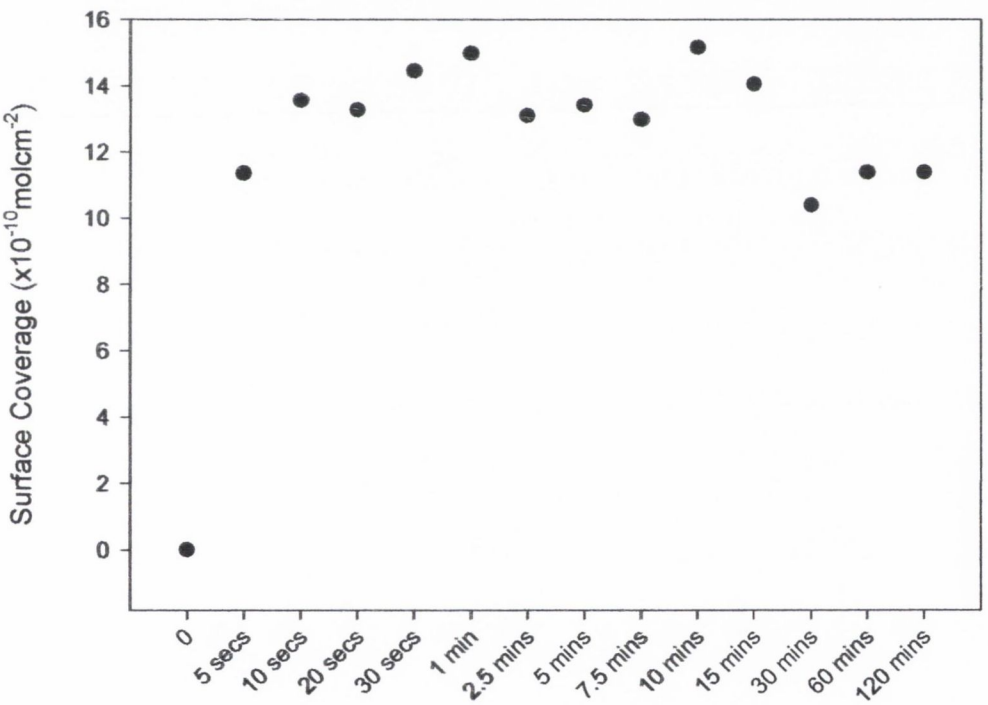


Figure 4.17. Surface Coverage as a function of deposition time calculated from cyclic voltammetry showing the deposition of 12Fc thiol from a 0.1mM solution at room temperature. All scans were carried out in 0.1M $HClO_4$ at 0.02Vs^{-1} scan rate.

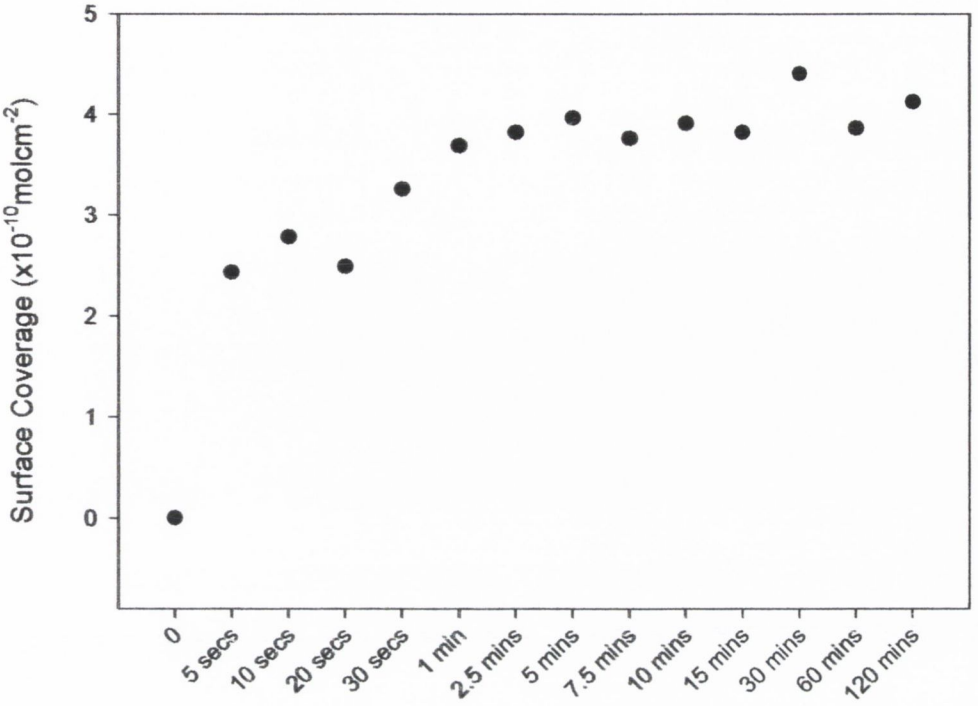


Figure 4.18. Surface Coverage as a function of deposition time calculated from cyclic voltammetry showing the deposition of 12Fc thiol from a 0.1mM solution at 40°C. All scans were carried out in 0.1M $HClO_4$ at 0.02Vs^{-1} scan rate.

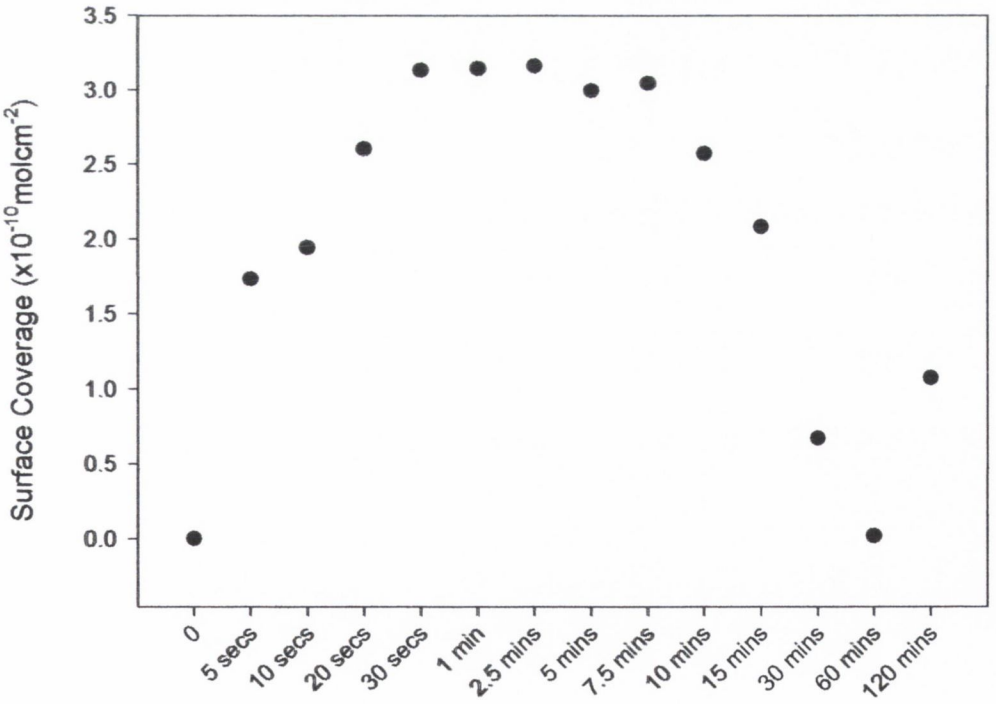


Figure 4.19. Surface Coverage as a function of deposition time calculated from cyclic voltammetry showing the deposition of 12Fc thiol from a 0.1mM solution at 60°C. All scans were carried out in 0.1M $HClO_4$ at 0.02Vs^{-1} scan rate.

12Fc 1mM Results. Finally deposition of 12Fc at RT, 40°C and 60°C at a concentration of 1mM is examined. Figures 4.20, 4.21 and 4.22 show plots of surface coverage vs. deposition time calculated from CVs recorded for the deposition of 12Fc thiol at 1mM concentration at RT, 40°C.and 60°C. Again in this case as in the case of 8Fc and 10Fc thiols good quality monolayers are formed at all temperatures at 1mM concentration.

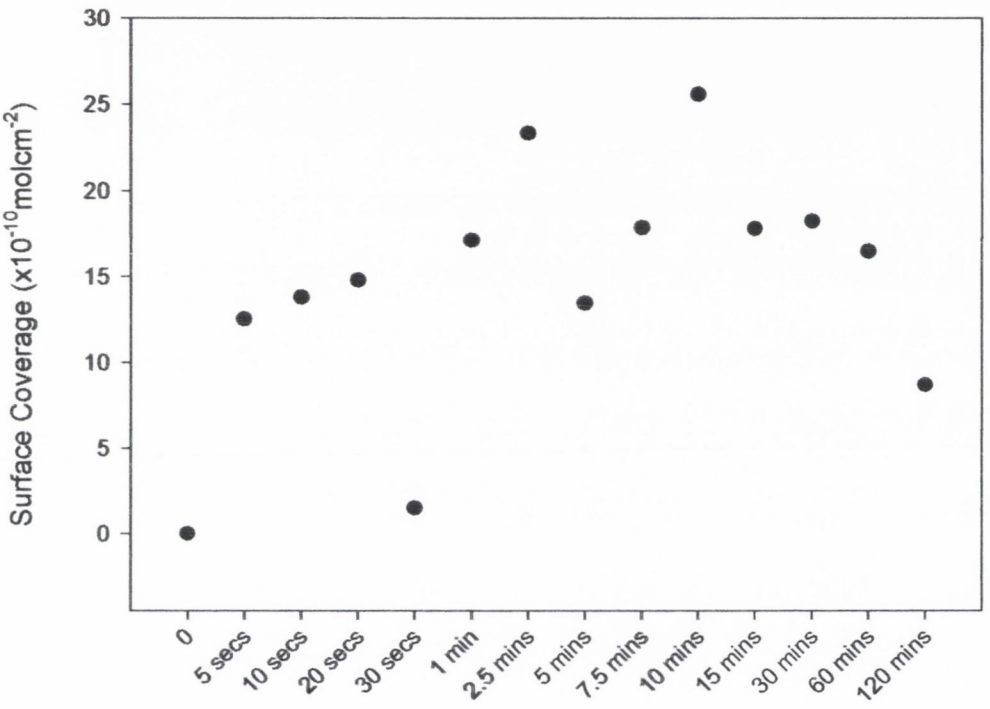


Figure 4.20. Surface Coverage as a function of deposition time calculated from cyclic voltammetry showing the deposition of 12Fc thiol from a 1mM solution at temperature. All scans were carried out in 0.1M $HClO_4$ at 0.02Vs^{-1} scan rate.

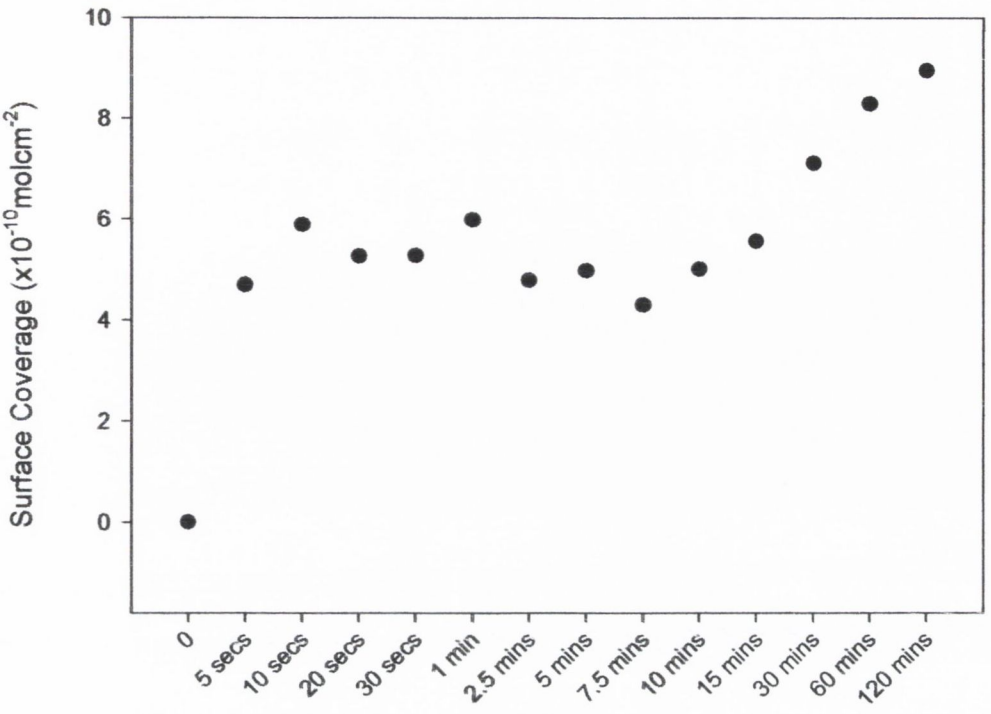


Figure 4.21. Surface Coverage as a function of deposition time calculated from cyclic voltammetry showing the deposition of 12Fc thiol from a 1mM solution at 40°C. All scans were carried out in 0.1M $HClO_4$ at 0.02Vs^{-1} scan rate.

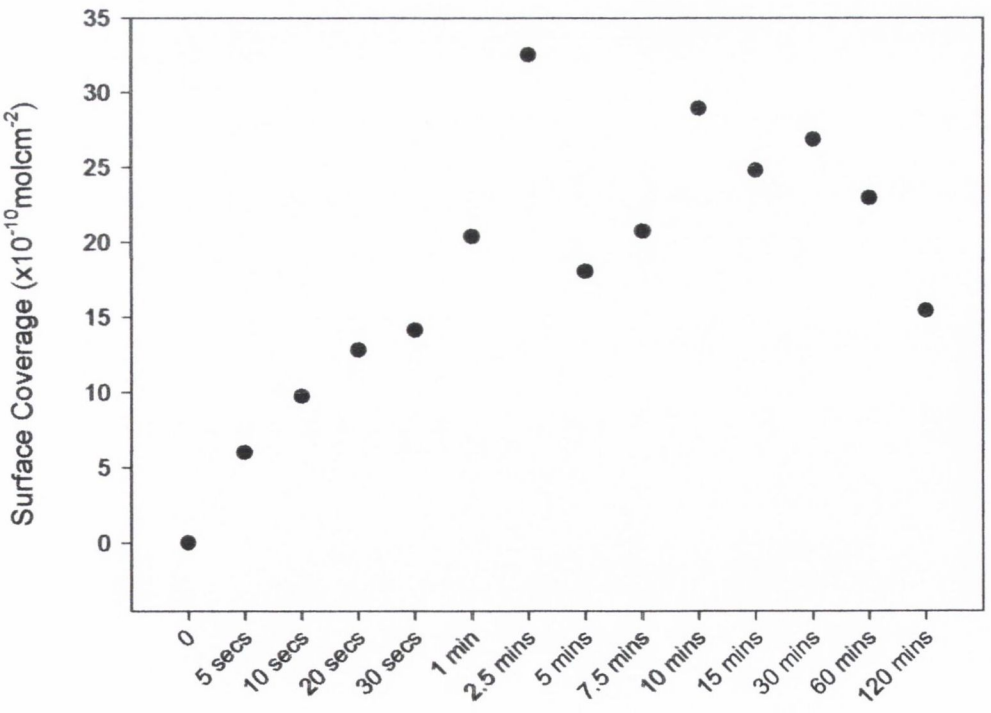


Figure 4.22. Surface Coverage as a function of deposition time calculated from cyclic voltammetry showing the deposition of 12Fc thiol from a 1mM solution at 60°C. All scans were carried out in 0.1M $HClO_4$ at 0.02Vs^{-1} scan rate.

4.3.2 Electrochemical Quartz Crystal Microbalance Study

Following the macroelectrode investigation of adsorption from solutions an Electrochemical Quartz Crystal Microbalance (EQCM) was employed to yield further insight into the deposition process. Previously EQCM studies were employed directly to measure the mass change occurring on the electrode surface as alkanethiol molecules were adsorbed[37, 38, 39]. Schneider et al.[40] employed EQCM studies to monitor the mass change occurring during the reductive desorption of the alkanethiol molecules from the gold surface as a method of determining the surface coverage. This section will attempt to describe the formation of SAMs using a combination of CV and EQCM. In ferrocene terminated SAMs pendant ferrocene groups form an ion pair with ClO_4^- in a perchloric acid electrolyte during oxidation[41] causing a mass change on the surface of the monolayer film. The resulting mass change may be monitored via EQCM and associated with the number of perchlorate ions forming ion pairs where the mass of one perchlorate molecule may be easily calculated as 1.6×10^{-22}g. To retain charge neutrality at the SAM-electrolyte interface one perchlorate ion pairs with one oxidised pendant ferrocene group (Fc^+). Thus using EQCM we may establish the number of perchlorate ions on the surface of the SAM during oxidation and hence infer the number of pendant Fc^+ groups on the surface of the SAM. Questions may be posed as to the value of this technique since it has already been shown in the previous section that the surface coverage of ferrocene terminated alkanethiol molecules can be determined from CV studies by calculating the charge associated with the oxidation wave. This method however yields far more insight into the quality of the monolayer. It is known for instance that during formation of the SAM that alkanethiol molecules are prone to coiling (Figure 4.2, Scheme B) which may render some pendant ferrocene groups effectively folded over such that they occupy space within the alkanethiol spacer. Such molecules would contribute to the oxidation current registered by CV examination and from which previous surface coverages have been calculated but would not register as a mass change (corresponding to an ion pair) during EQCM studies. Thus using a combination of CV and EQCM it is possible to distinguish between a well-ordered monolayer with a canopy of ferrocene molecules on the surface only and a monolayer in a more disordered state. Other features of monolayer formation which may be evident is the permeation of solvent into the layer during the oxidation of the SAM. Solvent may

permeate a partially formed monolayer quite easily and would be registered as a mass change on the surface of the electrode.

4.3.2.1 8Fc thiol – Discussion of 0.01mM, 0.1mM and 1mM Results

Figures 4.12, 4.13 and 4.14 show the CV and EQCMs recorded for the deposition of a monolayer of 8Fc thiol from a 0.01, 0.1 and 1mM solutions respectively. Tables 4.21, 4.22 and 4.23 show the diagnostics associated the results for 0.01, 0.1 and 1mM depositions. These tables show the surface coverage as determined by CV and the corresponding mass change expected if each of the electroactive ferrocene groups were to form an ion pair with a perchlorate molecule. They also show the mass change actually recorded from the EQCM traces. Finally a ratio is taken of the measured mass change to the expected mass change.

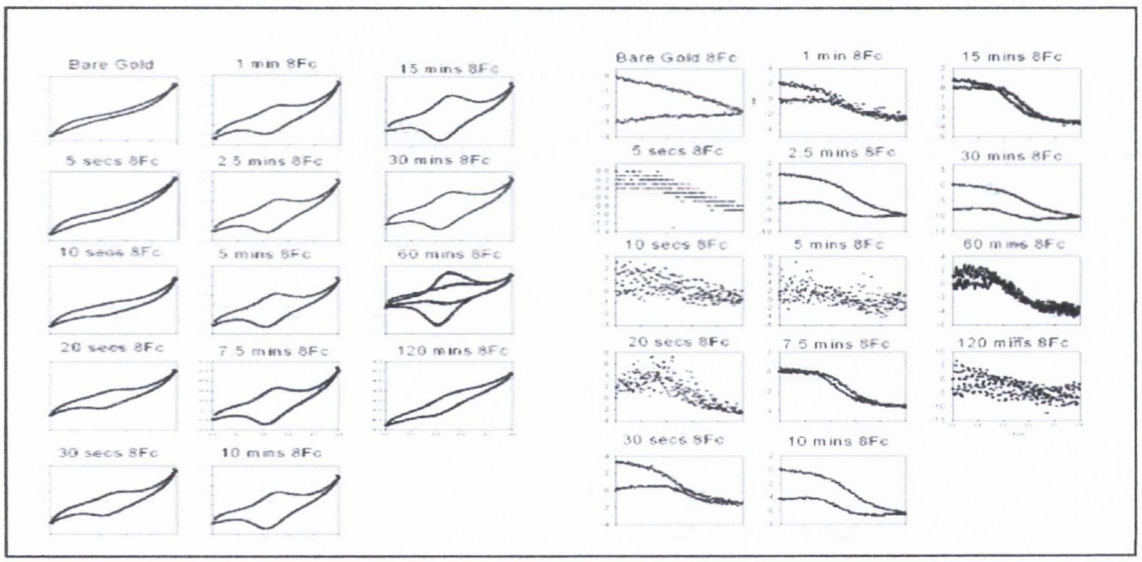


Figure 4.12. Combined cyclic voltammetry and EQCM study showing the deposition of 8Fc thiol from a 0.01mM solution at room temperature. All scans were carried out in 0.1M $HClO_4$ at $0.02Vs^{-1}$ scan rate.

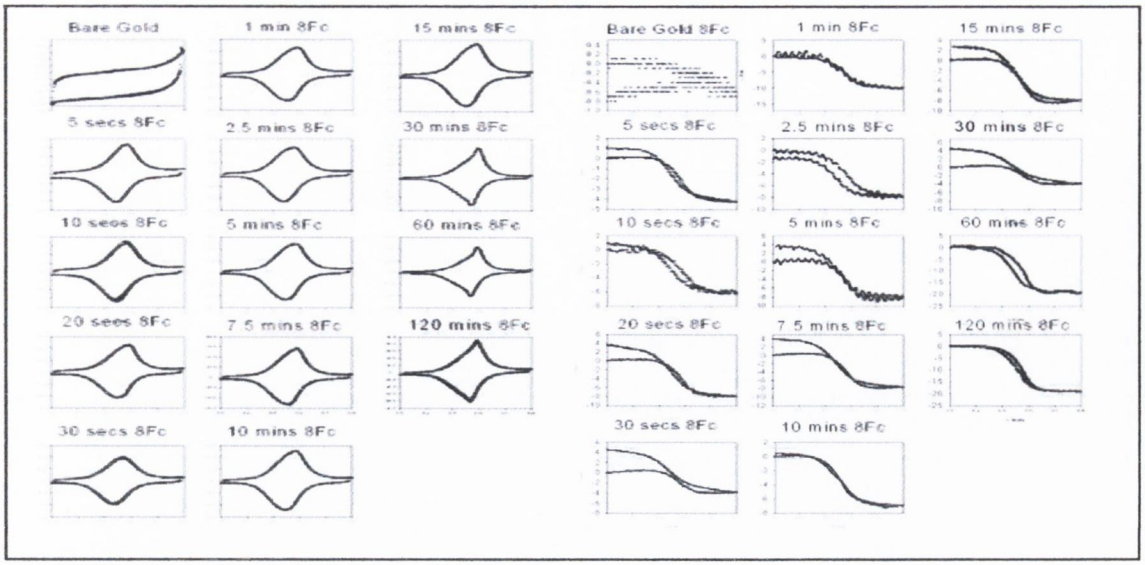


Figure 4.13. Combined cyclic voltammetry and EQCM study showing the deposition of 8Fc thiol from a 0.1mM solution at room temperature. All scans were carried out in 0.1M $HClO_4$ at $0.02Vs^{-1}$ scan rate.

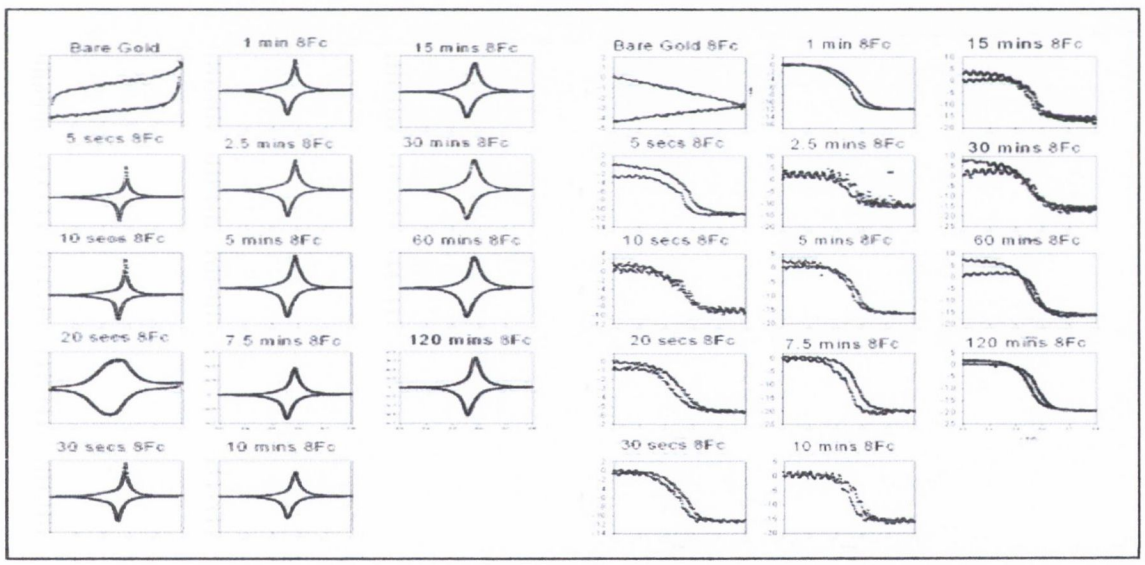


Figure 4.14. Combined cyclic voltammetry and EQCM study showing the deposition of 8Fc thiol from a 1mM solution at room temperature. All scans were carried out in 0.1M $HClO_4$ at $0.02Vs^{-1}$ scan rate.

Immersion Time	Surface Coverage ($x10^{-10}$ mol.cm^{-2})	Expected Mass Change, ΔM_E (ng)	Measured Mass Change, ΔM_m (ng)	$\frac{\Delta M_M}{\Delta M_E}$
5 secs	--	--	1.0	--
10 secs	0.13	0.24	--	--
20 secs	0.32	0.61	--	--
30 secs	0.30	0.57	5.3	9.30
1 min	0.40	0.76	3.3	4.28
2.5 mins	0.54	1.03	8.9	8.70
5 mins	0.59	1.11	--	--
7.5 mins	0.55	1.04	4.8	4.60
10 mins	0.56	1.05	7.9	7.53
15 mins	0.69	1.31	4.8	3.70
30 mins	0.49	0.92	12.8	13.93
60 mins	0.84	1.59	5.4	3.39
120 mins	0.51	0.96	--	--

Table 4.21 – Showing the mass change and surface coverage diagnostics for the deposition of a 8Fc thiol monolayer from a 0.01mM solution at RT.

Immersion Time	Surface Coverage ($x10^{-10}$ mol.cm^{-2})	Expected Mass Change, ΔM_E (ng)	Measured Mass Change, ΔM_m (ng)	$\frac{\Delta M_M}{\Delta M_E}$
5 secs	1.8	3.4	3.6	1.05
10 secs	1.9	3.6	8.4	2.34
20 secs	2.7	5.1	10.9	2.14
30 secs	2.4	4.5	6.0	1.33
1 min	2.9	5.5	12.4	2.26
2.5 mins	3.0	5.6	10.0	1.79
5 mins	3.1	5.9	12.2	2.06
7.5 mins	3.5	6.6	11.4	1.72
10 mins	3.2	6.1	9.8	1.61
15 mins	3.4	6.4	12.3	1.90
30 mins	4.6	8.7	19.7	2.26
60 mins	5.1	9.7	27.1	2.78
120 mins	4.7	9.0	26.7	2.98

Table 4.22 – Showing the mass change and surface coverage diagnostics for the deposition of a 8Fc thiol monolayer from a 0.1mM solution at RT.

Immersion Time	Surface Coverage ($x10^{-10}$ mol.cm^{-2})	Expected Mass Change, ΔM_E (ng)	Measured Mass Change, ΔM_m (ng)	$\frac{\Delta M_M}{\Delta M_E}$
5 secs	7.8	14.6	14.4	0.98
10 secs	9.3	17.5	12.9	0.74
20 secs	3.2	6.1	7.4	1.21
30 secs	8.4	15.9	15.4	0.97
1 min	8.6	16.3	16.3	0.99
2.5 mins	9.5	17.9	17.9	1.00
5 mins	10.7	20.3	23.1	1.14
7.5 mins	11.7	22.1	27.9	1.26
10 mins	11.3	21.3	22.2	1.04
15 mins	10.4	19.7	23.2	1.18
30 mins	9.0	17.0	25.2	1.48
60 mins	9.2	17.3	16.5	0.95
120 mins	10.9	20.6	27.2	1.32

Table 4.23 – Showing the mass change and surface coverage diagnostics for the deposition of a 8Fc thiol monolayer from a 1mM solution at RT.

Figure 4.15 below is a plot of $\Delta M_M/\Delta M_E$. This ratio is extremely significant in determining what deposition concentration forms the most ordered SAM. It is obvious from this plot that deposition from a 1mM solution forms the most highly ordered SAM. At all times during deposition the ratio of pendant ferrocene molecules forming ion pairs to the number of electroactive ferrocene molecules is almost unity. This is indicative of a well ordered SAM with all pendant ferrocene molecules lying on the surface of the SAM and each forming a single ion pair with a perchlorate molecule. A consequence of this observation is that little or no solvent is able to permeate the SAM. As expected the next most ordered SAM is that deposited from a 0.1mM solution. In this case the change in mass observed is on average approximately twice that expected from cyclic voltammetry. This would imply solvent permeation into the monolayer showing that the monolayer formed from a 0.1mM solution is not as compact as that formed from the higher concentration. Finally we look at the case of the SAM formed from a 0.01mM concentration. In this case the monolayer appears to be extremely disordered with the mass change at the surface of the electrode being in all cases much greater than that expected from cyclic voltammetry. This points to a very disordered monolayer undergoing a high amount of solvent permeation during oxidation. It is also notable from Figure 4.12 that a number of EQCM traces are extremely scattered and for this reason results from these plots are left out of the both Table 4.21 and Figure 4.15. This scattering of frequencies

can be attributed to a very disordered SAM that is constantly letting in and releasing solvent from the layer during the potential sweep.

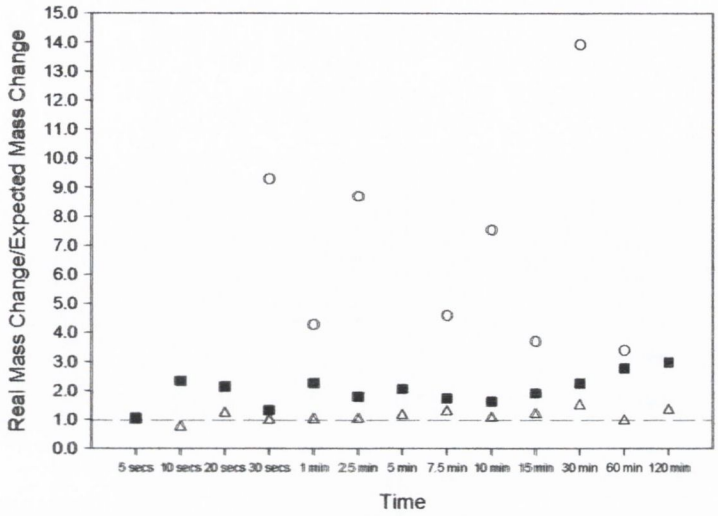


Figure 4.15 – Ratio of the mass change determined from EQCM studies to the mass change expected from CV studies a function of deposition time for the deposition of a monolayer of 8Fc thiol at concentration of 0.01mM (∫), 0.1mM (□) and 1mM (∫). The dashed line traces the ideal ratio of unity.

4.3.2.2 10Fc thiol – Discussion of 0.01mM, 0.1mM and 1mM Results

Figures 4.16, 4.17 and 4.18 show the CV and EQCMs recorded for the deposition of a monolayer of 10Fc thiol from a 0.01, 0.1 and 1mM solution. Tables 4.24, 4.25 and 4.26 show the diagnostics associated the results for 0.01, 0.1 and 1mM depositions.

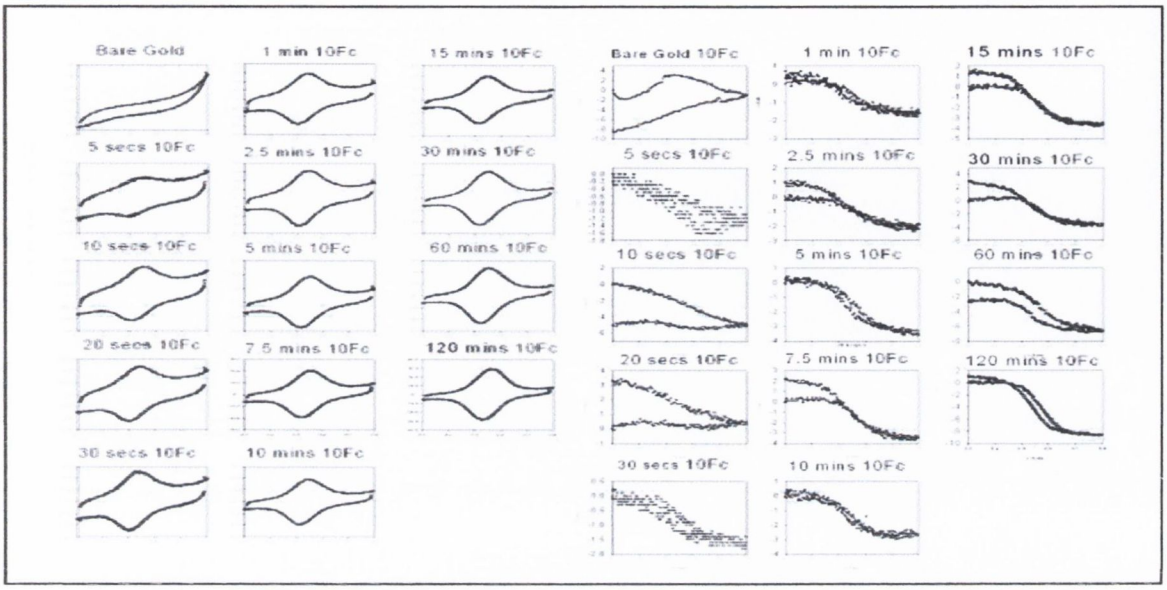


Figure 4.16. Combined cyclic voltammetry and EQCM study showing the deposition of 10Fc thiol from a 0.01mM solution at room temperature. All scans were carried out in 0.1M $HClO_4$ at $0.02Vs^{-1}$ scan rate.

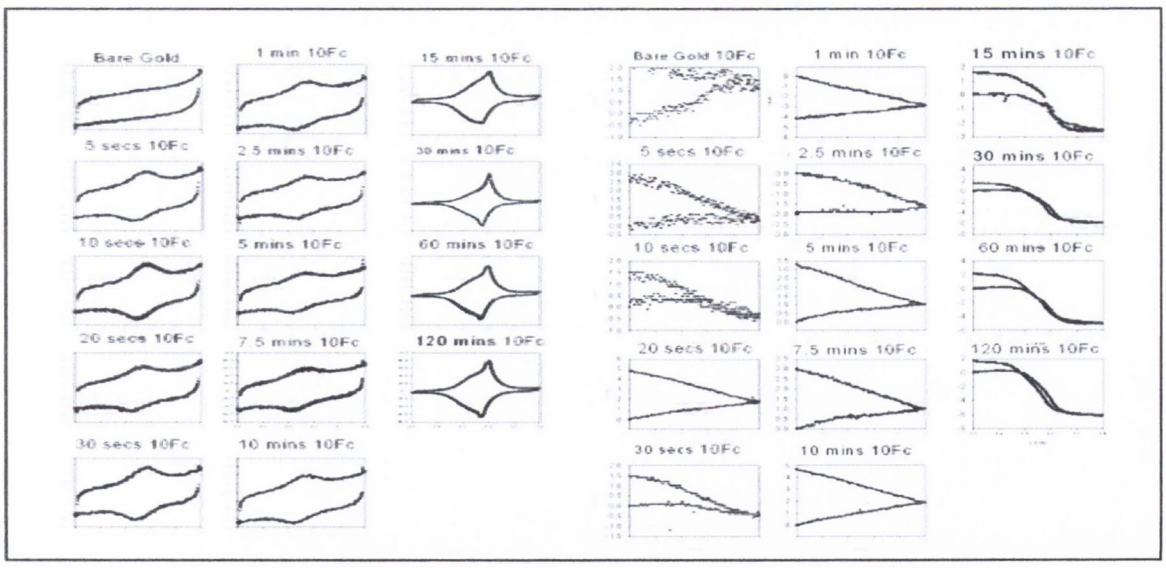


Figure 4.17. Combined cyclic voltammetry and EQCM study showing the deposition of 10Fc thiol from a 0.1mM solution at room temperature. All scans were carried out in 0.1M $HClO_4$ at $0.02Vs^{-1}$ scan

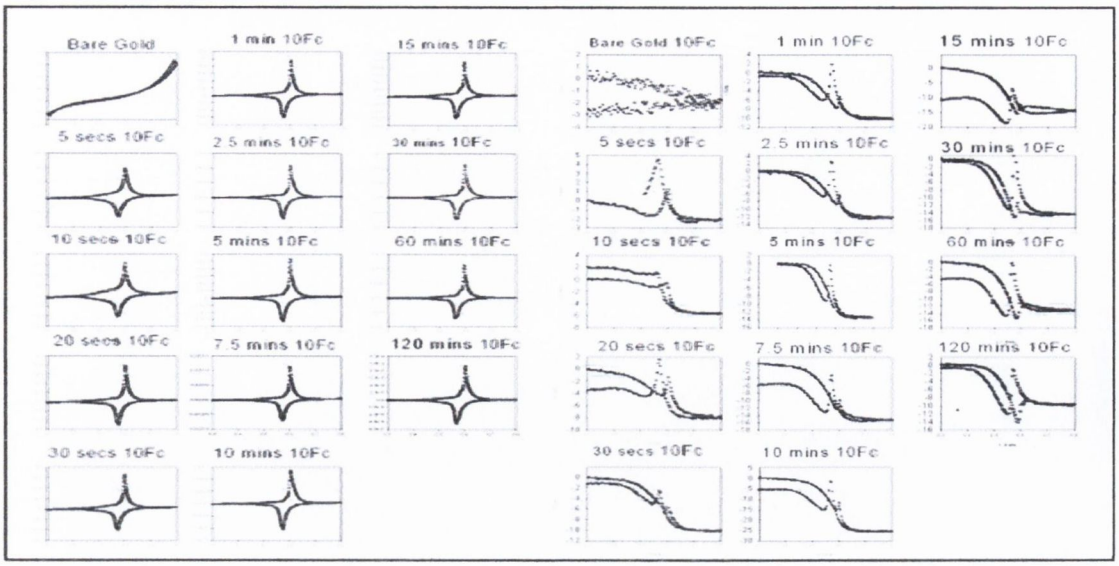


Figure 4.18. Combined cyclic voltammetry and EQCM study showing the deposition of 10Fc thiol from a 1mM solution at room temperature. All scans were carried out in 0.1M $HClO_4$ at $0.02Vs^{-1}$ scan

Immersion Time	Surface Coverage ($x10^{-10}$ mol.cm^{-2})	Expected Mass Change, ΔM_E (ng)	Measured Mass Change, ΔM_m (ng)	$\frac{\Delta M_M}{\Delta M_E}$
5 secs	0.3	0.6	1.8	3.19
10 secs	0.5	1.0	6.7	6.70
20 secs	0.5	1.0	--	--
30 secs	0.6	1.1	1.9	1.74
1 min	0.7	1.3	2.3	1.68
2.5 mins	0.9	1.6	2.7	1.66
5 mins	1.1	2.0	4.4	2.19
7.5 mins	1.2	2.2	5.3	2.37
10 mins	1.1	2.0	3.4	1.67
15 mins	1.2	2.2	4.9	2.17
30 mins	1.4	2.6	5.7	2.21
60 mins	1.5	2.8	6.9	2.46
120 mins	1.8	3.4	12.0	3.57

Table 4.24 – Showing the mass change and surface coverage diagnostics for the deposition of a 10Fc thiol monolayer from a 0.01mM solution at RT.

Immersion Time	Surface Coverage ($x10^{-10}$ mol.cm^{-2})	Expected Mass Change, ΔM_E (ng)	Measured Mass Change, ΔM_m (ng)	$\frac{\Delta M_M}{\Delta M_E}$
5 secs	0.2	0.3	--	--
10 secs	0.2	0.3	0.9	2.8
20 secs	0.1	0.3	1.6	6.1
30 secs	0.2	0.3	0.6	1.8
1 min	0.1	0.2	2.7	11.4
2.5 mins	0.1	0.2	1.8	10.8
5 mins	1.1	2.0	1.0	0.5
7.5 mins	0.1	0.3	0.8	3.0
10 mins	0.1	0.2	1.8	7.9
15 mins	2.4	4.6	3.7	0.8
30 mins	4.0	7.5	8.5	1.1
60 mins	3.7	6.9	7.4	1.1
120 mins	3.9	7.3	8.9	1.2

Table 4.25 – Showing the mass change and surface coverage diagnostics for the deposition of a 10Fc thiol monolayer from a 0.1mM solution at RT.

Immersion Time	Surface Coverage ($x10^{-10}$ mol.cm^{-2})	Expected Mass Change, ΔM_E (ng)	Measured Mass Change, ΔM_m (ng)	$\frac{\Delta M_M}{\Delta M_E}$
5 secs	7.9	14.9	2.9	0.20
10 secs	6.5	12.2	7.4	0.60
20 secs	11.4	21.5	9.8	0.46
30 secs	10.1	19.1	16.0	0.84
1 min	13.4	25.3	14.2	0.56
2.5 mins	16.0	30.2	17.4	0.57
5 mins	15.5	29.3	18.8	0.64
7.5 mins	15.5	29.3	20.7	0.70
10 mins	21.9	41.3	35.5	0.86
15 mins	14.1	26.7	18.8	0.70
30 mins	17.8	33.5	20.3	0.60
60 mins	16.7	31.5	17.7	0.56
120 mins	15.1	28.5	14.5	0.51

Table 4.26 – Showing the mass change and surface coverage diagnostics for the deposition of a 10Fc thiol monolayer from a 1mM solution at RT.

Figure 4.19 below shows a plot for the $\Delta M_M/\Delta M_E$ for the deposition of a 10Fc SAM at three different concentrations.

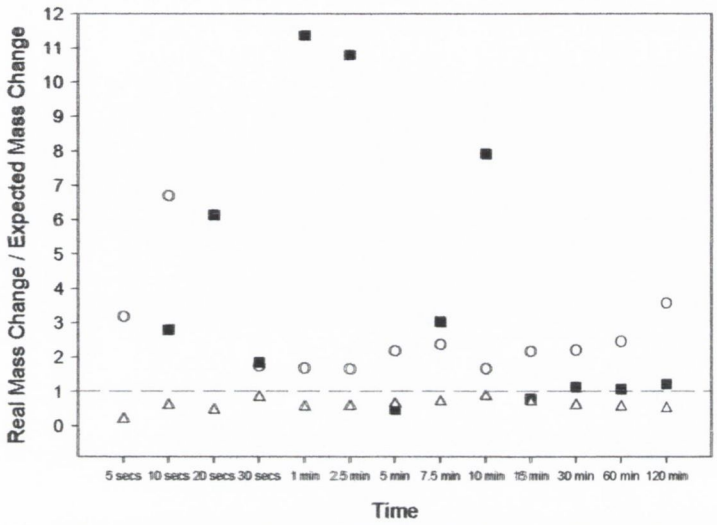


Figure 4.19 – Ratio of the mass change determined from EQCM studies to the mass change expected from CV studies a function of deposition time for the deposition of a monolayer of 10Fc thiol at concentration of 0.01mM (⌠), 0.1mM (□) and 1mM (⌠). The dashed line traces the ideal ratio of unity.

The inferences of this plot with respect to SAM quality are the same as those already discussed for the 8Fc case and thus will not be revisited. What is important to note is that once again, as expected, deposition from a 1mM solution provides the best quality SAM. It is notable that deposition from a 0.1mM solution does not approach the ideal value until after a period of 15 minutes assembly time. A similar observation was not noted for the case of 8Fc deposition solution from a 0.1mM solution and will be attributed to the specifics of this particular adsorption case. Finally we note that deposition from a 0.01mM solution appears to produce a much better quality SAM than in the case of 8Fc deposition. This may be attributed to the better packing of longer chain alkanethiols.

4.3.2.3 12Fc thiol – Discussion of 0.01mM, 0.1mM and 1mM Results

Figures 4.20, 4.21 and 4.22 show the CV and EQCMs recorded for the deposition of a monolayer of 10Fc thiol from a 0.01, 0.1 and 1mM solution. Tables 4.27, 4.28 and 4.29 show the diagnostics associated the results for 0.01, 0.1 and 1mM depositions.

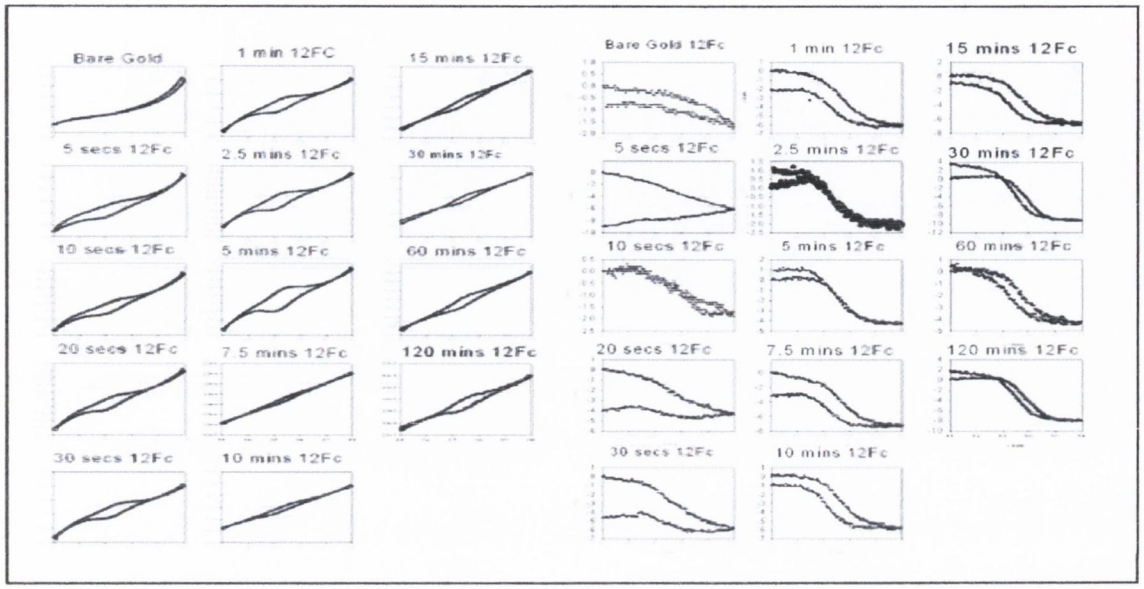


Figure 4.20. Combined cyclic voltammetry and EQCM study showing the deposition of 12Fc thiol from a 0.01mM solution at room temperature. All scans were carried out in 0.1M $HClO_4$ at $0.02Vs^{-1}$ scan

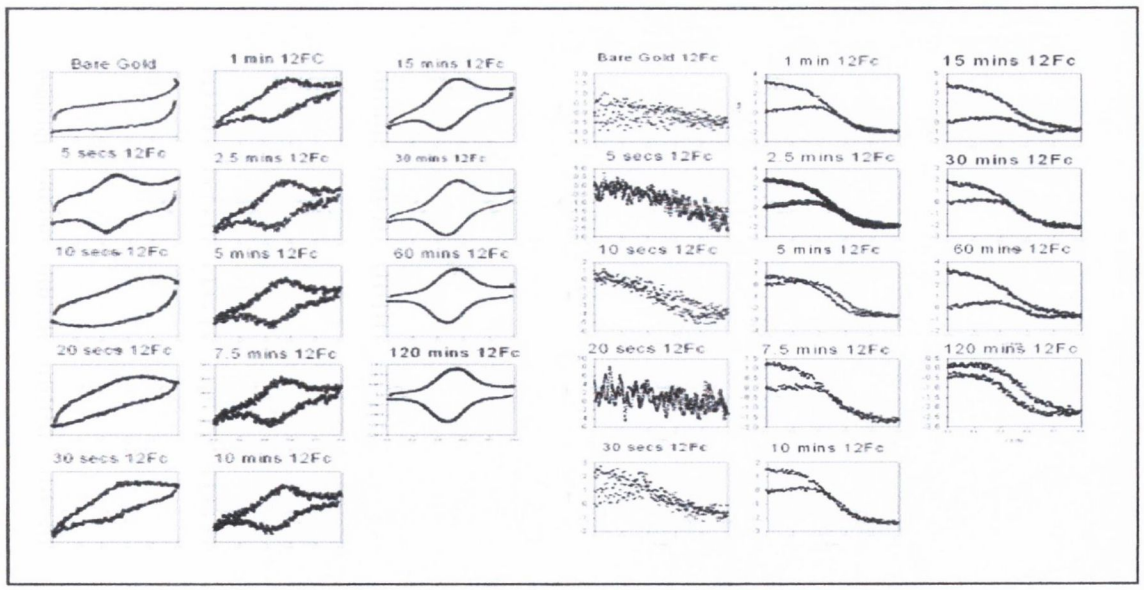


Figure 4.21. Combined cyclic voltammetry and EQCM study showing the deposition of 12Fc thiol from a 0.1mM solution at room temperature. All scans were carried out in 0.1M $HClO_4$ at $0.02Vs^{-1}$ scan

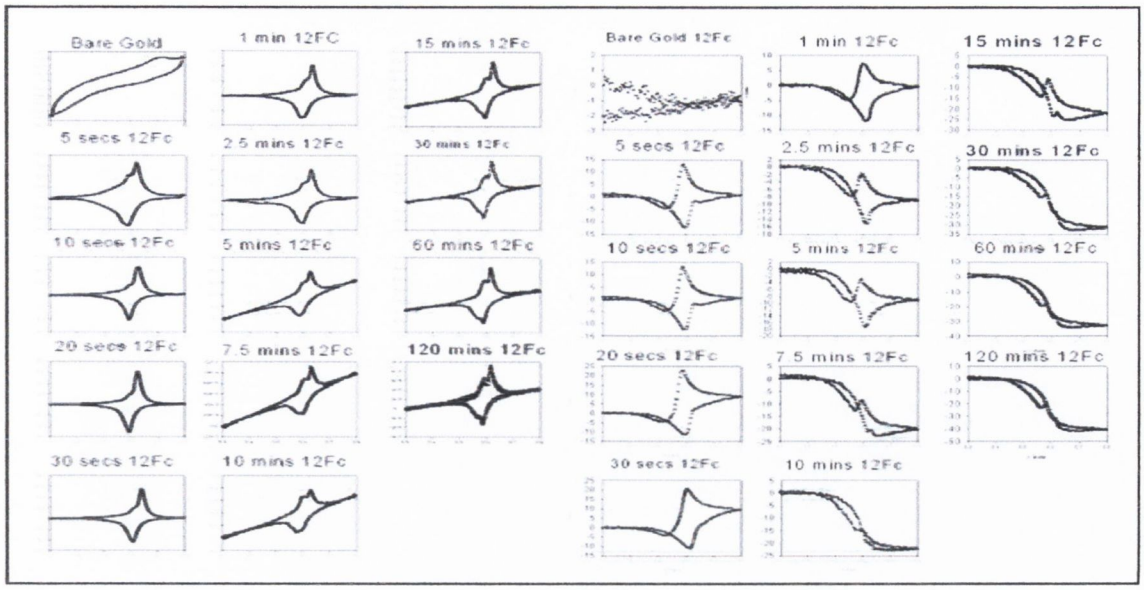


Figure 4.22. Combined cyclic voltammetry and EQCM study showing the deposition of 12Fc thiol from a 0.1mM solution at room temperature. All scans were carried out in 0.1M $HClO_4$ at $0.02Vs^{-1}$ scan rate.

Immersion Time	Surface Coverage ($x10^{-10}$ mol.cm^{-2})	Expected Mass Change, ΔM_E (ng)	Measured Mass Change, ΔM_m (ng)	$\frac{\Delta M_M}{\Delta M_E}$
5 secs	1.42	0.28	6.4	22.81
10 secs	1.23	0.23	2.5	10.96
20 secs	1.62	0.31	5.4	17.65
30 secs	3.16	0.59	7.1	11.89
1 min	3.89	0.73	7.9	10.73
2.5 mins	3.66	0.69	3.4	4.88
5 mins	4.06	0.77	6.2	8.13
7.5 mins	10.64	2.0	9.3	4.62
10 mins	11.29	2.13	7.7	3.62
15 mins	9.74	1.84	8.7	4.74
30 mins	12.02	2.27	13.6	6.0
60 mins	9.74	1.84	5.8	3.13
120 mins	8.52	1.61	11.7	7.25

Table 4.27 – Showing the mass change and surface coverage diagnostics for the deposition of a 12Fc thiol monolayer from a 0.01mM solution at RT.

Immersion Time	Surface Coverage ($x10^{-10}$ mol.cm^{-2})	Expected Mass Change, ΔM_E (ng)	Measured Mass Change, ΔM_m (ng)	$\frac{\Delta M_M}{\Delta M_E}$
5 secs	0.28	0.5	2.5	4.83
10 secs	--	--	4.9	--
20 secs	--	--	--	--
30 secs	0.90	1.7	2.4	1.43
1 min	0.85	1.6	3.6	2.21
2.5 mins	1.09	2.1	3.4	1.65
5 mins	0.89	1.7	3.9	2.35
7.5 mins	1.01	1.9	2.4	1.24
10 mins	1.01	1.9	3.4	1.77
15 mins	0.93	1.8	2.1	1.18
30 mins	0.81	1.5	3.3	2.18
60 mins	0.90	1.7	1.9	1.10
120 mins	0.90	1.7	3.0	1.79

Table 4.28 – Showing the mass change and surface coverage diagnostics for the deposition of a 12Fc thiol monolayer from a 0.1mM solution at RT.

Immersion Time	Surface Coverage ($x10^{-10}$ mol.cm^{-2})	Expected Mass Change, ΔM_E (ng)	Measured Mass Change, ΔM_m (ng)	$\frac{\Delta M_M}{\Delta M_E}$
5 secs	6.8	12.8	2.4	0.18
10 secs	14.1	26.7	0.3	0.01
20 secs	16.0	30.1	10.8	0.36
30 secs	14.7	27.7	11.5	0.42
1 min	12.1	22.8	1.4	0.06
2.5 mins	13.3	25.1	13.2	0.53
5 mins	10.1	19.1	13.0	0.68
7.5 mins	11.3	21.3	29.9	1.41
10 mins	10.2	19.2	31.9	1.66
15 mins	15.1	28.5	35.3	1.24
30 mins	16.6	31.3	46.4	1.48
60 mins	15.0	28.3	48.1	1.70
120 mins	16.0	30.2	57.5	1.91

Table 4.29 – Showing the mass change and surface coverage diagnostics for the deposition of a 12Fc thiol monolayer from a 1mM solution at RT.

Figure 4.23 below shows a plot for the $\Delta M_M/\Delta M_E$ for the deposition of a 12Fc SAM at three different concentrations. Again it is clearly notable that deposition from a 1mM solution gives a good quality monolayer with an $\Delta M_M/\Delta M_E$ value which is consistently close to unity. The quality of the SAM formed from a 0.1mM solution is however also of excellent quality as deposition time increases. Again deposition from a 0.01mM solution yields a poor quality SAM. The most notable phenomenon regarding the deposition of a 12Fc SAM is that at 0.1mM concentrations a good

quality SAM can be achieved over a relatively short time period. This adds weight to the observation that longer chain alkanethiol molecules are likely form a more ordered layer than shorter chains.

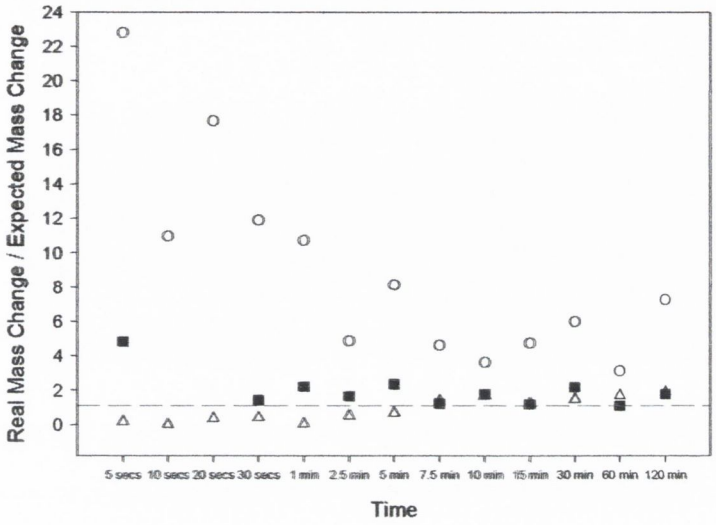


Figure 4.23 – Ratio of the mass change determined from EQCM studies to the mass change expected from CV studies a function of deposition time for the deposition of a monolayer of 12Fc thiol at concentration of 0.01mM (⌠), 0.1mM (□) and 1mM (⌠). The dashed line traces the ideal ratio of unity.

4.4 Conclusion

Using cyclic voltammetry (CV) and an Electrochemical Quartz Crystal Microbalance the adsorption kinetics and subsequent quality of monolayers of ferrocene terminated electroactive thiols was studied in this chapter. Firstly the effect of chain length, deposition solution concentration and deposition solution temperature on monolayer formation was examined. From cyclic voltammetry it was determined that at room temperature the fundamental factor affecting monolayer quality was the concentration of the deposition solution. Higher concentrations yielded better quality monolayers. At higher deposition solution temperatures longer chain lengths and higher deposition solution concentration was required to achieve SAM formation. It was seen that shorter chain alkane thiols at low concentrations did not form monolayers at elevated temperatures whereas, at higher concentrations, all chain lengths formed monolayers at increased temperatures. As the chain length increased in lower concentration solutions so too did the ability of such molecules to form monolayers at high temperatures.

EQCM was next employed as a tool to study the quality of monolayers formed as a function of thiol concentration and chain length. The ratio of measured mass change to expected mass change ($\Delta M_M/\Delta M_E$) was introduced as a means of evaluating SAM quality. Good quality monolayers were taken as those layers that exhibited a $\Delta M_M/\Delta M_E$ ration of unity. The results of this study were in keeping with present teaching. It was determined, again as expected, that longer chain lengths and high concentration yield are key to monolayer formation. For 1mM solutions at all chain lengths it was found that good quality monolayers were formed after only 5 seconds adsorption time. For 0.1mM solutions it was found that a period of at least 15 mins was necessary to guarantee good monolayer quality. In the case of 0.01mM solutions even adsorption for 2 hours was not sufficient to ensure good monolayer quality.

References

(1) M.D. Porter, C.A. Widrig and C.A. Alaves, *J. Am. Chem. Soc*, **1991**, *113*, 2805.

(2) D.K. Schwartz, *Annu. Rev. Phys. Chem*, **2001**, *52*, 107.

(3) Z.Y. Zhang, M.G. Lagally, *Science*, **1997**, *276*, 377.

(4) V. Kanager, H. Mohwald, P. Dutta, Rev. Mod. Phys, **1999**, *71(3)*, 779.

(5) C.D. Bain, E.B. Troughton, Y. Tao, J. Evall, G.M. Whitesides, R.G. Nuzzo, *J. Am. Chem. Soc.* **1989**, *111*, 321.

(6) K. Shimazu, I. Yagi, Y. Sato, K. Uosaki, *Langmuir*, **1992**, *8*, 1385.

(7) Y-T. Kim, R.L. McCarley, A.J. Bard, *Langmuir*, **1993**, *8*, 1941.

(8) C. Frubose, K. Doblhofer, *J. Chem. Soc. Faraday Trans*, **1995**, *91*, 1949.

(9) T.W. Schneider, D.A. Buttry, *J. Am. Chem. Soc.***1993**, *115*, 12391.

(10) D.S. Karpovich, G.J. Blanchard, *Langmuir*, **1994**, *10*, 3315.

(11) H.M. Schessler, D.S. Karpovich, G.J. Blanchard, *J. Am. Chem. Soc*, **1996**, 118, 9645.

(12) R.F. DeBono, G.D. Loucks, D. Dellamanna, U.J. Krull, *Can. J. Chem.* **1996**, *74*, 677.

(13) K.A. Peterlinz, R. Georgiadis, *Langmuir*, **1996**, *12*, 4731.

(14) M. Buck, M. Grunze, F. Eisert, J. Fischer, F. Trager, *J. Vac. Sci. Technol. A*, **1992**, *10*, 926.

(15) O. Dannenberger, M. Buck, M. Grunze, *J. Phys. Chem. B*, **1999**, *103*, 2202.

(16) M. Kawasaki, T. Sato, T. Tanaka, K. Takao, *Langmuir*, **2000**, *16*, 1719.

(17) K.D. Truong, P.A. Rowntree, *J. Phys. Chem*. **1996**, *100*, 19917.

(18) R.H. Terrill, T.A. Tanzer, P.W. Bohn, *Langmuir*, **1998**, *14*, 845.

(19) F. Bensebaa, R. Voicu, L. Huron, T.H. Ellis, E. Kruss, *Langmuir*, **1997**, *13*, 5335.

(20) M. Himmelhaus, F. Eisert, M. Buck, M. Grunze, *J. Phys. Chem. B*, **2000**, *104*, 576.

(21) R. Yamada, K. Uosaki, *Langmuir*, **1997**, *13*, 5218.

(22) R. Yamada, K. Uosaki, *Langmuir*, **1998**, *14*, 855.

(23) S. Xu, S.J.N. Cruchon-Dupeyrat, J.C. Garno, G.Y. Liu, G.K. Jennings, *J. Chem. Phys*, **1998**, *108*, 5002.

(24) O. Dannenberger, J.J. Wolff, M. Buck, *Langmuir*, **1998**, *14*, 4679.

(25) Kreuzer, H. J. *Surf. Sci.* **1995**, *344*, L1264.

(26) Arumainayagam, C. R.; Stinnett, J. A.; McMaster, M. C.; Madix, R. *J. Chem. Phys.* **1991**, *95*, 5437.

(27) H.B. Shao, H.Z. Yu, G.J. Cheng, H.L. Zhang, Z.F. Lui, *Ber. Bunsenges. Phys. Chem*, **1998**, *102*, 111.

(28) Pan, W.; Durning, C. J.; Turro, N. J. *Langmuir* **1996**, *12*, 4469.

(29) L.S. Jung, C.T. Campbell. *Phys Rev. Lett.* **2000**, *84*, 5164.

(30) I. Doudevski, W.A. Hayes, D.K. Schwartz, *Phys. Rev. Lett.* **1998**, *81*, 4927.

(31) I. Doudevski, D.K. Schwartz, *Phys Rev. B.* **1999**, *60*, 14.

(32) J. G. Amar, F.Family, *Phys. Rev. B.* **1994**, ***50***, 8781.

(33) A.M. Napper, H. Lui and D.H. Waldeck, *J. Phys. Chem. B.*, **2001**, *105*, 7699

(34) Y. Sato, S. Ye and K. Uosaki, *Langmuir*, **1997**, *13*, 3157.

(35) D. Collard and M.A. Fox, *Langmuir*, **1991**, *7*, 1192

(36) E. Delamarche, B.Michel, Ch. Gerber, D. Anselmetti, H.-J. Gentherodt, H. Wolf, H. Ringsdorf, *Langmuir*, **1994**, *10*, 2860.

(37) D.S. Karpovich and G.J. Blanchard, *Langmuir*, **1994**, *10*, 3315

(38) D.H. Kim, J. Noh, M. Hara, H. Lee, *Bull Korean Chem. Soc.* **2001**, *22*, No. 3

(39) W. Pan, C.J. Durning, N.J. Turro, *Langmuir*, **1996**, *12*, 4469

(40) T.W. Schneider and D.A. Buttry, *J. Am. Chem. Soc*, **1993**, *115*, 12391

(41) Y. Sato, F. Mizutani, K. Shimazu, S. Ye, K. Uosaki, *J. Electroanal. Chem.* **1999**, *474*, 94.

CHAPTER 5 –

FORMATION OF ELECTROACTIVE MIXED MONOLAYERS

5. Formation of Electroactive Mixed Monolayers.

5.1 Introduction.

In *Chapter 3, Section 3.3.2* it was determined that deviations from ideal electron transfer characteristics occur in fully formed monolayers of electroactive SAMs. Such deviations are due to the repulsive/attractive interactions occurring between neighboring electroactive surface moieties. Such interactions give rise to complications when attempting to study the fundamentals underlying electron transfer processes as described by Marcus theory. One way to negate such interactions is via the formation of mixed monolayers. By forming mixed monolayers it is possible to deposit molecules that are electroactive at modest electrode potentials in a matrix of insulating/non-electroactive molecules. Such molecules are not susceptible to the interactions mentioned above and thus provide an ideal basis to study the fundamentals of electron transport. This chapter will explore mechanisms for the formation of mixed monolayers. Cyclic voltammetry and an electrochemical quartz crystal microbalance will be used in tandem for the first time to investigate the initial stages of mixed monolayer formation. The use of these two mechanisms has the ability to provide new insights into the formation of mixed monolayers. Two methods, namely place exchange and coadsorption, are developed and studied. An introduction to the mixed monolayer system studied in this work will now be given. This will be followed by a description of the two mechanisms of mixed monolayer formation.

As already mentioned it is desirable to prepare electroactive monolayers in which the electroactive molecules have the ability to act ideally. To do this mixed monolayer formation is convenient. The mixed monolayer system described in this section is comprised of molecules bearing the electroactive ferrocene headgroup and insulating molecules bearing a CH_3 headgroup. This system is depicted schematically below in Figure 5.1 It has been calculated that the maximum surface coverage of ferrocene terminated alkanethiol SAMs on an electrode has been shown to be 4.5×10^{-10} $mol.cm^{-2}$ by modeling the pendant ferrocene molecules as spheres of diameter 6.6Å. However the ferrocene coverage on an electrode may be controlled the formation mixed monolayers[1,2] composed of diluent thiols and ferrocene terminated thiols

providing the ability, in theory, to investigate the electron transfer processes of single or at least ideally behaving redox sites.

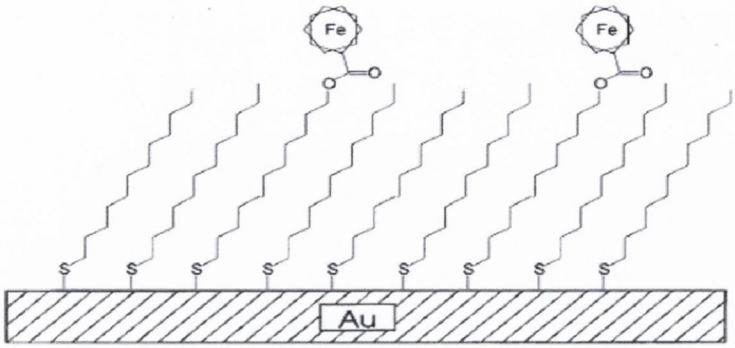


Figure 5.1. Schematic depicting a mixed monolayer of electroactive, ferrocene terminated molecules and insulating CH_3 terminated molecules Reproduced from Reference (1).

Two main methods exist for the formation of such mixed monolayers. The first was described by Chidsey et al.[3]. In this method the mixed monolayers are self-assembled from solutions containing various mole fractions of the two constituents. This method produced ideally behaving cyclic voltammetry (CV) at low ferrocenylalkanethiol mole fractions as the spacing between the ferrocene groups was great enough such that they did not interact. It has noted been however that this method is not experimentally trivial and it can be difficult to prepare reproducible mixed monolayers of defined proportions. This irreproducibility stems from the fact that alkanethiols with different terminal groups and different chain lengths have different free energies in solution. It has been noted that the relationship between the mole fraction of ferrocene terminated alkanethiols in solution and the fraction of the mixed SAM comprised of ferrocene terminated alkanethiols is not linear[3,4]. Although this situation has been treated thermodynamically[1] it remains experimentally challenging to deposit mixed monolayers of redox active thiols in a dilution matrix reproducibly using the method based on mole fractions.

The second main method of preparing mixed monolayers, and the one upon which this study is based, involves the exchange/replacement of a fraction of the thiols in an existing monolayer by incubating this monolayer in the solution of a different

thiol[3,5]. These experiments detail cases of the replacement of one ferrocene-terminated thiol for another, the exchange of a nonelectroactive thiol for a ferrocene terminated thiol (gain of electroactive coverage) and the exchange of a terminated ferrocene alkanethiol for an unsubstituted thiol (loss of electroactive coverage). These exchanges are reported to occur over a period of hours to days.

In this work we attempt to challenge and elucidate upon some of the theories put forward for the exchange/replacement method of creating mixed monolayers of ferrocene terminated and unsubstituted alkanethiols as these monolayers most applicable to the investigation of electron transfer dynamics in a single molecule.

Firstly we electrochemically investigate the work of Lee et al.[6]. This study asserts that a when an electrode modified with a ferroceneylalkanethiol SAM is incubated in a solution of unsubstituted alkanethiols a coadsorption process occurs as opposed to a place exchange process as reported above[3,5]. It was shown that $CH_3(CH_2)_{11}SH$ molecules coadsorbed between $FcCO_2(CH_2)_{11}SH$ molecules in a SAM. This caused rotation of the C-O single bond on the carbonyl side of the ester. In effect it was shown that when the $CH_3(CH_2)_{11}SH$ coadsorb they push the ferrocene groups upwards to make room for themselves. This can result in the overall reorientation of the $FcCO_2(CH_2)_{11}SH$ molecules. It is proposed that it is this reorientation of the terminal ferrocene groups as opposed to any place exchange mechanism that causes an observed decrease in ferrocenylalkanethiol surface coverage. This method will hitherto be known as coadsorption. The proposed mechanism for mixed monolayer formation by coadsorption is shown in Figure 5.2 below.

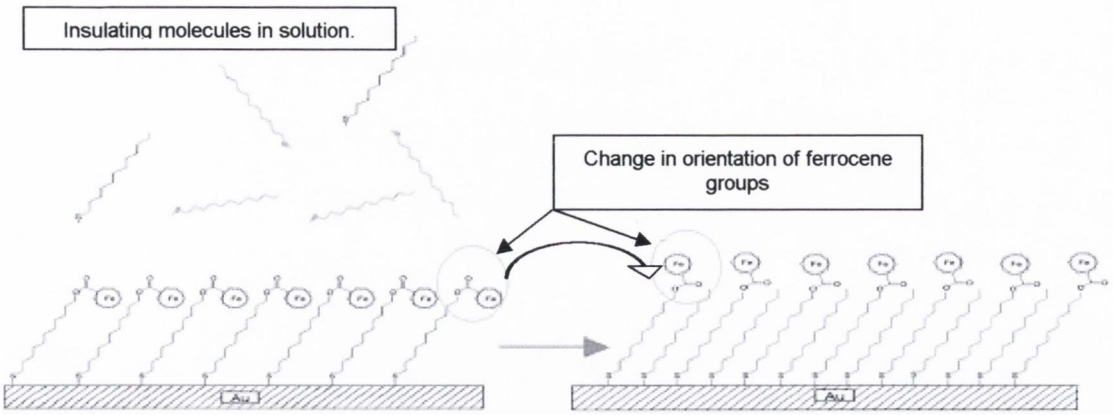


Figure 5.2. Schematic depicting the formation of mixed monolayer by coadsorption. The left hand side of the diagram depicts a fully formed electroactive layer being incubated in a solution of insulating molecules for a known period of time. The right hand side of the diagram shows insulating molecules being accommodated into the free volumes between the electroactive molecules. The coadsorption mechanism is accompanied by a reorientation of the terminal ferrocene groups.

Secondly we monitor the effect of incubating an electrode modified with an unsubstituted alkanethiol SAM in a solution of a ferrocene terminated, electroactive, alkanethiol monolayer using cyclic voltammetry and EQCM. This method of mixed monolayer formation will hitherto be known as place exchange. The proposed mechanism for this type of mixed monolayer formation is shown in Figure 5.3.

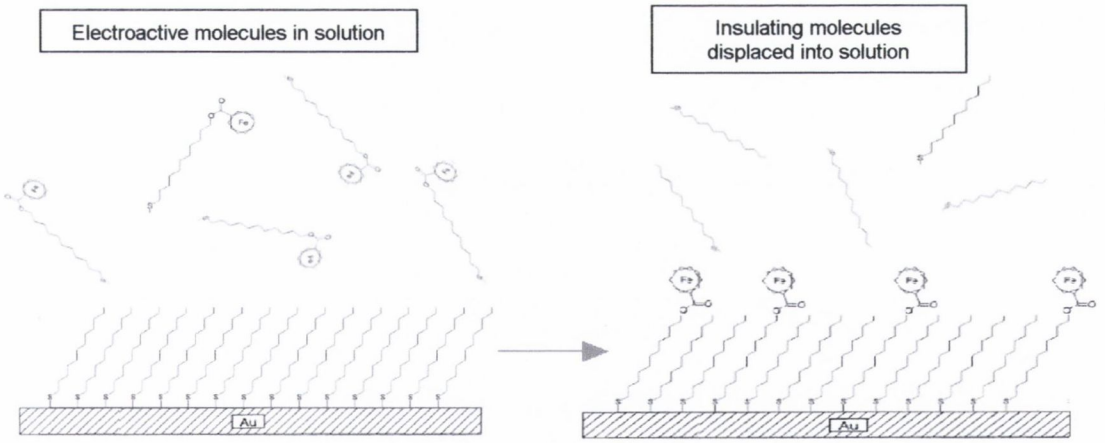


Figure 5.3. Schematic depicting the formation of mixed monolayer by place exchange. The left hand side of the diagram depicts a fully formed insulating layer being incubated in a solution of electroactive molecules for a known period of time. The right hand side of the diagram shows insulating molecules being displaced into solution and replaced by the electroactive molecules.

It will be shown in both cases that the formation of a mixed monolayer that has a profound effect on the electrochemical response of the system occurs in matter of minutes rather than over a period of hours or days. Using a combination of CV and EQCM the number of electroactive sites that are in an ordered orientation on the surface of the monolayer will be calculated. As well as this the number of water molecules that permeate the layer during redox activity at various stages of mixed monolayer formation will be calculated. Such calculations have the ability to provide a much more comprehensive understanding of the mechanisms involved in mixed monolayer formation.

5.2 Experimental

Electrochemical Measurements. All electrochemical measurements were carried out on a CH Instruments Model 440 potentiostat as described in *Section 2.2.1.*

Gold Substrate. The gold substrate used whether it be a standard macroelectrode or an EQCM electrode is as described in *Section 2.1.1.*

Electrode Pre-Treatment. The method used for electrode pre-treatment is described in *Section 2.3.1.*

Formation of Mixed Monolayers. Coadsorbed monolayers were deposited by immersing the gold substrate in a 1mM ethanolic solution of the various ferrocene-terminated alkanethiols for a period of 48hrs. Following immersion the gold substrate was thoroughly rinsed in ethanol to remove any physisorbed species. The modified electrodes were then immersed in 1mM ethanolic solutions of their respective alkanethiols for periods of 2.5, 5, 7.5 and 15 mins. This was followed by further rinsing in ethanol. Place exchanged monolayers were formed by an identical but reverse method. Here a monolayer of insulating, CH_3-terminated, molecules were deposited from 1mM ethanolic solutions of the molecule in question. Following immersion the gold substrate was thoroughly rinsed in ethanol to remove any physisorbed species. The modified electrodes were then immersed in 1mM ethanolic solutions of their respective ferrocene-terminated alkanethiols for periods of 2.5, 5, 7.5 and 15 mins. This was followed by further rinsing in ethanol.

Electrolyte Solutions. The electrolyte solutions used in all experiments were 0.1M Perchloric Acid unless otherwise stated. *Section 2.1.4* provides further details.

5.3 Results and Discussion

5.3.1 Mixed Monolayer Formation via Coadsorption

Figures 5.4-5.6 show the cyclic voltammetry responses of the ferrocene alkanethiol monolayers, $FcCO_2H(CH_2)_nSH$ (n=8,10,12) that have undergone coadsorption with $CH_3(CH_2)_nSH$ (n=7,9,11). It can be clearly seen that the peak heights decrease substantially upon coadsorption of the unsubstituted thiol. Since it has been shown that the coadsorption of the $CH_3(CH_2)_{11}SH$ molecules does not cause desorption of the ferrocene terminated molecules[4] it is postulated that the reorientation of the ferrocene molecules renders them less likely to undergo oxidation or reduction leading to the decreased peak heights in Figures 5.4-5.6 and decreased values of surface coverage as shown in Figure 5.7. After coadsorption it is quite difficult to differentiate between CV scans and hence their data is presented in Tables 5.1-5.3.

It is also noted from Tables 5.1-5.3 that as the amount of thiol coadsorption increases so too does the value of the Peak Width Half Maximum (E_{PWHM}) of the cyclic voltammograms. The cyclic voltammogram for the pure ferrocene alkanethiol SAM exhibits sharp oxidation and reduction peaks. Such sharp peaks are obtained when the redox centers form a densely packed and well-ordered monolayer. The value of E_{PWHM} for the $FcCO_2(CH_2)_{10}S$ monolayer is 43.8 mV which is well below the expected value of 90.6/n mV for an ideal electroactive SAM. This can be attributed to the fact that a monolayer with a high surface concentration of redox centers will have strong interactions between the redox centers.

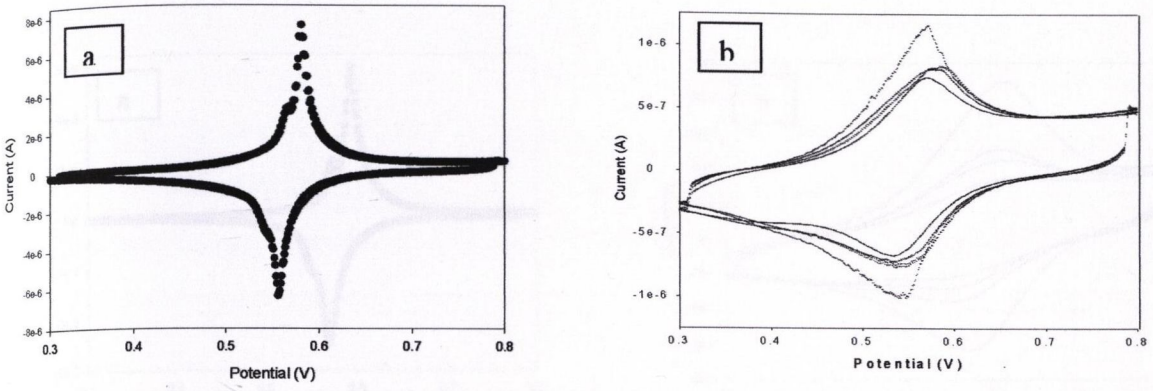


Figure 5.4. Cyclic voltammogram of (a) a purely $FcCO_2H(CH_2)_8S$ monolayer and (b) the $FcCO_2(CH_2)_8S$ immersed in 1mM $CH_3(CH_2)_7SH$ for various periods of time (2.5mins, 5mins, 7.5mins, 15mins). Decreasing peak heights indicate longer coadsorption times. The electrolyte was 0.1M $HClO_4$. Scan rate 0.02V/s.

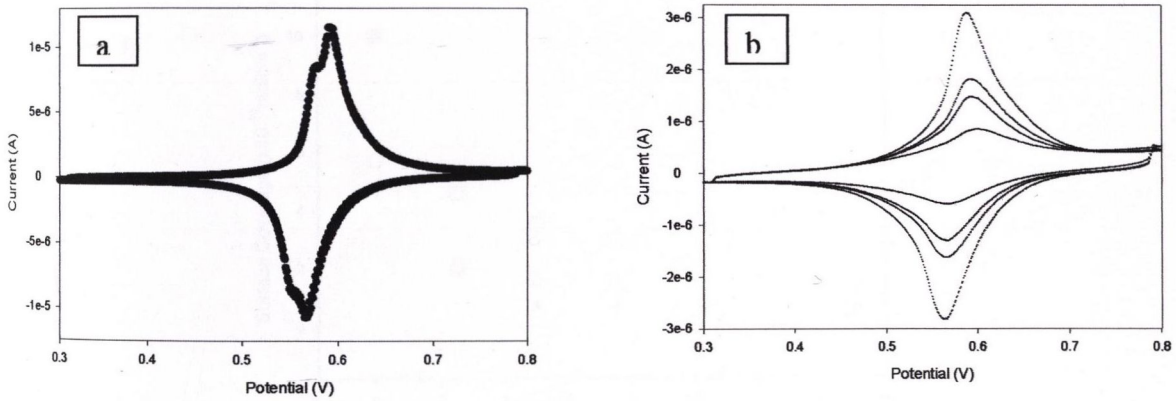


Figure 5.5. Cyclic voltammogram of (a) a purely $FcCO_2H(CH_2)_{10}S$ monolayer and (b) the $FcCO_2(CH_2)_{10}S$ immersed in 1mM $CH_3(CH_2)_9SH$ for various periods of time (2.5mins, 5mins, 7.5mins, 15mins). Decreasing peak heights indicate longer coadsorption times. The electrolyte was 0.1M $HClO_4$. Scan rate 0.02V/s.

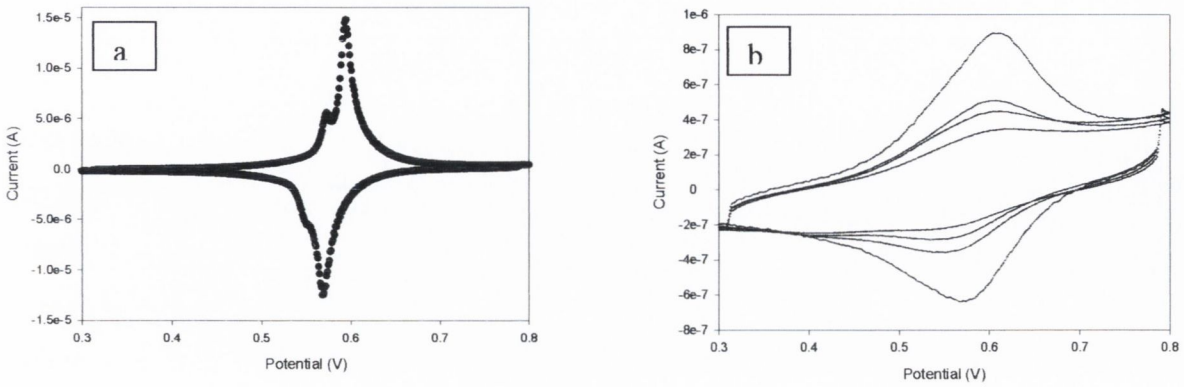


Figure 5.6. Cyclic voltammogram of (a) a purely $FcCO_2H(CH_2)_{12}S$ monolayer and (b) the $FcCO_2(CH_2)_{12}S$ immersed in 1mM $CH_3(CH_2)_{11}SH$ for various periods of time (2.5mins, 5mins, 7.5mins, 15mins). Decreasing peak heights indicate longer coadsorption times. The electrolyte was 0.1M $HClO_4$. Scan rate 0.02V/s

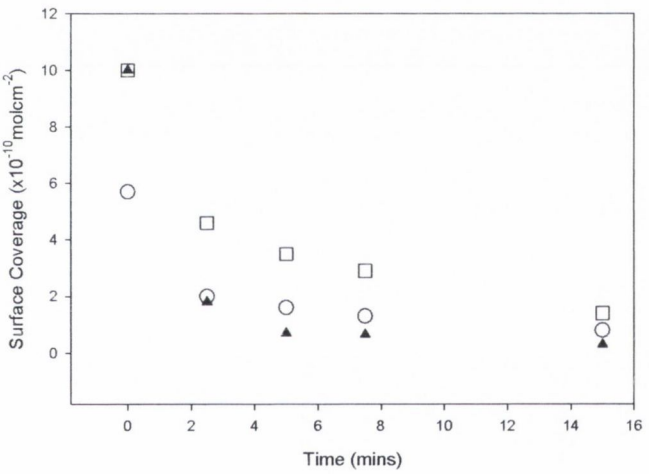


Figure 5.7. Showing the decrease in surface coverage of a $FcCO_2H(CH_3)_nSH$ (n=8, 10, 12) monolayers when treated with a 1mM solution of their corresponding unsubstituted thiol. n=8(circles), n=10(squares), n=12 (triangles).

These interactions have been considered by considering the activity coefficients for the oxidised and reduced forms of the electroactive group[7], or by classical[8] and statistical

mechanical interaction energies[9,10]. Values of E_{PWHM} can be either broader or narrower than 90.6/n mV depending on whether the interactions are either repulsive or attractive. It can be determined from Figure 5.4 that the interactions are attractive in the pure ferrocene alkanethiol SAM since the value of E_{PWHM} is less than 90.6/n mV. As the amount of coadsorption increases these interactions are reduced and the value of E_{PWHM} approaches the theoretical value indicating that the interactions between the ferrocene molecules decrease as the amount of coadsorbed thiol increases. This can be attributed to the fact that as an increased amount of ferrocene molecules are "deactivated" due to their coadsorption induced reorientation the amount of attractive interactions are decreased and hence the value of E_{PWHM} approaches the theoretical. A similar trend is observed when considering the cyclic voltammetry of the $FcCO_2(CH_2)_8S$ and $FcCOO(CH_2)_{12}S$ SAMs coadsorbed with $CH_3(CH_2)_7S$ and $CH_3(CH_2)_{11}S$ respectively.

Immersion Time (mins)	**I_P (A) ($x10^{-6}$)**	**E_{Pa} (mV)**	**E_{Pc} (mV)**	**E^0 (mV)**	**E_{PWHM} (mV)**
0	7.2	58	55	56.5	16.8
2.5	1.2	57	54	55.5	67.3
5	0.8	59	54	56.5	79.1
7.5	0.8	58	53	55.5	84.0
15	0.7	57	53	55	73.9

Table 5.1. Data for the cyclic voltammograms shown in Figure 5.4.

Immersion Time (mins)	**I_P (A) ($x10^{-6}$)**	**E_{Pa} (mV)**	**E_{Pc} (mV)**	**E^0 (mV)**	**E_{PWHM} (mV)**
0	11.3	59	57	58	43.8
2.5	3.1	58	56	57	66.0
5	1.8	59	56	57.5	79.7
7.5	1.5	59	56	57.5	80.0
15	0.85	60	56	58	95.0

Table 5.2. Data for the cyclic voltammograms shown in Figure 5.5.

Immersion Time (mins)	I_P (A) ($x10^{-6}$)	E_{Pa} (mV)	E_{Pc} (mV)	E^0 (mV)	E_{PWHM} (mV)
0	15.3	59	57	58	18.3
2.5	0.9	61	57	59	100
5	0.5	60	55	57.5	83
7.5	0.4	61	54	57.5	110
15	0.3	62	52	57	Indeterminate

Table 5.3. Data for the cyclic voltammograms shown in Figure 5.6.

Further study of Figure 5.4 yields further information on the nature of the thiol coadsorption. The SAM consisting of pure ferrocene alkanethiol exhibits a small redox shoulder occurring before the main oxidation peak at 58mV. This indicates phase segregation between ferrocene molecules orientated in slightly different manner. Interestingly this shoulder disappears in the SAMs where coadsorption has occurred. This indicates that the coadsorption of C_{10} may cause the remaining ferrocene molecules that have not been "deactivated" to orientate themselves in an ordered manner.

Hence the main conclusion of the latter experiments is that the reorientation of the ferrocene moieties leads to a decrease in the amount of electroactivity in the ferrocene thiol SAMs.

Further to this an electrochemical quartz crystal microbalance (EQCM) was employed to investigate the mass changes on the surface of the monolayer during the redox processes of the ferrocenylalkanethiol SAM. $FcCO_2(CH_2)_nSH$ monolayers allow electron transfer between the gold electrode and the electrolyte through the alkane chain. During the redox oxidation of the ferrocenylalkanethiol SAM the normally neutral terminal ferrocene group is transformed to the positive ferrocenium cation (Fc^+). As the terminal group becomes positively charged anions from the perchloric acid electrolyte (ClO_4^-) are attracted towards the surface of the SAM. An ion pair is

then formed between the terminal Fc^+ ion and the ClO_4^- molecule. The incorporation of the ClO_4^- anion onto the surface results in a mass change that can be measured via EQCM. An increase in the loading on the surface of the quartz crystal corresponds to a damping in its resonance frequency. The formation of the ion pair on the SAM surface will cause such a damping. Thus a decrease in the recorded frequency corresponds to an increase in the mass of the monolayer. When the ferrocene molecule is reduced back to its neutral state the electrostatic interaction necessary for the formation of the ion pair is no longer present. The ion pair is thus broken and the ClO_4^- molecule discarded back into the electrolyte. Mixed monolayer formation has never been treated in such a manner. This work will detail a method to calculate the number of redox sites that are active on the monolayer surface as mixed monolayer formation progresses for both the coadsorption and place exchange formation methods.

This simple treatment of ion pairing at the SAM/electrolyte interface described above has the ability to monitor the amount of electroactive sites on the surface that undergo ion pairing during oxidation. However as well as ion pairing interactions causing an increase in mass on the surface of the layer it is also possible to have the ingress of water molecules into the layer causing a mass increase. In this report the simple treatment of ion pairing is extended to calculate the number of water molecules encroaching into the monolayer. To aid the reader's understanding a sample calculation is presented below to determine: (a) the number of electroactive sites that are actually forming ion pairs, (b) the number of water molecules that ingress into the layer at each redox site during oxidation.

Sample Calculation

Figures 5.10-5.12 display the frequency changes accompanying the oxidation and reduction of the CVs in Figures 5.4-5.6. The surface coverages of electroactive thiols after each coadsorption period are given in Tables 5.4, 5.5 and 5.6, calculated from Figures 5.4, 5.5 and 5.6 respectively.

This calculation will be based on the purely electroactive monolayer (i.e. 0 mins immersion time in insulating thiol) described in Table 5.4.

The surface coverage of this electroactive monolayer is $5.7x10^{-10}$mol.cm^{-2}, thus the number of electroactive molecules on the surface is: $3.4x10^{14}$molecules.cm^{-2} (using Avogadros constant). Thus on the surface of the electrodes used in this work with area 0.196cm^2 the number of electroactive molecules is $6.6\ x10^{13}$. Should each of these electroactive sites form an ion pair with a perchlorate ion of weight $1.6x10^{-22}$g the expected mass change on the surface is

$$\text{Expected Mass Change} = (6.6\ x10^{13}\text{molecules})(1.6x10^{-22}\text{g.molecule}^{-1})$$
$$= 10.5\text{ng}$$

The actual mass change recorded by EQCM is 20ng which is an excess mass change. Thus 100% of the electroactive sites on the surface are forming ion pairs with perchlorate ions in solution. As well as this there is an ingress of 20ng –10.5ng = 9.5ng worth of water molecules into the layer during oxidation. The number of water molecules being incorporated into the layer (per redox site) can be calculated thus:

Should each redox site allow the ingress of one water molecule of weight $2.99x10^{-23}$g a mass change calculated below is expected.

$$\text{Mass Change due to } H_20 \text{ ingress} = (6.6\ x10^{13}\text{molecules})(2.99x10^{-23}\text{g.molecule}^{-1})$$
$$= 1.9\text{ng}$$

However an excess mass change of 10.5ng has been recorded. Thus there are 10.5ng/1.9ng = 5.5 water molecules being incorporated at each redox site of the layer during oxidation.

Many results such as that presented in Table 5.4 are given in this report and all figures presented are calculated as shown here.

Figures 5.4–5.6 and Figures 5.10-5.12 display the cyclic voltammetry and EQCM responses for electroactive monolayers that have been incubated in solutions of insulating thiols for varying periods of time. Tables 5.4, 5.5 and 5.6 display the diagnostics associated with each response as well as the number of water molecules incorporated and the number of electroactive molecules that are active on the surface of

the monolayer. Attention is now turned to Tables 5.4-5.5 as this data is expected to give the greatest insight into the nature of the processes occurring during coadsorption. As an instructive example of how these tables are interpreted Table 5.6, which deals with the coadsorption of a $FcCO_2(CH_3)_{12}SH$ electroactive monolayer with $CH_3(CH_2)_{11}SH$, will be examined. Firstly it is noted that at all stages during the coadsorption process 100% of the electroactive surface moieties are active. This means that all of the surface sites detected by cyclic voltammetry are registered as forming ion pairs with perchlorate ions and thus in an ordered orientation on the surface of the layer. Attention is now turned to the number of water molecules that are incorporated into the layer during oxidation. It has be shown that the maximum number of water molecules that can be incorporated into a purely ferrocene alkanethiol monolayer is 12-13[11] per alkanethiol molecule. This is possible because water molecules can occupy the free space in a ferrocene alkanethiol SAM which results from the discrepancy in area occupied by the ferrocene molecule and that occupied by the alkane chain. This is depicted in Figure 5.8 below.

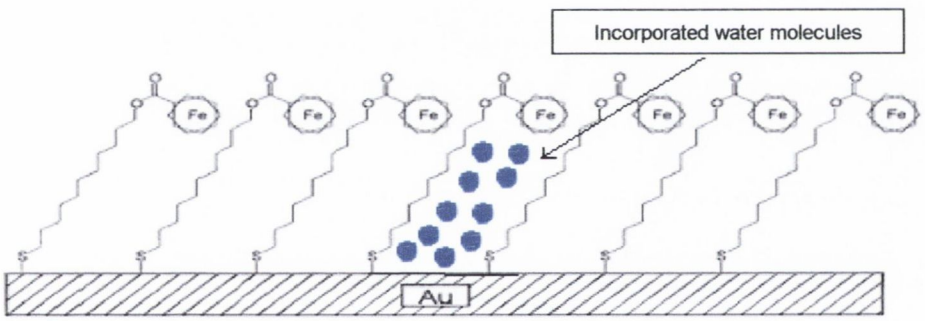


Figure 5.8. Showing how water molecules can be incorporated between the chains in a ferrocene terminated alkanethiol SAM. The water molecules are depicted as navy circles.

The presence of H_2O molecules in the bulk hydrocarbon section of the SAM may not be what is expected given the hydrophobic nature of this region. However H_2O molecules have shown the ability to readily transverse cell membranes formed from lipid bilayers of similar structure to the alkanethiol molecules used in this study[12]. Thus the possibility of H_2O molecule incorporation into this region should not be ruled out.

As already mentioned it is known that upon coadsorption the insulating molecules adsorb into the spaces between the ferrocene terminated chains causing a reorientation of the ferrocene moieties. Indeed the insulating molecules adsorb in exactly the place where water molecules are thought to permeate the layer (see Figure 5.2). Thus it is to be expected that as coadsorption proceeds the insulating molecules would block any permeation of water molecules into the layer. Now examine Table 5.6. Before any coadsorption the number of water molecules calculated to be incorporated at each redox site is 6.8. However after 2.5 mins coadsorption the number of water molecules rises greatly to 34.2 being incorporated at each site. The question that must be asked is why this is happening since the coadsorption of insulating molecules is expected to block water permeation? An explanation is proposed thus. At small coadsorption times only a fraction of the available ferrocene terminated sites have an insulating chain coadsorbed next to them. Consider one particular ferrocene moiety that has been reoriented due to this process. The ferrocene moiety next to it may not be reoriented. The combination of neighboring ferrocene moieties next to one another in different orientations with no insulating molecule in the space between could allow a large amount of water molecules to permeate. This effect is depicted in Figure 5.9.

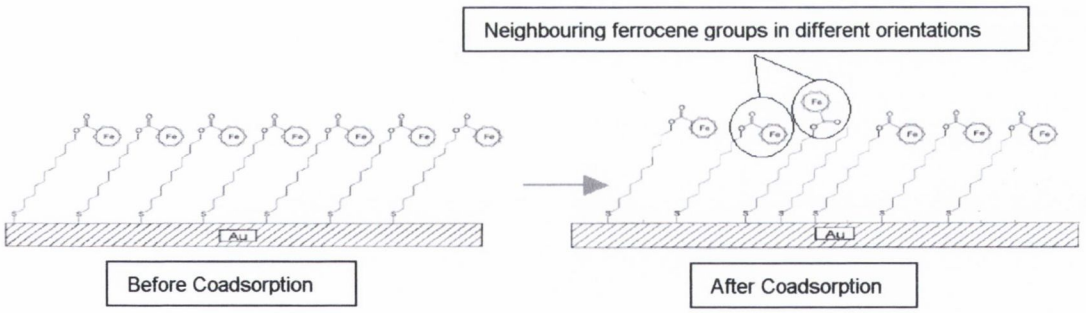


Figure 5.9. Depicting the mechanism proposed by which an increased amount of water molecules are allowed to permeate the SAM film after coadsorption. Shown are two ferrocene groups adopting differing orientations after coadsorption. The leftmost ferrocene resides in its standard state. The rightmost ferrocene is reoriented due to the coadsorption of an insulating molecule beside it.

As the coadsorption continues in Table 5.6 the number of water molecules incorporated at each redox site increases still further to 52.9 after 5 mins coadsorption time. As the coadsorption time increases still further to 7.5 and 15 mins the number of incorporated water molecules is seen to fall. Such an effect may be explained as an increased number

of insulating molecules being present on the surface beginning to block water molecule permeation and offset effects due to mismatches in neighboring ferrocene orientations. Quite similar trends are seen in Tables 5.4 and 5.5 corresponding to the coadsorption of $FcCO_2(CH_3)_nSH$ (n=8 and 10) electroactive monolayers with $CH_3(CH_2)_nSH$ (n=7 and 9) respectively.

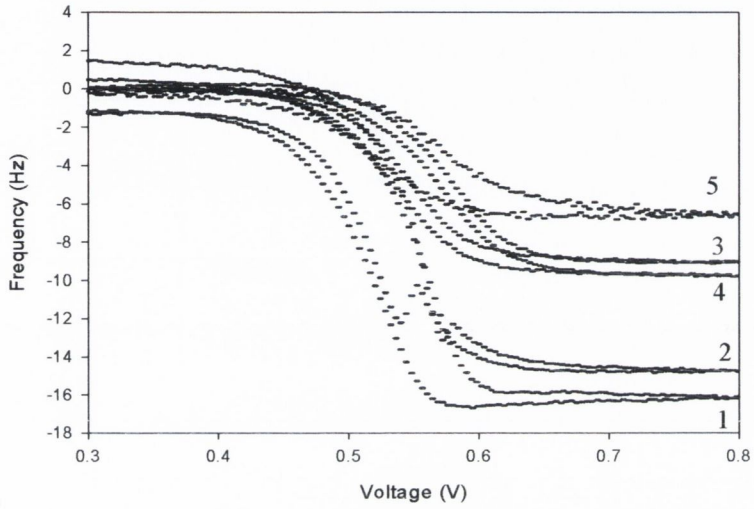


Figure 5.10. EQCM response of a $FcCO_2H(CH_2)_8SH$ monolayer immersed in 1mM $CH_3(CH_2)_7SH$ in 0.1M $HClO_4$ for various periods of time. 0mins (1) , 2.5mins (2), 5mins (3), 7.5mins (4), 15mins (5). Scan rate 20mV/s.

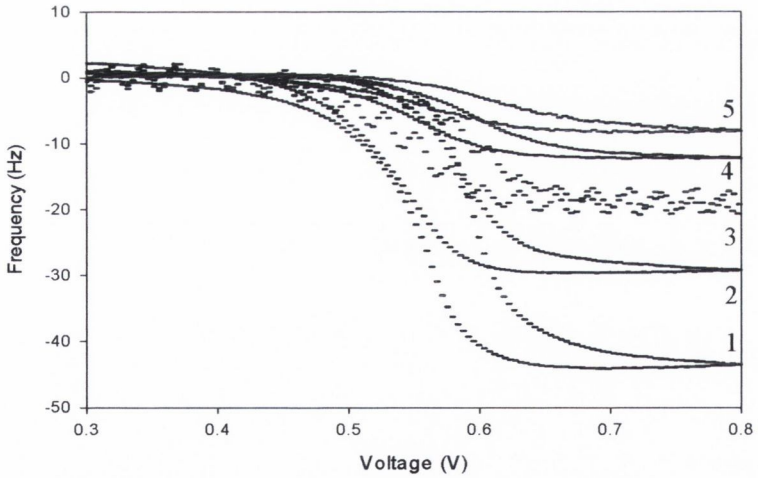


Figure 5.11. EQCM response of a $FcCO_2H(CH_2)_{10}SH$ monolayer immersed in 1mM $CH_3(CH_2)_9SH$ in 0.1M $HClO_4$ for various periods of time. 0mins (1), 2.5mins (2), 5mins (3), 7.5mins (4), 15mins(5). Scan rate 20mV/s.

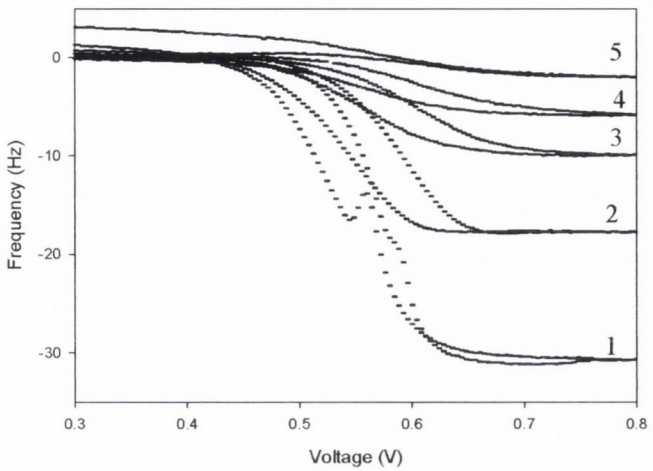


Figure 5.12. EQCM response of a $FcCO_2H(CH_2)_{12}SH$ monolayer immersed in 1mM $CH_3(CH_2)_{11}SH$ in 0.1M $HClO_4$ for various periods of time. 0mins (1), 2.5mins (2), 5mins (3), 7.5mins (4), 15mins(5). Scan rate 20mV/s.

Surface Coverage ($x10^{-10}$mol.cm^{-2})	Frequency Change (Hz)	Expected Mass Change (Ng)	Mass Change (ng)	Water Molecules Incorporated per Redox Site	% Electroactive Sites Active
5.7	14.3	10.8	20.0	4.6	100
2.0	15.8	3.8	22.1	25.9*	100
1.6	9.2	3.0	12.8	17.3	100
1.3	9.5	2.4	13.3	23.6	100
0.8	6.1	1.5	8.5	24.7	100

Table 5.4. Surface Coverages (from Figure 5.7) for a monolayer of $FcCO_2H(CH_3)_8SH$ incubated in a 1mM solution $CH_3(CH_2)_7SH$ for various periods of time and EQCM data from Figure 5.10. .*This value exceeds the theoretical amount of 12-13 water molecules[11] that can be incorporated per redox site. It indicates a period of extreme disorder in the layer possibly do to its reorientation. It is likely that a proportion of the monolayer is very permeable to the electrolyte. All values above 12-13 from here onwards are described likewise.

Surface Coverage ($x10^{-10}$mol.cm^{-2})	Frequency Change (Hz)	Expected Mass Change	Mass Change (ng)	Water Molecules Incorporated per Redox Site	% Electroactive Sites Active
10	42.2	18.9	59.1	11.4	100
4.6	28.5	8.7	39.9	19.2	100
3.5	18.1	6.6	25.3	15.1	100
2.9	11.5	5.5	16.1	10.4	100
1.4	7.3	2.6	10.2	15.3	100

Table 5.5. Surface Coverages (from Figure 5.7) for a monolayer of $FcCO_2H(CH_3)_{10}SH$ incubated in a 1mM solution $CH_3(CH_2)_9SH$ for various periods of time and EQCM data from Figure 5.11.

Surface Coverage ($x10^{-10}$mol.cm^{-2})	Frequency Change (Hz)	Expected Mass Change	Mass Change (ng)	Water Molecules Incorporated	% Electroactive Sites Active
10	30.7	18.9	42.9	6.8	100
1.8	17.9	3.4	25.1	34.2	100
0.7	10.3	1.3	14.4	52.9	100
0.6	5.6	1.1	7.8	31.5	100
0.3	2.3	0.6	3.2	24.9	100

Table 5.6. Surface Coverages (from Figure 5.7) for a monolayer of $FcCO_2H(CH_3)_{12}SH$ incubated in a 1mM solution of $CH_3(CH_2)_{11}SH$ for various periods of time and EQCM data from Figure 5.12.

5.3.2 Mixed Monolayer Formation via Place Exchange.

Figures 5.13-5.15 show the cyclic voltammetry responses of the unsubstituted alkanethiol monolayers, $CH_3(CH_2)_nSH$ where (n=7,9,11), that have been treated with the corresponding 1mM ethanolic solutions of $FcCO_2(CH_2)_nSH$, (n=8,10,12). It can be clearly seen in each case that electron transfer processes between the substrate and the electrolyte is completely blocked (except for a negliable amount due to pinholes) for a purely unsubstituted SAM. Incubation in solutions of the ferrocene terminated alkanethiols results in the exchange of some unsubstituted thiol with ferrocene terminated thiol in similar manner to that described by Collard and Fox[30] when they observed the replacement of $CH_3(CH_2)_{15}SH$ with $Fc(CH_2)_{16}SH$. One possible reason for such a substitution is due to the fact that the ferrocene terminated thiols have a higher free energy in solution than do the unsubstituted thiols making it energetically more favorable for the ferrocene terminated species to adsorb replacing the unsubstituted thiols which return to solution. Tables 5.7-5.10 show data corresponding to the cyclic voltammograms in Figures 5.13-5.15. Figure 5.16 shows the increase in surface coverage of ferrocene alkanethiols after different incubation periods.

It can be seen from Tables 5.7-5.9 that as the incubation time in the solutions of the ferrocene terminated thiols increases the value of the E_{PWHM} decreases in contrast to the situation occurring when the unsubstituted thiol is added to the ferrocenylalkanethiol monolayer. This increase in E_{PWHM} is a result of the increased population of ferrocene terminated species on the substrate. As this population increases the amount of interactions occurring between the ferrocene moieties also increases. This causes greater deviations from the ideal Nernstian value of 90/n mV for E_{PWHM} and is further evidence of a greater number of ferrocene terminated molecules place exchanging with the unsubstituted thiols on the substrate.

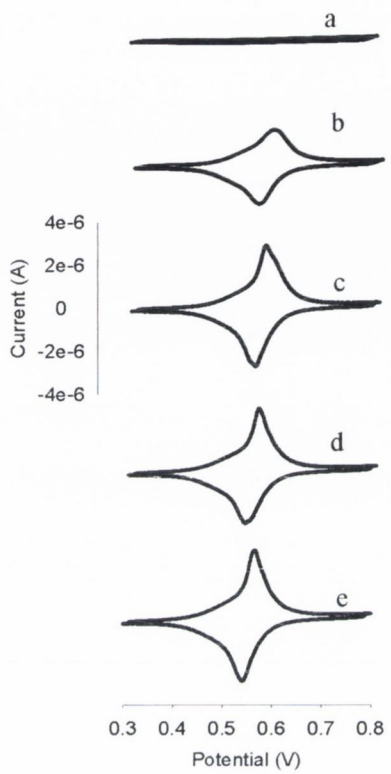


Figure 5.13. Cyclic voltammogram of (a) a $CH_3(CH_2)_7SH$ monolayer immersed in 1mM $FcCO_2H(CH_2)_8S$ for various periods of time (b)2.5mins, (c)5mins, (d)7.5mins, (e)15mins. The electrolyte was 0.1M $HClO_4$. Scan rate 0.02V/s.

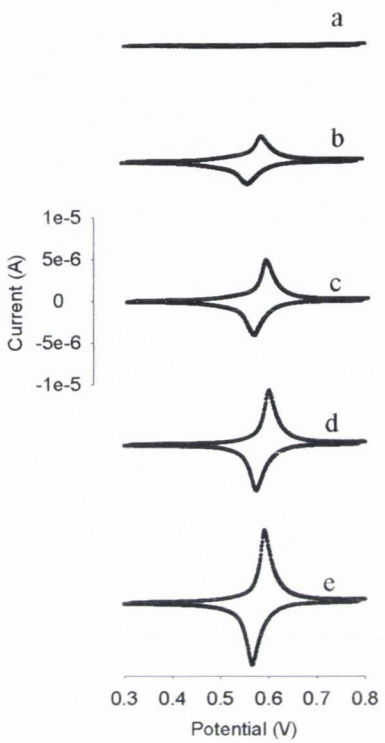


Figure 5.14. Cyclic voltammogram of (a) a $CH_3(CH_2)_9SH$ monolayer immersed in 1mM $FcCO_2H(CH_2)_{10}S$ for various periods of time (b)2.5mins, (c)5mins, (d)7.5mins, (e)15mins. The electrolyte was 0.1M $HClO_4$. Scan rate 0.02V/s.

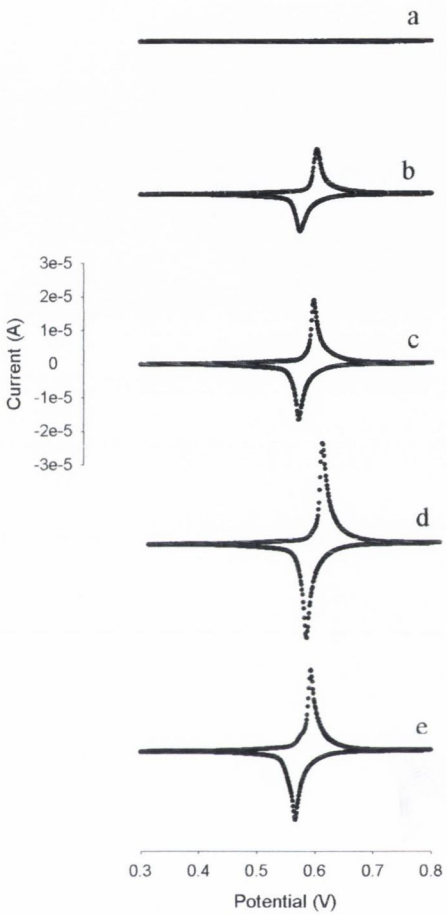


Figure 5.15. Cyclic voltammogram of (a) a $CH_3(CH_2)_{11}SH$ monolayer immersed in 1mM $FcCO_2H(CH_2)_{12}S$ for various periods of time (b)2.5mins, (c)5mins, (d)7.5mins, (e)15mins. The electrolyte was 0.1M $HClO_4$. Scan rate 0.02V/s.

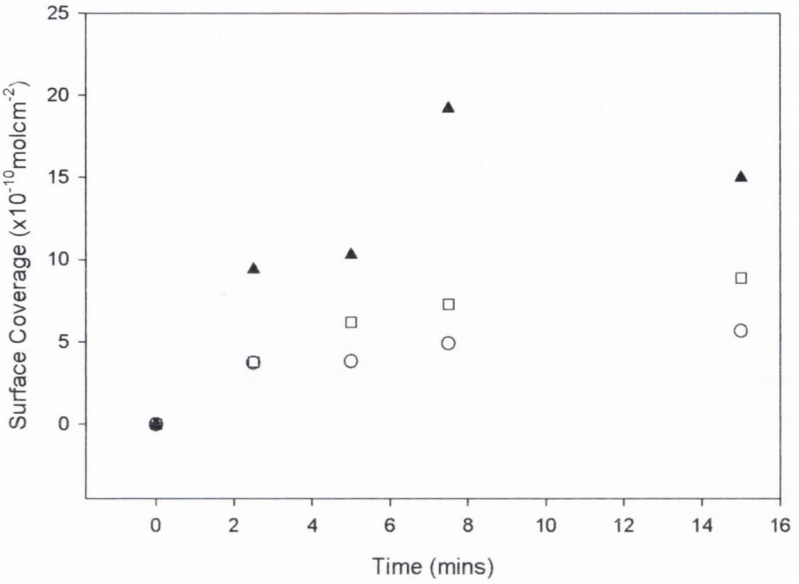


Figure 5.16. Showing the increase in surface coverage of $FcCO_2H(CH_3)_nSH$ (n=8, 10, 12) in a $CH_3(CH_2)_nSH$ (n=7, 9, 11) monolayer as a function of time. n=8(circles), n=10(squares), n=12 (triangles).

Immersion Time (mins)	I_P (A) (x10^{-6})	E_{Pa} (mV)	E_{Pc} (mV)	E^0 (mV)	E_{PWHM} (mV)
2.5	1.7	58.1	55.1	56.6	81
5	2.9	57.1	54.9	56	59
7.5	2.9	56	53.3	54.6	49
15	3.3	56.7	54.2	55.4	48

Table 5.7. Data for the cyclic voltammograms shown in Figure 5.13.

Immersion Time (mins)	I_P (A) (x10^{-6})	E_{Pa} (mV)	E_{Pc} (mV)	E^0 (mV)	E_{PWHM} (mV)
2.5	3	58.9	56.3	57.6	41
5	4.8	58.8	56.3	57.6	32
7.5	6.4	60	57.4	58.7	30
15	7.8	59	56.5	57.8	29

Table 5.8. Data for the cyclic voltammograms shown in Figure 5.14.

Immersion Time (mins)	I_P (A) (x10^{-6})	E_{Pa} (mV)	E_{Pc} (mV)	E^0 (mV)	E_{PWHM} (mV)
2.5	13.3	60.2	57.5	58.9	17
5	18.9	59.7	57.2	58.5	14
7.5	29.2	59.8	57.1	58.5	15
15	25.7	59.3	56.5	57.9	14

Table 5.9. Data for the cyclic voltammograms shown in Figure 5.15.

As in the case of the coadsorption study an EQCM was employed to gain further information regarding the exchange processes. Figures 5.17-5.19 show the frequency changes occurring as a result of the oxidation and reduction of the place exchanged mixed monolayers shown in Figures 5.13-5.15. Tables 5.10-5.12 display the data corresponding to the EQCM responses in Figures 5.17-5.19. As expected the amount of ion pairing observed increases as the incubation time in the electroactive alkanethiol solution increases. Attention is now turned to Tables 5.10–5.12. Again it is instructive to consider one of these tables as a basis upon which to consider all results. In this case Table 5.10, corresponding to the place exchange of a $CH_3(CH_2)_7SH$ monolayer with $FcCO_2H(CH_3)_8SH$ molecules, is considered. Data for the purely insulating monolayer, i.e. 0 mins immersion time is omitted from the table as a completely featureless response characteristic of such a layer is observed. After 2.5 mins immersion in an

electroactive solution a surface coverage of $3.7x10^{-10}mol.cm^{-2}$ of electroactive molecules have place exchanged onto the surface of the electrode as detected by cyclic voltammetry. However using EQCM it is determined that only 25.8% of these place exchanged, electroactive molecules have an orientation suitable to form ion pairs. As the place exchange time is increased the number of electroactive molecules in an ordered orientation increases until finally after 15 mins coadsorption time 100% of the molecules are in a position on the surface to form ion pairs. Again in the case of place exchanged monolayers the number of water molecules permeating the SAM is of interest. The number of water molecules permeating the SAM continues to decrease throughout the place exchange process as the ferrocene moieties become more ordered. At all stages the number of water molecules permeating the SAM structure is well below the number that permeated during the coadsorption method of mixed monolayer formation. This is an interesting observation in itself and most likely arises from the fact that when an electroactive molecule place exchanges into an insulating layer molecules capable to blocking water permeating surround it. Effects such as mismatches in ferrocene orientations that give rise to excess water permeation are not likely to be observed in the case of place exchanged monolayers. Tables 5.11 and 5.12 describe similar findings.

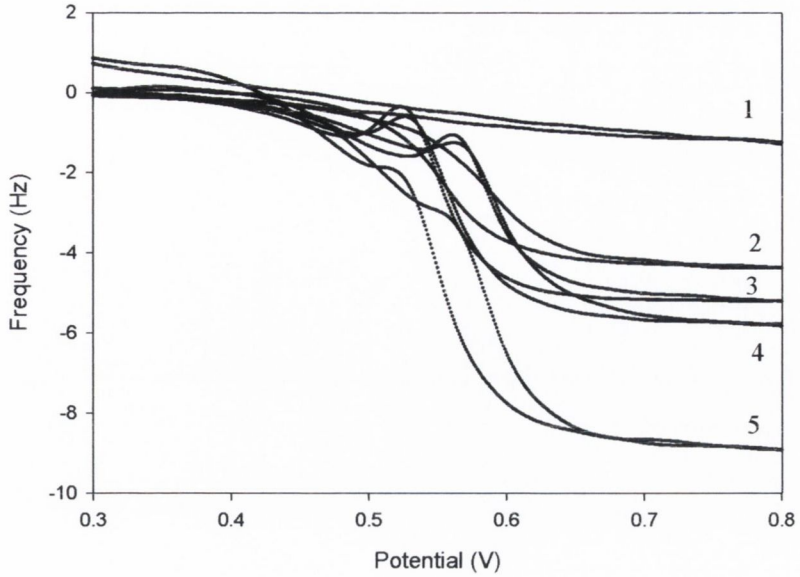


Figure 5.17. EQCM response of a $FcCO_2H(CH_2)_8SH$ monolayer immersed in 1mM $CH_3(CH_2)_7SH$ in 0.1M $HClO_4$ for various periods of time. (1) 0mins, (2) 2.5mins, (3) 5mins, (4) 7.5mins, (5) 15mins. Scan rate 20mV/s.

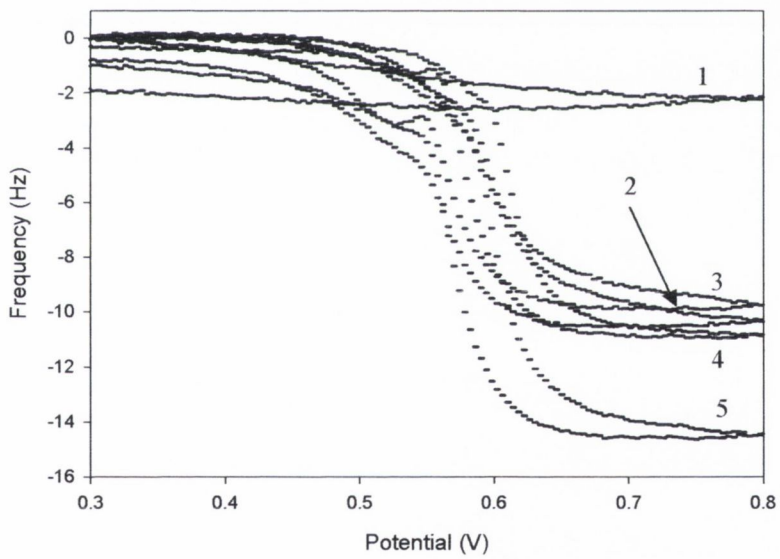


Figure 5.18. EQCM response of a $FcCO_2H(CH_2)_{10}SH$ monolayer immersed in 1mM $CH_3(CH_2)_9SH$ in 0.1M $HClO_4$ for various periods of time. (1) 0mins, (2) 2.5mins, (3) 5mins, (4) 7.5mins, (5) 15mins. Scan rate 20mV/s.

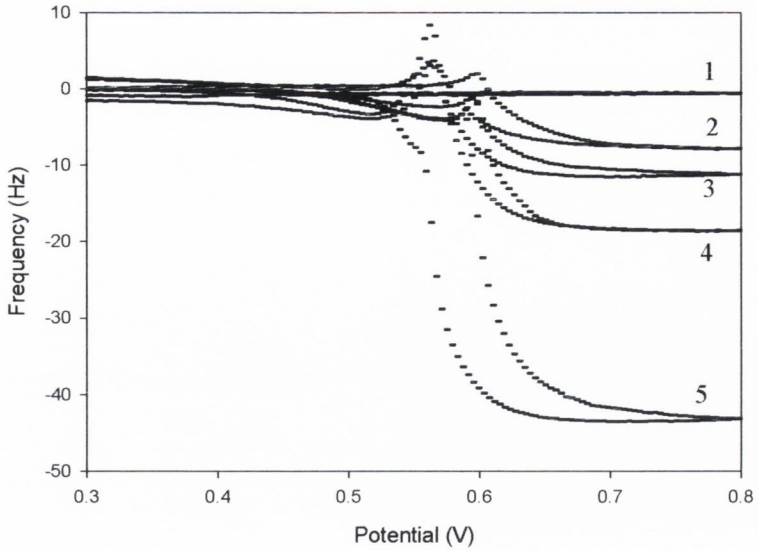


Figure 5.19. EQCM response of a $FcCO_2H(CH_2)_{12}SH$ monolayer immersed in 1mM $CH_3(CH_2)_{11}SH$ in 0.1M $HClO_4$ for various periods of time. (1) 0mins, (2) 2.5mins, (3) 5mins, (4) 7.5mins, (5) 15mins. Scan rate 20mV/s.

Immersion Time (mins)	Surface Coverage ($x10^{-10}$mol.cm^{-2})	Expected Mass Change (ng)	Frequency Change (Hz)	Mass Change (ng)	No Water Molecules Incorporated per Redox Site	% Electroactive Sites Active
2.5	3.7	6.9	1.3	1.8	3.9	25.8
5	3.8	7.2	4.2	5.8	1.0	80.8
7.5	4.9	9.3	5.6	7.8	0.8	84.3
15	5.7	10.8	8.9	12.5	0.8	100

Table 5.10. Surface Coverages (from Figure 5.16) for a mixed monolayer of $CH_3(CH_2)_7SH$ and incubated in a 1mM solution of $FcCO_2H(CH_3)_8SH$ for various periods of time and EQCM data from Figure 5.17.

Immersion Time (mins)	Surface Coverage ($x10^{-10}$mol.cm^{-2})	Expected Mass Change (ng)	Frequency Change (Hz)	Mass Change (ng)	No Water Molecules Incorporated per Redox Site	% Electroactive Sites Active
2.5	3.8	7.2	2.1	2.9	3.2	40.4
5	6.2	11.7	10.3	14.1	1.2	100.0
7.5	7.3	13.8	9.5	13.3	0.2	96.5
15	8.9	16.8	14.5	20.3	1.1	100.0

Table 5.11. Surface Coverages (from Figure 5.16) for a mixed monolayer of $CH_3(CH_2)_9SH$ and incubated in a 1mM solution of $FcCO_2H(CH_3)_{10}SH$ for various periods of time and EQCM data from Figure 5.18.

Immersion Time (mins)	Surface Coverage ($x10^{-10}$mol.cm^{-2})	Expected Mass Change (ng)	Frequency Change (Hz)	Mass Change (ng)	No Water Molecules Incorporated per Redox Site	% Electroactive Sites Active
2.5	9.4	17.8	8.0	11.2	1.9	63.1
5	10.3	19.5	10.8	15.1	1.2	77.6
7.5	19.2	36.3	18.4	25.8	1.5	71.1
15	15.0	28.3	42.7	59.8	5.9	100

Table 5.12. Surface Coverages (from Figure 5.16) for a mixed monolayer of $CH_3(CH_2)_{11}SH$ and incubated in a 1mM solution of $FcCO_2H(CH_3)_{12}SH$ for various periods of time and EQCM data from Figure 5.22.

5.3.3 Chain Length Comparisons

For completeness in this study of mixed monolayer formation the effect of chain length on the adsorption kinetics was studied. In simple terms the nature of place exchange and coadsorption was examined when the chain lengths of either constituent were not equal.

5.3.3.1 Coadsorption

In this section the effect of coadsorbing monolayers of $FcCO_2H(CH_3)_nSH$ (n = 8,10,12) with unsubstituted thiols of different chain lengths will be examined. Thus a monolayer of $FcCO_2H(CH_3)_8SH$ will be coadsorbed with unsubstituted molecules with n=10 and n=12. A monolayer of $FcCO_2H(CH_3)_{10}SH$ coadsorbed with unsubstituted molecules with n=8 and n=12 and finally a monolayer of $FcCO_2H(CH_3)_{12}SH$ with unsubstituted molecules of n=8 and n=10. No notable difference is observed between the findings for the coadsorption process in the case of unequal chain lengths as in the case of equal chain lengths. For this reason the results are not individually discussed however the reader is advised to draw similar conclusions as were detailed in *Section 5.3.1*. Also given in this case are comparisons adsorption kinetics of the two species with differing chain length when coadsorbed onto a monolayer of a third chain length. For example Figure 5.20 describes the kinetics of coadsorption of insulating thiols with 10 and 12 CH_2 units when coadsorbed onto an insulating layer of 8 CH_2 units. It is found throughout that as the length of the coadsorbing chain increases so too does the rate at which they are coadsorbed into the previously deposited monolayer. An exception to this is shown in Figure 5.22. Here insulating thiols with 8 and 10 CH_3 units are coadsorbed into a $FcCO_2H(CH_3)_{12}SH$. In this case the adsorption kinetics are almost identical. This most likely due to the fact that the reorientation rate of ferrocene moiety in the longer chain $FcCO_2H(CH_3)_{12}SH$ is independent of length when the coadsorbants are of shorter chain length than it.

Figure 5.20 depicts the change in surface coverage of a $FcCO_2H(CH_3)_8SH$ monolayer when coadsorbed with 1mM solutions of $CH_3(CH_2)_nSH$ (n=10 and 12). Table 5.13 shows the diagnostics associated with the combined CV and EQCM measurements.

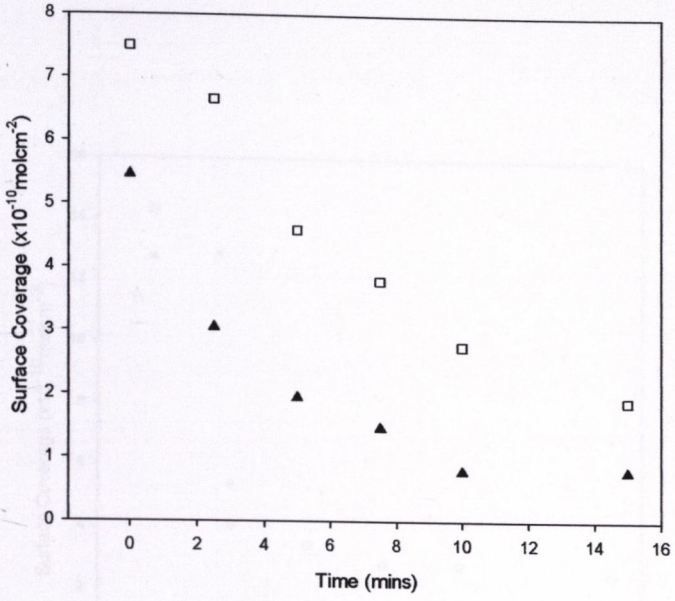


Figure 5.20. Comparison of the decrease in surface coverage of a $FcCO_2H(CH_3)_8SH$) monolayer treated with a 1mM solution of unsubstituted thiols of varying chain length. n=10(squares) and n=12 (triangles).

Time (mins)	Surface Coverage (x10^{-10}mol.cm^{-2})		Frequency Change (Hz)		Mass Change (ng)		Water Molecules Incorporated per Redox Site		% Electroactive Sites Active	
	n=10	**n=12**	**n=10**	**n=12**	**n=10**	**n=12**	**n=10**	**n=12**	**n=10**	**n=12**
0	7.5	5.5	-	28.4	-	39.8	-	15.2	-	100
2.5	6.6	3.1	23.5	26.3	32.9	36.8	8.7	28.3	100	100
5	4.6	1.9	20.4	10.8	28.6	15.1	12.3	17.2	100	100
7.5	3.8	0.8	16.9	6.1	23.7	8.5	12.3	24.8	100	100
15	1.9	0.8	5.8	3.4	8.1	4.8	6.7	11.6	100	100

Table 5.13. Surface Coverages (from Figure 5.20) for a monolayer of $FcCO_2H(CH_3)_8SH$ incubated in a 1mM of $CH_3(CH_2)_{11}SH$ (n=10 and 12) solution of for various periods of time

Figure 5.21 depicts the change in surface coverage of a $FcCO_2H(CH_3)_{10}SH$ monolayer when coadsorbed with 1mM solutions of $CH_3(CH_2)_nSH$ (n=8 and 12).

Table 5.14 shows the diagnostics associated with the combined CV and EQCM measurements.

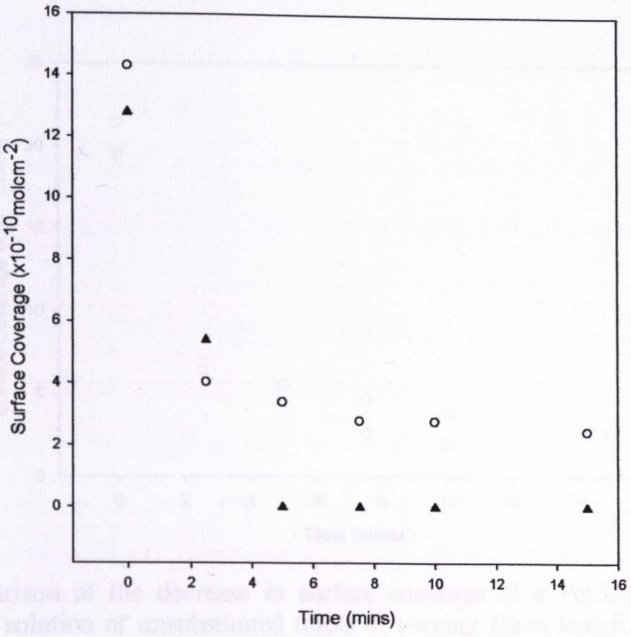


Figure 5.21. Comparison of the decrease in surface coverage of a $FcCO_2H(CH_3)_{10}SH$ monolayer treated with a 1mM solution of unsubstituted thiols of varying chain length. n=8(circles) and n=12 (triangles).

Time (mins)	Surface Coverage (x10^{-10}mol.cm^{-2})		Frequency Change (Hz)		Mass Change (ng)		Water Molecules Incorporated per Redox Site		% Electroactive Sites Active	
	n=8	**n=12**	**n=8**	**n=12**	**n=8**	**n=12**	**n=8**	**n=12**	**n=8**	**n=12**
0	14.3	12.8	41.1	55.2	57.5	77.3	6.0	11.8	100	100
2.5	4.0	5.4	12.4	6.9	17.4	9.7	6.9	0.2	100	95.1
5	3.4	0	7.9	2.2	11.1	3.1	3.9	-	100	0
7.5	2.8	0	5.4	1.4	7.6	2.0	2.3	-	100	0
15	2.5	0	3.5	1.0	4.9	1.4	0.2	-	100	0

Table 5.14. Surface Coverages (from Figure 5.21) for a monolayer of a $FcCO_2H(CH_3)_{10}SH$ incubated in a 1mM solution of $CH_3(CH_2)_nSH$ (n=8 and 12) for various periods of time

Figure 5.22 depicts the change in surface coverage of a $FcCO_2H(CH_3)_{10}SH$ monolayer when coadsorbed with 1mM solutions of $CH_3(CH_2)_nSH$ (n=8 and 12). Table 5.15 shows the diagnostics associated with the combined CV and EQCM measurements.

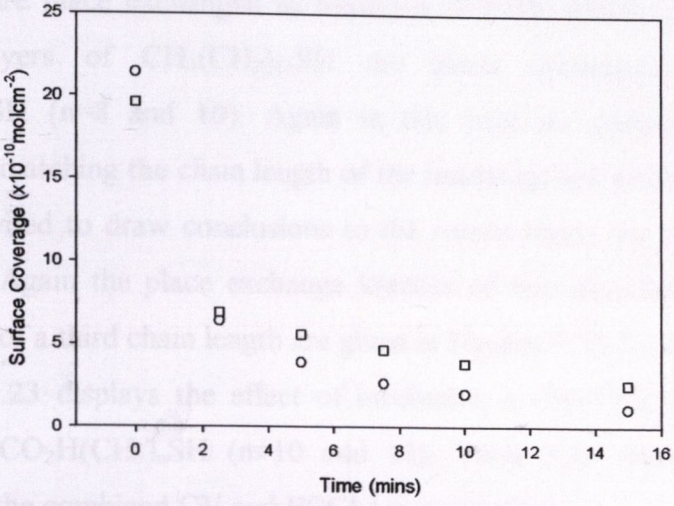


Figure 5.22. Comparison of the decrease in surface coverage of a $FcCO_2H(CH_3)_{12}SH$ monolayer treated with a 1mM solution of unsubstituted thiols of varying chain length. n=8(circles) and n=10 (squares).

Time (mins)	Surface Coverage (x10^{-10}mol.cm^{-2})		Frequency Change (Hz)		Mass Change (ng)		Water Molecules Incorporated per Redox Site		% Electroactive Sites Active	
	n=8	**n=10**	**n=8**	**n=10**	**n=8**	**n=10**	**n=8**	**n=10**	**n=8**	**n=10**
0	21.4	19.6	51.2	56.1	71.7	78.5	4.1	5.9	100	100
2.5	6.4	6.9	38.0	39.3	53.2	55.0	18.2	17.2	100	100
5	3.9	5.6	14.5	34.7	20.3	48.6	9.4	19.2	100	100
7.5	2.0	3.9	7.7	28.6	10.8	40.0	9.9	23.7	100	100
15	1.1	2.6	2.9	9.6	4.1	13.4	5.2	9.3	100	100

Table 5.15. Surface Coverages (from Figure 5.22) for a monolayer of a $FcCO_2H(CH_3)_{12}SH$ incubated in a 1mM solution of $CH_3(CH_2)_nSH$ (n=8 and 10) for various periods of time.

5.3.3.2 Place Exchange

This section examines the effect of incubating insulating monolayers in solutions of electroactive monolayers of differing chain length. Thus monolayers of $CH_3(CH_2)_7SH$ are place exchanged in solutions of $FcCO_2H(CH_3)_nSH$ (n=10 and 12). Monolayers of $CH_3(CH_2)_9SH$ are place exchanged in solutions of $FcCO_2H(CH_3)_nSH$ (n=8 and 12). Finally monolayers of $CH_3(CH_2)_{11}SH$ are place exchanged in solutions of $FcCO_2H(CH_3)_nSH$ (n=8 and 10). Again in this case no appreciable difference is observed by mismatching the chain length of the insulating and electroactive chains and the reader is invited to draw conclusions to the results based the description given in *Section 5.3.2*. Again the place exchange kinetics of two electroactive chains into a insulating SAM of a third chain length are given in Figures 5.23-5.25.

Figure 5.23 displays the effect of incubating a $CH_3(CH_2)_7SH$ SAM in 1mM solutions of $FcCO_2H(CH_3)_nSH$ (n=10 and 12). Table 5.16 shows the diagnostics associated with the combined CV and EQCM measurements.

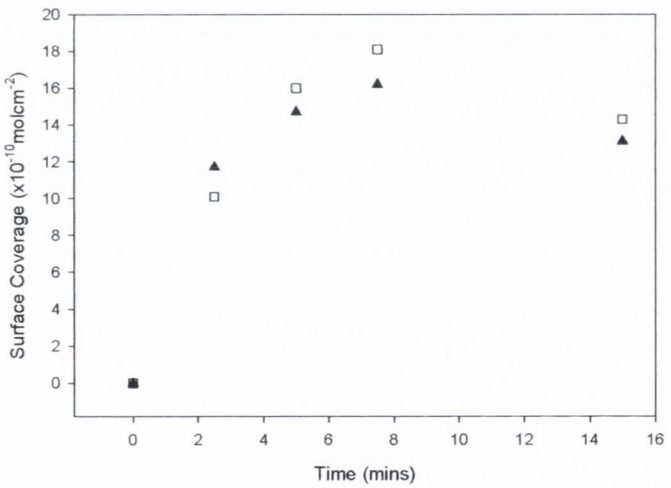


Figure 5.23. Showing the increase in surface coverage of $FcCO_2H(CH_3)_nSH$ (n=10 and 12) in a $CH_3(CH_2)_7SH$ monolayer as a function of time. n=10(squares), n=12 (triangles).

Time (mins)	Surface Coverage ($x10^{-10}$mol.cm^{-2})		Frequency Change (Hz)		Mass Change (ng)		Water Molecules Incorporated per Redox Site		% Electroactive Sites Active	
	n=10	n=12	n=10	n=12	n=10	n=12	n=10	n=12	n=10	n=12
2.5	10.1	11.7	16.3	29.7	22.8	41.6	1.0	4.9	100	100
5	16.0	14.7	22.7	48.43	31.8	67.8	0.3	7.9	100	100
7.5	18.1	16.2	22.8	50.4	31.9	70.6	0.4	7.2	93.3	100
15	14.3	13.1	19.1	47.9	26.7	67.1	0.1	9.4	98.9	100

Table 5.16. Surface Coverages (from Figure 5.23) for a monolayer of $CH_3(CH_2)_7SH$ and incubated in a 1mM of $FcCO_2H(CH_3)_nSH$ (n=10 and 12) solution of for various periods of time

Figure 5.24 displays the effect of incubating a $CH_3(CH_2)_9SH$ SAM in 1mM solutions of $FcCO_2H(CH_3)_nSH$ (n=8 and 12). Table 5.17 shows the diagnostics associated with the combined CV and EQCM measurements

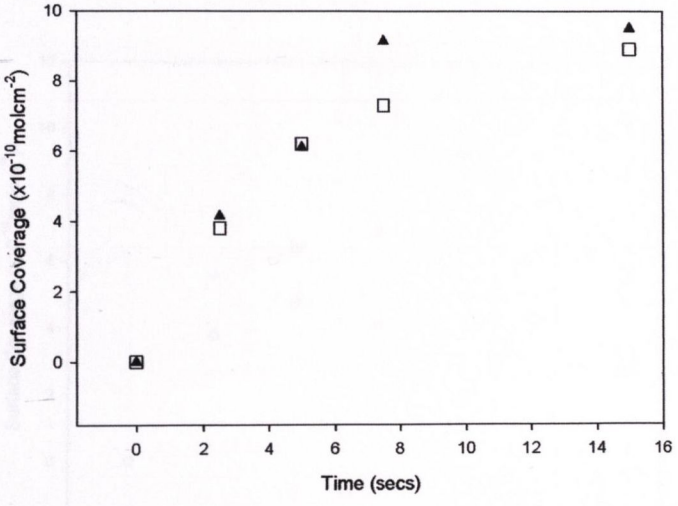


Figure 5.24. Showing the increase in surface coverage of $FcCO_2H(CH_3)_nSH$ (n=8 and 12) in a $CH_3(CH_2)_9SH$ monolayer as a function of time. n=8(circles, n=12 (triangles).

Time (mins)	Surface Coverage ($x10^{-10}$mol.cm^{-2})		Frequency Change (Hz)		Mass Change (ng)		Water Molecules Incorporated per Redox Site		% Electroactive Sites Active	
	n=8	**n=12**	**n=8**	**n=12**	**n=8**	**n=12**	**n=8**	**n=12**	**n=8**	**n=12**
2.5	6.5	4.2	13.2	5.5	18.5	7.7	2.7	0.2	100	97.1
5	7.9	6.1	20.2	8.1	28.3	11.3	4.8	0.1	100	98.1
7.5	10.4	9.1	29.5	9.7	41.3	13.6	5.9	1.1	100	79.1
15	13.5	9.5	41.8	22.9	58.5	32.1	6.9	4.2	100	100

Table 5.17. Surface Coverages (from Figure 5.24) for a monolayer of $CH_3(CH_2)_9SH$ and incubated in a 1mM of $FcCO_2H(CH_3)_nSH$ (n=8 and 12) solution of for various periods of time

Figure 5.25 displays the effect of incubating a $CH_3(CH_2)_{11}SH$ SAM in 1mM solutions of $FcCO_2H(CH_3)_nSH$ (n=8 and 10). Table 5.18 shows the diagnostics associated with the combined CV and EQCM measurements

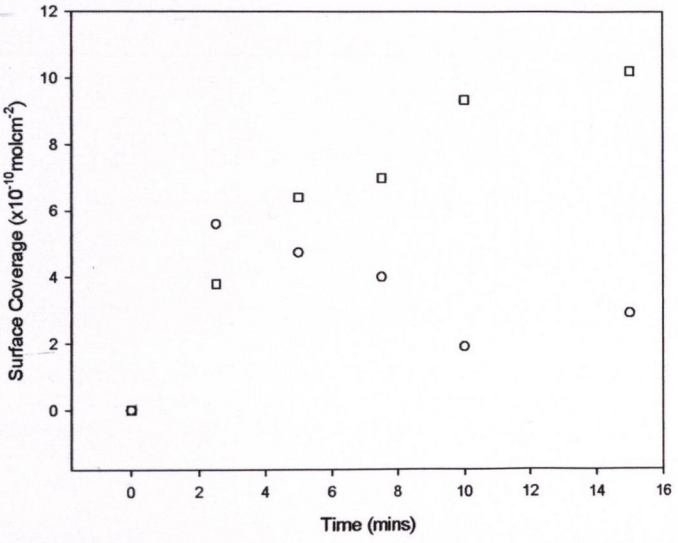


Figure 5.25. Showing the increase in surface coverage of $FcCO_2H(CH_3)_nSH$ (n=8, 10) in a $CH_3(CH_2)_{11}SH$ monolayer as a function of time. n=8(circles), n=10(squares).

Time (mins)	Surface Coverage ($x10^{-10}$mol.cm^{-2})		Frequency Change (Hz)		Mass Change (ng)		Water Molecules Incorporated per Redox Site		% Electroactive Sites Active	
	n=8	n=10	n=8	n=10	n=8	n=10	n=8	n=10	n=8	n=10
2.5	5.6	3.8	18.9	8.9	26.5	12.5	8.1	3.9	100	100
5	4.7	6.4	15.0	18.4	21.0	25.8	7.3	6.1	100	100
7.5	4.0	6.9	11.9	18.7	16.7	26.2	6.5	5.4	100	100
15	2.9	10.2	17.3	22.3	24.2	31.2	18.3	3.1	100	100

Table 5.18. Surface Coverages (from Figure 5.25) for a monolayer of $CH_3(CH_2)_{11}SH$ and incubated in a 1mM of $FcCO_2H(CH_3)_nSH$ (n=8 and 10) solution of for various periods of time

5.4 Conclusion

This work has used electroactive thiols to investigate the rates of formation of mixed monolayers using two complimentary methods.

The first mechanism involved the coadsorption of an insulating, CH_3, terminated alkane chain into the free space between the ferrocene terminated chains. Initially a study was carried out using electroactive and insulating thiols with equal alkane chain lengths. It was determined throughout the coadsorption process that 100% of the electroactive sites remained in a position where ion pairing could occur with the electrolyte ions as determined using EQCM. However, it was also determined that once the coadsorption process began, the number of water molecules incorporated into the layer during the redox processes increased vastly. Neighboring terminal ferrocene groups with mismatching orientations is an explanation put forward to describe the increase in water molecule incorporation. As well as this the effect on the coadsorption process when using insulating and electroactive thiols of differing chain length was investigated. No notable difference from the coadsorption process using alkane chains of equal chain length was noted.

The second mechanism investigated was the place exchange method. In this method a pre-deposited, insulating, SAM was incubated in a solution of electroactive thiols. This caused the replacement of insulating molecules by electroactive molecules on the surface of the electrode. Firstly the effect of place exchange using electroactive and insulating molecules of equal chain length was examined. It was determined in all cases that as the incubation time in the electroactive solution increased the amount of electroactivity registered on the electrode surface also increased. In all cases 100% of electroactive molecules place-exchanged into the layer were ordered in an orientation where ion pairing with the electrolyte could occur after 15 mins place exchange time. The number of water molecules incorporated during the redox process at various stages of the place exchange process was also examined. It was determined, in general, that that as the number of electroactive molecules incorporated into the layer increased the number of water molecules permeating the layer decreased. It is proposed that terminal ferrocene orientation mismatches such as those that occurred during the coadsorption method do not occur during mixed monolayer formation using this method. Thus a

decreased amount of water molecule incorporation was observed. Variations in the chain lengths were examined in the place exchanged monolayers also. Again no appreciable effect was observed in these studies.

The ideality of electron transfer mechanisms was also investigated in this study by examining the peak width half maximum values (PWHM) and comparing them to the ideal PWHM value of 90mV for electroactive monolayers.

It was determined using the coadsorption mechanism that the ideal 90mV could be neared to some extent after approximately 10-15 mins coadsorption.

The voltammetry of place exchanged monolayers was also examined for ideality. In the case of place exchanged monolayers the PWHM values never neared 90mV in general. It was determined that as the amount of electroactive thiol on the surface increased the PWHM values decreased indicating an increasing amount of interactions between neighboring electroactive molecules.

In conclusion, it has been determined that from a quality point of view place exchanged monolayers are the better choice for forming mixed monolayers. This is evident from their decreased amount of water incorporation during redox processes relative to mixed monolayers formed from coadsorption. From the point of view of electron transfer studies coadsorbed monolayer offer a better option as evidenced from their PWHM values which were closer to 90mV than in the case of place exchanged monolayers.

References

(1) G.K. Rowe, S.E. Creager, *Langmuir*, **1994**, *10*, 1186

(2) J.F. Smalley, S.W. Feldberg, C.E.D. Chidsey, M.R. Linford, M.D. Newton and Y.P. Lui, *J. Phys. Chem*, **1995**, *99*, 13141

(3) C.D. Bain, J. Evall and G.M. Whitesides, *J. Am. Chem. Soc.*, **1989**, *111*, 7155

(4) C.E.D Chidsey, C.R. Bertozzi, T.M. Putvinski and A.M. Mujsce, *J. Am. Chem. Soc.*, **1990**, *112*, 4301

(5) X. Yao, J. Wang, F. Zhou, J. Wang and N. Tao, *J. Phys. Chem. B*, **2004,** *108(22)*, 7206

(6) M. Lee and C. Chung, *Bull. Korean Chem. Soc.* **1999**, Vol. 20, No. 2

(7) A.P. Brown and F.C Anson, *J Electroanal. Chem.* **1978,** 92:133

(8) H. Daifuku, K. Aoki, K. Tokuda and H. Matsuda, *J Electroanal. Chem.* **1985,** 183:1

(9) K. Aoki, K. Tokuda and H. Matsuda, *J Electroanal. Chem.* **1987,** 217:1

(10) K. Aoki, K. Tokuda and H. Matsuda, *J Electroanal. Chem.* **1987,** 217:15

(11) X. Yao, J.Wang, F. Zhou, J. Wang, N. Tao, *J. Phys. Chem. B.*, **2004**, *108*, 7206

(12) L. Stryer. *Biochemistry*, 3rd edition, **1988**, Ch. 12, 219

CHAPTER 6 –

MAGNETIC FIELD EFFECTS ON ELECTROACTIVE SELF-ASSEMBLED MONOLAYERS

6. Magnetic Field Effects on Electroactive Monolayers

6.1 Introduction

In this section of work the effect of an applied magnetic field on electron transfer processes through self-assembled monolayers will be investigated. Such effects have not been reported before, indeed the area of magnetoelectrochemistry was not fully reviewed until 1983[1], and for this reason very little background information is available. However what follows is an introduction to the general area of magnetoelectrochemistry as it has been developed up to now.

Magnetoelectrochemistry was first reviewed by Fahidy[1] in 1983. In this paper the effects imposed by magnetic fields on electrochemical systems were reviewed. Four main areas were identified in the paper in which magnetic fields played a major role in the system electrochemistry. These sections were mass transport, reaction kinetics, cathodic metal deposition and anodic metal deposition. In the case of this report the main area of interest of these four subsections is the effect of magnetic fields on mass transport. In an electrochemical system there are three main forms of mass transport. They are diffusion, convection and migration. Diffusion is essentially the movement of a species down a concentration gradient. Convection is the movement of species due to mechanical forces and can be effectively eliminated on a short timescale. Convection can have a large influence on current density. Migration is the movement of charged species due to a potential gradient. This is the mechanism through which charge passes through an electrolyte. The forces leading to migration are electrostatic and hence the charge can be carried by any ionic species in solution.

The effect of a magnetic field on mass transport is well established and has been shown in a number of studies to induce convection in the electrolyte solution, known sometimes as the magnetohydrodynamic (MHD) effect, thereby reducing the diffusion layer thickness and consequently increasing the rate of mass transport. One such study that verified this phenomenon was carried out by Hinds et al.[2]. Here the effect of an applied magnetic field on the electrodeposition of copper from concentrated $CuSO_4$ solution was investigated. A large enhancement (~300%) on the deposition rates of copper was observed. The effect of the magnetic field was thought to be equivalent to rotating the electrode. A similar study was carried out by Uhlemann et al.[3] in which the electrodeposition of Co in the presence of an external

magnetic field was investigated. Again it was determined that the presence of an external magnetic field increased the rate of mass transport to the surface thereby increasing the amount of Co deposited. Magnetic fields up to a strength of 13T were applied and it was found that as the field strength increased so too did the amount of Co deposited. Thus in general it can be noted that the effect of magnetic fields on the area of mass transport in electrochemical systems is well established. Normally the effect of the magnetic field on electrolyte convection is treated with the well established Navier-Stokes equation which describes the motion of fluid flow.

A much more controversial area however relates to the effect of an external magnetic field on the dynamics of electron transfer processes in electrochemical systems. Devos et al.[4] studied the effect of an external magnetic field on the charge-transfer properties of the ferri-ferrocyanide couple at a platinum electrode surface. It was determined that the applied magnetic field had no effect on the charge transfer properties.

This work aims to provide a definitive test on whether external magnetic fields have the ability to influence the nature of interfacial electron transfer processes. Using redox active moieties tethered to the surface of a self-assembled monolayer provides a convenient method by which such a test can be carried out. This is due to the fact that an anchored redox active group should preclude any effects due to electrode convection caused by the magnetic field and thus attention may be focused solely on the electron transfer processes. Cyclic voltammetry, chronoamperometry and an electrochemical quartz crystal microbalance will be used to elucidate the phenomenon occurring when the external magnetic field is applied to the electrode coated with a redox active self-assembled monolayer.

6.2 Experimental

Electrochemical Measurements. All electrochemical measurements were carried out on a CH Instruments Model 440 potentiostat as described in *Section 2.2.1.*

Gold Substrate. The gold substrate used whether it be a standard macroelectrode or an EQCM electrode is as described in *Section 2.1.1.*

Electrode Pre-Treatment. **Electrode Pre-Treatment**. The method used for electrode pre-treatment is described in *Section 2.3.1.*

Monolayer Deposition. All monolayers were deposited using solution deposition. The method used is described in *Section 2.3.2.*

Magnetic Field. Magnetic fields were applied using a cylindrical magnet, the Halbach Cylinder, supplied by Prof. J.M.D. Coey of Magnetic Solutions Ltd. The magnet had a field strength of 0.5 Tesla. The magnet was formed from sintered Nd-Fe-B and consisted of twelve segments providing a homogeneous magnetic field in the circular bore (diameter of 5.4 cm).

Macroelectrode experiments involved performing cyclic voltammetry on a fully formed electroactive SAM in the absence of the magnetic field to ensure SAM quality and provide a baseline scan. The electrochemical cell was then placed in the bore of the magnet with the direction of the magnetic field running parallel to the surface of the working electrode and hence perpendicular to the direction of the alkane chains on the surface of the monolayer. For clarity the direction of the magnetic field with respect to the alkane chains on the surface of the layer of shown in Figure 6.1. As can be seen from the diagram the direction of the magnetic field runs parallel to the surface of the working electrode and thus perpendicular to the alignment of the alkanethiol molecules on the electrode surface.

Cyclic voltammograms were then run continuously between the upper and lower voltage limits and scans performed after defined time intervals in the bore of the magnet were selected for analysis. Certain experiments involved analysis of the SAM redox activity when the field was removed. In this case the electrochemical cell

was removed from the bore of the magnet after analysis and subsequent cyclic voltammetry was performed in the absence of the magnetic field.

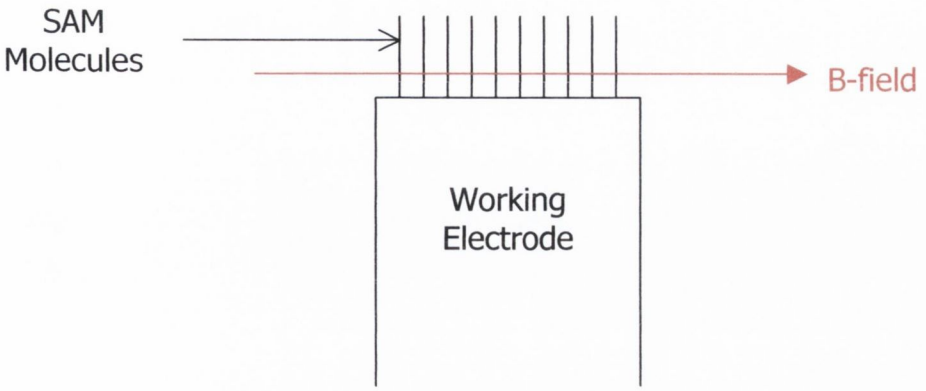


Figure 6.1. Direction of the applied magnetic field with respect to the molecules constituting a deposited self-assembled monolayer

During EQCM experiments the entire Teflon cell was carefully placed into the bore. Because of the design of the EQCM cell little could be done to ensure that the orientation of the B-field relative to the electrodes was exactly the same during different experiments. However the technique for voltammetric analysis in the presence of the magnetic field was identical to that used in the case of macroelectrodes.

Electrolyte Solutions. The electrolyte solutions used in all experiments were 0.1M Perchloric Acid unless otherwise stated. *Section 2.1.4* provides further details.

6.3 Results and Discussion

6.3.1 Effect of B-field on Redox Activity

As an initial examination on the effect an external magnetic field has on electron transfer mechanisms cyclic voltammetry was carried out before and after the application of the magnetic field. In all cases it was found that this resulted in diminished ferrocene alkanethiol redox activity manifested by diminished CV peak heights. A typical CV response taken before and after the application of the magnetic field is shown in Figure 6.2 below.

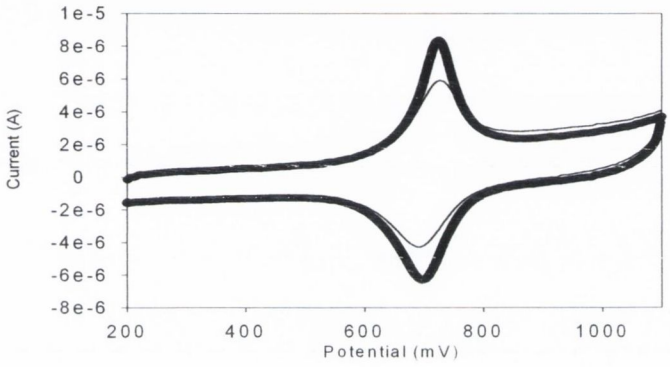


Figure. 6.2. Cyclic voltammograms of an electrode modified with an $SH(CH_2)_{12}CO_2HFc$ SAM before (heavy line) and after (light line) the application of a 0.5T B-field parallel to the surface of the modified electrode.

It is now noted and will be evident in the following results that the application of the magnetic field, whilst having an effect on the redox activity of the SAMs in all cases did not yield reproducible results. This lack of reproducibility can most likely be attributed to differences in the structures of individually prepared SAMs arising from differences in electrode surface morphology, the presence of certain contaminants or possible inherent differences in electrode polishing between monolayer depositions.

6.3.1.1 Effect of Chain Length

Following the initial observation made in the previous section that the application of an external magnetic field has a readily observable effect on the redox activity of an electroactive SAM it was decided to carry out identical tests on redox active monolayers of different alkane linker lengths in an attempt to determine any trends that were evident. Figure 6.3 below shows the results of this experiment. It is immediately apparent that the change in redox activity of the electroactive SAMs does not follow any immediately observable trends. The change in surface coverage upon application of the external B-field changes to a varying extent in the case of each alkane linker size. This observation adds credence to the postulate that the effect of the applied magnetic field is specific to each SAM structure.

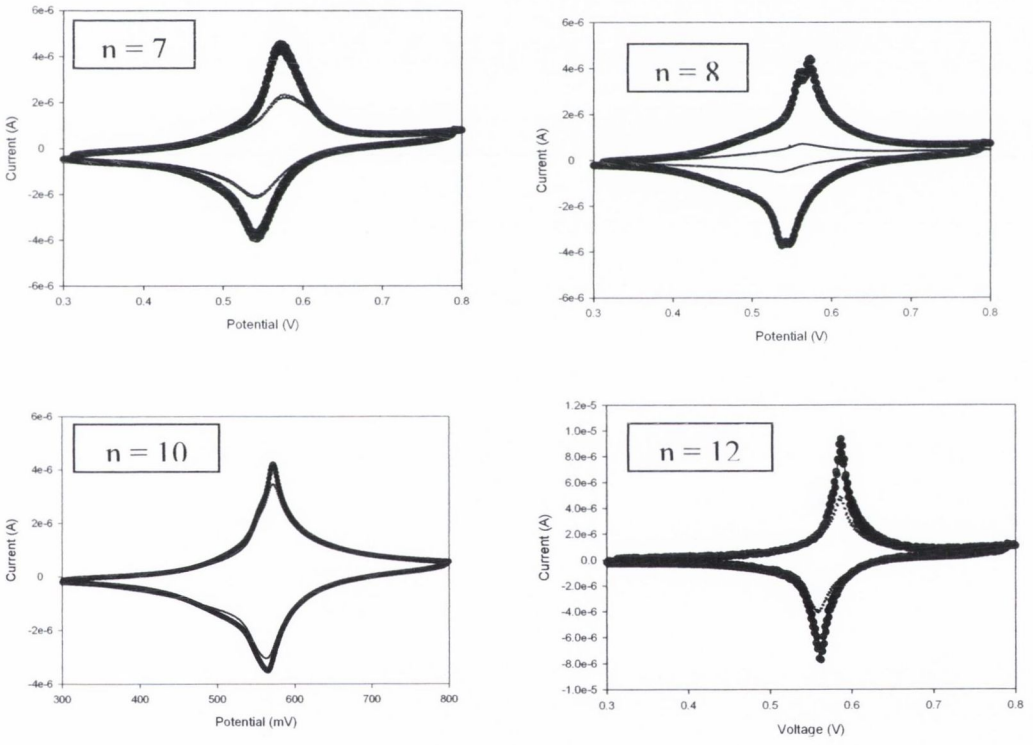


Figure. 6.3 Cyclic voltammograms of $S(CH_2)_nCO_2HFc$ (n=7, 8, 10, 12) modified electrodes before (heavy line) and after (light line) the application of a 0.5T B-field perpendicular to the surface of the electrode.

Table 6.1 shows the decrease in redox activity as a function of chain length upon application of the B-field.

n	Redox Active Surface Coverage, Γ, (B-field absent) ($x10^{-10}$ mol.cm^{-2})	Redox Active Surface Coverage, Γ_B, (B-field present) ($x10^{-10}$ mol.cm^{-2})	Γ_B/Γ
7	7.9	5.2	0.6
8	8.1	1.2	0.1
10	5.2	4.6	0.8
11	10.0	7.6	0.7

Table 6.1. Changes in the surface coverage of a redox active monolayer of an of $S(CH_2)_{10}CO_2HFc$ SAM as a function of chain length.

It is stressed that the decrease in the redox activity observed is not expected to be due to loss of SAM molecules from the surface of the electrode. It is also stressed that no drop in redox activity occurs without the field. The cyclic voltammograms recorded before the application of the magnetic field are stable and may be repeated exactly many times.

6.3.1.2 Effect of Solvent

In order to build up a greater degree of information regarding the nature of the magnetic field effects on electron transfer mechanisms electroactive monolayers formed from solutions of some different solvents were examined with and without B-field effects. The results of this study are shown in Figure 6.4.

The thinking behind this experiment was effectively to continue to build a stock of knowledge regarding the B-field effects. It was proposed that the application of a B-field parallel to the surface of the electrode (perpendicular to the alkanethiol linkers) may cause the alkane chains to become disordered and possibly to cause some pendant ferrocene redox sites to become buried in the surrounding alkane chain matrix. This burying of the redox active groups may limit their electroactivity and thus be responsible for the observed decrease in surface coverage upon application of the B-field as detailed in Table 6.1. The possibility of a pendant redox site being buried depends on how well the monolayer formed due to the fact that it will be more difficult to cause a pendant headgroup to bury itself in a well ordered, densely packed alkane matrix.

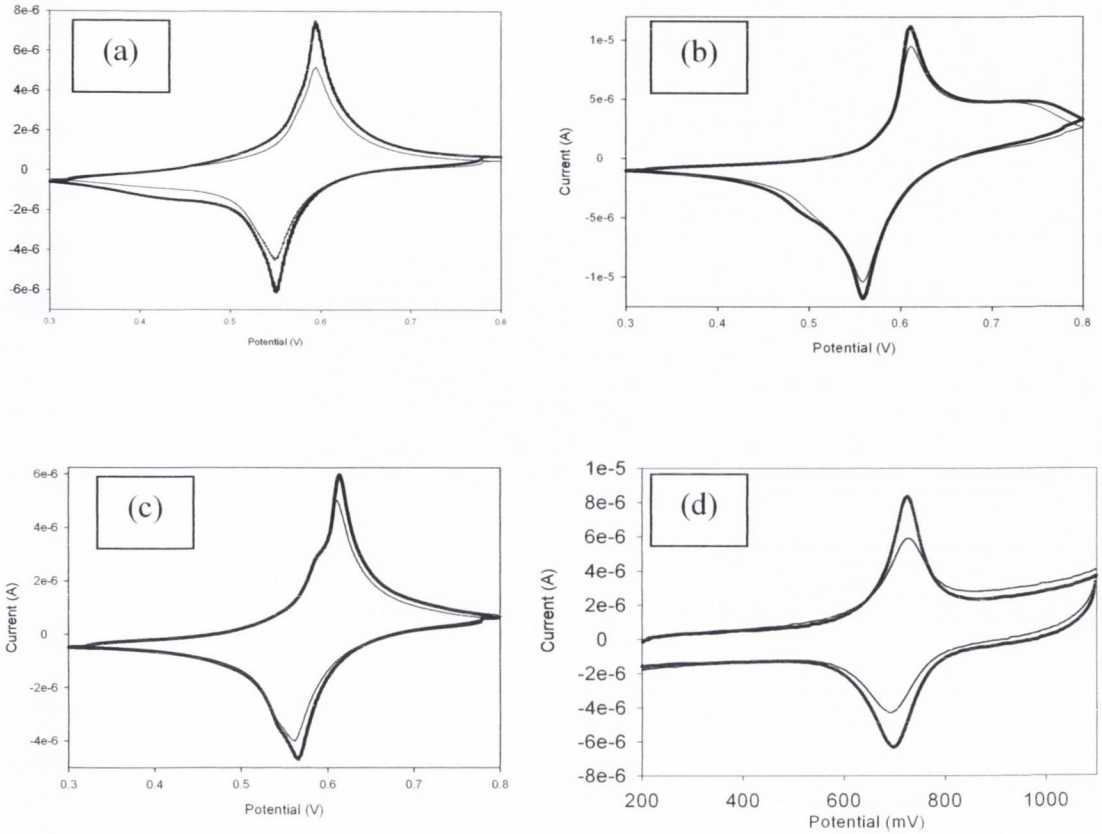


Figure. 6.4 Cyclic voltammograms of a $S(CH_2)_{10}CO_2HFc$ modified electrodes deposited from 1mM solutions in various solvents. (a) acetonitrile, (b) hexane, (c) toluene and (d) ethanol before (heavy line) and after (light line) the application of a 0.5T B-field perpendicular to the surface of the electrode.

Table 6.2 below examines the ΔE_p values corresponding to the CV responses in Figure 6.4.

Solvent	ΔE_p (mV) – Before Field	ΔE_p (mV) – During Field
Acetonitrile	45	44
Hexane	52	54
Toluene	48	49
Ethanol	29	33

Table 6.2. Diagnostics for the CV responses in Figure 6.4 of $S(CH_2)_{10}CO_2HFc$ monolayers prepared from various solvents before and after the application of a 0.5T B-field.

What is most notable from Table 6.2 is that the values of ΔE_p do not change to any large degree when the B-field is absent and when the B-field is present. What can be taken from this section of study is that the application of a magnetic field parallel to the surface of the electrode does not substantially change the quality of that SAM as determined by ΔE_p measured values. Should the application of the magnetic field change the structure of the layer substantially a large difference in the hydrophobicity of the layer would be expected. Such a change would be manifested as a relatively large change in the ΔE_p value however no such change is observed.

Thus it is postulated from this section of work that the application of a magnetic field parallel to the surface of an electrode modified with a self-assembled monolayer does not substantially alter the ordering of that layer.

6.3.2 Chronoamperometry

Further investigation into the effects of an applied B-field to electron transfer events in electroactive self-assembled monolayers was examined using chronoamperometry. Figure 6.5 below shows the results of chronoamperometry performed both before and during the application of the magnetic field. Again two rate constants can be extracted as was described in *Section 3.3.4*. These are shown in Table 6.3. It is immediately apparent from the chronoamperometric response shown that the rate of electron transfer is dramatically increased in the presence of an external magnetic field in Region 1. This is a very unexpected result. In order to illustrate the point further a plot of normalised current against time is shown inset in Figure 6.5.

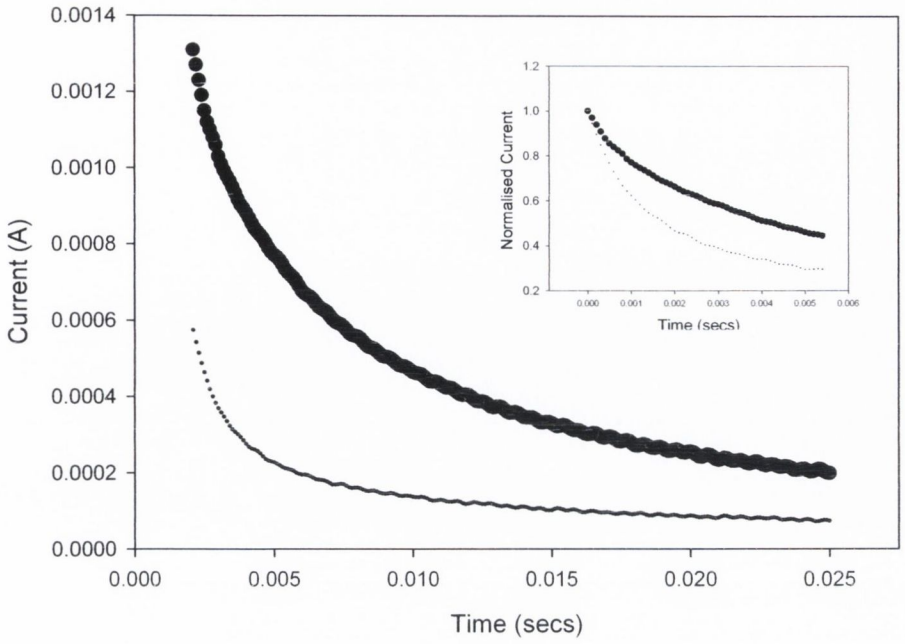


Figure 6.5. Showing the chronoamperometric response of a $S(CH_2)_{10}CO_2HFc$ modified electrode before (dark line) and during (light line) the application of a 0.5T magnetic field parallel to the electrode surface. *Inset.* Normalised current versus time plot for the same data.

Electron Transfer Rate Constant (s^{-1})		
	Region 1	**Region 2**
Before Field	193	52
During Field	370	36

Table 6.3 The electron transfer rate constants extracted from the oxidative chronoamperometry response of an $FcCO_2H(CH_2)_{10}SH$ monolayer.

Similar observations are recorded for alkane chain linkers of differing length as shown below in Figure 6.6. Again a normalised current is presented as this method provides the best presentation for comparison. From these plots two rate constants can be taken. These are shown in Tables 6.4 below.

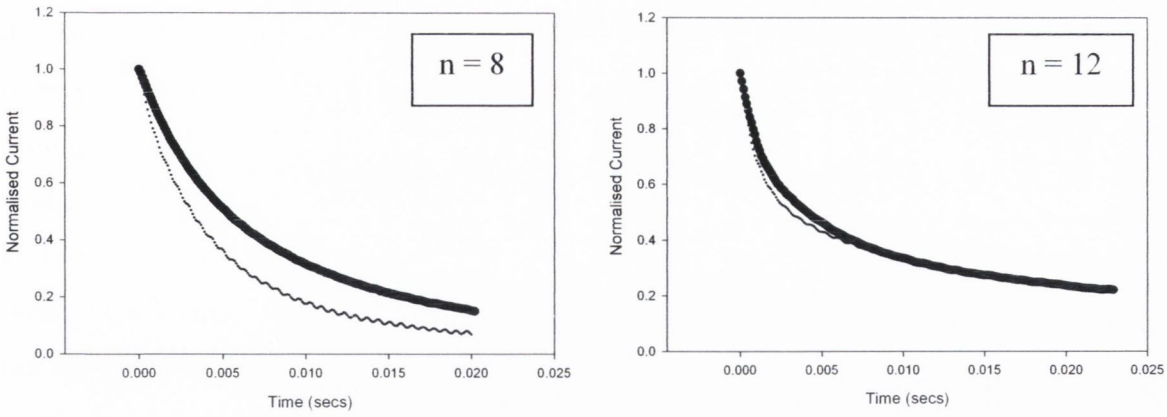


Figure 6.5. Normalised chronoamperometric response of a $S(CH_2)_nCO_2HFc$ (n=8,12) modified electrode before (dark line) and during (light line) the application of a 0.5T magnetic field parallel to the electrode surface.

Electron Transfer Rate Constant (s^{-1})		
n = 8	**Region 1**	**Region 2**
Before Field	135	72
During Field	196	71
n = 12		
Before Field	235	31
During Field	276	30

Table 6.4 The electron transfer rate constants extracted from the oxidative chronoamperometry response of an S $(CH_2)_nCO_2HFc$ (n=8,12) monolayer.

Towards the end of *Section 6.3.1.2* it was proposed that the applied magnetic field could cause the pendant ferrocene groups to coil into the surrounding alkane matrix. It was proposed that such an effect could account for the decrease in surface coverage observed when an external magnetic field was applied. This can now be combined with what has been revealed by the chronoamperometry results that have been presented in this section. These results show an increase in the rate of electron transfer occurring in the presence of an external magnetic field. Sumner and Creager[6] carried out voltammetric studies on ferrocene moieties that were artificially buried in a surrounding matrix of alkane chains. This was achieved by forming mixed monolayers comprised of a small percentage of alkanethiol molecules with pendant electroactive ferrocene groups coadsorbed with insulating, CH_3 terminated chains that were much longer. Two main findings are reported for buried ferrocene moieties in

this work. Firstly it was determined that when the ferrocene groups were buried into the alkane chain matrix the redox potentials at which the oxidation/reduction occurred were shifted to much higher potentials relative to monolayers in which the ferrocene groups were exposed to the electrolyte. It was determined from the magnetic field studies that have been presented that only a decrease in the observed surface coverage is seen whilst no shift is seen in the oxidation/reduction potentials. Thus this first point would seem to indicate that the application of an external magnetic field does not cause a burying of the pendant ferrocene groups. The second observation in the work by Sumner and Creager is that burying of the pendant ferrocene redox group causes a large decrease in the observed electron transfer rate constant ($40{,}000s^{-1}$ in the case of surface ferrocene groups vs. $200s^{-1}$ in the case of buried groups). An increase in the rate of electron transfer is observed upon application of the external magnetic field was nowhere near this magnitude a decrease was nonetheless observed. Thus the second main finding of the Sumner and Creager study would also appear to support the hypothesis that burying of the ferrocene groups does not occur upon application of an external magnetic field.

Thus at this stage of the examination of magnetic field effects of electron transfer mechanisms in self-assembled monolayers the postulate that an applied field causes pendant ferrocene groups to be buried in the surrounding alkane layer seems unlikely due to the conflicting comparisons with previous work carried out by Sumner and Creager. Because of this an electrochemical quartz crystal microbalance was employed to give further insight into the effects of an externally applied B-field.

6.3.3 Electrochemical Quartz Crystal Microbalance Study

It has already been shown that there is a decrease in apparent SAM surface coverage upon the application of a magnetic field. The phenomenon was further investigated using EQCM to observe the frequency response of the ferrocene-terminated alkanethiol SAMs both in and out of the field. Figure 6.6 below depicts the frequency change corresponding to the oxidation and reduction of the electroactive monolayers of a number of different chain lengths both before and after exposure to the 0.5T B-field.

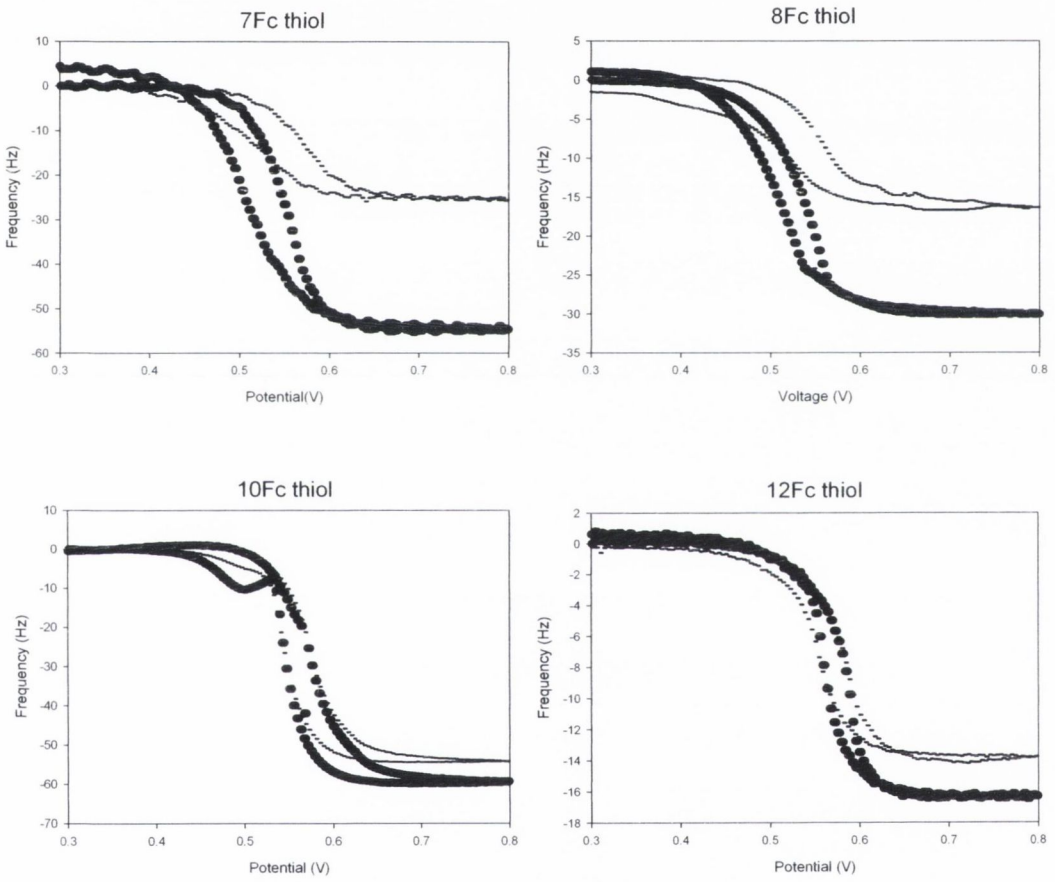


Figure 6.6. Frequency change corresponding to the oxidation and reduction of $S(CH_2)_nCO_2HFc$ (n = 7, 8, 10, 12) SAMs before (heavy line) and after (light line) the application of a 0.5T B-field perpendicular to the surface of the electrode.

It is immediately apparent from Figure 6.6 that the extent of ion pairing occurring in the presence of the externally applied magnetic field decreases. The EQCM results show the frequency changes corresponding to the CVs presented in Figure 6.3 showing the decrease in redox activity due to the B-field. Frequency changes and corresponding mass changes are shown in Table 6.5.

n	Δf (Hz) (B-field absent)	Δf (Hz) (B-field present)	Δm (ng) (B-field absent)	Δm (ng) (B-field present)
7	55	25	77	35
8	29	15	41	21
10	58	54	82	75
12	17	14	23	19

Table 6.5. Frequency and mass changes corresponding to $S(CH_2)_nCO_2HFc$ (n = 7, 8, 10, 11) both in and out of the B-field

This frequency change must now be correlated with the decrease in redox activity registered using cyclic voltammetry in Figure 6.3. As a sample calculation the situation of the n = 7 alkane chain linker will be taken.

Sample Calculation. The surface coverage calculated from the cyclic voltammetry response in Figure 6.3 for the $S(CH_2)_7CO_2HFc$ monolayer is 7.9×10^{-10}mol.cm^{-2} and 5.2×10^{-10}mol.cm^{-2} after the application of the magnetic field. The corresponding surface mass change for the monolayer before and after the application of the magnetic field is 77ng and 35ng respectively.

Before the application of the magnetic field, should each of the electroactive sites form an ion pair with a perchlorate ion of weight 1.6×10^{-22}g the expected mass change on the surface is

$$\text{Expected Mass Change, } (M_{ex}) = N_a.(7.9 \times 10^{-10}\text{molecules})(1.6 \times 10^{-22}\text{g.molecule}^{-1})$$

$$M_{ex} = 76\text{ng}$$

Where N_a is Avogadro's Constant. The registered mass change before the application of the magnetic field is 77ng thus it is evident that all of the redox active sites on the surface of the monolayer form ion pairs during oxidation. As well as this a very small amount of solvent is incorporated into the surface of the layer weighing 1ng. To all intents and purposes this monolayer is acting ideally from the EQCM perspective.

When the magnetic field is applied the surface coverage of electroactive sites, as calculated from Figure 6.3 is 5.2×10^{-10}mol.cm^{-2}. Should each of these sites form an ion pair with one perchlorate ion the expected mass change is 50ng. The registered mass change after the application of an external magnetic field is 35ng. Thus there is now a discrepancy occurring between the mass changes, 50ng worth of ion pairing is

expected to occur but only 35ng is actually occurring. This result would indicate that quite a large proportion of sites on the surface of the monolayer are no longer forming ion pairs with the electrolyte upon application of the magnetic field. It can be said that only 35 out of 50 or 70% of the electroactive sites in this monolayers are performing electroactively and are in a position to form ion pairs after the application of the magnetic field. Such calculations were carried out for the different alkane chain lengths and the results are shown in Table 6.6.

If a more comprehensive description of this calculation is required please refer to the sample calculation in *Section 5.3.1.*

Alkane Linker Length	Surface Coverage ($x10^{-10}$ $mol.cm^{-2}$)	Expected Mass Change (ng)	Actual Mass Change (ng)	% Redox Sites Electroactive	No. Water Molecules Incorporated per Redox Site
n = 7					
B-field absent	7.9	76	77	100	0
B-field present	5.2	50	35	70	0
n = 8					
B-field absent	8.1	78	41	53	0
B-field present	1.2	9	21	100	5.5
n = 10					
B-field absent	5.2	50	82	100	3.5
B-field present	4.6	44	75	100	3.9
n = 12					
B-field absent	10.0	96	23	24	0
B-field present	7.6	73	19	26	0

Table 6.6. Data corresponding to the combined CV and EQCM responses for a $S(CH_2)_nCO_2HFc$ (n = 7, 8, 10, 12) modified electrodes both in and out of the B-field.

The data presented above in Table 6.5 does not appear to show any trend in a particular direction. In the case of the n = 7 alkane linker it is noted that no water molecule incorporation occurs either before or after the application of the magnetic field whereas in the case of the n = 8 linker the amount of water molecule incorporation increases upon application of the field. In the n = 12 case the amount of water molecule incorporation decreases upon application of the magnetic field. Although the results of the EQCM study seem conflicting there are some definite findings that can be taken from it.

Firstly it would seem evident that intrinsic structural deformations to the monolayer do not occur upon application of the magnetic field. With the exception of the n = 8 chain approximately the same number of water molecules are incorporated

per redox site before and after the application of the magnetic field in all cases. Should any considerable structural changes take place it is likely that a large change in the number of water molecules incorporated per redox site would be observed.

Secondly it is apparent that when the external B-field is applied there is a decrease in the redox activity of the surface bound electroactive ferrocene groups. It has been shown beyond doubt that this decrease in the electroactivity corresponding to the application of an external B-field is followed by a decrease in the amount of ion pairing that occurs. Thus an intrinsic link is evident between electron transfer processes and ion pairing events. The relationship between ion pairing events and the rate of electron transfer events has been dealt with in some detail by Marcus[7] for the case of bridged donor-acceptor molecules. Three cases were considered for such a system: (1) Electron transfer occurred first, (2) Ion pairing occurs first, (3) Electron transfer and ion pairing occurred simultaneously. It was determined for each of these three cases that a slow ion transport step decreased the rate of charge transport. However it has been shown in this work that the application of an external field actually increases the rate of electron transfer whilst diminishing the amount of ion pairing that occurs. Thus again it would appear that conflicting results appear when dealing with the application of an external magnetic field effect.

A theory to account for the combination of an increased rate of electron transport combined with a decreased amount of ion pairing is now presented in terms of mixed monolayers formed via coadsorption as described in *Section 5.3.1.* It relates to work by Lee et. al[8] who have shown that the pendant ferrocene group on the surface of the SAM can rotate such that the C=O bond between it and the alkane chain of the SAM is rotated from perpendicular to parallel relative to the electrode surface. In the case of Lee et al. this rotation was a result of the coadsorption of unsubstituted alkanethiols. This is shown in Figure 6.7 below.

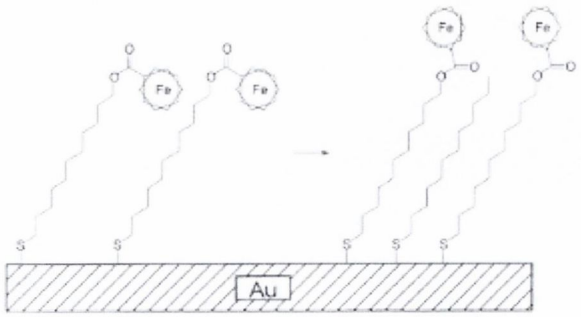


Figure 6.7. A schematic representation for the reorientation of the $S(CH_2)_{11}CO_2HFc$ monolayer self-assembled on gold before and after the coadsorption of $SH(CH_2)_{11}CH_3$. Reproduced from Ref. (8).

It was shown in *Section 5.3.1* that as an increased amount of coadsorption occurred a decreased amount of ion pairing occurred. Thus it was evident that the rotation of the pendant ferrocene groups upon coadsorption to a new orientation shown in Figure 6.7 caused a decrease in the amount of ion pairing occurring as well as a decrease in the surface coverage/electroactivity of the layer. Chronoamperometry was then employed to evaluate the electron transfer rate constants corresponding to varying stages of coadsorption were then examined. Figure 6.8 below shows the chronoamperometric response for a ferrocene-terminated SAM monolayer that has undergone coadsorption with $CH_3(CH_2)_{11}SH$ insulating monolayer by incubation in a 1mM solution for 15 minutes.

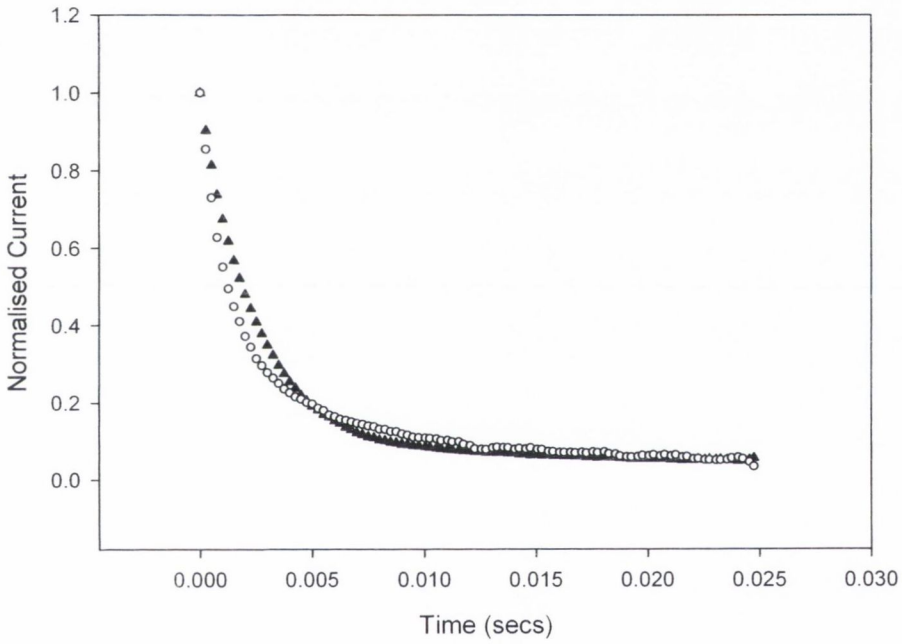


Figure 6.8. Normalised chronoamperometry response of a $S(CH_2)_{12}CO_2HFc$ both before (▲) and after (○) coadsorption with $CH_3(CH_2)_{11}SH$ molecules for 15 mins.

It is evident from Figure 6.8 that an increased rate of electron transfer occurs upon coadsorption. The initial fast electron transfer rate constant increases from $354s^{-1}$ to $455s^{-1}$ upon coadsorption. What is evident here is that the same set of criteria are being met when looking at mixed monolayers formed from coadsorption and when an external magnetic field is applied to an electroactive self assembled monolayer, i.e. in both cases a decrease in the amount of electroactivity is observed via cyclic voltammetry, in both cases a decrease in the amount of ion pairing is observed via

EQCM studies and in both cases an increase in the electron transfer rate constant is observed via chronoamperometry. Thus it is postulated that a mechanism similar to that depicted in Figure 6.7 occurs when an external magnetic field is applied to the ferrocene-terminated self-assembled monolayer.

6.3.4 Magnetic Field and Time Dependence

It has been shown in thus far that the application of the B-field parallel to the surface of a SAM modified electrode causes a decrease in the redox activity as well as a decrease in the amount of ion pairing/dissociation occurring when a redox active monolayer deposited on an electrode is oxidised/reduced.

In order to gain further insight into the mechanism by which the applied magnetic field affects the surface coverage it was proposed that surface coverage of redox molecules change as a function of time was monitored. Shown in Figure 6.9 below are the surface coverages as a function of time for electrodes modified with $S(CH_2)_nCO_2HFc$ (n=7, 8, 10, 11) SAMs. Unexpectedly it is noted that as the time the electroactive monolayer spends under the influence of the magnetic field increases so too does the effect the magnetic field on the redox activity of the SAM. More unexpectedly it is noted that the observed surface coverage continues to decrease after the B-field has been removed. This result indicates that the structural reorientation of the SAM continues after the magnetic field has been removed. It must be noted when examining Figure 6.9 that the surface coverage corresponding to t = 0 corresponds to the surface coverage calculated before the monolayer was exposed to the magnetic field.

In order to gain further insight into the processes occurring the redox activity change as a function of time was monitored using an electrochemical quartz crystal microbalance. Figure 6.10 the results of this study on an electrode modified with a $S(CH_2)_{12}CO_2HFc$ monolayer. As expected the surface coverage is found to decrease as a function of time both during the application of the magnetic field and after the application of the field. As well as this the extent of the ion pairing is found to decrease also. Table 6.7 summarises the results gained from this study. A number of points can be taken from Table 6.6. Firstly it is evident that during the application of the magnetic field, as the surface decreases so too does the amount of ion pairing occurring. This however has already been established in *Section 6.3.3* previously.

More unexpectedly it is also determined that following the removal of the field, the continuing surface coverage decrease is followed by a decrease in the amount of ion pairing. It is determined throughout the experiment that 100% of the ferrocene sites that are detected from cyclic voltammetry form ion pairs with perchlorate ions in solution.

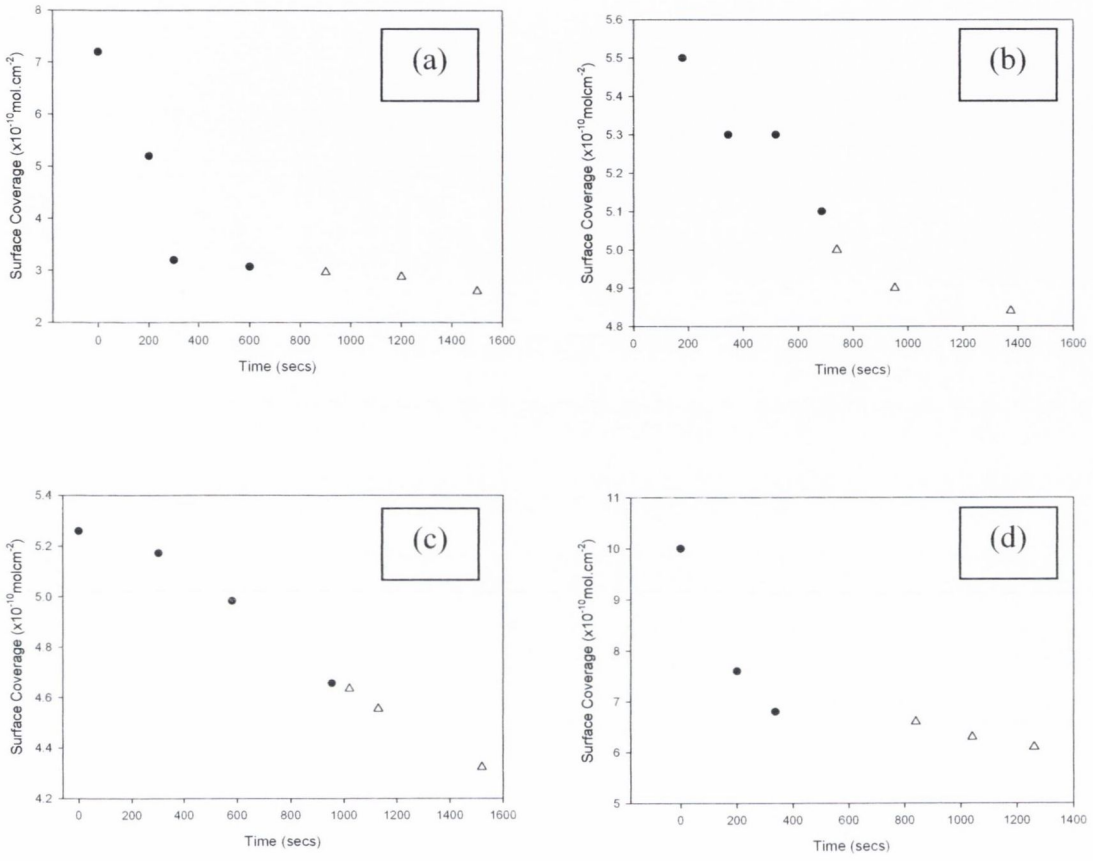


Figure. 6.9. Graph of redox active surface coverage against time for $S(CH_2)_nCO_2HFc$ ((a) n = 7, (b) n = 8, (c) n = 10 and (d) n = 11) modified electrodes. The surface coverage calculated before the magnetic field is applied appears at t=0. (•) during the application of the B-field (△) after the magnetic field has been removed.

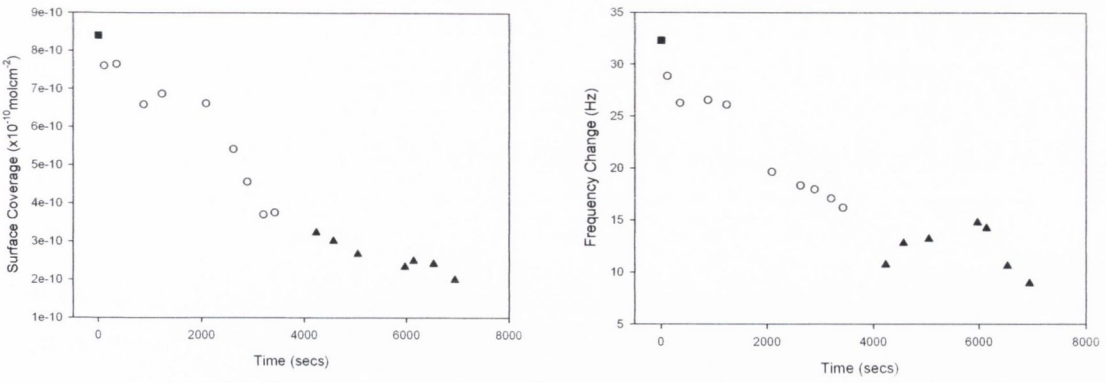


Figure. 6.10. Graph of redox active surface coverage against time for $S(CH_2)_{12}CO_2HFc$ modified electrodes.

Time (secs)	Surface Coverage ($x10^{-10}$mol.cm^{-2})	Expected Mass Change (ng)	Actual Mass Change (ng)	% Redox Sites Electroactive	No. Water Molecules Incorporated per Redox Site
Before Field					
0	8.4	81.0	45.2	100	2.4
In the Magnetic Field					
113	7.6	73.3	40.4	100	2.4
355	7.6	73.7	36.7	100	2.7
880	6.6	63.5	37.2	100	2.2
1230	6.9	66.2	36.5	100	2.4
2086	6.6	63.7	27.5	100	3.0
2622	5.4	52.2	25.6	100	2.7
2890	4.6	43.9	25.1	100	2.3
3203	3.7	35.7	23.9	100	1.8
3425	3.8	36.2	22.7	100	2.0
After the Magnetic Field					
4232	3.2	31.2	15.0	100	2.8
4571	3.0	29.0	17.9	100	2.1
5047	2.7	25.7	18.5	100	1.5
5965	2.3	22.5	20.7	100	0.4
6135	2.5	24.0	19.9	100	0.9
6527	2.4	23.2	14.8	100	1.9
6943	1.9	19.2	12.5	100	1.9

Table 6.7. Data corresponding to the combined CV and EQCM responses for a $S(CH_2)_{12}CO_2HFc$ modified electrodes before, during and after the application of an external magnetic field.

As well as the formation of ion pairs it is possible to again calculate the number of water molecules that are incorporated into the self assembled monolayer during the redox processes. It is found throughout the experiment however that the amount of water molecules incorporated does not change substantially. This indicates that the

structure of the monolayer does not change substantially. This is an especially interesting finding in the case of the surface coverage changes occurring when the magnetic field has been removed.

Thus far it has been postulated that the application of a magnetic field parallel to the surface of an electrode causes a rotation of the pendant ferrocene groups in a manner similar to that described in Figure 6.7. This section has presented evidence that the rotation process, if responsible for the decrease in electroactivity of the layer, continues even after the B-field has been removed.

6.3.5 Effect of Magnetic Field Orientation

In this section the effect of the orientation of the applied magnetic field relative to the electrode will be examined. It has already been shown that the application of a magnetic field parallel to the surface of the electrode has an effect on the electrochemical response of an electroactive monolayer deposited that electrode. In this section comparisons will be made between the responses of an electroactive monolayer coated electrode to a magnetic field applied parallel and perpendicular to the surface of the electrode. For clarity Figure 6.11 below shows the two complimentary field directions relative to the surface of the electrode.

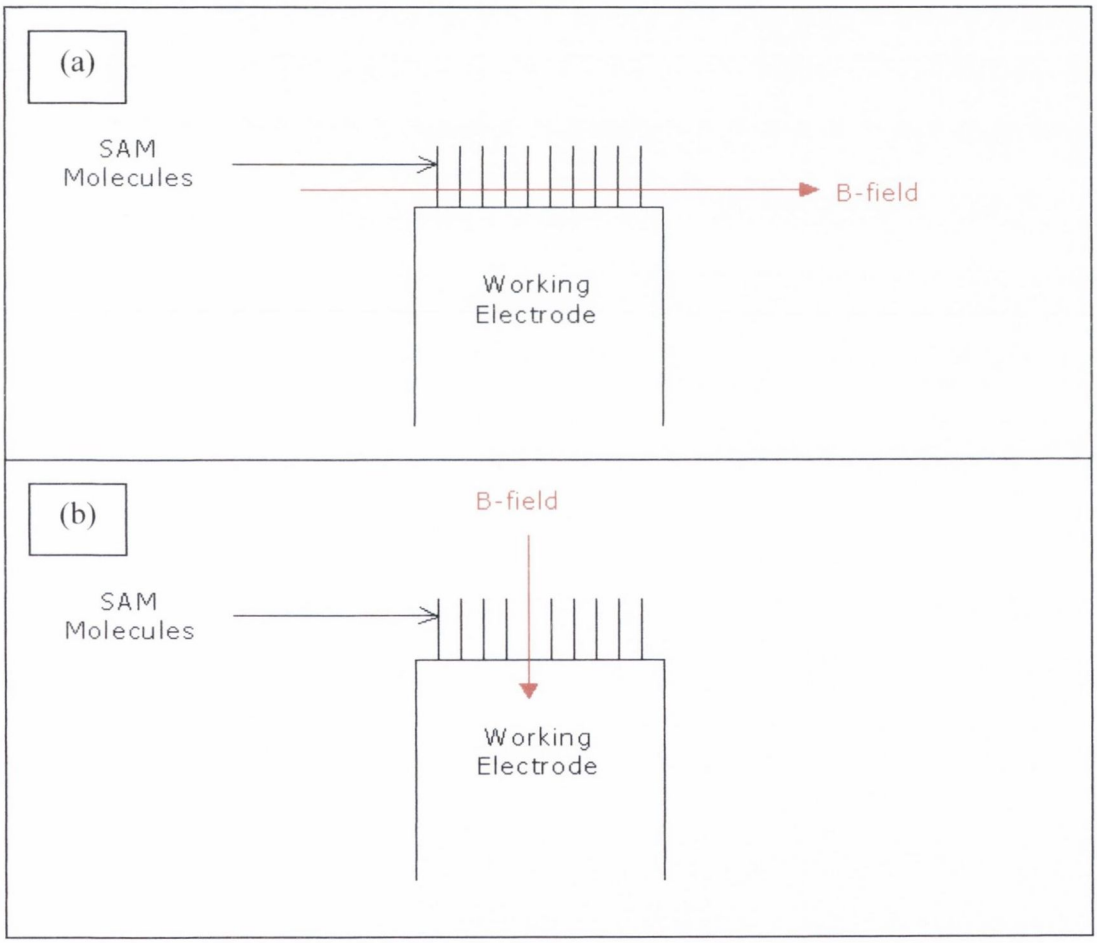


Figure 6.11. Direction of the applied magnetic field with respect to the molecules constituting a deposited self-assembled monolayer. (a) Magnetic Field orientation parallel to the surface of the electrode, (b) Magnetic field orientated perpendicular to the surface of the electrode.

Figure 6.12 below shows the cyclic voltammetric response of an electrode modified with a self-assembled monolayer of $S(CH_2)_{10}CO_2HFc$ when subjected to an external magnetic field in varying orientations. Also shown is the cyclic voltammetry response after the parallel field has been removed. For clarity the exact method of field application is now explained. Firstly a cyclic voltammogram was recorded prior to any magnetic field being applied. The magnetic field was then applied to the electrode in the perpendicular orientation and after 15 mins a cyclic voltammogram was recorded. The magnetic field was then applied to the electrode in the parallel orientation and after 15 mins a cyclic voltammogram was recorded. Finally the magnetic field was removed and after a further 15 mins a final cyclic voltammogram was recorded. This procedure gave rise to the response shown in Figure 6.12.

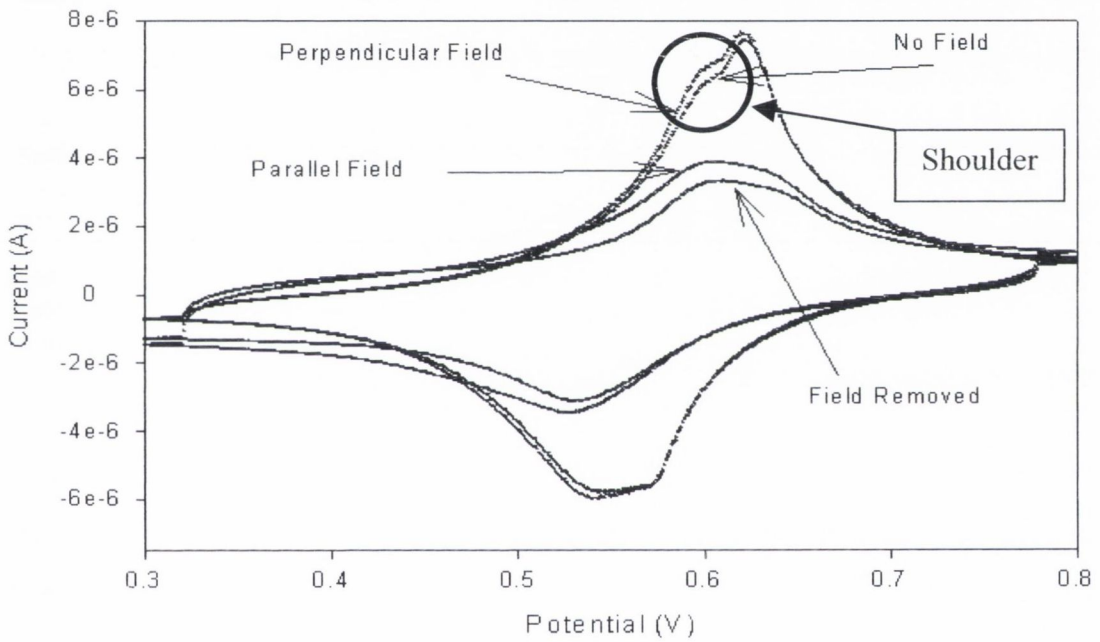


Figure 6.12. Cyclic voltammetric response of a gold electrode modified with a SAM of $S(CH_2)_{10}CO_2HFc$ to a 0.5T magnetic field applied in different orientations with respect to the electrode surface.

The first thing that can be taken from Figure 6.12 is that almost no surface coverage change can be detected when the magnetic field is orientated perpendicular to the surface of the electrode whilst a large surface coverage decrease is seen once the magnetic field is applied parallel to the surface of the electrode. Again as expected the surface coverage continues to decrease after the magnetic field has been removed. The recorded surface coverages are shown in Table 6.8. The second point of note

from Figure 6.12 is that the shoulder on the peak corresponding to the cyclic voltammogram recorded before the application of the field and occurring at approximately 580mV. The fact that this shoulder is present both in the absence of any applied magnetic field and when the field is applied in the perpendicular orientation but is not present when the field is applied parallel to the surface of the electrode or after the field has been removed is noteworthy. These shoulder peaks are attributed to electroactive molecules orientated in slightly different manner than the molecules in the bulk SAM (See *Section 3.1.1.2*). The fact that these peaks disappear upon application of the magnetic field in the parallel orientation may indicate that that this field application causes a reorientation of all molecules in the layer in a common manner.

	Before Magnetic Field	**Perpendicular Orientation**	**Parallel Orientation**	**Magnetic Field Removed**
Surface Coverage ($x10^{-10}$mol.cm^{-2})	19.0	20.0	7.8	7.5

Table 6.8. Surface coverages calculated from the cyclic voltammetric response of a $S(CH_2)_{10}CO_2HFc$ modified electrodes that have been exposed to a 0.5T magnetic field in varying orientations. Also shown is the surface coverage recorded both before and after the application of the field.

In order to gain further insight into this phenomenon chronoamperometry was carried out to examine the rate of electron transfer through the monolayer. This examination is presented below in Figure 6.1.3.

From this chronoamperometry response it is immediately apparent that the rate of electron transfer through the monolayer is not affected when the magnetic field is applied perpendicular to the surface ($k_{ET} = 139.3s^{-1}$ both before the application of the magnetic field and when the field is applied in the perpendicular orientation). However when the field is applied parallel to the surface of the electrode the electron transfer rate is increased as expected ($k_{ET} = 207.6s^{-1}$ when the field is applied parallel to the surface of the electrode and when the field has been removed).

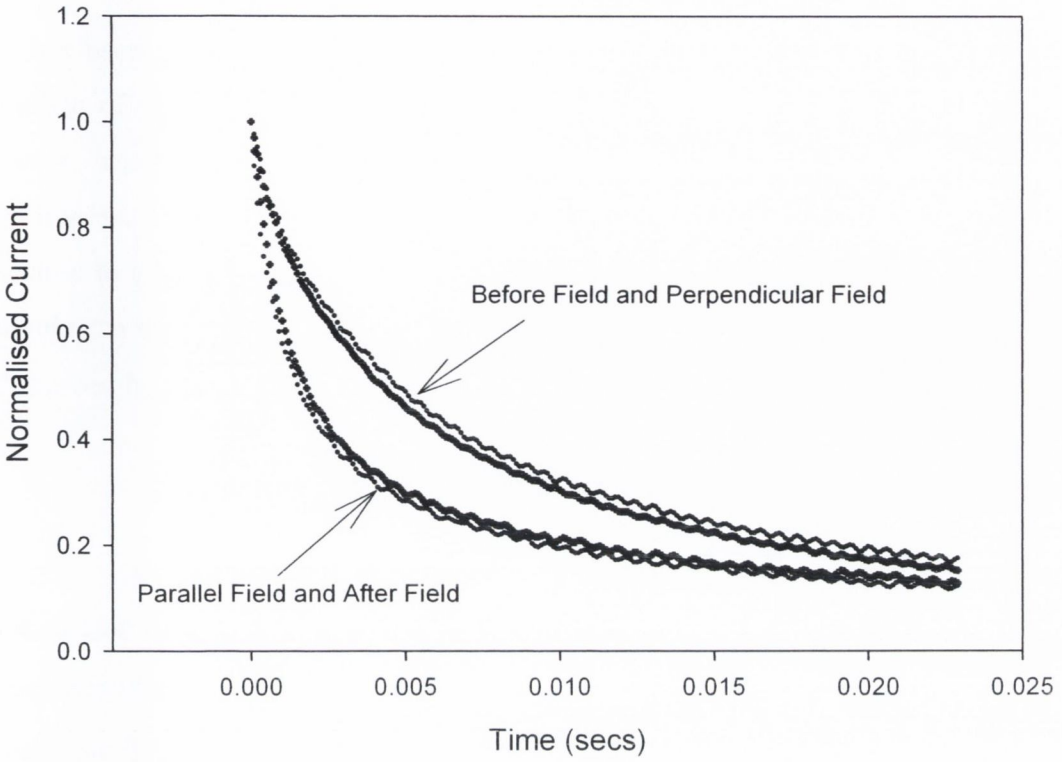


Figure 6.13. Chronoamperometry response of a gold electrode modified with a $S(CH_2)_{10}CO_2HFc$ monolayer to a 0.5T magnetic field applied in different orientations with respect to the electrode surface. The light traces correspond to the response for the perpendicular field orientation and the response when the field has been removed.

A number of findings can thus be taken from this section of study. Firstly it is noted that the application of a magnetic field perpendicular to the surface of an electrode modified with an electroactive SAM does not have an effect worthy of comment on the observed surface coverage when studied using cyclic voltammetry. Secondly it has been found that the application of a magnetic field in the perpendicular orientation does not have an effect on the rate of electron transfer. The final notable result from this section is that following the removal of the magnetic field there is the now expected decrease in surface coverage (*Section 6.3.4*). However this decrease in surface coverage following the removal if the field is not followed by a change in the rate of electron transfer as determined in Figure 6.13.

6.5.3.1 Magnetodynamic Considerations

It has been shown above that the orientation of the magnetic field relative to the surface of the electrode, and hence relative to the SAM molecules, is an important factor when calculating the observed surface coverage of electroactive SAM molecules. This consideration of the magnetic field orientation is extended in this section to consider magnetodynamic effects. This is because the system investigated involves a moving charge in the presence of a magnetic field. Such a system may be described by the Lorentz equation shown below in Equation 6.1.

$$\vec{F} = \vec{i} \times \vec{B} \tag{6.1}$$

the vector product implying that the Lorentz force $\vec{F}$ on the charged particle is perpendicular to the current $\vec{i}$ associated with the motion of the particle, and to the magnetic field $\vec{B}$. Another form of Equation 6.1 is:

$$F = i.B\sin\theta \tag{6.2}$$

where θ is the angle between the directions of the magnetic field and the current.

When the magnetic field is in the so-called parallel orientation, i.e. in the plane of the monolayer shown in Figure 6.14(a), the direction of the field is perpendicular to the direction of the current flow. In this case $\theta = 90^{o}$ and thus the Lorentz force on the charge carriers is a maximum and is directed perpendicular to the plane of the Figure. The force therefore imposes a perpendicular component to the trajectories of the charges from the (which in the absence of the field were largely direct paths along the alkanethiol chains). As a result the current associated with the flow might be expected to be reduced.

When the magnetic field is in the so-called perpendicular orientation, i.e. along the direction of the alkanethiol chains shown in Figure 6.14(b), the field is approximately parallel to the current flow. In this case $\theta = 0^{o}$ and $\vec{F} = 0$. Thus when the magnetic field is perpendicular to the current flow the deflecting force on the moving charge particles is expected to be greatest and when it is parallel to the flow the force acting on the charged particles is expected to be least.

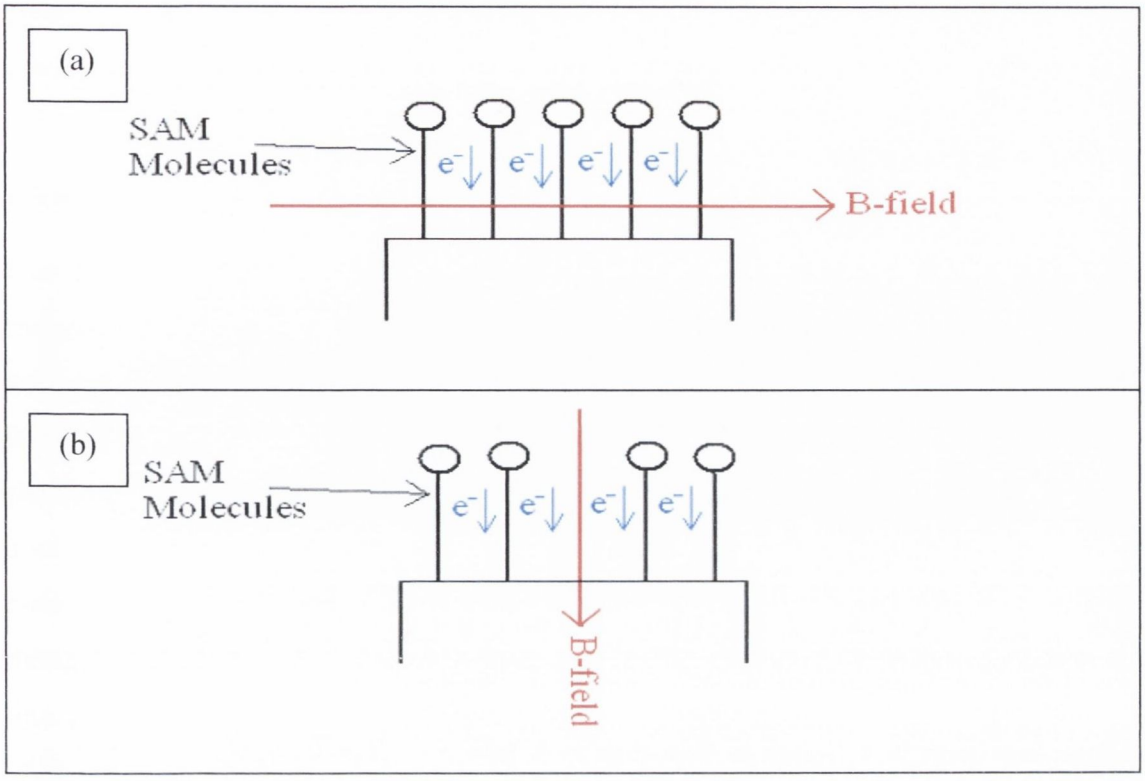


Figure 6.14. Direction of the applied magnetic field with respect to the molecules constituting a deposited self-assembled monolayer. (a) Magnetic Field orientation parallel to the surface of the electrode. In this orientation the direction of the magnetic field is perpendicular to the direction of current flow ($\theta = 90^{\circ}$) and the deflecting Lorentz force is greatest. (b) Magnetic field orientated perpendicular to the surface of the electrode. In this orientation the direction of the magnetic field is parallel to the direction of current flow ($\theta = 0^{\circ}$) and the deflection is least.

This observation may now be considered in tandem with the experimental findings presented in Figure 6.12. In Figure 6.12 it was shown that when the magnetic field was applied parallel to the electrode surface (thus perpendicular to the direction of current flow) an effect was seen on the observed surface coverage of electroactive molecules. This would indicate that the applied magnetic field was responsible for a force on the electrons traveling from the pendant redox moieties to the electrode. In the case of Figure 6.14(a) the right hand rule determines that this force would be in a direction coming out of the page. This force would, in effect, be sweeping the charge carrying electrons away form the surface of the electrode and hence diminish the observed surface coverage. It was also shown in Figure 6.12 that a magnetic field applied perpendicular to the electrode surface (thus parallel to the direction of electron motion) had no effect on the observed surface coverage. Again this agrees with the predictions of Equations 6.1 and 6.2. When the field is applied parallel to the direction

of current motion the no force on electrons moving from the redox moiety to the electrode surface is expected. Figure 6.12 shows no change in the observed surface coverage upon application of a magnetic field in this direction.

6.3.6 Magnetic Field Forces in Aqueous Electrolytes

One final brief explanation that may be put forward to explain the effects of the magnetic field on the various aspects of SAM redox activity relates to the effect that an applied B-field has on solution ions. The forces acting upon aqueous electrolytes because of the application of an external magnetic field have been described previously by Lyons et al.[9]. In this study 10 distinct forces are identified due to the application of the external B-field. Of these forces the one most applicable to the presently discussed system is termed the Electrokinetic Force (F_E). This force is thought to arise from the interaction of the magnetic field and electric current and is thought to induce convection in aqueous electrolytes acting at a distance of a few nanometers from the electrode surface.

Consider the case of the perchloric acid electrolyte. Should this electrolyte be subject to this stirring close to the surface of the self-assembled monolayer – this stirring may have an effect on the ability of perchlorate ions to form ion pairs. It has already been discussed that electron transfer events are linked to ion pairing interactions according to work by Marcus[7]. Thus it is worth considering that the stirring of the perchloric acid electrolyte close to the surface of the monolayer makes ion-paring events more difficult. This decrease in ion-pairing events would explain the observations made previously using CV and EQCM of a decrease in electroactivity and a corresponding decrease in the observed ion pairing events respectively.

6.4 Conclusion

This section has examined the effects of an external magnetic field on the mechanism of electron transfer using cyclic voltammetry, chronoamperometry and an electrochemical quartz crystal microbalance.

The effect of the magnetic field on redox active monolayers prepared from $S(CH_2)_nCO_2HFc$ (n=7,8,10,12) was examined using cyclic voltammetry. It was determined that the effect of the externally applied field did not scale in any immediately notable way. Although it was obvious that the magnetic field had an effect on the redox activity of the monolayer the extent of the effect was of a different magnitude in the case of each chain length. The effect of the magnetic field on redox active monolayers prepared using different solvents was also investigated using cyclic voltammetry. It was determined that the magnetic field had an effect on the redox activity in all cases.

Chronoamperometry studies were then carried out to examine the effect of the applied magnetic field on the kinetics of electron transfer. It was determined that the application of an externally applied field caused an increase in the rate of electron transfer through the redox active monolayers. At this stage of the investigation it was possible to discount the possibility of pendant ferrocene groups being buried in the surrounding alkane chains. Should the pendant ferrocene groups be buried a decrease in the rate of electron transfer is expected. However when an external magnetic field is applied an increase the rate is measured.

An electrochemical quartz crystal microbalance was then employed to study the effects of an externally applied magnetic field. It was determined that as well as having an effect on the redox activity of the self assembled monolayers, the externally applied magnetic field also has an effect on the extent of ion pairing that occurs. It was determined by examining the number of water molecules incorporated into the layer during the redox activity of the monolayer that no significant structural deformations take place upon application of the magnetic field. The intrinsic link between ion pairing and electron transfer events in redox active self-assembled monolayers was observed in this section. A model to account for the experimental findings thus far given was presented. This model was based on previous work involving the formation of self-assembled monolayers by coadsorption[8] and involves the rotation of the pendant ferrocene group. Identical redox diagnostics including an

observed decrease in redox activity of the SAM, an increase in the rate of electron transfer through the SAM and a decrease in the amount of ion pairing occurring are observed in the case of redox active mixed monolayers formed via coadsorption and redox active monolayers under the influence of an external magnetic field.

The effect of the magnetic field orientation on the redox activity of self-assembled monolayers was investigated. It was determined that when the magnetic field was applied perpendicular to the surface of the electrode no effect on the redox activity of the SAM was detected either by cyclic voltammetry or chronoamperometry. When the magnetic field was switched parallel to the surface of the electrode the expected decrease in surface coverage and increase in electron transfer rate constant was seen. Finally it was noted that when the magnetic field in the parallel orientation was removed the expected continuing decrease in surface coverage was not followed by any change in the electron transfer rate constant. This indicates that the elect of the externally applied magnetic field may be two-pronged and involve both a change in the conformation of the layer as well as the direct action of the magnetic field on the transported electrons, possibly by a Lorentz Force.

Finally a theory was put forward involving the stirring of the perchloric acid electrolyte due to the application of an external magnetic field. The Electrokinetic Force was identified as the force most likely to induce convection close to the surface of the self-assembled monolayer causing an effect on the ability of the pendant ferrocene molecules to form ion pairs.

References

(1) T.Z. Fahidy, *J. Appl. Electrochem.* **1983,** *13,* 553.

(2) G. Hinds, F. E. Spada, J. M. D. Coey, T. R. Ni Mhiochain and M. E. G. Lyons *J. Phys. Chem. B,* **2001**, *105,* 9487.

(3) M. Uhlemann, A. Krause, J. P. Chopart and A. Geberta, *J. Electrochem Soc.* **2005**, *152*, C817

(4) O.Devos, O. Aaboubi, J.-P. Chopart, A. Olivier C. Gabrielli and B. Tribollet, *J. Phys. Chem. A* **2000,** *104,* 1544.

(5) C.-C. Lee and T.-C. Chou, *Electrochimica Acta*, **1995,** *40,* 965.

(6) J.J. Sumner and S. E. Creager, *J. Phys. Chem. B,* **2001**, *105,* 8739.

(7) R.A. Marcus, *J. Phys. Chem. B,* **1998**, *102*, 10071.

(8) M. Lee and C. Chung, *Bull. Korean Chem. Soc.* **1999,** Vol. 20, No. 2

(9) M.E.G. Lyons, G. Hinds, J.M.D. Coey, *Electrochemistry Communications,* **2001**, *3*, 215.

CHAPTER 7 –

SELF-ASSEMBLED MONOLAYERS AND ENZYMES

7. Self-Assembled Monolayers and Enzymes

7.1 Introduction

The preceding chapters in this work have focused mainly on the theoretical considerations relating to self-assembled monolayers particularly electroactive, ferrocene terminated self-assembled monolayers. In this chapter a more practical aspect of self-assembled monolayers will be investigated, that being the immobilisation of redox active enzymes onto electrode surfaces modified with self-assembled monolayers. Two enzymes will be immobilised, these being glucose oxidase and cytochrome c. There will now be an introduction to the use of self-assembled monolayers in relation to enzyme immobilisation followed by an introduction to both enzymes.

7.1.1 Introduction to Enzymes and Self-Assembled Monolayers

One of the major obstacles to be overcome in the development of new biosensors is the issue of how to optimise electron transport between the enzymes' active site (prosthetic group) and the electrode surface. Marcus theory dictates that the kinetics of electron transfer between two sites is determined by the potential difference between the sites, the energy needed to reorganise the two species and the distance between the two redox centres. It is possible deposit enzymes directly onto the surface of an electrode. However when this is done the orientation of the prosthetic group in the enzyme with respect to the electrode surface is random such and the feasibility of electron transfer is ill-defined. Such orientations are shown below in Figure 7.1.

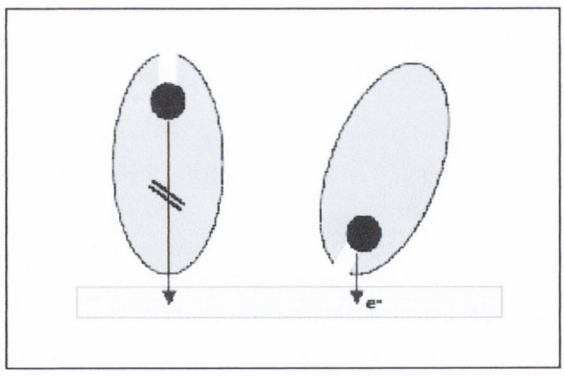


Figure 7.1. Depicting the effect of prosthetic group orientation on electron transfer. The prosthetic group is symbolised by the dark circle. On the left a prosthetic group is shown, well shielded by the surrounding protein shell from the electrode surface making electron transfer difficult. On the right the prosthetic group is shown in an orientation favourable to electron transfer.

In the case of an electrode with many enzyme molecules deposited upon it the overall orientation of the enzyme prosthetic groups are likely to be far from optimum. In the ideal situation all of the enzyme prosthetic groups deposited onto the surface of the electrode would be orientated such that electron transfer between them and the electrode surface would be as facile as possible.

Self-assembled monolayers provide one approach to optimise the electron transfer processes between the enzyme and the electrode surface. SAMs demonstrate a number of advantages as a platform for the immobilisation of enzyme species: (1) They are easily prepared and exhibit a high degree of structural order. (2) SAMs based on alkanethiol molecules in particular exhibit a membrane-like environment that is suitable for the study of biological molecules. (3) The chemistry of the SAM may be easily tailored. This includes variation of the packing structure of the SAM or in the headgroup chemistry. The headgroup chemistry can be particularly important when considering immobilising enzyme molecule on the SAM surface. Figure 7.2 below shows the effect achieved by immobilising an enzyme on an electrode modified with an appropriate SAM compared to an electrode that has enzyme molecules deposited directly onto its surface.

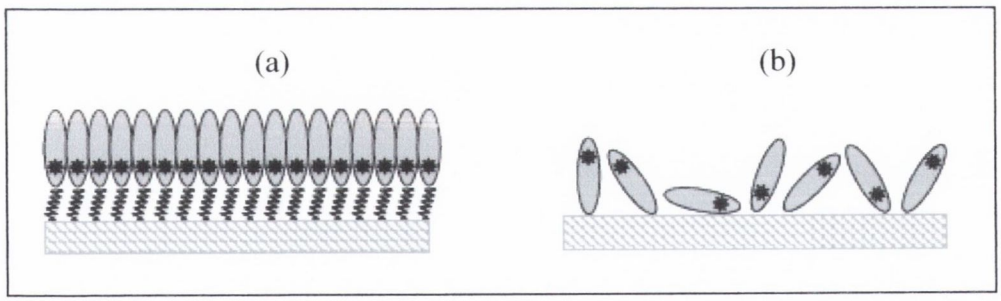


Figure 7.2. Comparison between (a) an enzyme immobilised on the surface of the appropriate self-assembled monolayer and (b) an enzyme that has been deposited directly onto the surface of an electrode. Note that the prosthetic group of the enzyme (indicated by a dark star) is orientated in a more manner more suitable to electron transfer with respect to the electrode surface when the electrode surface has been modified with a SAM.

For a more detailed introduction to previous work relating to enzymes immobilised on electrodes modified with SAMs the reader is invited to refer to *Section 1.3.4.1* of this report.

7.1.2 Introduction to Glucose Oxidase

This section will attempt, for the benefit of unfamiliar readers, to provide an introduction to the glucose oxidase enzyme.

An enzyme is a protein that has the ability to catalyse a chemical reaction. An enzyme may catalyse several million reactions per second. Enzymes are essential to life as most biological reactions would occur too slowly or would yield different products in their absence. Enzymes are normally specific to the reaction they catalyse. This specificity is achieved by selective binding between the enzyme and a specific reactant molecule (substrate). This is sometimes known as the 'lock and key' model.

Glucose oxidase is a dimeric protein containing one tightly bound flavin adenine dinucleotide (FAD) unit per monomer as a cofactor (a cofactor is an additional component needed by certain enzymes in order to exhibit full catalytic activity) Glucose oxidase catalyses the oxidation of β-D-glucose to produce D-glucono-1,5-lactone and hydrogen peroxide using molecular oxygen as an electron acceptor. This reaction is shown below in Figure 7.3.

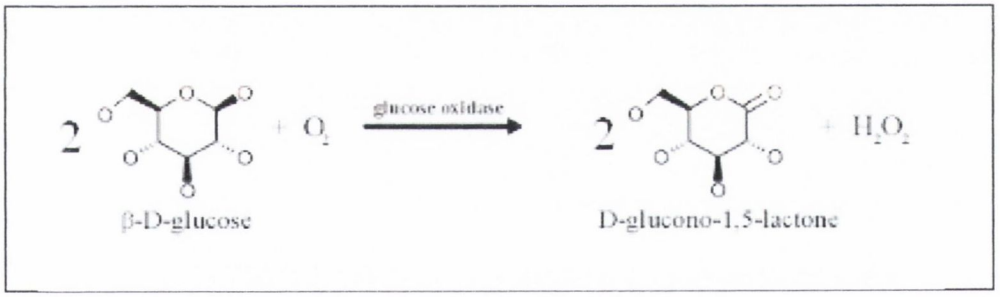


Figure 7.3 – Schematic depicting the conversion of α-D-glucose to produce D-glucono-1,5-lactone in the presence of glucose oxidase.

Glucose oxidase is an essential feature in modern biosensor devices that measure the amount of glucose present in the blood. Glucose oxidase is used due to the fact that glucose is traditionally difficult to detect in blood samples. If an electrode modified with glucose oxidase is introduced to a blood sample however all of the glucose present in that sample will be converted to D-glucono-1,5-lactone with the production of H_2O_2 also according to Figure 7.3. The H_2O_2 produced can be easily detected at the electrode surface and the magnitude of the signal it produces is proportional to the amount of glucose in the blood sample. Essentially the basis of

glucose oxidase sensors is converting glucose, which is difficult to detect electrochemically, into H_2O_2, which is easy to detect electrochemically.

The work presented in this report is based on attempts to improve the electrical communication between the glucose oxidase enzymes and the underlying gold electrode by orientating the enzymes in an ordered manner on a gold electrode modified with a particular self-assembled monolayer. It is possible to deposit glucose oxidase directly onto the surface of a gold electrode. However when this is done the orientation of the glucose oxidase is random and thus the electron transfer process between the enzyme and the electrode surface cannot be well controlled. As well as the increase in order expected by the introduction of self-assembled monolayers some other advantages arise when using the electrode/SAM/glucose oxidase system namely the ability of SAMs to selectively remove electrical contributions from inhibitor molecules. It was detailed above that traditionally H_2O_2 was detected at the electrode surface however this work will use soluble redox mediators to shuttle charge back and forth between the enzyme and electrode surface.

7.1.3 Introduction to Cytochrome C

This section will again, for the benefit of unfamiliar readers, provide an introduction to cytochrome c.

A cytochrome is a hemoprotein whose main function is electron transfer. The heme group is essentially an iron (or sometimes another metal) group contained at the centre of a large heterocyclic ring. This is a highly conjugated ring system – meaning its electrons are extremely mobile. Cytochromes can thus be readily oxidised and reduced reversibly. Several types of cytochrome molecules exist and they may be distinguished using spectroscopy. Probably the most widely studied of the various types of cytochromes is cytochrome c. This is mainly due to the fact that cytochrome c is a readily soluble protein unlike other types of cytochromes. Cytochrome c is a relatively small protein (M_w ~ 12,000 Daltons) and consists of a chain of proteins containing about 100 amino acids. A schematic showing the structure of the heme group of cytochrome c is shown below in Figure 7.4. The single iron atom at the centre of the heme group is shown. This central iron atom is linked to the four nitrogen atoms of the four pyrrole rings that make up the porphyrin ring of the heme group. The heme group in cytochrome c is covalently linked to the protein by links from its vinyl groups. This is seen to occur twice in the top left hand side of Figure

7.4. Depicted is the situation where the vinyl groups have been linked to the S-H groups of the cysteine amino acids of the protein shell. In the free heme molecule a double bond is present between the two carbon atoms of the vinyl side-chain (-$CH{=}CH_2$). However when the protein shell is linked to the heme group this bond becomes a single C-C bond and the spare electrons form a thioether bond to the sulfur on the cysteine side. (-C-CH_3-S-CH_2). Also worth noting are the carboxyl groups at the bottom right hand side of Figure 7.4. These groups may be deprotonated at neutral pH.

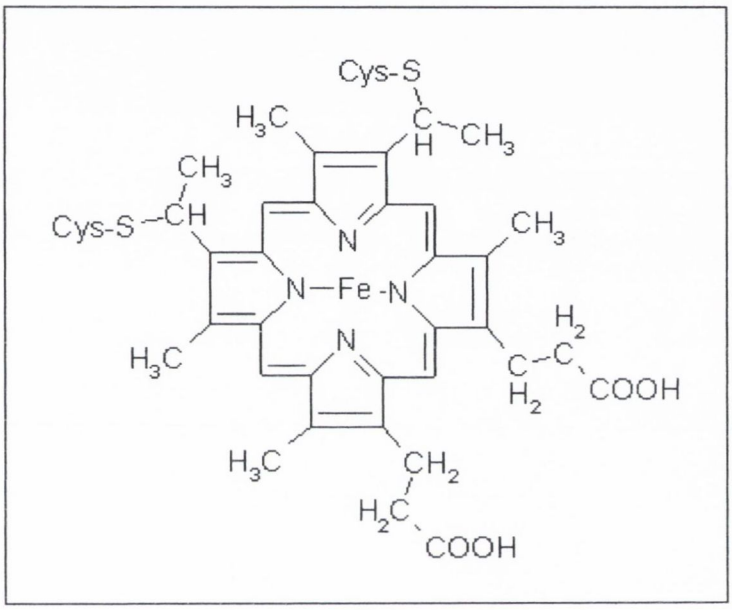


Figure 7.4 – Schematic depicting the structure of the heme group of cytochrome c. Shown in the top left hand side of the diagram is the heme group bound covalently to the protein shell via a thioelther bond with cysteine amino acids.

The reason why cytochrome c is of interest to researchers is due to the fact that it plays a role in two major biological functions. Ironically these two functions are somewhat opposing in their outcomes. Firstly cytochrome c plays an important role in the production of energy needed for the functioning of the body and secondly it plays a role in apoptosis which is a fundamental process in the demise of the body. Cytochrome c has also been used in studies of evolutionary divergence by examining the sequence of amino acids that make up the protein shell.

The role played by cytochrome c in generating the energy required by a living organism is as follows: the 'currency' of energy used by all living things is adenosine triphosphate (ATP). ATP is produced by the enzyme ATP synthase. ATP in turn is

powered by a transmembrane process known as the electron transport chain which is essentially an electrochemical potential gradient. This potential gradient is established via a series of redox reactions which can be separated into component parts. In general the electron transfer chain in living organisms can be divided into four distinct steps which are normally defined by the redox active molecules that are involved in each particular step. Electron transfer between the third and fourth stages (molecules) in the electron transfer chain is carried out by cytochrome c. Cytochrome c has the ability to accept an electron from cytochrome reductase (the third of the molecular stages in the electron transfer chain) and subsequently carries this electron until it collides with cytochrome oxidase (the final stage of the molecular stages in the electron transfer chain) whence it donates the electron. Thus in this case it is shown how the ability of cytochrome c to be readily and reversibly oxidised and reduced plays an important role in the production of ATP and subsequently the body's energy.

As well as its role in energy production, cytochrome c also plays a vital role in apoptosis. Apoptosis is basically a controlled form of cell death that the body uses to dispose of any unwanted cells. Morphological changes in the structure of the cell undergoing apoptosis are observed and these morphological changes are triggered by enzymes known as caspases which have the ability to cleave other enzymes. Cytochrome c has a role in the production of caspase 9 which is an initiator caspase that cleaves inactive forms of effector caspases and thus activating them to perform the apoptotic process. Caspase 9 in turn is formed from the action of apoptosome which is a large multi-protein structure. The apoptosome molecule is formed when two cytochrome c molecules bind to the cytosolic protein APAF 1 and the nucleotide dATP forming a apoptosome structure. Apoptosis is an extremely important function in the human body. A lack of apoptitic activity can result in uncontrolled cell growth leading to the formation of cancerous tumors whereas too much apoptitic activity may result in cell growth disorders.

A final interesting use of cytochrome c lies in the area of evolutionary divergance. Cytochrome c has been used in such studies because it is present in all living things from bacteria to humans. However slight differences in the amino acid sequences that make up the protein of the enzyme have been found. The sequences have been examined to determine if any trend exists in the amino acid mutations. i.e is there a logical progression in the mutations from, say, bacteria to canine to human. Should this be the case it would provide strong evidence that the the cytochrome c

present in all living things accrues from a common ancestor. If a logical progression is not found as the complexity of the animal increases it is likely that the cytochrome c molecule is optimised depending on the environment it occupies. i.e. the cytochrome c present in each animal will tailor its amino acid sequence in such a way that it serves its purpose best.

Thus it has been shown that cytochrome c is of interest over a wide range of topics. Both its role in the electron transfer chain and in the apoptosis cycle involve its ability to transfer electrons. Because of this the electron transfer mechanisms of cytochrome c are of large interest to researchers. In this chapter it will be attempted to provide a platform for the studies of cytochrome c redox processes using self-assembled monolayers in much the same way as described for the glucose oxidase enzyme described in the previous section (*Section 7.1.2*). The reason for using self-assembled monolayers as a platform for cytochrome c adsorption on electrodes is twofold. Firstly, as was the case with glucose oxidase adsorption, it is desirable to orientate the heme groups in an ordered manner with respect to the surface. Secondly it has been shown in various studies that cytochrome c adsorbed onto Au[1] and Ag[2] surfaces undergoes large changes in conformation akin to the denaturing of the protein. Such effects can lead to irreversible electron transfer between the electrode surface and the heme group of the cytochrome c. Self-assembled monolayers with their ability to easily modify an electrode surface at the molecular level provide an ideal platform upon which to tether cytochrome c molecules for electron transfer studies.

7.2 Experimental

Electrochemical Measurements. All electrochemical measurements were carried out on a CH Instruments Model 440 potentiostat as described in *Section 2.2.1.*

Gold Substrate. The gold substrate used whether it be a standard macroelectrode or an EQCM electrode is as described in *Section 2.1.1.*

Electrode Pre-Treatment. The method used for electrode pre-treatment is described in *Section 2.3.1.*

7.2.1 Glucose Oxidase

Materials. Glucose oxidase (grade VII from *aspergillus niger*) was obtained from Sigma Aldrich and used as received. α-D-glucose was obtained from Sigma Aldrich. Mutarotation of α-D-glucose to β-D-glucose was achieved by storing solutions of α-D-glucose in phosphate buffer overnight at 4°C. Phosphate buffer solution (pH 7) was obtained from Sigma Aldrich. Ferrocene carboxylic acid was obtained from Sigma Aldrich. Uric acid and ascorbic acid were purchased from Sigma Aldrich. 11-mercapto-undecanoic acid was purchased from Sigma Aldrich. 1-decanethiol was purchased from Sigma Aldrich. Cysteamine was purchased from Sigma Aldrich. Glutaric dialdehyde was purchased from Sigma Aldrich.

Preparation of Electrodes. Gold working electrodes were coated with the appropriate self-assembled monolayer by immersing them in a 1mM ethanolic solution of that molecule for a period of 24 hours. Glucose oxidase coatings were then prepared by applying a 10μl droplet of glucose oxidase/phosphate buffer solution (1mg ml^{-1}) onto the electrode surface. This droplet was allowed to evaporate at room temperature. Following the evaporation of the droplet the glucose oxidase was cross-linked by holding the electrode over a few drops of glutaric dialdehyde for 1 hour. This method produced a glucose oxidase film atop of a self-assembled monolayer that was found to be stable following repeated electrochemical measurements.

Electrolyte Solutions. In this section electrolyte solutions were comprised of phosphate buffer solutions in all cases with various additions as described in the text.

7.2.2 Cytochrome c

Materials. Cytochrome c from equine heart was purchased from Sigma Aldrich. The molecules used to form self-assembled monolayers are as described in *Section 7.2.1.*

Preparation of electrodes. Gold working electrodes were coated with the appropriate self-assembled monolayer by immersing them in a 1mM ethanolic solution of that molecule for a period of 24 hours. Coatings of cytochrome c were then applied by immersing the electrode in a 1mg ml^{-1} solution of cytochrome c in 0.44mM phosphate buffer solution, pH 7.4, ionic strength 1mM.

Electrolyte Solutions. Solutions of 4.4mM potassium phosphate buffer, pH 7.4, ionic strength 10mM were used as the electrolyte when carrying out electrochemical measurements.

7.3 Results and Discussion

7.3.1 Glucose Oxidase

7.3.1.1 Inhibition of Interferers. One great advantage of using self-assembled monolayers is their ability to selectively inhibit the redox reaction of certain solution redox mediators with the electrode surface whilst the reaction of other redox mediators is permitted. The ability of self-assembled monolayers to selectively inhibit the electroactivity of undesirable interferer molecules is of interest when considering commercial glucose sensor design. Typical interferers in modern glucose biosensors are ascorbic and uric acid that are present in the blood and whose electroactivity can mask the response of the glucose electroactivity. Figure 7.5 below shows the response of a gold electrode modified with three alkanethiol monolayers, with different headgroups namely CH_3, NH_2 and CO_2H, to a solution containing ascorbic acid.

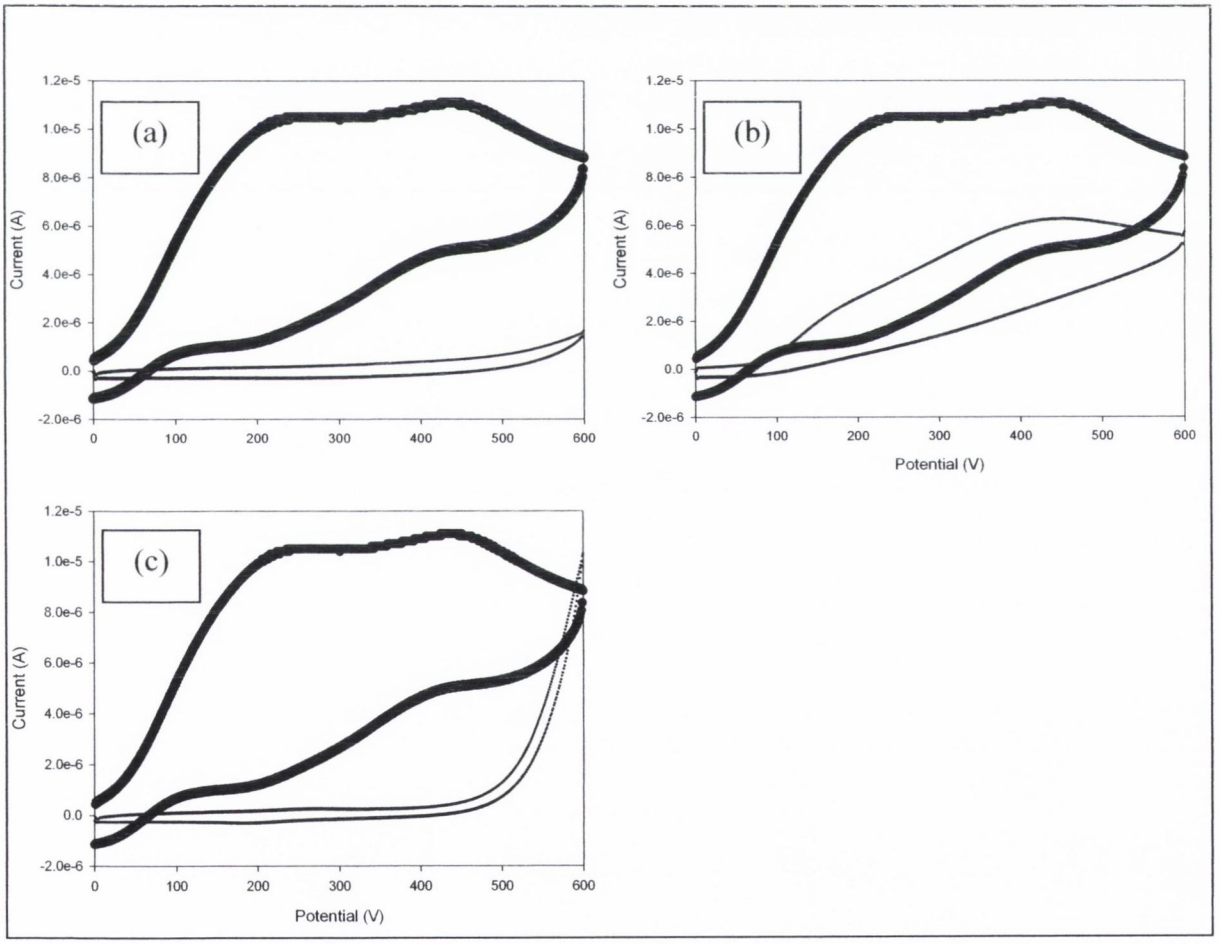


Figure 7.5. Comparison of the response of a gold electrode modified with (a) CH_3, (b) NH_2 and (c) CO_2H terminated SAMs and the response of a bare gold electrode in the presence of ascorbic acid. The electrolyte solution was a phosphate buffer solution containing 1mM ascorbic acid. The thicker trace present in all three graphs is the response of the bare gold electrode and the lighter trace is the response of the electrode modified with the appropriate SAM. Scan rate $0.1 Vs^{-1}$.

Figure 7.6 below shows the comparison between the response of a bare gold electrode and an electrode modified with self-assembled groups with CH_3, NH_2 and CO_2H to a solution containing uric acid.

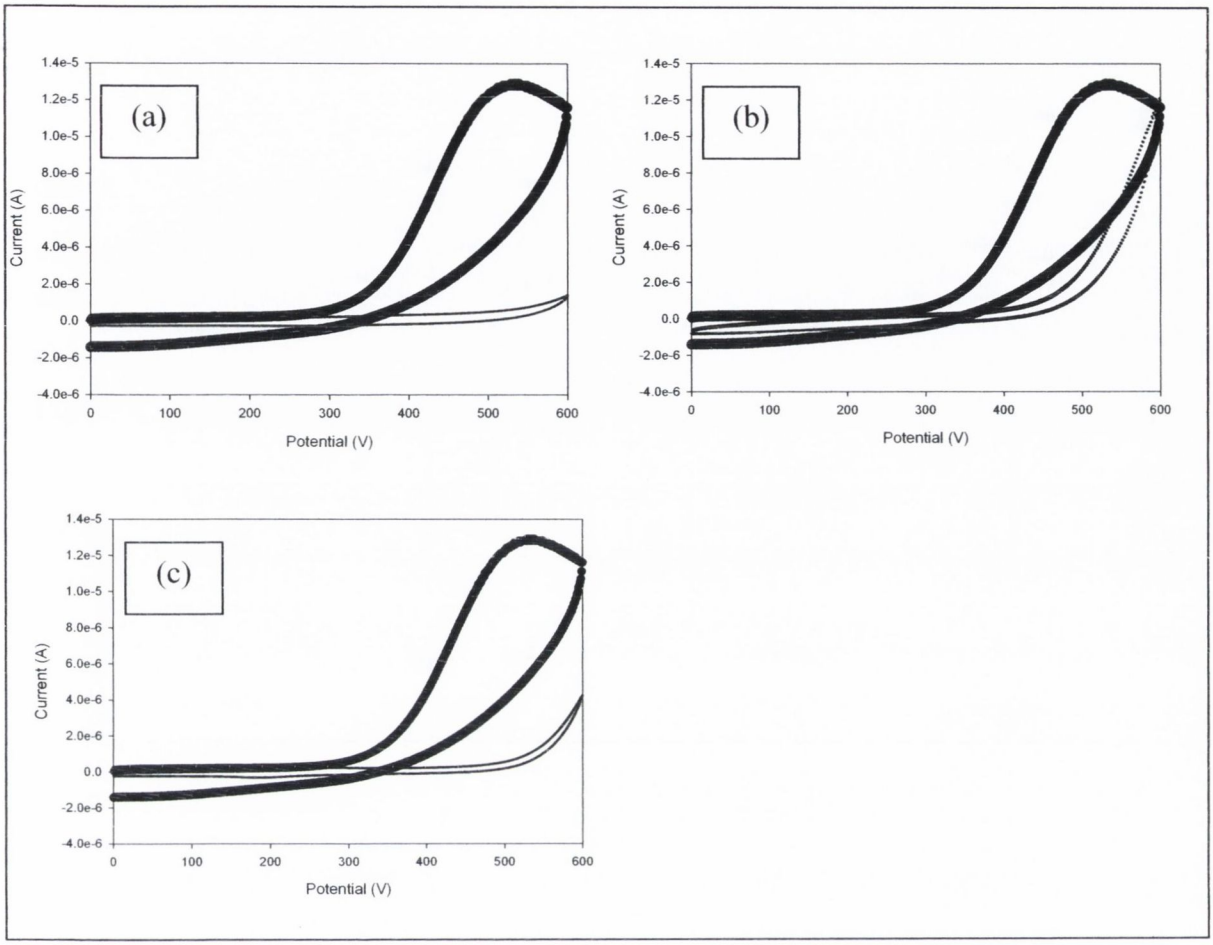


Figure 7.6. Comparison of the response of a gold electrode modified with (a) CH3, (b) NH2 and (c) CO_2H terminated SAMs and the response of a bare gold electrode in the presence of uric acid. The electrolyte solution was a phosphate buffer solution containing 1mM uric acid. The thicker trace present in all three graphs is the response of the bare gold electrode and the lighter trace is the response of the electrode modified with the appropriate SAM. Scan rate $0.1Vs^{-1}$.

It can be clearly seen from the response of the gold electrode when compared to the monolayer coated electrodes that the signal corresponding to the redox process of the ascorbic/uric acid is dramatically reduced when the electrode has been coated with a self-assembled monolayer. This effect is observed because the molecules of ascorbic/uric acid are not permitted close approach to the electrode surface once it has been coated with a self-assembled monolayer. Thus any electron redox process is forced to occur over long range across the SAM which according to the distance dependence factor in Marcus theory makes the probability of this occurring extremely low. Thus any redox reaction involving the ascorbic/uric acid molecules is likely to occur at 'pinhole' (See *Section 1.2.6.5* for further reading on pinhole sites) sites

within the SAM. Thus, should a well ordered SAM be formed, the possibility of ascorbic/uric acid having any electrical activity and thus interfering with the glucose sensitivity should be vastly diminished. Therefore it has been shown that SAMs formed with CH_3, NH_2 and CO_2H headgroups all have the ability to act as inhibitors to the action of ascorbic and uric acid as electrochemical interferers.

However the ability of the deposited self-assembled monolayers also has some drawbacks when applied to the area of glucose sensing. This is due to the fact that gold electrodes that have been modified with self-assembled monolayers are found to also to inhibit the electroactivity of hydrogen peroxide. This is undesirable as the redox action of this analyte is central to the operation of conventional biosensors. Figure 7.7 below shows the comparison between the response of a bare gold electrode and an electrode modified with self-assembled groups with CH_3, NH_2 and CO_2H to H_2O_2.

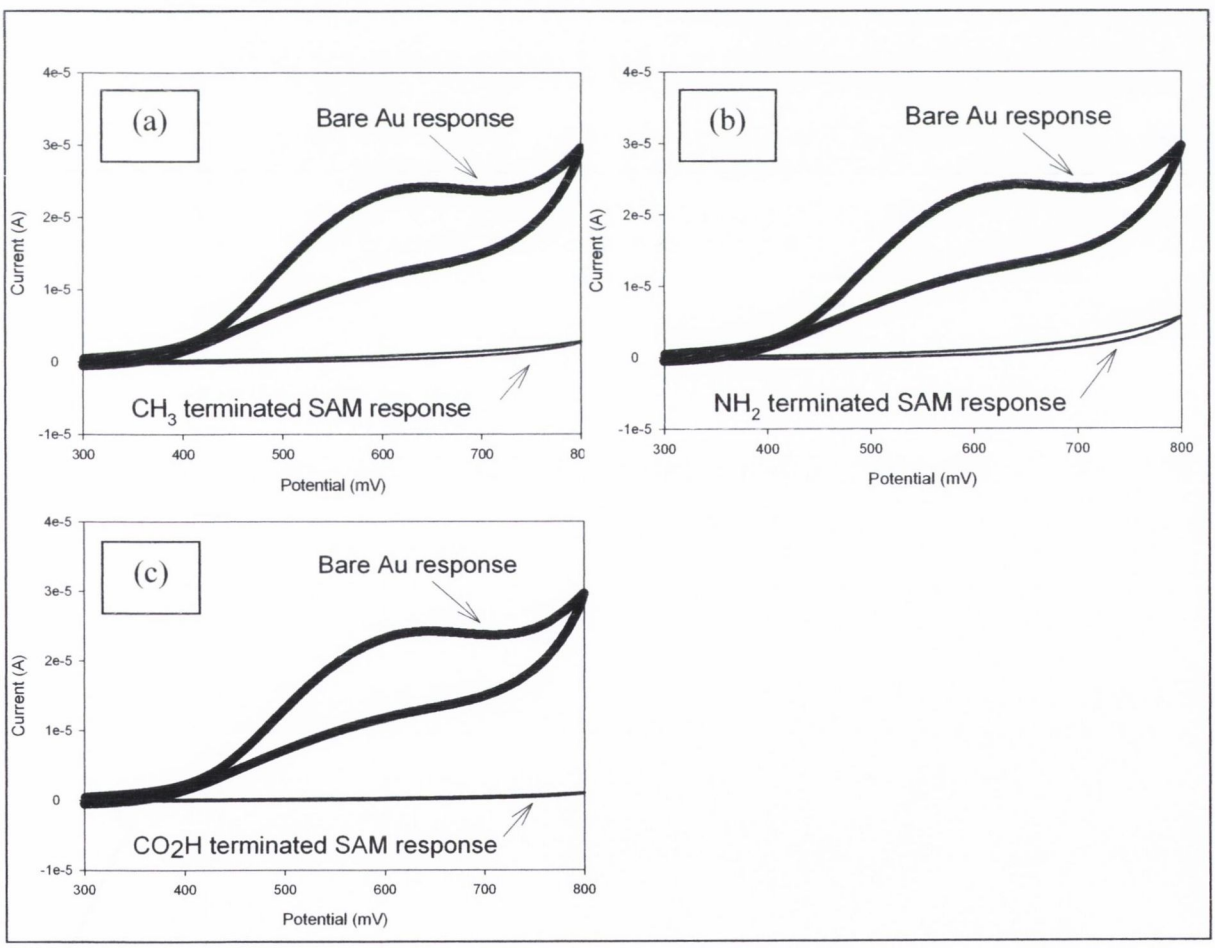


Figure 7.7. Comparison of the response of a gold electrode modified with (a) CH3, (b) NH2 and (c) CO_2H terminated SAMs and the response of a bare gold electrode in the presence of hydrogen peroxide. The electrolyte solution was a phosphate buffer solution containing 1M hydrogen peroxide. The dark trace present in all three graphs is the response of the bare gold electrode and the lighter trace is the response of the electrode modified with the appropriate SAM. Scan rate $0.1 Vs^{-1}$.

Luckily however, the redox activity of all solution phase molecules are not suppressed at electrodes coated with self-assembled monolayers. Figure 7.8 below shows the response of an electrode modified with self-assembled groups of CH_3, NH_2 and CO_2H in the presence of ferrocene carboxylic acid ($FcCO_2H$) which is a common redox active molecule.

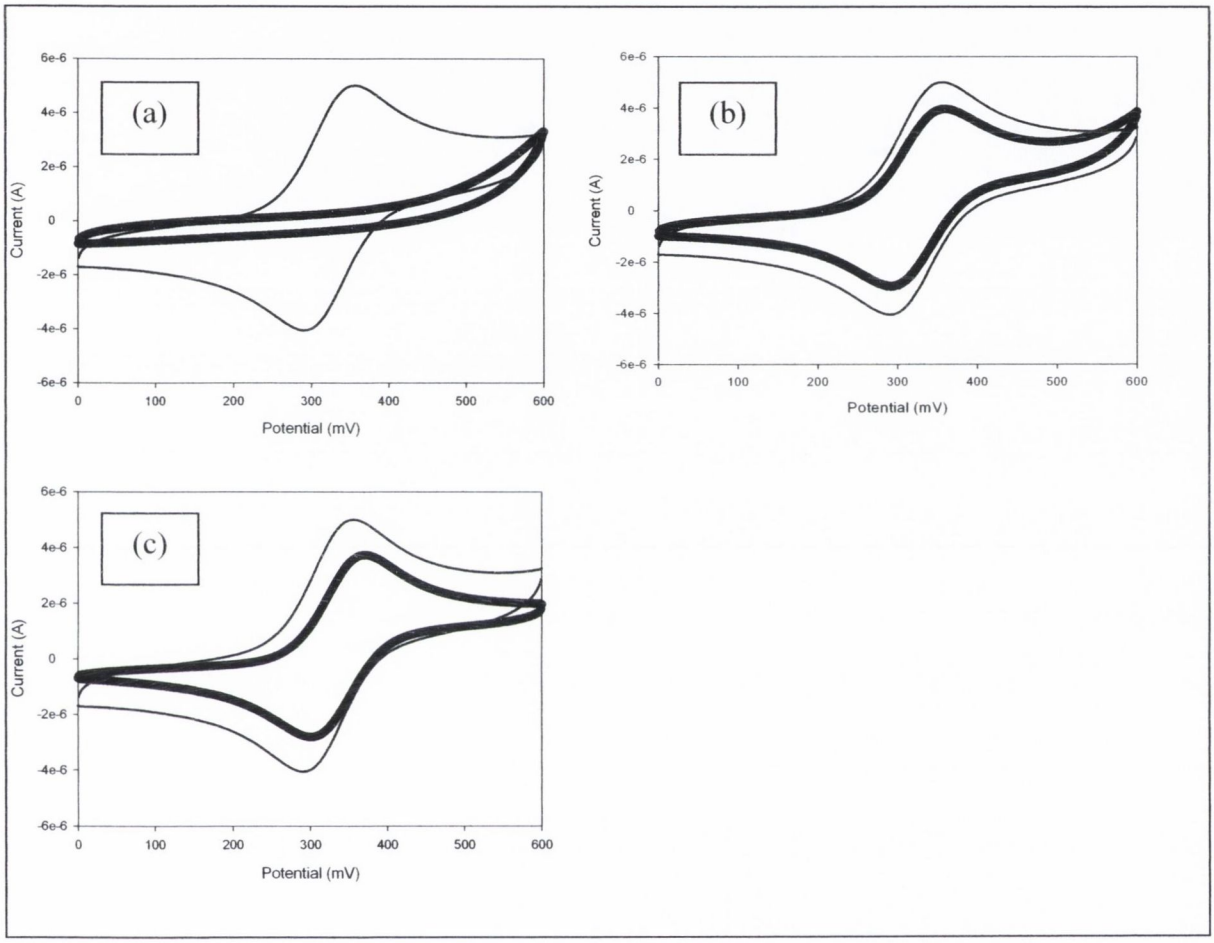


Figure 7.8. Comparison of the response of a bare gold electrode and one modified with (a) CH3, (b) NH2 and (c) CO_2H terminated SAMs in the presence of ferrocene carboxylic acid. The lighter trace present in all three graphs is the response of the bare gold electrode and the thicker trace is the response of the electrode modified with the appropriate SAM. The electrolyte solution was a phosphate buffer solution containing 1mM $FcCO_2H$. Scan rate $0.1Vs^{-1}$.

The set of cyclic voltammograms in Figure 7.8 provides some important information regarding the use of self-assembled monolayers as a platform for glucose biosensors.

Firstly it provides evidence that not all interfacial electron transfer reactions are impeded due to the presence of a self-assembled monolayer. Thus it has been

shown that employing self-assembled monolayers as a technique to modify the electrode surface provides the ability to discriminate between redox reactions of different molecules. While the unwanted redox activity of interferers (ascorbic and uric acid) is suppressed the redox activity of another species ($FcCO_2H$) is allowed. This provides the ability to develop a glucose sensor capable of blocking the activity of certain interferers whilst using a redox mediator such as ferrocene carboxylic acid that could be used to shuttle charge back and forth between a redox enzyme and the electrode surface.

The second aspect of importance that can be derived from Figure 7.8 regards the choice of self-assembled monolayer. It is clear that when using a solution phase redox mediator the choice of headgroup for the SAM is important. The voltammogram recorded for the electrode modified with a CH_3 terminated group does not show peaks corresponding to the oxidation/reduction of the ferrocene carboxylic acid whereas the voltammograms corresponding to the NH_2 and CO_2H terminated SAMs do show peaks indicating that the solution phase mediator is active at electrodes modified with these SAMs. This observation is likely due to the denser packing of the CH_3 terminated SAMs which do not allow close approach of the $FcCO_2H$ molecules whereas the other two SAMs are terminated with the bulkier NH_2 and CO_2H groups causing them to pack less densely. Thus the $FcCO_2H$ molecules are permitted close approach to electrodes modified with these groups. It is informative to briefly comment on the diagnostics of the voltammetric response for the NH_2 and CO_2H terminated SAMs. This can be done with reference to Table 7.1.

	Anodic Peak Current (A) ($x10^{-6}$)	**Cathodic Peak Current (A) ($x10^{-6}$)**	**E_{Pa} (mV)**	**E_{Pc} (mV)**	**E^0 (mV)**	**E_{Pa} - E_{Pc} (mV)**	**$\frac{i_p^{ox}}{i_p^{red}}$**
Bare Gold	4.4	-3.8	356	291	324	65	1.15
NH_2 terminated SAM	3.7	-3.2	357	291	324	66	1.15
CO_2H terminated SAM	3.7	-3.4	371	301	336	70	1.08

Table 7.1. Diagnostics corresponding to the cyclic voltammetry responses in Figure 7.8. Not included are any diagnostics corresponding to a gold electrode modified with a CH_3 terminated SAM (Figure 7.8(a)) as this response is featureless.

Firstly it is notable that the peak currents in the case of the SAM modified electrodes are diminished with respect to the gold electrode. This is to be expected as although the SAMs to permit $FcCO_2H$ molecules to permeate their structure there is likely to be some residual blocking effect to be attributed to the SAM. Secondly it is notable that the overall electron transfer diagnostics in all cases are shown to be essentially reversible with the difference between the anodic and cathodic peak potentials quite close to the ideal 59/n mV. As well as this the ratio of the anodic peak current to the cathodic peak current is always close to unity, again an indication of reversibility. Thus it has been shown that the electron transfer ability of the redox active $FcCO_2H$ molecules is blocked to some extent by the presence of a self-assembled monolayer, however neither the presence of the CO_2H nor the NH_2 terminated SAM has any effect, to any notable extent, on the degree of reversibility of the system

Thus far some interesting points have been put forward regarding the use of self-assembled monolayers as platforms for glucose sensor design before even before any enzyme has been introduced to the system. It has been shown that self-assembled monolayers have the ability to allow the access of particular redox active molecules to the electrode surface whilst selectively inhibiting others, an invaluable asset to biosensor design. Also noted however was that this ability depended to some extent on the choice of molecule used to for the SAM. It was shown that both NH_2 and CO_2H terminated SAMs allowed redox active $FcCO_2H$ molecules to reversibly access the electrode surface whilst CH_3 terminated SAMs did not. This observation was attributed to differences in packing densities of the different SAMs.

The next section will develop the study further by introducing a layer of glucose oxidase atop the self-assembled monolayers.

7.3.1.2 SAM/Glucose Oxidase System.

The previous section has described how SAMs formed from different molecules can be used to selectively inhibit/allow the action of redox active molecules. One significant problem encountered however, was the fact that the redox activity of hydrogen peroxide, the common analyte used in glucose sensors, was found to be inhibited. However the redox activity of $FcCO_2H$ molecules was found to be permitted. Any possible glucose sensor design will thus need to use $FcCO_2H$ (or similar electroactive molecules) as a redox mediator. Due to this necessity the use of SAMs terminated with CH_3 groups has been ruled out, as they do not allow close approach of $FcCO_2H$ molecules to the electrode surface.

Shown below in Figure 7.9 is the response, to a solution with glucose present, of an electrode modified with a self-assembled monolayer and on top of this SAM a layer of glucose oxidase. Also shown for comparison in this figure is the response of the electrode before any glucose has been added to the electrolyte solution.

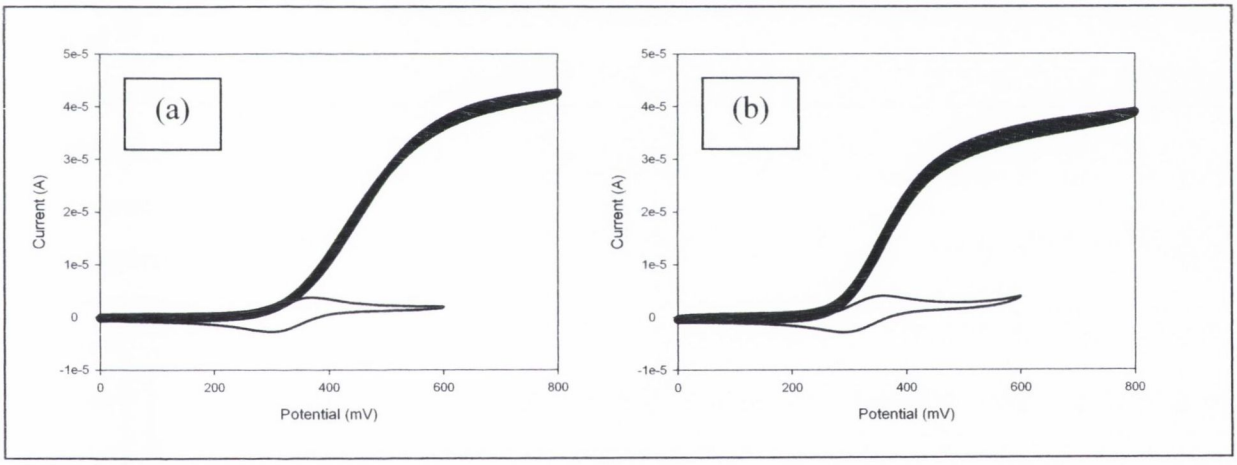


Figure 7.9. Comparison of the response of a bare gold electrode and one modified with (a) SAM-CO_2H/glucose oxidase layer and (b) SAM-NH_2/glucose oxidase layer in the presence of 1mM ferrocene carboxylic acid only (light trace), and in the presence of 1mM ferrocene carboxylic acid and 0.25M glucose (dark trace). Scan rate $0.1Vs^{-1}$.

It can clearly be seen from Figure 7.9 seen that the glucose is being catalysed by glucose oxidase to generate an electrical response at the electrode surface. Conventional biosensors are based on monitoring the production of hydrogen peroxide using molecular oxygen as a cofactor for the oxidation of glucose by glucose oxidase. This technique is somewhat different however. In this technique the ferricenium ion of the FCA molecule acts as the cofactor and in the process is

oxidised to the FCA^+ ion. The presence of the electrical signal at the electrode surface is thought to be due to the process depicted in Scheme 7.1 with the conversion of FCA^+ to FCA in step (2) resulting in the electrical signal observed. The FCA produced in step (2) may then be recycled to act once again as the cofactor in the oxidation of glucose by glucose oxidase.

$$\text{Glucose} + GOx_{(ox)} \rightarrow \text{gluconolactone} + GOx_{(red)} \quad (1)$$

$$GOx_{(red)} + 2FCA^+ \rightarrow GOx_{(ox)} + 2FCA + 2H^+ \quad (2)$$

$$2FCA^+ \rightleftharpoons 2FCA + 2e^- \quad (3)$$

Scheme 7.1. The method by which mediation occurs using ferrocene carboxylic acid as a redox mediator.

This result however is not particularly remarkable as the use of redox mediators has been recorded previously in relation to glucose oxidase[3,4]. For example, Bourdillion et al.[3] utilised ferrocene methanol to study the voltammetry of glucose oxidase layers bound to rabbit IgG (antigen) atop of a carbon electrode. The result only becomes of interest when the response of the Au/ SAM/glucose oxidase layers to the presence of glucose in solution are compared to those of the Au/glucose oxidase layers. This comparison is shown below in Figure 7.10.

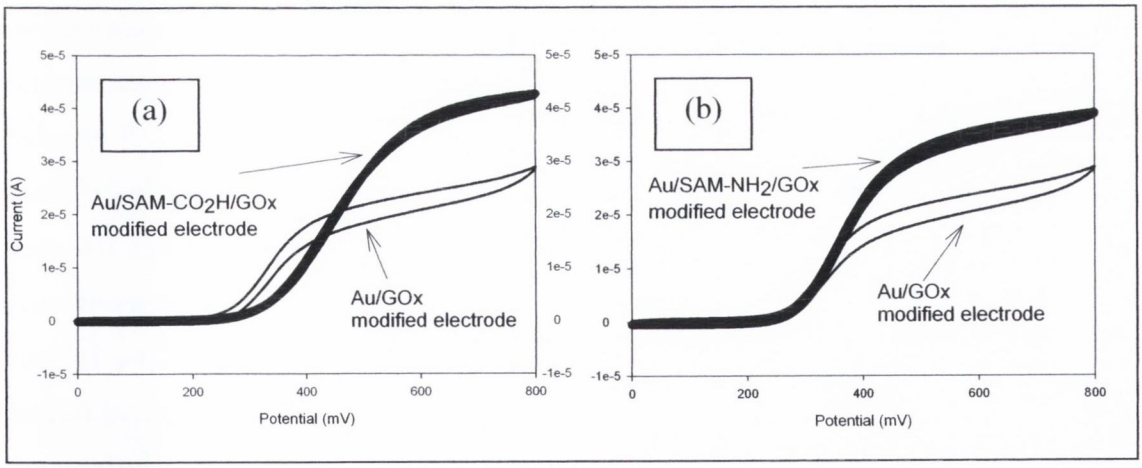


Figure 7.10. Comparison of the response of a bare gold electrode modified with a glucose oxidase layer (Au/GOx) and (a) SAM-CO_2H/glucose oxidase layer and (b) SAM-NH_2/glucose oxidase layer in the presence of 1mM ferrocene carboxylic acid and 0.25M glucose. The response of the Au/GOx modified electrode is shown as the light trace in both (a) and (b). The response of the Au/SAM/GOx electrode is shown as the dark tracers in both (a) and (b). Scan rate $0.1Vs^{-1}$.

The amplification of the response is clearly visible when the electrode is modified with a self-assembled monolayer due to the increase in the order of the enzyme orientation it brings.

Another notable feature of Figure 7.10 is the potential at which the catalysis of the glucose occurs. In Figure 7.10(a) corresponding to the Au/SAM-CO_2H/GOx electrode the catalysis is observed to occur at a higher potential than does the catalysis at the Au/GOx electrode. This observation may be explained by reference to Figure 7.8(c) and Table 7.1. It can be noted from these two that the oxidation of the ferrocene carboxylic acid occurs at a more positive potential at the electrode modified with a CO_2H terminated SAM than it does at the bare gold electrode (371 vs. 356mV). In Figure 7.10(b) corresponding to the Au/SAM-NH_2/GOx system the catalysis the potential at which catalysis occurs is the same as that at the Au/GOx electrode. Again reference to Figure 7.8(b) and Table 7.1 are informative. It is observed in this case that the oxidation of the ferrocene carboxylic acid occurs at the same potential at the electrode modified with the NH_2 terminated SAM and a bare gold electrode (356 vs. 357mV). These findings represent an important point regarding the operation of this glucose sensor in that they confirm the action of the ferrocene carboxylic acid in mediating the electron transfer. Figure 7.8(c) indicated that the oxidation of the $FcCO_2H$ molecules occurred at a slightly higher potential when acting at a CO_2H terminated SAM relative to the bare gold electrode. In order to observe a signal corresponding to the catalysis of glucose is necessary for ferrocene carboxylic acid to migrate towards the electrode surface and undergo a redox reaction - according to Scheme 7.1. It has been shown that this is possible at the CO_2H terminated SAM modified electrode but that it occurs at a slightly more positive potential relative to the bare Au case. This is reflected in Figure 7.10(a) where the potential at which the glucose catalysis occurs is slightly retarded relative to the bare Au electrode. In the case of an NH_2 terminated SAM modified electrode the oxidation of the $FcCO_2H$ molecules occur at the same potentials as in the case of the bare gold electrode. Thus the catalysis of the glucose is expected to occur at the same potential at the Au/SAM-NH_2/GOx electrode as it is at the Au/GOx electrode. This postulate is confirmed by the result in Figure 7.10(b) and adds weight to the mechanism derived in Scheme 7.1 relating to the operation of the system.

7.3.1.3 Michaelis-Menten Analysis of the SAM/Glucose Oxidase System.

In order to gain further information regarding the SAM/glucose oxidase system a Michaelis-Menten analysis was carried out on the SAM/glucose oxidase system. The Michaelis-Menten analysis can be used to account for how the reaction rate of an enzyme varies with substrate concentration. In the case of this system the Michaelis-Menten theory describes how the rate of glucose catalysis by the glucose oxidase enzyme changes with the concentration of glucose in solution. There now follows a mathematical description of the Michaelis-Menten theory similar to that presented by Briggs and Haldane in 1925[8].

According to the Michaelis-Menten theory an enzyme, E, catalyses a substrate, S, via the formation of an intermediate species, ES, as described in Equation 7.1.

$$E + S \rightleftharpoons ES \tag{7.1}$$

In this equation the rate constants for the forward and reverse direction of the reaction are k_1 and k_2 respectively. Once the reaction depicted by Equation 7.1 has been carried out a reaction to form the product, P, takes place along with the regeneration of the enzyme. This is described by Equation 7.2 below.

$$ES \rightarrow E + P \tag{7.2}$$

In this equation the rate constants for the reaction is denoted k_3. Combining Equations 7.1 and 7.2 yields:

$$E + S \rightleftharpoons ES \rightarrow E + P \tag{7.3}$$

With the rate constants k_1, k_2 and k_3 described for Equations 7.1 and 7.2 still applying. The rate at which the product, P, is formed can be thus written according to equation 7.4 below.

$$R = k_3[ES] \tag{7.4}$$

The rate of breakdown of the enzyme complex, ES, can be described by Equation 7.5 below:

$$\text{Rate of breakdown of ES} = (k_2 + k_3)[ES] \tag{7.5}$$

Similarly the rate of formation of ES can be described written as:

$$\text{Rate of formation of ES} = (k_1)[ES] \tag{7.6}$$

At equilibrium the rate of formation of ES is equal to the rate of breakdown of ES. Thus combining Equations 7.5 and 7.6 yields Equation 7.7 below.

$$(k_1)[ES] = (k_2 + k_3)[ES] \tag{7.7}$$

or

$$[ES] = \frac{1}{\left(\frac{k_2 + k_3}{k_1}\right)}[E][S] \tag{7.8}$$

The expression $\left(\frac{k_2 + k_3}{k_1}\right)$ can then be defined as the Michaelis constant, K_m. Equation 7.8 can then be simplified to read:

$$[ES] = \frac{[E][S]}{K_M} \tag{7.9}$$

It is then noted that as the enzyme catalysis progresses the concentration of the enzyme must be defined as the initial concentration of the enzyme, E_T, less the concentration of the enzyme-substrate complex. This can be written as:

$$[E] = [E_T] - [ES] \tag{7.10}$$

Substituting Equation 7.10 into Equation 7.9 yields Equation 7.11.

$$[ES] = \frac{([E_T] - [ES])[S]}{K_M} \tag{7.11}$$

Rearranging for [ES] yields:

$$[ES] = [E_T]\left(\frac{[S]/K_M}{1+[S]/K_M}\right) \tag{7.12}$$

or

$$[ES] = [E_T]\left(\frac{[S]}{[S]+K_M}\right) \tag{7.13}$$

If the reaction rate, R, given by Equation 7.4 is substituted into Equation 7.13 this yields Equation 7.14 below.

$$R = k_3[E_T]\left(\frac{[S]}{[S]+K_M}\right) \tag{7.14}$$

Equation 7.14 above can be used to predict how the reaction rate, R, varies with the substrate concentration, [S]. Take the case where the concentration of substrate, [S], in solutions is very large, so much so that [S] >> K_m. here the rate of the enzyme catalysed reaction will be at its maximum. The term $\left(\frac{[S]}{[S]+K_M}\right)$ in Equation 7.14 reduces to unity and Equation 7.14 reduces to:

$$R_{max} = k_3[E_T] \tag{7.15}$$

Substituting Equation 7.15 into Equation 7.14 then yields Equation 7.16.

$$R = R_{\max}\left(\frac{[S]}{[S]+K_M}\right) \tag{7.16}$$

This equation is a fundamental equation governing the reaction kinetics of an enzyme catalysed reaction and is generally known as the Michaelis-Menten equation.

The case where the substrate concentration is much smaller than K_m may also be taken into account. In this case the ([S] + K_m) denominator in Equation 7.16 can be approximated as K_m. Equation 7.16 may then be written as:

$$R = \frac{R_{\max}[S]}{K_M} \tag{7.17}$$

This Equation 7.17 dictates that at low concentrations of substrate in solution the rate of the enzyme catalysed reaction is directly proportional to that substrate concentration.

Finally the case where the substrate concentration, [S], is equal to K_m may be considered. In this case the Equation 7.16 reduces to:

$$R = \frac{R_{\max}}{2} \tag{7.18}$$

Equation 7.18 dictates that when the solution substrate concentration is equal to K_m the reaction rate will be half of its maximum possible value. Lyons[6] has previously described, theoretically, a Michaelis-Menten analysis of a system taking into account the effect of diffusion of the solution phase redox mediator on the reaction flux. This analysis is quite involved however and for simplicity the standard Michaelis-Menten analysis will be applied.

A Michaelis-Menten analysis was carried out on the SAM/glucose oxidase system using CO_2H terminated SAM as well as the case of a bare gold electrode modified with glucose oxidase only for comparison. This was carried out by the additions of known quantities of glucose to an electrolyte solution and measuring the response of an electrode modified with the SAM/glucose oxidase system. The additions of glucose were made whilst the electrode was held at a potential of 0.6V vs. Ag/AgCl which was a potential deemed suitable for the catalysis of solution phase

glucose as determined from Figure 7.10(a). The response of the electrode to this system is shown below in Figure 7.11. Each step in Figure 7.11 represents the addition of a specific aliquot of glucose solution. It can be noted that the response of the system is quite fast as the steps occur almost immediately upon addition of the glucose under the conditions of this experiment. From this trace a plot of the steady state current against the glucose concentration may be plotted as the electrochemical equivalent of the Michaelis-Menten plot. This is shown in Figure 7.12.

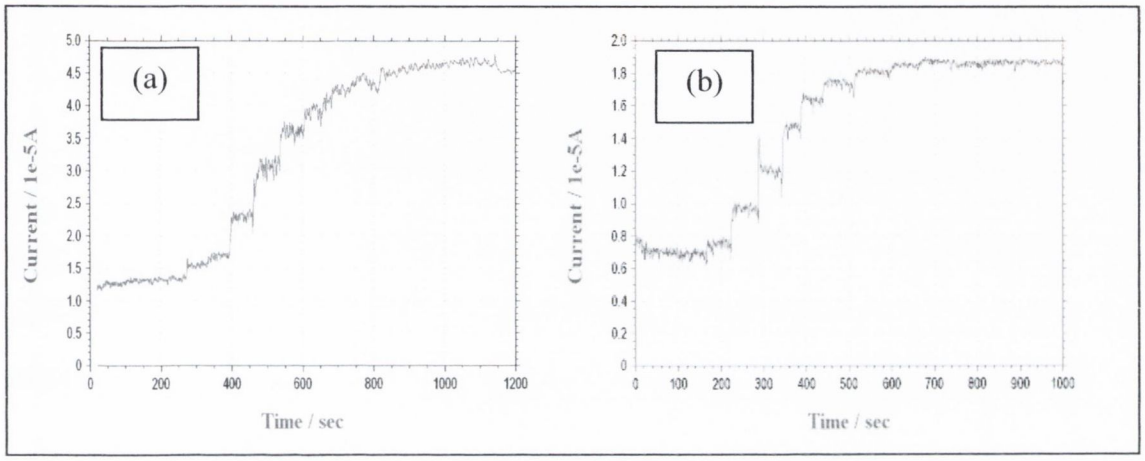


Figure 7.11. Amperometric response of a bare gold electrode modified with a (a) SAM-CO_2H/glucose oxidase layer and (b) glucose oxidase only to the serial addition of glucose to a stirred solution of 1mM ferrocene carboxylic acid. The electrode potential was held at 0.6V vs. Ag/AgCl.

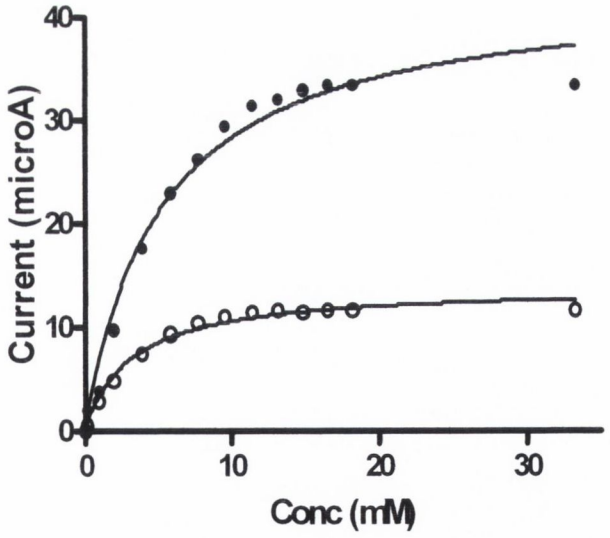


Figure 7.12. Comparison of the steady state current against concentration from the amperometric response in Figure 7.11. (o) Au/glucose oxidase, (•) Au/SAM-CO_2H/glucose oxidase.

The data in Figure 7.12 has been fitted to the Michaelis-Menten equation governing enzyme kinetics described by Equation 7.16 in this report. From this fitting values of V_{max} and K_m can be determined. These values are displayed below in Table 7.2.

	V_{max}(A)	K_m(mM)
Au/Glucose Oxidase	19	1.5
Au/ SAM-CO_2H/Glucose Oxidase	43	5.2

Table 7.2. Comparison of the V_{max} and K_m values determined from Figure 7.12.

The response described in Figure 7.12 is exactly that predicted by Bourdillion et al.[7] who examined the response of a glucose oxidase layer immobilised onto a glassy carbon electrode. In this work Equation 7.19 below is derived to describe the amperometric response of an enzyme-catalysed reaction between two substrates.

$$J = \frac{J_{\max}}{1 + \frac{K_1}{S_1^0} + \frac{K_2}{S_2^0}} \tag{7.19}$$

where J is the product flux, J_{max} is the maximum chemical flux when the enzyme is working under zero-order kinetics, K_1 and K_2 are the Michaelis constants for oxygen and glucose respectively S_1^0 and S_2^0 are the substrate concentrations. This equation can be written in a more appropriate manner to deal with the system considered in this study, i.e. with the use of $FcCO_2H$ as a redox mediator as:

$$I = \frac{I_{\max}}{1 + \frac{K_{glu}}{C_{glu}} + \frac{K_{FCA}}{C_{FCA}}} \tag{7.20}$$

According to Equation 7.20, at low glucose concentrations the response of the electrode is expected to be linear with a slope of I_{mzx}/K_{glu} and at high glucose concentrations a limiting current response is expected with half the limiting current when $K_{glu}/C_{glu} = 1 + (K_{FCA}/C_{FCA})$. Although this analysis will not be expanded upon here it is reasonable to arrive at the conclusion, from inspection of Figure 7.12, that

the overall characteristics of the analysis presented by Bourdillion in Equation 7.10 are being adhered to. i.e. an initial period of linearity corresponding to low substrate concentrations followed by the onset of a limiting current corresponding to high glucose concentrations.

Following this analysis the effect of the mediator concentration on the amperometry response was measured. The results of this analysis is shown below in Figure 7.13.

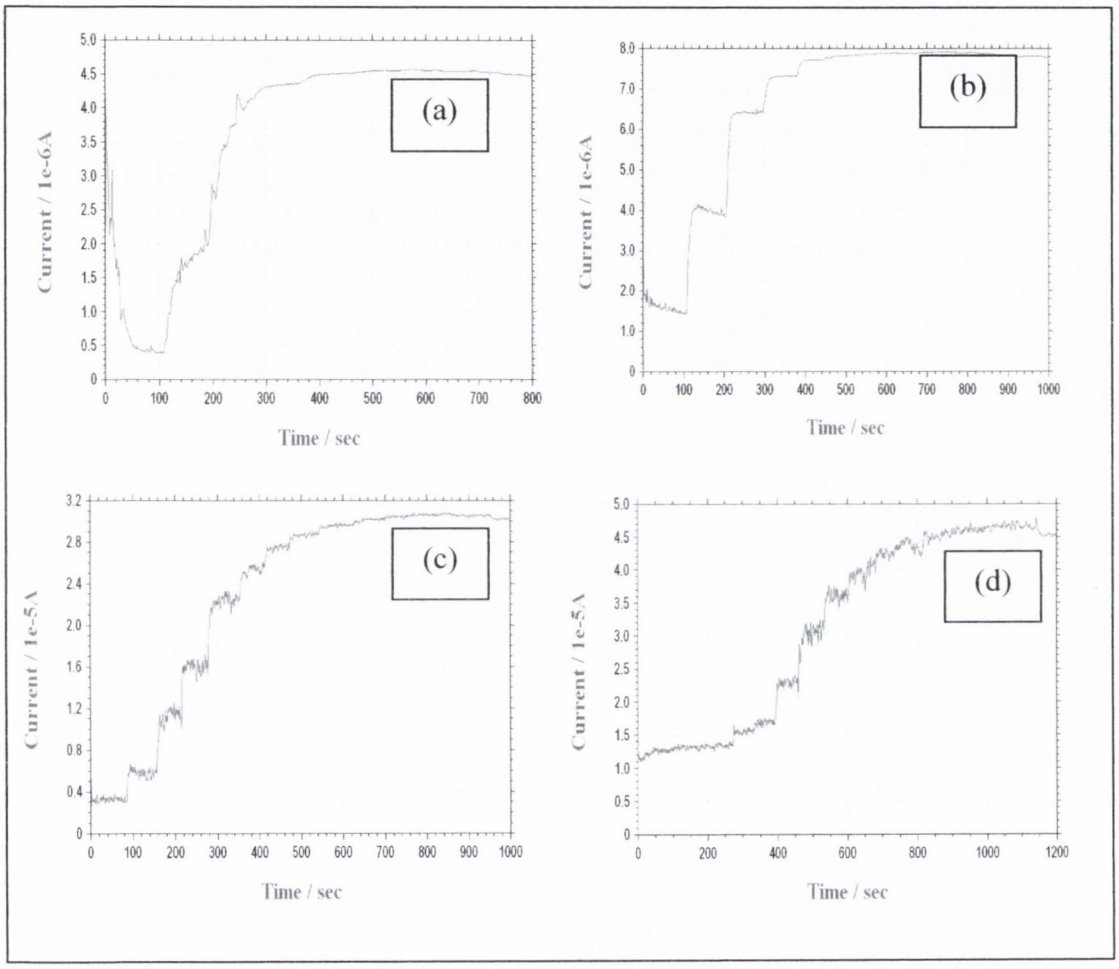


Figure 7.13. Amperometric response of a bare gold electrode modified with a SAM-CO_2H/glucose oxidase layer to the serial addition of glucose with varying concentrations of solution phase redox mediator. (a) 0.25mM $FcCO_2H$ (b) 0.5mM $FcCO_2H$ (c) 0.75mM $FcCO_2H$ and (d) 1mM $FcCO_2H$. The electrode potential was held at 0.6V vs. Ag/AgCl.

From the responses in Figure 7.13 a Michaelis-Menten analysis could again be carried out. This analysis is shown for the four mediator concentrations in Figure 7.14 below.

From this fitting values of V_{max} and K_m could be calculated for the four mediator concentrations. These values are presented in Table 7.3.

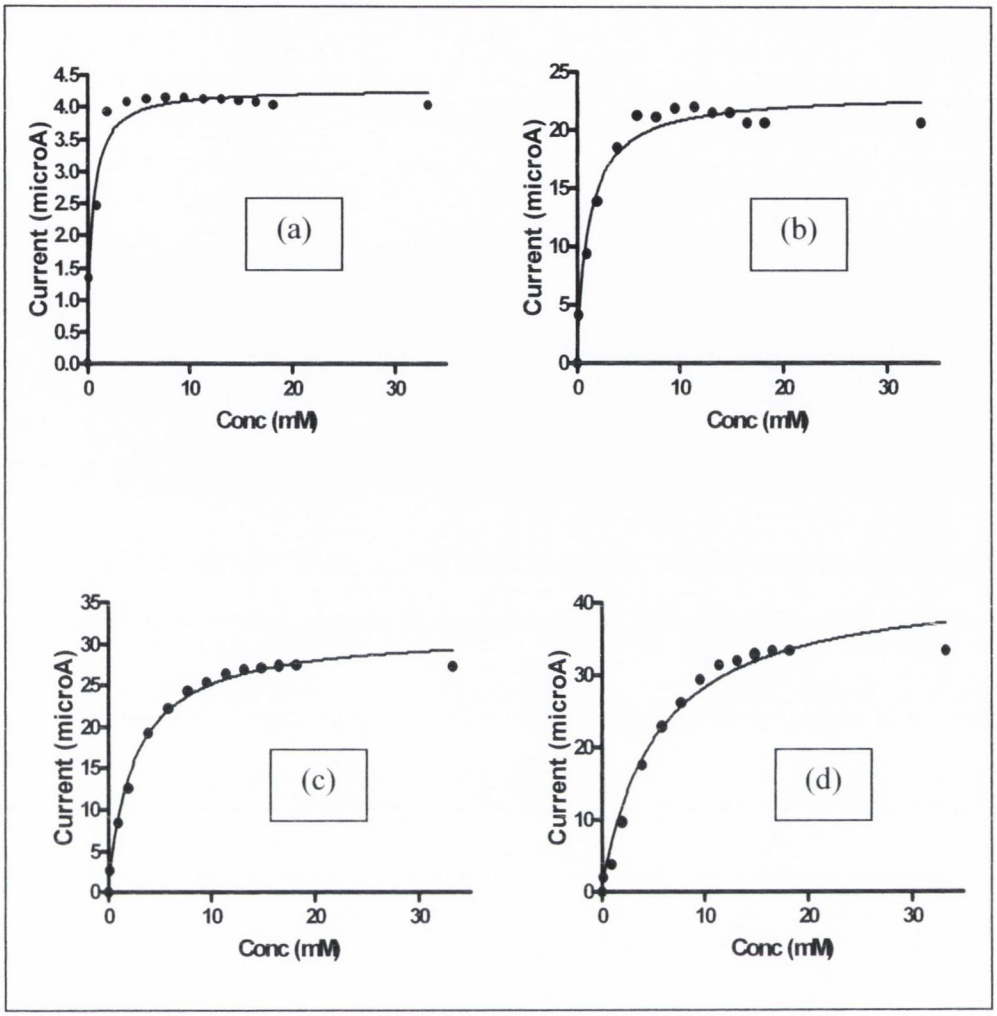


Figure 7.14. Michaelis-Menten fitting of the steady state response to the serial addition of glucose to a solution of varying mediator concentration. (a) 0.25mM $FcCO_2H$ (b) 0.5mM $FcCO_2H$ (c) 0.75mM $FcCO_2H$ and (d) 1mM $FcCO_2H$.

Mediator Concentration	V_{max}(A)	K_m(mM)
0.25mM	4.9	0.46
0.5mM	23.1	1.13
0.75mM	31.5	2.5
1mM	43.1	5.2

Table 7.3. Comparison of the V_{max} and K_m values for different mediator concentrations determined from Figure 7.14.

Firstly it is noted from Table 7.3 above that the limiting current increases as the concentration of mediator in solution increases. As well as this the value of the Michaelis-Menten constant, K_m, which is essentially an indication of the affinity between the enzyme and the substrate, is seen to rise as the mediator concentration increases. A small value of K_m indicates that there is a large degree of association between the enzyme and the substrate meaning that little product is formed. It is noted that as the mediator concentration increases, the value of K_m decreases, indicating that the formation of product is more facile at higher mediator concentrations. This result would point to the fact that the interaction between the reduced form of the enzyme and the oxidised form of the redox mediator (as described in Scheme 7.1(2)) is at least partly rate limiting in this system.

7.3.2 Cytochrome c

The previous section of the report investigated a system of glucose oxidase immobilised atop of a self-assembled monolayer. It was shown in this case that an amplification of the sensitivity of electrodes modified in this manner to the presence of glucose in solution was observed relative to the bare gold electrode. This section will attempt to design a similar system involving the cytochrome c enzyme from horse heart with the hope of developing an electrochemical system capable of displaying improved electron transfer characteristics relative to the bare gold electrode.

Figure 7.15 below shows the response of a bare gold electrode that has been modified with a coating of cytochrome c (Au/cyt c).

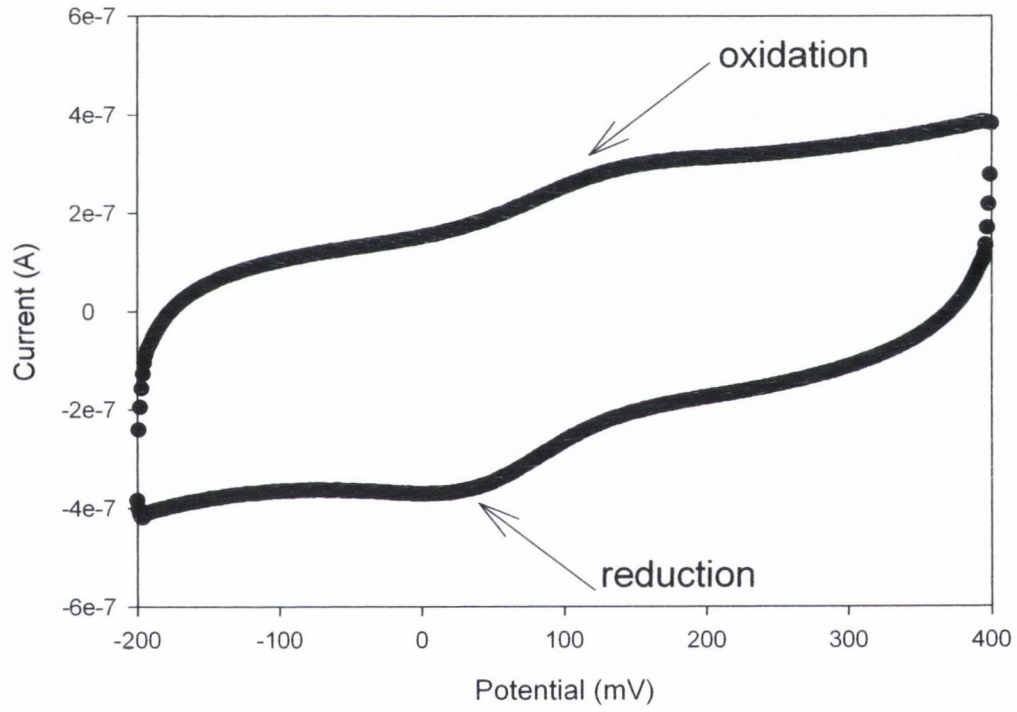


Figure 7.15. Response of an gold electrode modified with a layer of cytochrome c. The scan was carried out in 4.4mM potassium phosphate buffer, pH 7.4, ionic strength(μ) = 10mM. Scan rate $0.1 Vs^{-1}$.

Peaks corresponding to the quasi-reversible oxidation and reduction of the heme group of the cytochrome c enzyme are visible and are depicted by arrows in Figure 7.15. The diagnostics for the cyclic voltammetry response in Figure 7.11 are shown in Table 7.4.

Anodic Peak Current (A) ($x10^{-8}$)	Cathodic Peak Current (A) ($x10^{-8}$)	E_{Pa} (mV)	E_{Pc} (mV)	E^0 (mV)	$E_{Pa} - E_{Pc}$ (mV)	$\frac{i_p^{ox}}{i_p^{red}}$
5.5	8.9	142	29	85.5	113	0.6

Table 7.4 Diagnostics corresponding to the cyclic voltammetry responses in Figure 7.11.

The diagnostics in Table 7.4 immediately suggest that the oxidation/reduction of the cytochrome c molecules deposited on the bare gold electrode is sluggish and only quasi-reversible. The value of 113mV for the potential difference between the oxidation and reduction peaks is almost twice the ideal 59 mV expected for a one electron transfer. As well as this the ratio of the oxidative peak current to the reductive peak current is 0.6, much smaller than the ideal value of unity for completely reversible electron transfer. Thus the observations noted earlier that cytochrome c is denatured somewhat at Au surfaces would appear to be confirmed.

The surface coverage of cytochrome c deposited onto the bare gold electrode surface could be determined by integration under the oxidation peak to determine the charge. The charge was found to be 3.4 x 10^{-8}C which corresponded to a surface coverage of 11.5pmol cm^{-2}. This value is within reasonable experimental error of the theoretical surface coverage of a monolayer of cytochrome c molecules of 15 pmol cm^{-2} as determined by Song et al.[5] by assuming an area of 1000Å^2 / molecule. It must be noted however that this value only takes into account cytochrome c molecules that are detectably electroactive at the electrode surface.

This may be compared to the response of a bare gold electrode in the phosphate buffer. This comparison is shown in Figure 7.16 below. Here the response of the bare gold electrode is shown as a dark trace and the response of the electrode modified with cytochrome c, as in Figure 7.15, is shown as the light trace. Firstly it is important to note that the response of the bare gold electrode does not exhibit any peaks in the presence of the buffer solution thus it is not possible to confuse the peaks that are present in the case of the cytochrome c modified electrode (Figure 7.15) with any reversible solution ion activity. Secondly, it is obvious from Figure 7.16 that the layer of cytochrome c deposited on the gold surface provides a barrier to the redox activity of solution ions in the buffer solution with the electrode surface. This is evident in the lack of charging current observed in the case of the cytochrome c

modified electrode between approximately –200 to –100mV vs. Ag/AgCl relative to the unmodified electrode and the decrease in the redox activity of the solution ions at the electrode surface above this potential. The decrease in the observed charging current is likely to arise from similar reasons to the decrease associated with the deposition of a self-assembled monolayer onto the electrode surface (See *Section 1.2.7.2*).

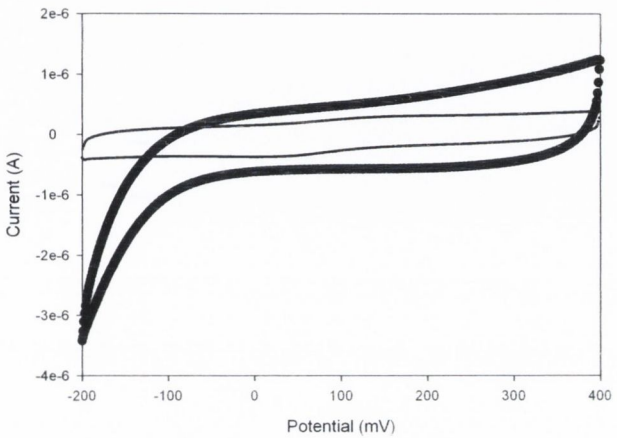


Figure 7.16. Comparison of the response of a bare gold electrode (dark trace) and the response of a gold electrode modified with a layer of cytochrome c (light trace). The scan was carried out in 4.4mM potassium phosphate buffer, pH 7.4, μ = 10mM. Scan Rate 0.1Vs^{-1}.

7.3.2.1 SAM/Cytochrome c System.

As mentioned previously, the aim of this section was to use self-assembled monolayers as a platform to design a system capable of improved electrical response with a view to furthering the understanding of the redox processes occurring in cytochrome c. The response of an electrode modified with a self-assembled monolayer with cytochrome c deposited on top of the monolayer is shown below in Figure 7.17. Before discussing the deposition of cytochrome c molecules onto the surface of the self-assembled monolayers with differing headgroups it is necessary to briefly discuss the chemistry of the cytochrome c molecule. The structure of cytochrome c has been described in detail previously[9,10]. Cytochrome *c* consists of a single polypeptide chain of 104 amino acids which are covalently attached to a heme group. The heme group is surrounded by tightly packed hydrophobic side chains. Only one edge of the planar heme ring is accessible to the surface. The cationic side chains of several lysine and arginine residues are clustered at the surface on one face of the molecule. The molecule is particularly rich in lysine. On the opposing face of

the molecule, a cluster of anionic residues including glutamic and aspartic acids exist. Cytochrome *c* has 19 positively charged lysine residues, plus two arginines also positively charged, but only 12 acidic residues (aspartic or glutamic acids). Because of this the surface of the cytochrome c molecule is likely to bear a positive charge. This charge must be taken into account when discussing the deposition of cytochrome c onto a SAM modified surface. The deposition and resulting electron-transfer characteristics of the cytochrome c molecules residing on the SAMs with CH_3, NH_2 and CO_2H headgroups will now be examined.

Au/SAM-CH_3/cytochrome c system. It can be seen from Figure 7.17(a) below that no cytochrome c appears to be deposited atop of the CH_3 terminated SAM. A CH_3 terminated SAM is likely to impart hydrophobic surface chemistry to the electrode surface. It would appear that it is not favourable for the positively charged cytochrome c protein shell to deposit on to the surface of this SAM.

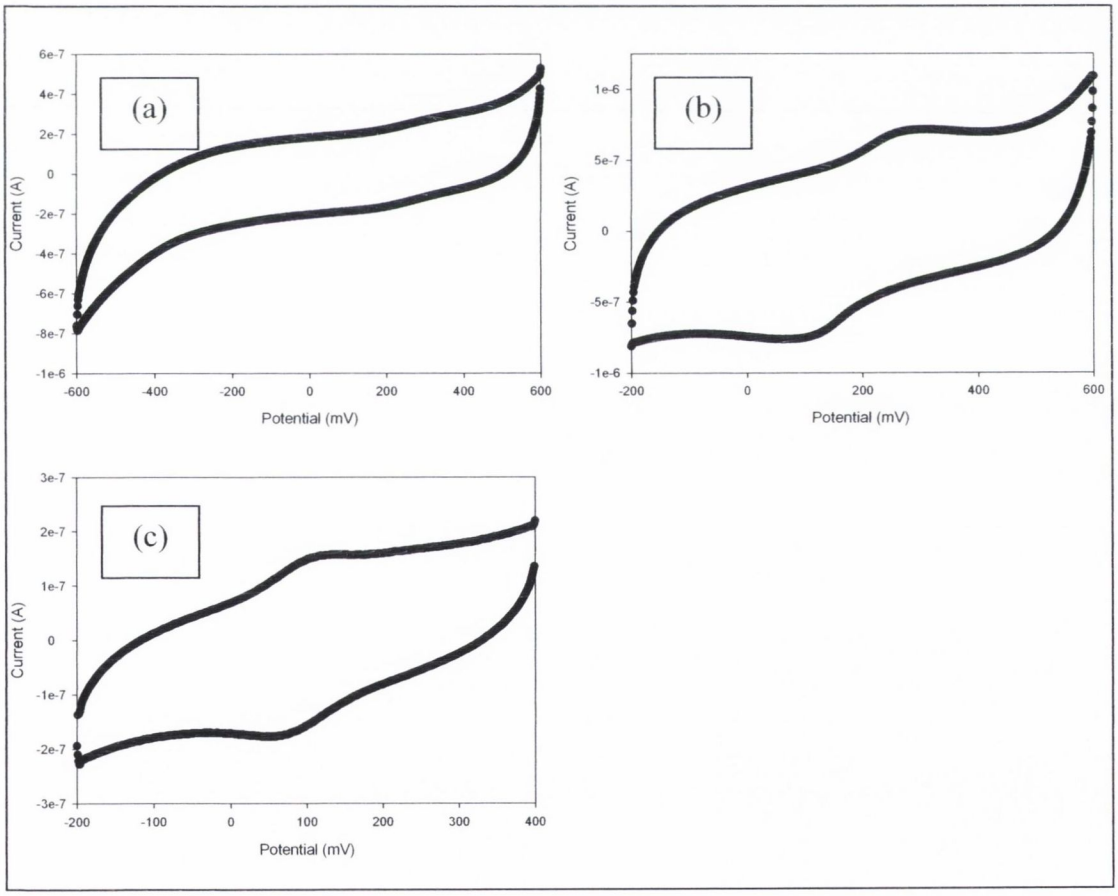


Figure 7.17. The response of an electrode modified with cytochrome c deposited on top of (a) CH_3, (b) NH_2 and (c) CO_2H terminated SAMs. The scan was carried out in 4.4mM potassium phosphate buffer, pH 7.4, μ = 10mM. Scan rate $0.1 Vs^{-1}$.

Au/SAM-NH_2/cytochrome c system. Figure 7.17(b) depicts the response of an electrode modified with an NH_2 terminated SAM upon which cytochrome c molecules have been deposited. Firstly it is noted that cytochrome c molecules are definitely deposited onto the surface unlike the case of the CH_3 terminated SAM. The deposition of an NH_2 terminated SAM is likely to generate a positive charge to the surface of the electrode[11]. Taking into account the positive charge of the cytochrome c shell it is strange that cytochrome c molecules are deposited onto this surface. One possible explanation is that the anionic glutamic and aspartic acids of the protein shell are attracted to the positively charged surface and induce surface binding. Integration of the oxidative peak in for the Au/SAM-NH_2/cytochrome c system yields a charge of 7.6×10^{-8} C which corresponds to a surface coverage of 25.9 pmol cm^{-2}. This value is almost twice the theoretical value of 15 pmol cm^{-2} quoted earlier. This increased surface coverage is likely to be due to increased surface roughness at the electrode surface. It is still reasonable to conclude that the observed peaks are due to the redox activity of adsorbed cytochrome c molecules. The diagnostics for the cyclic voltammetry of the Au/SAM-NH_2/cytochrome c system are given in Table 7.5. Standard tests for reversibility can again be commented upon here. A large separation between the oxidative and reductive peak potential is evident (158mV) indicating only quasi-reversibility of this system. As well as this the ratio of the oxidative to the reductive peak current is less than unity (0.59) which again indicates that the system is not fully reversible. Another notable point is that the formal potential (E^0) was determined as 189mV vs. Ag/AgCl for the Au/SAM-NH_2/cytochrome c system. It is instructive to compare this potential to that determined in Table 7.4 for bare gold which is 85.5mV. It can be thus determined that cytochrome c adsorbed on top of an NH_2 terminated SAM is a good deal more difficult to oxidise/reduce than in the case where the cytochrome c is deposited directly onto the electrode surface. This observation would seem to suggest that the cytochrome c might be denatured when adsorbed onto this surface due to the positively charged surface leading to a less facile orientation of the heme group relative to the electrode surface. Also it is possible that the negatively charged aspartic or glutamic acids have bound to the positively charged surface of the SAM leading to the cytochrome c molecules adsorbed in an orientation unfavourable to electron transfer.

	Anodic Peak Current (A) ($x10^{-6}$)	Cathodic Peak Current (A) ($x10^{-6}$)	E_{Pa} (mV)	E_{Pc} (mV)	$E_{Pa} - E_{Pc}$ (mV)	E^0 (mV)	$\frac{i_p^{ox}}{i_p^{red}}$
NH_2 terminated SAM	0.13	-0.22	268	110	158	189	0.59
CO_2H terminated SAM	0.98	-0.86	134	61	73	98	1.1

Table 7.5. Diagnostics corresponding to the cyclic voltammetry responses in Figure 7.17. Not included are any diagnostics corresponding to a gold electrode modified with a CH_3 terminated SAM (Figure 7.17(a)) as this response is featureless.

Au/SAM-CO_2H/cytochrome c system. Figure 7.17(c) depicts the response of an electrode modified with an CO_2H terminated SAM upon which cytochrome c molecules have been deposited. The deposition of a CO_2H terminated SAM will impart a negative charge to the electrode surface[12]. Because of this negative charge it is to be expected that some cytochrome c molecules would be deposited onto the surface. Integration of the current under the oxidation peak of Figure 7.17(c) yields a charge of 6.9 x 10^{-8} C which corresponds to a surface coverage of 22.7 pmol cm^{-2} which is slightly lower than that observed for the NH_2 terminated SAM system. The diagnostics for the cyclic voltammetry of the Au/SAM-CO_2H/cytochrome c system are given in Table 7.5. Again the standard tests for reversibility can be carried out. The potential difference between the oxidation and reduction processes is 73mV. Although this is still greater than the ideal peak separation of 0mV for a reversible system it still represents an improvement on the Au/SAM-NH_2/cytochrome c system which yielded a peak separation of 158mV. It also represents an improvement to the case where cytochrome c was adsorbed directly onto the gold electrode (113mV, Table 7.4). As well as this the ratio of the oxidative to the reductive peak current is 1.1 much closer to the ideal value of unity than in the case of either the Au/SAM-NH_2/cytochrome c system or the Au/cytochrome c system which yielded values of 0.59 and 0.6 respectively. Again the formal potential of this system is instructive. For this system the formal potential is found to be 98mV. This value of formal potential is lower than either the Au/SAM-NH_2/cytochrome c system or the Au/cytochrome c system which yielded values of 158mV and 113mV respectively. Thus it is noted that the oxidation/reduction of the cytochrome c when deposited upon a CO_2H terminated layer is more facile than in the case of either the Au/SAM-NH_2/cytochrome c system

or the Au/cytochrome c system. This leads to the conclusion that the cytochrome c molecules are orientated in a manner suitable for electron transfer. It is likely that the plentiful, positively charged lysine groups are strongly bound electrostatically to the negatively charged monolayer surface.

One final point of note can be gained by observation of Figure 7.18 below. This figure compares the response of the Au/SAM-CO_2H/cytochrome c system and the Au/cytochrome c system. It is noted that a much larger charging current occurs in the absence of the self-assembled monolayer between the gold electrode and the cytochrome c molecules. This would indicate that, as well as having an effect on the orientation of the cytochrome c molecules on the surface, the SAM also presents a barrier to the migration and corresponding reaction of solution molecules at the surface of the electrode. Thus it is likely that the presence of the SAM also isolates the electron transfer processes occurring in the cytochrome c molecules from others that are coincidentally occurring in the system.

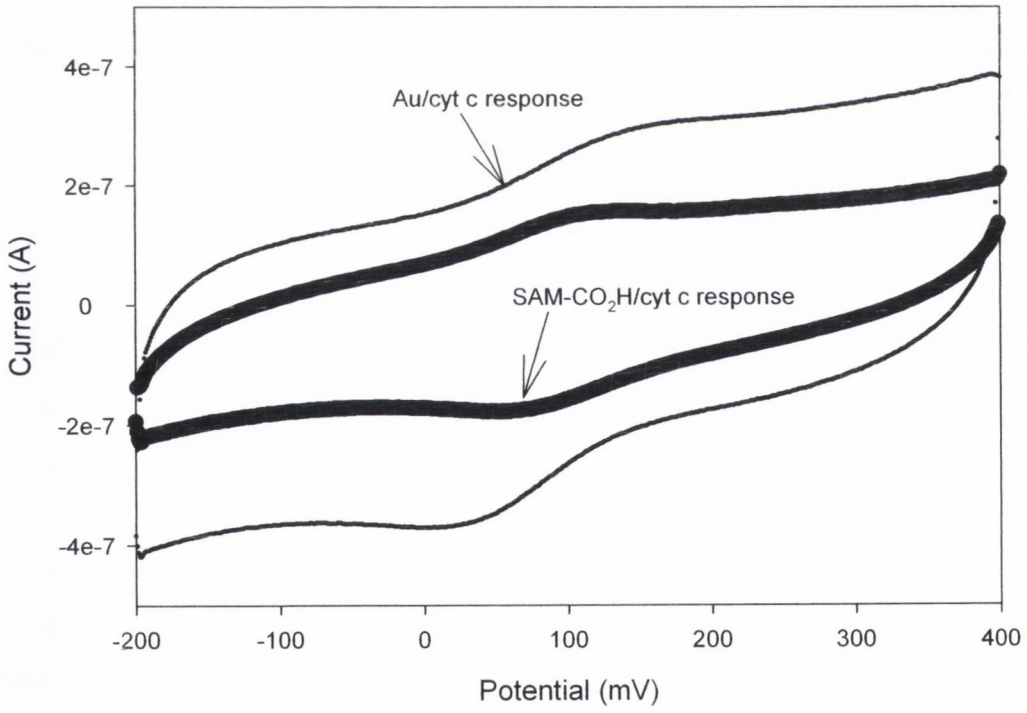


Figure 7.18. Comparison of the response of a bare gold electrode modified with cytochrome c and one modified with cytochrome c deposited on top of a CO_2H terminated SAMs. The scan was carried out in 4.4mM potassium phosphate buffer, pH 7.4, μ = 10mM. Scan rate $0.1Vs^{-1}$.

Thus far it has been established that it is possible to deposit cytochrome c molecules onto bare gold electrodes, onto gold electrodes modified with NH_2 and CO_2H terminated self-assembled monolayers. It has been shown that cytochrome c does not deposit onto a CH_3 terminated self-assembled monolayer under the above conditions. Examination of the voltammetry produced in Figure 7.17 yielded some insight into the nature of the adsorption of the cytochrome c molecules. Cytochrome c molecules deposited onto a SAM terminated with a CO_2H group were shown to exhibit the most reversible electron transfer characteristics. The next most reversible electron transfer was observed when the cytochrome c directly adsorbed onto the gold electrode surface. Cytochrome c adsorbed onto the NH_2 was shown to exhibit the least reversible electron transfer most likely owing to denaturing interactions between the positively charged lysine groups and the positively charged surface or interactions between the negatively charged aspartic or glutamic acids and the surface resulting in an unfavourable conformation of the heme group for electron transfer.

Finally it was noted that the presence of the self-assembled monolayer had the effect of minimising the redox activity of solution ions thus increasing the selectivity of the system towards the electron transfer processes occurring due to the oxidation/reduction of the cytochrome c heme group.

7.3.2.2 Electron Transfer Rates.

It has been postulated thus far that the adsorption of cytochrome c onto the surface of self-assembled monolayers causes the enzyme to lie in a particular orientation dependant on the headgroup chemistry of the relevant SAM. It is instructive to examine the electron transfer rates between the heme group of the cytochrome c molecule and the electrode surface when the cytochrome c has been deposited on these electrode surfaces. The chronoamperometry responses over the oxidative peak of cytochrome c deposited onto gold and NH_2 and CO_2H terminated SAMs corresponding to the traces in Figure 7.15 and 7.17(b) and (c) respectively are shown below in Figure 7.19. Again the response of the electrode modified with a CH_3 terminated SAM is omitted because no cytochrome c was seen to be deposited in this case.

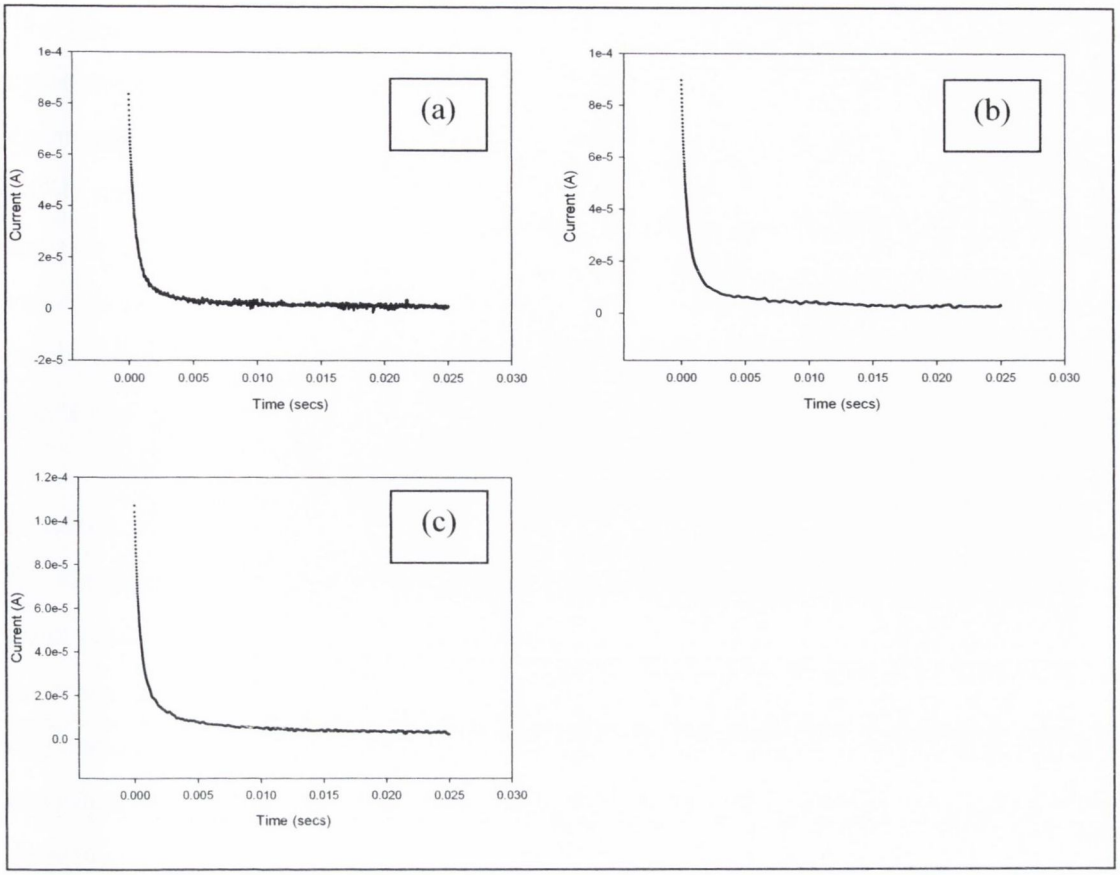


Figure 7.19. Chronoamperometry response of various electrodes modified with cytochrome c deposited on top of (a) bare Au electrode and (b) NH_2 and (c) CO_2H terminated SAMs. The scan was carried out in 4.4mM potassium phosphate buffer, pH 7.4, μ = 10mM.

The electron transfer rate constants are calculated according to the procedure described in *Section 3.3.4* for the three cases shown in Figure 7.19 above. These are presented in Table 7.6 below.

Electron Transfer Rate Constants (s^{-1})		
	Region 1	**Region 2**
Bare Au	982	58
CO_2H terminated SAM	855	41
NH_2 terminated SAM	772	14

Table 7.6. The electron transfer rate constants extracted from the oxidative chronoamperometry response of an Au/cyt c, Au/cyt c/SAM-NH_2 and a Au/cyt c/SAM-CO_2H modified electrode. Five values for each chain length are calculated owing to the intrinsic dispersion of rate constants throughout the layer.

The first thing to note from the electron transfer rates reported in Table 7.6 is that cytochrome c molecules deposited onto the bare gold electrode exhibit the highest electron transfer rates. This is followed in magnitude by the system of Au/cyt c/SAM-CO_2H and finally by Au/cyt c/SAM-NH_2. It is to be expected that the highest electron transfer rates are attributed to the cytochrome c molecules deposited onto bare gold, since, as it has been discussed previously in this work that the rate of electron transfer is hindered to an extent by the presence of an alkane spacer between the electron donor and acceptor (See *Section 3.3.4, Figure 3.11).*

The main point to take from this section however is that even with the presence of the self-assembled monolayers between the cytochrome c molecules and the electrode surface, the rates of electron transfer are not drastically affected. This point taken in tandem with the previously shown ability of self-assembled monolayers to improve the overall reversibility of the electron transfer processes between the cytochrome c molecules and the electrode surface, still makes self-assembled monolayers an attractive choice for substrate modification prior to cytochrome c deposition.

7.4 Conclusion

This work has utilised cyclic voltammetry (CV), chronoamperometry (CA) and amperomtery to study the ability of self-assembled monolayers to tailor the chemistry of an electrode surface as a platform upon which to deposit enzyme molecules with a view to improved enzyme stability and electrical communication between the enzyme and the electrode surface. The study has focused on two enzymes namely glucose oxidase and cytochrome c. The systems developed in the study of either enzyme were different in each case.

In the case of the glucose oxidase enzyme the system developed was done so with a view to improving the glucose sensing performance of the glucose oxidase enzyme deposited on an electrode surface.

In the case of the cytochrome c enzyme the system developed was somewhat simpler and involved only the attempt to improve the electron transfer characteristics between the heme centre of the cytochrome c molecule and the electrode surface. This is because the ability to donate and accept electrons is central to the biological action of cytochrome c molecules.

In the case of the glucose oxidase system a number of findings were presented. Firstly the ability of self-assembled monolayers of differing headgroup chemistry, namely CH_3, NH_2 and CO_2H terminated SAMs, to screen the electrochemical activity of uric and ascorbic acid, which are typical interferers in glucose sensors was demonstrated. However it was also demonstrated that self-assembled monolayers screened the activity of hydrogen peroxide which is central to the operation of conventional biosensors. The screening properties of the SAMs pointed to the need for a redox mediator to shuttle charge back and forth between the enzyme and the electrode. It was determined that ferrocene carboxylic acid could be used as this mediator providing the SAM had either NH_2 or CO_2H headgroups. Thus a system was developed in which glucose oxidase was deposited atop of SAMs bearing either of the aforementioned headgroups. Such systems showed the ability to detect the presence of glucose in solution using $FcCO_2H$ as the redox mediator The system utilising a CO_2H terminated SAM displayed slightly better detection quality with regard to electrochemical signal. This was followed by observing the response of the CO_2H terminated system to the addition of small quantities of glucose to an electrolyte solution using amperometry. It was shown that the system had the ability to sense

millimolar quantities of glucose almost immediately upon addition. The system was shown to adhere to the traditional Michaelis-Menten analysis. An improved response level was observed when comparing glucose oxidase deposited atop of a SAM modified electrode relative to glucose oxidase deposited directly onto a bare gold surface. It is likely that this is due to a denaturing of the enzyme when in contact with the gold surface. The effect of redox mediator concentration on the response of the system was also investigated. It was determined that higher concentrations of redox mediators led to an improved amperometric response. As well as this the value of the Michaelis constant, K_m, was seen to increase as the concentration of mediator in solution increased. This observation indicated that as the concentration of the mediator increased the conversion of the enzyme-substrate into product became more facile.

Following the development of the glucose oxidase system the voltammetry of the cytochrome c enzyme deposited atop of a SAMs bearing differing headgroups was examined. In this study cytochrome c was deposited atop of electrodes modified with CH_3, NH_2 and CO_2H terminated SAMs. The voltammetric response of such electrodes was compared with that of cytochrome c deposited onto an unmodified gold electrode. It was determined that cytochrome c absorbed onto electrodes modified with both NH_2 and CO_2H terminated SAMs however it did not adsorb onto electrodes modified with CH_3 terminated SAMs. The reason for these observations is thought to accrue from the fact that that CO_2H and NH_2 headgroups impart negative and positively charged surface chemistries respectively. The imparted charge is thought to interact with certain sections of the cytochrome c protein shell. The neutral CH_3 terminated SAM is not thought to interact with the protein shell for this reason. It was found that the voltammetry of the CO_2H SAM exhibited the best reversibility. It was also determined that the presence of the alkane linker in such SAMs is responsible for a diminishment of the charging current observed during voltammetry as it presents a barrier to the redox reaction of solution ions with the electrode surface.

Finally the electron transfer rates between the heme groups of the cytochrome c molecule and the electrode surface were examined. It was determined that the presence of the alkane spacer in the CO_2H and NH_2 terminated SAMs did not impede the electron transfer rates between the enzyme and the electrode to any great extent.

References

(1) C. Hinnen, C. Parsons and R. Nikki, *J. Electroanal. Chem*, **1983**, *147*, 329.

(2) D.E. Reed, F.M. Hawkridge, *Anal. Chem*. **1987**, *59*, 2334

(3) C. Bourdillon, C. Demaille,lb J. Cueris, J. Moiroux, J.-M. Sav6ant *J. Am. Chem. Soc.* **1993**,*115*, 12264.

(4) K. Yoneyama, E. Tamiya and I. Karube, *J. Electroanal. Chem*., **1989**, *273*, 107.

(5) S. Song, R. A. Clark E. F. Bowden and M. J. Tarlov. *J. Phys. Chem*. **1993**, *97*, 6564.

(6) M.E.G. Lyons, *Sensors,* **2003,** *3,* 19.

(7) C. Bourdillion, J.P. Bourgeois and D. Thomas, *J. Am. Chem. Soc.* **1980,** *102,* 4231

(8) G.E. Briggs, J.B.S. Haldane, *J. Biochem,* **1925,** *19*, 339.

(9) H.A. Harbury and P.A Loach, *J. Biol. Chem*. **1960**, 235, 3640.

(10) R.E Dickerson and R Timkovich,. *The Enzymes*. (P. Boyer Ed.) New York: Academic Press, **1975**

(11) P. Zhu, Y. Masuda and K. Koumoto, *Biomaterials*, **2004**, *17*, 3915.

(12) M. Agashe, V. Raut, S. J. Stuart, and R. A. Latour, *Langmuir* **2005,** *21,* 1103.

CHAPTER 8 –

GENERAL CONCLUSIONS AND FUTURE RECOMMENDATIONS

8. General Conclusions and Future Recommendations

8.1 General Conclusions

The vast majority of this work focused on the redox properties of electroactive self – assembled monolayers. This work was motivated by the need to expand the available knowledge regarding nanoscale systems. To highlight the importance of nanotechnology research it is noted that the Irish Council for Science, Technology and Innovation (ICSTI) has estimated that the area of nanotechnology could be worth approximately €13 billion to the Irish economy by 2010. It has been forecasted that the nanotechnology industry worldwide may be worth up to $1 trillion by this time.

The first results section of this work (*Chapter 3*) characterised the electrochemistry of ferrocene terminated electroactive SAMs using both cyclic voltammetry (CV), chronoamperometry (CA) and an electrochemical quartz crystal microbalance (EQCM). The effect of chain length on monolayer quality was examined. Longer chains were found to pack more closely than shorter chains. Molecular interactions between the pendant electroactive groups were evaluated using a modified Brown-Anson model. It was found that molecular interactions between the pendant ferrocene groups increased as the close packing of the chains increased, i.e. with increasing chain length. Finally the dependence of the electron transfer rate on the length of the alkane linker between the electrode and the pendant electrode group was examined. It was determinaed that the addition of one CH_2 linker unit caused a 17% decrease in the electron transfer probability between the electrode surface and the pendant ferrocene groups.

The second results section of this work (*Chapter 4*) examined the adsorption characteristics of self-assembled monolayers using the electroactive ferrocene terminated molecules to effectively provide an electrochemical label of the presence of an alkanethiol molecule deposited onto the surface of the electrode. This work utilised both CV and an EQCM. The effect of alkane chain length, deposition solution temperature and deposition solution concentration was examined. A balancing act was observed between temperature and concentration for all alkane chain lengths. It was determined that a combination of low deposition solution concentration and high temperature produced either a poorly formed monolayer or no monolayer at all. It was feasible to form excellent quality monolayers at high concentrations and high temperatures. Effects due to alkane chain lengths were observed and it was found that

better packing was observed for longer chain lengths irrespective of solution concentration/temperature.

The third section of results (*Chapter 5*) focused on the development of a mixed monolayer system consisting of electroactive, ferrocene terminated molecules and insulating CH_3 terminated molecules. Two complimentary methods named 'place exchange' and 'coadsorption' were developed. A combination of CV and EQCM was used to monitor the formation of such mixed monolayers. Voltammetric analysis showed that the formation of such mixed monolayers led to an improvement in the ideality of the observed electron transfer processes. It was determined that the 'place exchange' method which involved incubating a fully formed insulating SAM in a solution of electroactive thiols was the best method to form such SAMs. This is because decreased quantities of water molecules were incorporated into the layer during this process relative to the 'coadsorption' mechanism.

The fourth section of results (*Chapter 6*) studies the effect of an externally applied magnetic field on the electron transfer properties of electroactive SAMs. A combination of CV, CA and EQCM was used to examine the system. Initially the effect of the magnetic field on electroactive SAMs of differing chain lengths and prepared from different solvents was examined. It was determined that the presence of the magnetic field had the effect of diminishing the observed surface coverage of electroactive molecules in all cases however no clear trend was identified. The effect of the magnetic field on the rate of electron transfer between the electrode and the pendant ferrocene molecules was also examined. It was determined that the magnetic field caused an increase in this rate. An EQCM was also employed to elucidate the effects of the magnetic field. It was determined that a decrease in the amount of solution anion-pendant electroactive group ion pairing events was observed upon application of the field. The effect of the orientation of the magnetic field with respect to the electrode surface was also examined. It was determined that magnetic field effects are only observed for the case of a magnetic field orientated parallel to the electrode surface. Some theories were put forward regarding the nature of the magnetic field effects. These theories involved comparing the application of the magnetic field to the formation of a mixed monolayer and the identification of the electrokinetic force that has the effect of stirring solution ions.

The fifth and final results section (*Chapter 7*) dealt with the immobilising enzymes atop of self-assembled monolayers. The oxidoreductases, glucose oxidase and cytochrome c were chosen for this purpose. Firstly the immobilisation of glucose oxidase was examined on SAMs of varying surface chemistry. It was determined that an improved response to solution phase glucose was obtained when the glucose oxidase was deposited onto a SAM bearing a CO_2H headgroup. Ferrocene carboxylic acid was used as a solution phase mediator. It was shown that the sensitivity of the system scaled with the concentration of the mediator as determined from a Michaelis-Menten analysis. Next the deposition of cytochrome c was examined. It was shown that cytochrome c deposited atop of a CO_2H terminated SAM displayed improved voltammetric characteristics relative to an NH_2 terminated SAM and a bare gold electrode. No cytochrome c was seen to be deposited atop of a CH_3 terminated SAM. The electron transfer rate constants between the cytochrome c molecules and the electrode surface were examined in the case of the CO_2H and NH_2 terminated SAMs and it was determined that the presence of the alkane spacer layer did not have a significant effect on this rate constant.

8.2 Future Recommendations

My recommendations regarding an this work would centre around the development of the theory regarding the magnetic field effects on the electron transport properties of the redox active self-assembled monolayers. This work has increased the amount of empirical data regarding the system as well as putting forward a number of possible explanations regarding the nature of the processes involved. However a definitive explanation of the magnetic field effects has yet to be put forward.

Apart from magnetic field effects a recommendation would be made to continue the development of enzyme deposition atop of self-assembled monolayers. Particular attention should be paid to the chemical and temporal stability of such systems particularly in the case of the glucose oxidase system which would be intended, ultimately, to be used in vivo.

APPENDIX

8Fc thiol - 0.01mM, 0.1mM and 1mM results

The results below are associated with section 4.3.1.1 of this thesis.

8Fc 0.01mM Results.

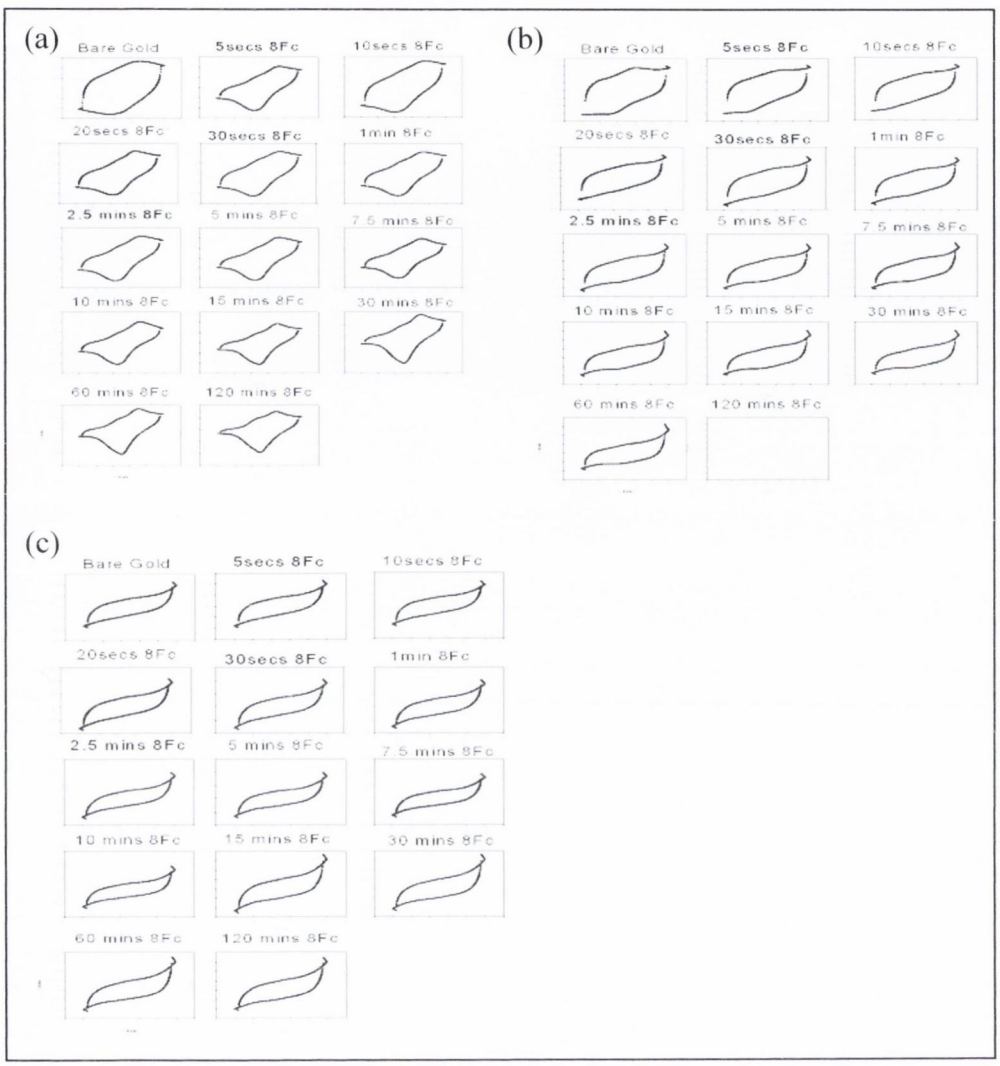


Figure 1. Cyclic voltammetry showing the deposition of 8Fc thiol from a 0.01mM solution at (a) Room Temperature, (b) 40°C and (c) 60°C. All scans were carried out in 0.1M $HClO_4$ at 0.02Vs^{-1} scan rate.

Immersion Time	Oxidation Potential (E_{ox})	Reduction Potential (E_{red})	I_{ox} x10-6 (A)	I_{red} x10-6 (A)	E^0 (V)	Peak Separation (mV)	PWHM (mV)	Surface Coverage ($x10^{-10}$ mol.cm^{-2})
0.00	--	--	--	--	--	--	--	0.00
5 secs	0.55	0.45	0.30	0.69	0.50	10.30	184	0.06
10 secs	0.55	0.46	0.25	0.37	0.51	13.40	52	0.14
20 secs	0.55	0.49	0.64	0.47	0.52	9.10	121	0.42
30 secs	0.56	0.49	0.44	0.47	0.53	11.60	97	0.33
1 min	0.57	0.50	0.53	0.68	0.54	10.90	139	0.48
2.5 mins	0.57	0.51	0.56	0.88	0.54	11.30	132	0.48
5 mins	--	--	--	--	--	--	--	-
7.5 mins	0.60	0.52	0.78	0.68	0.56	9.80	160	0.69
10 mins	0.61	0.52	0.69	0.71	0.57	9.90	125	0.60
15 mins	0.61	0.53	0.84	0.86	0.57	9.20	151	0.78
30 mins	0.64	0.54	0.94	0.88	0.59	6.10	162	0.70
60 mins	0.67	0.54	1.00	0.92	0.61	6.00	159	0.81
120 mins	0.66	0.55	0.87	0.80	0.61	6.40	170	0.69

Table 1 – Showing the cyclic voltammetry diagnostics for the deposition of an 8Fc thiol monolayer from a 0.01mM solution at room temperature

8Fc 0.1mM Results.

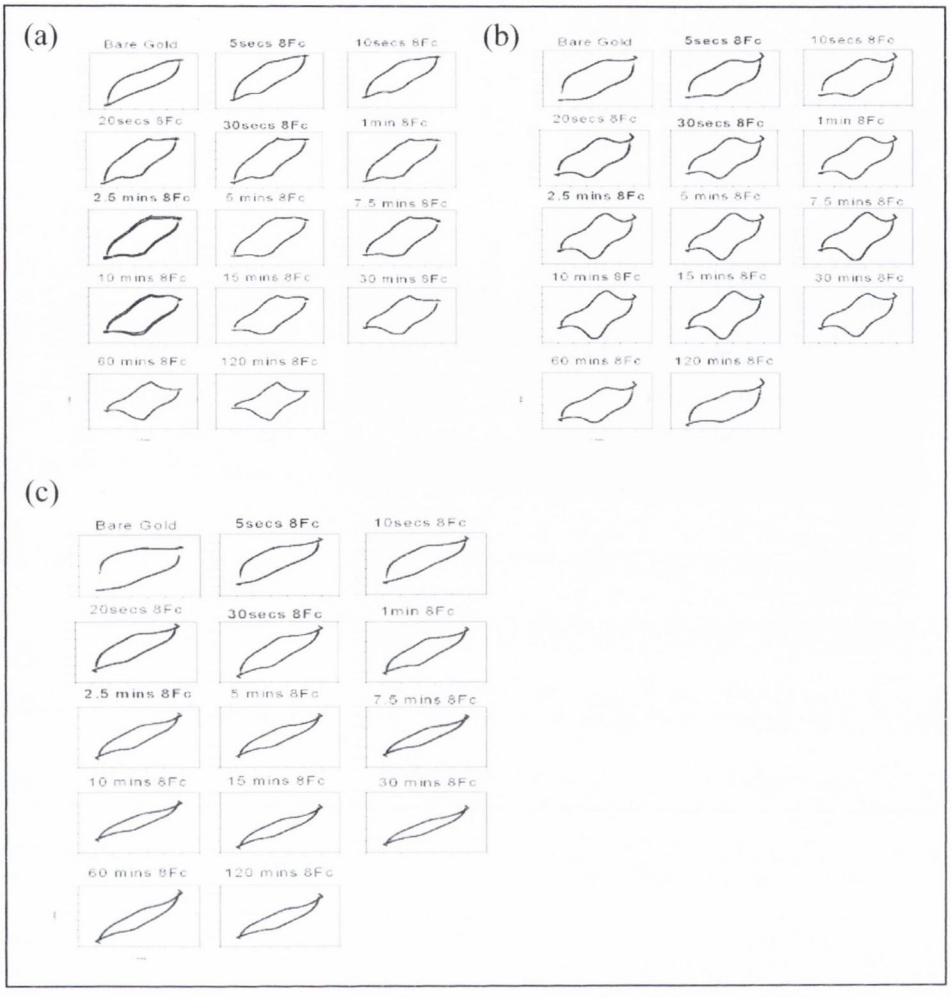


Figure 2. Cyclic voltammetry showing the deposition of 8Fc thiol from a 0.1mM solution at (a) Room Temperature, (b) 40°C and (c) 60°C. All scans were carried out in 0.1M $HClO_4$ at 0.02Vs^{-1} scan rate.

Immersion Time	Oxidation Potential (E_{ox})	Reduction Potential (E_{red})	I_{ox} x10-6 (A)	I_{red} x10-6 (A)	E^0 (V)	Peak Separation (mV)	PWHM (mV)	Surface Coverage ($x10^{-10}$ mol.cm^{-2})
0.00	--	--	--	--	--	--	--	0.00
5 secs	0.54	0.48	1.71	2.12	0.51	6.06	--	0.24
10 secs	0.56	0.49	1.82	2.06	0.52	7.25	--	0.30
20 secs	0.60	0.55	2.24	1.72	0.58	4.90	--	0.33
30 secs	0.60	0.55	2.29	1.80	0.58	5.02	--	0.58
1 min	0.60	0.55	2.22	1.78	0.58	4.97	--	0.45
2.5 mins	0.60	0.55	2.21	1.76	0.58	5.10	--	0.38
5 mins	0.60	0.49	2.13	2.04	0.55	11.76	198	0.44
7.5 mins	0.60	0.49	2.23	2.02	0.55	11.31	192	0.47
10 mins	0.60	0.49	2.18	2.02	0.55	11.50	192	0.48
15 mins	0.60	0.50	2.09	2.05	0.55	10.26	244	0.59
30 mins	0.60	0.52	2.10	1.99	0.56	7.98	96	0.53
60 mins	0.60	0.55	2.06	1.98	0.57	5.10	100	0.58
120 mins	0.70	0.55	2.04	2.09	0.62	14.64	106	0.75

Table 2 – Showing the cyclic voltammetry diagnostics for the deposition of an 8Fc thiol monolayer from a 0.1mM solution at room temperature

Immersion Time	Oxidation Potential (E_{ox})	Reduction Potential (E_{red})	I_{ox} x10-6 (A)	I_{red} x10-6 (A)	E^0 (V)	Peak Separation (mV)	PWHM (mV)	Surface Coverage ($x10^{-10}$ mol.cm^{-2})
0.00	--	--	--	--	--	--	--	0.00
5 secs	0.61	0.50	1.27	1.28	0.55	10.40	72	0.14
10 secs	0.62	0.50	1.33	1.35	0.56	11.11	92	0.12
20 secs	0.60	0.51	1.37	1.42	0.56	9.47	114	0.21
30 secs	0.61	0.52	1.41	1.47	0.56	9.02	92	0.27
1 min	0.61	0.52	1.49	1.55	0.56	8.88	102	0.29
2.5 mins	0.61	0.52	1.58	1.62	0.56	8.63	105	0.47
5 mins	0.61	0.52	1.63	1.68	0.57	8.36	115	0.45
7.5 mins	0.61	0.53	1.67	1.73	0.57	7.92	111	0.50
10 mins	0.61	0.53	1.69	1.73	0.57	7.65	111	0.53
15 mins	0.61	0.54	1.66	1.74	0.57	6.99	121	0.52
30 mins	0.61	0.54	1.47	1.58	0.57	6.86	117	0.40
60 mins	0.62	0.53	1.06	1.12	0.58	8.18	140	0.21
120 mins	0.62	0.53	1.69	0.69	0.57	8.98	indt	0.12

Table 3 – Showing the cyclic voltammetry diagnostics for the deposition of an 8Fc thiol monolayer from a 0.1mM solution at 40°C.

Immersion Time	Oxidation Potential (E_{ox})	Reduction Potential (E_{red})	I_{ox} x10-6 (A)	I_{red} x10-6 (A)	E^0 (V)	Peak Separation (mV)	PWHM (mV)	Surface Coverage ($x10^{-10}$ mol.cm^{-2})
0.00	0.50	--	--	--	--	--	--	0.22
5 secs	0.52	--	0.34	--	--	--	--	0.27
10 secs	0.54	0.51	0.52	0.24	0.51	1.10	--	0.40
20 secs	0.54	0.52	0.65	0.39	0.53	1.20	--	0.23
30 secs	0.54	0.52	0.55	0.45	0.53	1.70	--	0.45
1 min	0.54	0.53	0.56	0.50	0.53	0.10	--	0.30
2.5 mins	0.54	0.53	0.46	0.40	0.54	0.20	--	0.24
5 mins	0.54	0.54	0.36	0.31	0.54	-0.30	--	0.20
7.5 mins	0.54	0.54	0.36	0.30	0.54	0.10	--	0.17
10 mins	0.54	0.54	0.33	0.24	0.54	0.00	--	0.14
15 mins	0.54	0.54	0.24	0.17	0.54	-0.30	--	0.15
30 mins	0.55	0.54	0.18	0.21	0.54	-0.40	--	0.11
60 mins	0.55	0.54	0.16	0.16	0.55	1.10	--	0.10
120 mins	0.50	0.55	0.15	0.18	0.55	-0.20	--	0.22

Table 4 – Showing the cyclic voltammetry diagnostics for the deposition of an 8Fc thiol monolayer from a 0.1mM solution at 60°C.

8Fc 1mM Results



Figure 3. Cyclic voltammetry showing the deposition of 8Fc thiol from a 1mM solution at (a) Room Temperature, (b) 40°C and (c) 60°C. All scans were carried out in 0.1M $HClO_4$ at 0.02Vs^{-1} scan rate.

Immersion Time	Oxidation Potential (E_{ox})	Reduction Potential (E_{red})	I_{ox} x10-6 (A)	I_{red} x10-6 (A)	E^0 (V)	Peak Separation (mV)	PWHM (mV)	Surface Coverage ($x10^{-10}$ mol.cm^{-2})
0.00	--	--	--	--	--	--	--	0.00
5 secs	0.60	0.56	11.50	10.64	0.58	4.54	13	2.27
10 secs	0.61	0.56	6.37	5.86	0.59	4.58	60	2.21
20 secs	0.61	0.56	5.16	4.88	0.58	5.29	83	2.07
30 secs	0.61	0.55	4.44	4.57	0.58	6.27	100	1.83
1 min	0.61	0.56	5.18	4.92	0.58	5.16	80	2.12
2.5 mins	0.61	0.56	5.25	5.10	0.58	4.77	79	2.06
5 mins	0.60	0.55	4.83	4.85	0.58	5.42	88	1.94
10 mins	0.60	0.55	5.21	5.13	0.58	5.10	76	2.05
15 mins	0.60	0.55	4.79	4.97	0.57	4.90	91	2.23
30 mins	0.60	0.55	5.21	5.41	0.58	5.09	84	2.29
60 mins	0.59	0.55	4.97	5.33	0.57	4.64	91	2.39
120 mins	0.60	0.55	6.10	6.32	0.58	5.02	55	2.59

Table 5 – Showing the cyclic voltammetry diagnostics for the deposition of an 8Fc thiol monolayer from a 1mM solution at RT

Immersion Time	Oxidation Potential (E_{ox})	Reduction Potential (E_{red})	I_{ox} x10-6 (A)	I_{red} x10-6 (A)	E^0 (V)	Peak Separation (mV)	PWHM (mV)	Surface Coverage ($x10^{-10}$ mol.cm^{-2})
0.00	--	--	--	--	--	--	--	0.00
5 secs	0.58	0.57	1.96	1.76	0.57	0.70	54	0.87
10 secs	0.58	0.57	2.55	2.25	0.57	0.60	61	1.13
20 secs	0.57	0.56	2.31	2.13	0.57	0.80	56	0.85
30 secs	0.57	0.56	5.18	4.06	0.57	0.70	51	1.03
1 min	0.57	0.56	3.22	2.82	0.57	0.70	58	1.35
2.5 mins	0.57	0.57	5.12	4.14	0.57	0.20	76	2.13
5 mins	0.57	0.57	4.91	4.05	0.57	0.40	56	1.62
7.5 mins	0.57	0.56	4.15	3.46	0.57	0.70	47	1.51
10 mins	0.57	0.56	4.53	3.70	0.57	0.70	46	1.71
15 mins	0.57	0.56	5.58	4.47	0.57	0.70	54	2.14
30 mins	0.57	0.56	5.18	4.06	0.57	0.70	56	2.08
60 mins	0.57	0.56	5.74	4.26	0.57	0.70	59	2.64
120 mins	0.57	0.56	6.02	4.32	0.57	0.80	67	3.05

Table 6 – Showing the cyclic voltammetry diagnostics for the deposition of an 8Fc thiol monolayer from a 1mM solution at 40°C

Immersion Time	Oxidation Potential (E_{ox})	Reduction Potential (E_{red})	I_{ox} x10-6 (A)	I_{red} x10-6 (A)	E^0 (V)	Peak Separation (mV)	PWHM (mV)	Surface Coverage ($x10^{-10}$ mol.cm^{-2})
0.00	--	--	--	--	--	--	--	0.00
5 secs	0.57	0.57	1.50	1.73	0.57	0.20	72	0.40
10 secs	0.57	0.57	1.53	1.65	0.57	0.20	79	0.77
20 secs	0.57	0.56	1.46	1.55	0.57	0.50	87	0.78
30 secs	0.57	0.57	2.13	2.12	0.57	0.10	79	1.06
1 min	0.58	0.58	3.46	3.36	0.58	0.90	55	1.41
2.5 mins	0.59	0.58	5.51	4.94	0.59	0.20	68	2.53
5 mins	0.57	0.57	4.07	3.24	0.57	0.70	77	2.01
7.5 mins	0.57	0.56	3.65	2.81	0.57	0.70	86	1.91
10 mins	0.57	0.56	3.08	2.46	0.57	0.10	97	1.91
15 mins	0.57	0.57	4.50	3.57	0.57	0.40	73	2.29
30 mins	0.57	0.56	3.58	2.72	0.57	0.80	96	2.13
60 mins	0.57	0.56	4.62	3.50	0.57	0.90	85	2.51
120 mins	0.57	0.57	5.70	4.86	0.57	0.30	85	3.00

Table 7 – Showing the cyclic voltammetry diagnostics for the deposition of an 8Fc thiol monolayer from a 1mM solution at 60°C

10Fc thiol - 0.01mM, 0.1mM and 1mM results

The results presented below are associated with section 4.3.1.2 of this thesis.

10Fc 0.01mM Results.

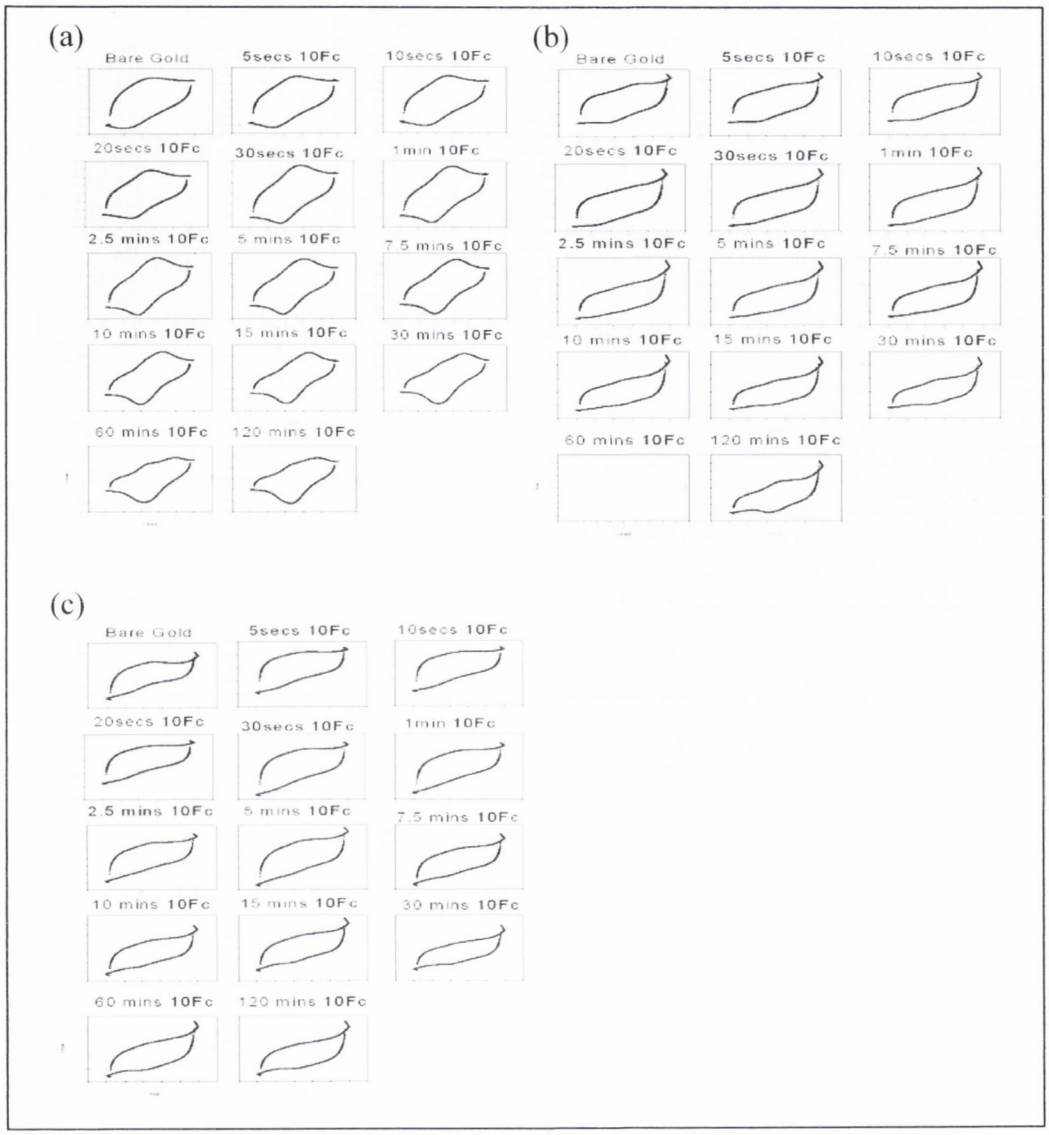


Figure 4. Cyclic voltammetry showing the deposition of 10Fc thiol from a 0.01mM solution at (a) Room Temperature, (b) 40°C and (c) 60°C. All scans were carried out in 0.1M $HClO_4$ at 0.02Vs^{-1} scan rate.

Immersion Time	Oxidation Potential (E_{ox})	Reduction Potential (E_{red})	I_{ox} x10-6 (A)	I_{red} x10-6 (A)	E^0 (V)	Peak Separation (mV)	PWHM (mV)	Surface Coverage ($x10^{-10}$ mol.cm^{-2})
0.00								0.00
5 secs	0.55	0.45	0.46	0.19	0.50	10.22	--	0.00
10 secs	0.55	0.46	0.47	0.20	0.50	9.08	--	0.00
20 secs	0.55	0.49	0.48	0.13	0.52	6.71	--	0.00
30 secs	0.57	0.49	0.60	0.36	0.53	7.30	--	0.20
1 min	0.57	0.50	0.56	0.44	0.54	7.02	62	0.21
2.5 mins	0.58	0.51	0.57	0.57	0.54	7.08	68	0.20
5 mins	0.59	0.51	0.65	0.62	0.55	8.11	70	0.25
7.5 mins	0.60	0.52	0.65	0.73	0.56	8.26	67	0.30
10 mins	0.61	0.52	0.76	0.79	0.57	8.93	75	0.38
15 mins	0.61	0.53	0.80	0.83	0.57	8.66	87	0.42
30 mins	0.64	0.54	0.52	0.88	0.59	10.80	100	0.47
60 mins	0.67	0.54	0.31	0.84	0.61	13.56	72	0.44
120 mins	0.66	0.55	0.24	1.00	0.61	10.29	112	0.47

Table 8 – Showing the cyclic voltammetry diagnostics for the deposition of an 10Fc thiol monolayer from a 0.01mM solution at RT.

10Fc 0.1mM Results.



Figure 5. Cyclic voltammetry showing the deposition of 10Fc thiol from a 0.1mM solution at (a) Room Temperature, (b) 40°C and (c) 60°C. All scans were carried out in 0.1M $HClO_4$ at $0.02Vs^{-1}$ scan rate.

Immersion Time	Oxidation Potential (E_{ox})	Reduction Potential (E_{red})	I_{ox} x10-6 (A)	I_{red} x10-6 (A)	E^0 (V)	Peak Separation (mV)	PWHM (mV)	Surface Coverage ($x10^{-10}$ mol.cm^{-2})
0.00	--	--	--	--	--	--	--	0.00
5 secs	0.54	0.58	0.29	0.98	0.56	-42	--	0.09
10 secs	0.60	0.58	0.32	1.93	0.59	20	239	1.26
20 secs	0.61	0.59	0.39	1.44	0.60	27	230	0.97
30 secs	0.62	0.59	0.66	1.52	0.60	31	216	0.97
1 min	0.61	0.58	0.79	1.99	0.60	31	210	1.28
2.5 mins	0.60	0.59	0.88	1.89	0.59	11	232	1.31
5 mins	0.60	0.58	1.08	2.11	0.59	15	206	1.20
7.5 mins	0.60	0.58	0.47	1.75	0.59	22	250	1.30
10 mins	0.60	0.55	0.66	1.86	0.57	52	235	1.31
15 mins	0.60	0.59	0.77	1.91	0.59	13	241	1.12
30 mins	0.60	0.58	1.37	2.53	0.59	17	190	1.15
60 mins	0.60	0.60	2.43	3.13	0.60	5	56	0.86
120 mins	0.59	0.59	2.00	2.76	0.59	4	234	1.27

Table 9 – Showing the cyclic voltammetry diagnostics for the deposition of an 10Fc thiol monolayer from a 0.1mM solution at RT.

Immersion Time	Oxidation Potential (E_{ox})	Reduction Potential (E_{red})	I_{ox} x10-6 (A)	I_{red} x10-6 (A)	E^0 (V)	Peak Separation (mV)	PWHM (mV)	Surface Coverage ($x10^{-10}$ mol.cm^{-2})
0	--	--	--	--	--	--	--	0.00
5 secs	0.56	0.52	0.06	0.13	0.54	40	--	0.06
10 secs	0.55	0.52	0.29	0.32	0.54	30	118	0.15
20 secs	0.56	0.54	0.42	0.48	0.55	30	101	0.28
30 secs	0.57	0.54	0.53	0.55	0.55	30	105	0.31
1 min	0.57	0.54	0.63	0.63	0.56	30	104	0.4
2.5 mins	0.57	0.53	0.74	0.67	0.55	30	114	0.48
5 mins	0.58	0.54	0.97	0.76	0.56	50	106	0.93
7.5 mins	0.59	0.56	1.09	0.92	0.57	30	102	0.66
10 mins	0.58	0.56	1	0.9	0.57	30	111	0.65
15 mins	0.59	0.56	1.18	1	0.57	20	104	0.71
30 mins	0.58	0.57	1.45	1.23	0.58	10	102	0.85
60 mins	0.58	0.57	1.68	1.35	0.58	10	98	0.93
120 mins	0.58	0.57	1.56	1.23	0.58	10	107	0.97

Table 10 – Showing the cyclic voltammetry diagnostics for the deposition of an 10Fc thiol monolayer from a 0.1mM solution at 40°C.

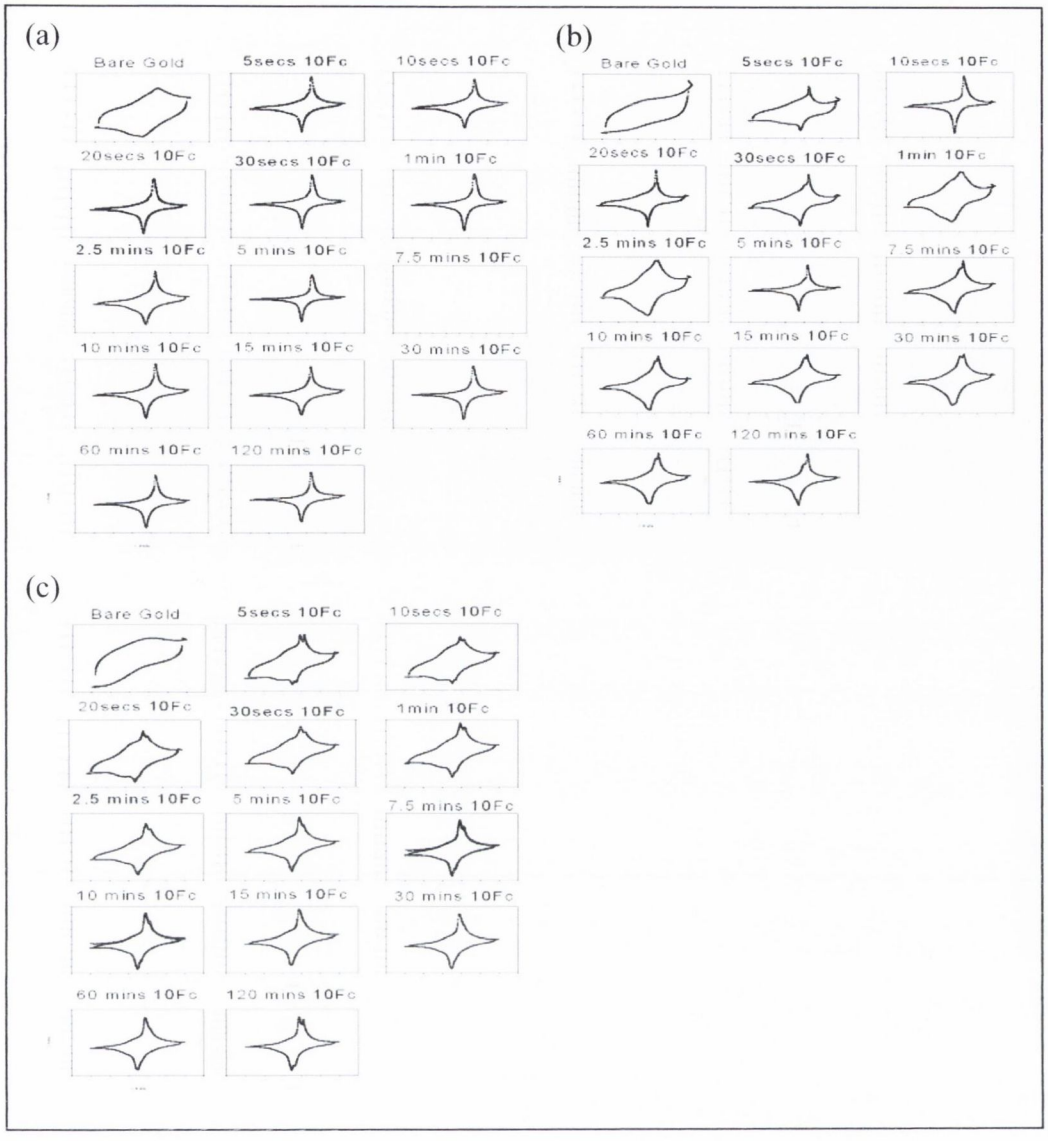


Figure 6. Cyclic voltammetry showing the deposition of 10Fc thiol from a 1mM solution at (a) Room Temperature, (b) 40°C and (c) 60°C. All scans were carried out in 0.1M $HClO_4$ at 0.02Vs^{-1} scan rate.

Immersion Time	Oxidation Potential (E_{ox})	Reduction Potential (E_{red})	I_{ox} x10-6 (A)	I_{red} x10-6 (A)	E^0 (V)	Peak Separation (mV)	PWHM (mV)	Surface Coverage ($x10^{-10}$ mol.cm^{-2})
0	--	--	--	--	--	--	--	0.00
5 secs	0.6	0.6	1.17	0.96	0.6	10	22	2.96
10 secs	0.61	0.6	1.06	0.78	0.6	10	25	2.61
20 secs	0.61	0.6	1.36	1.13	0.6	10	27	3.22
30 secs	0.61	0.6	1.54	1.3	0.6	10	28	3.45
1 min	0.61	0.6	1.61	1.38	0.6	10	29	3.83
2.5 mins	0.6	0.59	8.59	5.6	0.6	10	30	4.14
5 mins	0.61	0.59	19.9	18.06	0.6	10	31	4.61
7.5 mins	--	--	--	--	--	--	--	--
10 mins	0.6	0.59	12.05	8.66	0.6	10	27	3.12
15 mins	0.6	0.59	10.95	7.24	0.6	10	25	2.76
30 mins	0.6	0.59	15.53	12.64	0.6	10	19	3.78
60 mins	0.6	0.59	13.66	10.39	0.6	10	25	3.15
120 mins	0.6	0.59	14.77	11.43	0.6	10	25	3.61

Table 11 – Showing the cyclic voltammetry diagnostics for the deposition of an 10Fc thiol monolayer from a 1mM solution at RT.

Immersion Time	Oxidation Potential (E_{ox})	Reduction Potential (E_{red})	I_{ox} x10-6 (A)	I_{red} x10-6 (A)	E^0 (V)	Peak Separation (mV)	PWHM (mV)	Surface Coverage ($x10^{-10}$ mol.cm^{-2})
0	--	--	--	--	--	--	--	0
5 secs	0.61	0.61	2.26	1.8	0.61	10	17	0.59
10 secs	0.61	0.6	16.12	15.87	0.6	10	30	3.93
20 secs	0.6	0.6	7.11	5.76	0.6	10	14	1.43
30 secs	0.61	0.6	4.58	3.92	0.61	10	34	1.38
1 min	0.59	0.58	1.96	1.77	0.59	10	83	1.01
2.5 mins	0.59	0.58	2.3	2.07	0.59	0	83	1.24
5 mins	0.6	0.6	13.58	12.4	0.6	10	33	3.83
7.5 mins	0.6	0.6	5.88	4.69	0.6	0	45	2.11
10 mins	0.6	0.6	5.04	4.2	0.6	10	61	2.03
15 mins	0.6	0.59	5.21	4.18	0.59	20	52	2.25
30 mins	0.61	0.58	5.46	4.56	0.59	20	61	2.72
60 mins	0.6	0.6	7.52	5.68	0.6	0	48	2.94
120 mins	0.6	0.6	11.69	9.59	0.6	10	48	3.85

Table 12 – Showing the cyclic voltammetry diagnostics for the deposition of an 10Fc thiol monolayer from a 1mM solution at 40°C

Immersion Time	Oxidation Potential (E_{ox})	Reduction Potential (E_{red})	I_{ox} x10-6 (A)	I_{red} x10-6 (A)	E^0 (V)	Peak Separation (mV)	PWHM (mV)	Surface Coverage ($x10^{-10}$ mol.cm^{-2})
0	--	--	--	--	--	--	--	0
5 secs	0.6	0.57	1.98	1.98	0.59	30	100	0.77
10 secs	0.57	0.57	1.76	1.79	0.57	0	41	0.71
20 secs	0.58	0.57	2.05	2.02	0.57	0	44	1.09
30 secs	0.58	0.57	2.56	2.4	0.58	0	43	0.82
1 min	0.58	0.57	3.36	2.96	0.57	0	47	1.16
2.5 mins	0.58	0.57	3.93	3.48	0.57	0	50	1.39
5 mins	0.57	0.57	5.33	4.49	0.57	0	40	1.69
7.5 mins	0.57	0.57	6.38	5.18	0.57	0	40	1.99
10 mins	0.57	0.57	6.48	5.3	0.57	0	40	1.94
15 mins	0.57	0.56	5.9	4.51	0.57	10	38	1.83
30 mins	0.57	0.57	6.79	5.17	0.57	0	39	2.25
60 mins	0.57	0.57	6.52	4.89	0.57	0	43	2.26
120 mins	0.57	0.57	8.17	6.63	0.57	0	44	1.86

Table 13 – Showing the cyclic voltammetry diagnostics for the deposition of an 10Fc thiol monolayer from a 1mM solution at 60°C

12Fc thiol - 0.01mM, 0.1mM and 1mM results

The results presented below are associated with section 4.3.1.3 of this thesis.

12Fc 0.01mM Results.

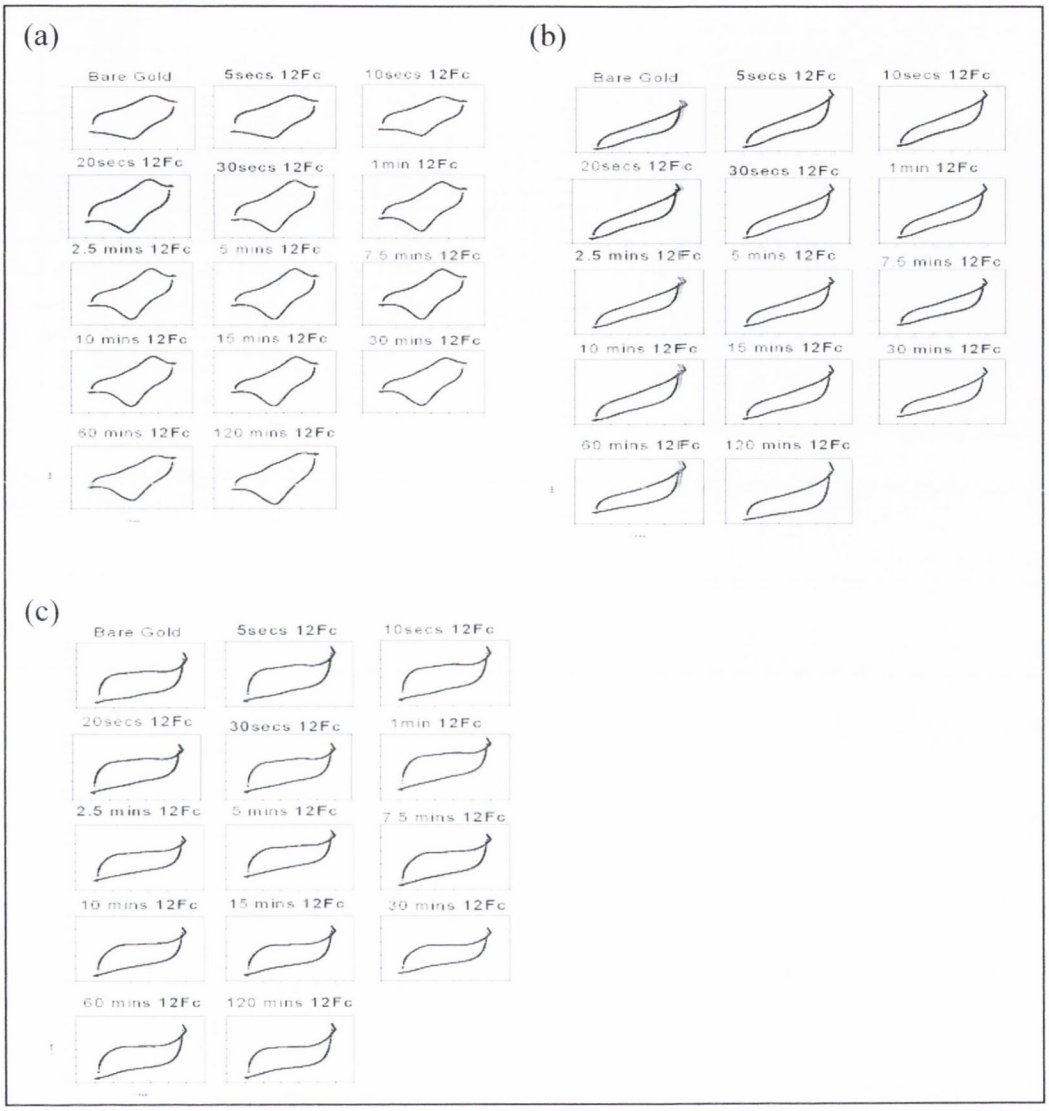


Figure 7. Cyclic voltammetry showing the deposition of 12Fc thiol from a 0.01mM solution at (a) Room Temperature, (b) 40°C and (c) 60°C. All scans were carried out in 0.1M $HClO_4$ at 0.02Vs^{-1} scan rate.

Immersion Time	Oxidation Potential (E_{ox})	Reduction Potential (E_{red})	I_{ox} x10-6 (A)	I_{red} x10-6 (A)	E^0 (V)	Peak Separation (mV)	PWHM (mV)	Surface Coverage ($x10^{-10}$ mol.cm^{-2})
0.00								0
5 secs	0.65	0.56	0.40	0.43	0.60	90	99	0.28
10 secs	0.65	0.56	0.47	0.43	0.60	90	101	0.33
20 secs	0.65	0.56	0.56	0.47	0.60	80	116	0.36
30 secs	0.64	0.56	0.60	0.49	0.60	80	118	0.44
1 min	0.65	0.56	0.65	0.52	0.60	80	123	0.43
2.5 mins	0.64	0.56	0.72	0.55	0.60	80	121	0.44
5 mins	0.65	0.57	0.72	0.55	0.61	80	105	0.40
7.5 mins	0.65	0.57	0.73	0.57	0.61	80	124	0.50
10 mins	0.65	0.57	0.71	0.52	0.61	80	121	0.47
15 mins	0.65	0.57	0.68	0.50	0.61	90	129	0.52
30 mins	0.66	0.57	0.57	0.44	0.62	100	111	0.32
60 mins	0.67	0.57	0.47	0.32	0.62	100	indt	0.43
120 mins	0.70	0.57	0.37	0.68	0.63	130	indt	0.38

Table 14 – Showing the cyclic voltammetry diagnostics for the deposition of an 12Fc thiol monolayer from a 0.01mM solution at RT.

12Fc 0.1mM Results.



Figure 8. Cyclic voltammetry showing the deposition of 12Fc thiol from a 0.1mM solution at (a) Room Temperature, (b) 40°C and (c) 60°C. All scans were carried out in 0.1M $HClO_4$ at 0.02Vs^{-1} scan rate.

Immersion Time	Oxidation Potential (E_{ox})	Reduction Potential (E_{red})	I_{ox} x10-6 (A)	I_{red} x10-6 (A)	E^0 (V)	Peak Separation (mV)	PWHM (mV)	Surface Coverage ($x10^{-10}$ mol.cm^{-2})
0.00	--	--	--	--	--	--	--	0.00
5 secs	0.61	0.54	2.44	1.15	0.57	70.00	116	11.36
10 secs	0.62	0.54	2.05	1.20	0.58	80.00	150	13.55
20 secs	0.60	0.58	2.44	1.78	0.59	20.00	164	13.27
30 secs	0.60	0.59	2.63	1.87	0.59	10.00	147	14.45
1 min	0.60	0.58	2.66	1.82	0.59	20.00	147	14.98
2.5 mins	0.60	0.58	2.43	1.61	0.59	30.00	160	13.09
5 mins	0.60	0.58	2.55	1.71	0.59	20.00	150	13.41
7.5 mins	0.60	0.59	2.65	1.93	0.59	20.00	164	12.98
10 mins	0.60	0.58	2.82	2.04	0.59	20.00	159	15.16
15 mins	0.62	0.59	2.53	1.80	0.60	30.00	170	14.06
30 mins	0.60	0.58	2.28	1.78	0.59	20.00	148	10.40
60 mins	0.59	0.58	2.40	1.67	0.59	10.00	171	11.39
120 mins	0.59	0.58	2.47	1.91	0.59	10.00	136	11.39

Table 15 – Showing the cyclic voltammetry diagnostics for the deposition of a 12Fc thiol monolayer from a 0.1mM solution at RT.

Immersion Time	Oxidation Potential (E_{ox})	Reduction Potential (E_{red})	I_{ox} x10-6 (A)	I_{red} x10-6 (A)	E^0 (V)	Peak Separation (mV)	PWHM (mV)	Surface Coverage ($x10^{-10}$ mol.cm^{-2})
0.00	--	--	--	--	--	--	--	0.00
5 secs	0.57	0.56	0.48	0.40	0.56		Indt.	2.43
10 secs	0.55	0.56	0.58	0.56	0.56	-10	Indt.	2.78
20 secs	0.58	0.56	0.63	0.62	0.57	20	135.00	2.49
30 secs	0.57	0.55	0.72	0.76	0.56	20	Indt.	3.26
1 min	0.59	0.56	0.77	0.88	0.57	30	136	3.69
2.5 mins	0.59	0.56	0.84	0.99	0.57	30	133	3.82
5 mins	0.59	0.55	0.88	1.04	0.57	30	133	3.96
7.5 mins	0.58	0.57	0.86	1.17	0.58	20	132	3.76
10 mins	0.59	0.56	0.89	1.13	0.58	30	129	3.91
15 mins	0.59	0.56	0.89	1.15	0.58	30	126	3.82
30 mins	0.60	0.57	0.97	1.27	0.59	20	129	4.40
60 mins	0.60	0.57	0.92	1.27	0.58	30	123	3.86
120 mins	0.60	0.57	1.03	1.34	0.58	30	119	4.12

Table 16 – Showing the cyclic voltammetry diagnostics for the deposition of a 12Fc thiol monolayer from a 0.1mM solution at 40°C.

Immersion Time	Oxidation Potential (E_{ox})	Reduction Potential (E_{red})	I_{ox} x10-6 (A)	I_{red} x10-6 (A)	E^0 (V)	Peak Separation (mV)	PWHM (mV)	Surface Coverage ($x10^{-10}$ mol.cm^{-2})
0.00	0.52	--	0.28	--	--	--		0.00
5 secs	0.54	0.52	0.46	0.24	0.53	20.00	Indt.	1.73
10 secs	0.54	0.54	0.60	0.35	0.54	0.00	Indt.	1.94
20 secs	0.55	0.45	0.64	0.33	0.50	10.00	119	2.60
30 secs	0.54	0.52	0.76	0.42	0.53	20.00	Indt.	3.13
1 min	0.56	0.54	0.73	0.51	0.55	20.00	131	3.14
2.5 mins	0.57	0.55	0.71	0.53	0.56	20.00	133	3.16
5 mins	0.56	0.55	0.68	0.51	0.56	20.00	131	2.99
7.5 mins	0.56	0.55	0.70	0.50	0.55	10.00	Indt.	3.04
10 mins	0.57	0.54	0.59	0.43	0.55	30.00	129	2.57
15 mins	0.57	0.55	0.49	0.41	0.56	20.00	124	2.08
30 mins	0.55	0.56	0.20	1.30	0.55	0.00	Indt.	0.67
60 mins	0.57	0.56	0.06	0.03	0.56	10.00	Indt.	0.02
120 mins	0.52	--	0.28	--	--	--	Indt.	1.07

Table 17 – Showing the cyclic voltammetry diagnostics for the deposition of a 12Fc thiol monolayer from a 0.1mM solution at 60°C.

12Fc 1mM Results.



Figure 9. Cyclic voltammetry showing the deposition of 12Fc thiol from a 1mM solution at (a) Room Temperature, (b) 40°C and (c) 60°C. All scans were carried out in 0.1M $HClO_4$ at $0.02Vs^{-1}$ scan rate.

Immersion Time	Oxidation Potential (E_{ox})	Reduction Potential (E_{red})	I_{ox} x10-6 (A)	I_{red} x10-6 (A)	E^0 (V)	Peak Separation (mV)	PWHM (mV)	Surface Coverage ($x10^{-10}$ mol.cm^{-2})
0.00	0.60	--	--	--	--	--	--	0.00
5 secs	0.59	0.59	4.13	3.34	0.59	0	94	12.52
10 secs	0.60	0.59	4.35	3.35	0.59	10	107	13.80
20 secs	0.60	0.59	4.78	3.70	0.59	10	98	14.80
30 secs	0.62	0.59	5.05	4.02	0.60	30	90	1.50
1 min	0.62	0.59	5.51	4.32	0.61	30	100	17.10
2.5 mins	0.62	0.60	7.74	5.38	0.61	20	70	23.32
5 mins	0.61	0.59	4.47	3.30	0.60	20	129	13.46
7.5 mins	0.61	0.59	5.79	4.56	0.60	20	85	17.86
10 mins	0.62	0.60	8.22	5.91	0.61	20	68	25.58
15 mins	0.61	0.59	5.92	4.47	0.60	20	106	17.80
30 mins	0.61	0.59	6.08	4.37	0.60	20	160	18.23
60 mins	0.61	0.60	5.54	3.95	0.61	10	164	16.46
120 mins	0.60	0.59	2.63	2.29	0.59	10	121	8.70

Table 18 – Showing the cyclic voltammetry diagnostics for the deposition of a 12Fc thiol monolayer from a 1mM solution at RT.

Immersion Time	Oxidation Potential (E_{ox})	Reduction Potential (E_{red})	I_{ox} x10-6 (A)	I_{red} x10-6 (A)	E^0 (V)	Peak Separation (mV)	PWHM (mV)	Surface Coverage ($x10^{-10}$ mol.cm^{-2})
0.00	--	--	--	--	--	--	--	0.00
5 secs	0.59	0.59	1.72	1.46	0.59	2	85	4.7
10 secs	0.59	0.59	4.27	2.07	0.59	0	64	5.89
20 secs	0.59	0.58	2.55	2.02	0.59	2	66	5.26
30 secs	0.59	0.58	2.63	2.24	0.59	2	63	5.27
1 min	0.59	0.59	2.92	2.43	0.59	1	65	5.99
2.5 mins	0.59	0.59	2.39	2.07	0.59	1	64	4.79
5 mins	0.59	0.58	2.66	2.26	0.59	2	61	4.98
7.5 mins	0.59	0.59	2.04	1.63	0.59	0	70	4.3
10 mins	0.59	0.59	2.75	2.24	0.59	1	58	5.01
15 mins	0.59	0.59	3.03	2.24	0.59	2	59	5.56
30 mins	0.59	0.59	3.44	2.42	0.59	1	64	7.11
60 mins	0.59	0.58	4.26	3.33	0.59	2	131	8.29
120 mins	0.58	0.58	4.15	3.19	0.58	4	117	8.94

Table 19 – Showing the cyclic voltammetry diagnostics for the deposition of a 12Fc thiol monolayer from a 1mM solution at 40°C.

Immersion Time	Oxidation Potential (E_{ox})	Reduction Potential (E_{red})	I_{ox} x10-6 (A)	I_{red} x10-6 (A)	E^0 (V)	Peak Separation (mV)	PWHM (mV)	Surface Coverage ($x10^{-10}$ mol.cm^{-2})
0.00	--	--	--	--	--	--	--	0.00
5 secs	0.62	0.62	3.06	1.15	0.62	10	155	5.99
10 secs	0.62	0.61	3.68	2.45	0.62	10	51	9.73
20 secs	0.59	0.59	3.87	2.33	0.59	0	56	12.80
30 secs	0.59	0.59	4.24	2.65	0.59	0	59	14.10
1 min	0.59	0.59	7.36	3.93	0.59	0	65	20.34
2.5 mins	0.62	0.61	11.35	7.77	0.62	10	68	32.50
5 mins	0.59	0.59	6.26	2.98	0.59	10	86	18.00
7.5 mins	0.59	0.59	7.10	3.61	0.59	10	74	20.70
10 mins	0.59	0.59	9.73	6.25	0.59	0	69	28.90
15 mins	0.59	0.59	8.37	4.94	0.59	10	65	24.75
30 mins	0.59	0.59	9.16	5.56	0.59	10	57	26.81
60 mins	0.59	0.59	7.94	5.07	0.59	0	51	22.90
120 mins	0.60	0.59	5.06	2.82	0.60	10	60	15.37

Table 20 – Showing the cyclic voltammetry diagnostics for the deposition of a 12Fc thiol monolayer from a 1mM solution at 60°C.